NASA Contractor Report 189222

LIFE PREDICTION AND CONSTITUTIVE MODELS FOR ENGINE HOT SECTION ANISOTROPIC MATERIALS PROGRAM

Interim Report

D. M. Nissley and T. G. Meyer
UNITED TECHNOLOGIES CORPORATION

August 1992

NASA

(NASA-CR-189222) LIFE PREDICTION
AND CONSTITUTIVE MODELS FOR ENGINE
HOT SECTION ANISOTROPIC MATERIALS
PROGRAM Interim Report (United
Technologies Corp.) 177 p

N92-31534

Unclas

G3/07 0116469

TABLE OF CONTENTS

TABLE OF CONTENTS (Continued)

LIST OF ILLUSTRATIONS

LIST OF ILLUSTRATIONS (Continued)

LIST OF ILLUSTRATIONS (Continued)

LIST OF TABLES

SECTION 1.0

SUMMARY

The following tasks were completed and results obtained during this 35 month effort:

Base Program

o   Specimens were machined for the coated multiaxial tests.

o   Diffusion aluminide coating constitutive tests were completed. This data was obtained from thin aluminide coated PWA 1480 substrates subjected to cyclic stress relaxation in a manner consistent with that used to obtain overlay coating constitutive properties.

o   Level II uniaxial fatigue experiments were completed. The Level II TMF tests substantiated the finding that PWA 1480 crack initiation life is dependent on: 1) the presence of a coating, 2) the coating composition and microstructure, 3) single crystal orientation, 4) the cyclic strain-temperature-time relationship (i.e., the cyclic loading history), and 5) the severity of thermal exposure. These tests, along with those from Level I fatigue experiments, formed the database used to evaluate and select the TMF crack initiation life models for the overlay coating and PWA 1480 single crystal materials.

o   Overlay coating isothermal cyclic stress relaxation data was used to obtain model constants for the two coating constitutive models selected for further development: Moreno's Simplified Approach and Walker's Unified Viscoplastic Formulation. Based on overall correlation of the baseline data, ability in reproducing creep and TMF behavior, and ease of incorporation into a finite element code, the Walker model was selected as the final coating model. The Walker model for the overlay coating was subsequently incorporated into the MARC finite element computer code user subroutine, HYPELA.

o   The "micromechanistic" based Walker Unified Viscoplastic Formulation was chosen as the final single crystal constitutive model for PWA 1480. This model was subsequently modified to address low temperature strain rate insensitivity and nonisothermal cyclic conditions.

o   Candidate coating life models were evaluated using the results obtained in overlay coated PWA 1480 fatigue experiments. The coating life model selected for final development is a modified form of Ostergren's Hysteretic Energy Model.

o   Candidate life models for coated Ni-based single crystal superalloys were evaluated using the results obtained in coated PWA 1480 fatigue experiments. Two single crystal models applicable to TMF conditions were selected for final development. Both models are based on isotropic crack growth parameters: maximum mode I crack growth stress intensity factor, Kmax, and mode I crack tip opening displacement, CTOD, based on Kmax.

o   Uncoated monotonic tensile and creep and baseline coated TMF experiments for Alloy 185, the secondary single crystal alloy in this program, were conducted.

Option 1 Program

o   Finite element and boundary element analyses of candidate notched specimen designs were conducted to obtain stress concentrations and to guide selection of secondary crystalline orientations.

o   Specimen fabrication is nearly complete.

o   Fatigue tests of smooth and notched PWA 1480 specimens were initiated. Testing of notched uncoated PWA 1480 specimens has determined that crack initiation occurs at the maximum principle stress location, and not the maximum principle strain location. The crack initiation site for un-HIP'd (HIP'd = Hot Isostatically Pressed) PWA 1480 was identified as porosity located at, or near, the notch surface. Inspection of un-HIP'd notched specimen fracture surfaces indicate that a normal fatigue zone (i.e., thumbnail-like crack normal to the maximum principle stress) was initiated, followed by crystallographic crack growth along an octahedral slip plane. Testing has concentrated at 649°C (1200°F), but higher temperature tests were also conducted.

o   Initial correlations of notched and smooth data from the option program were completed. A stress range life model using elastic concentrated stress showed promising trends.

2

SECTION 2.0

INTRODUCTION

One of the more important developments in gas turbine blade materials has been the introduction of directionally solidified and single crystal castings. Among the advantages of these materials are:

o   Substantially increased high temperature creep and stress rupture strengths and enhanced oxidation/corrosion resistance due to the elimination of grain boundaries.

o   Increased low cycle fatigue life due to a thermal stress reduction incurred as a result of lower elastic modulus along the solidification direction.

o   Higher melting temperature and greater heat treatment flexibility resulting from the elimination of grain boundary strengthening elements.

This casting process has matured to the level where it is now routinely used in the production of commercial and military aircraft jet engine turbine blades. Unfortunately, metallurgical and processing advances have not been matched by corresponding advancements in the knowledge and understanding of the mechanics of these materials, their failure mechanisms, and methods for life prediction. In order to realize the full potential of these materials, it is necessary to determine the dominant life limiting parameters. Anisotropy introduces many life prediction questions, especially for stresses which are not parallel to the direction of solidification. Oxidation resistant coatings further complicate the questions. All of these issues are addressed in this NASA sponsored program.

The program consists of a base program and an optional program (Option 1). The base program addresses coated single crystal material subjected to relevant turbine airfoil temperatures and load histories. Option 1 addresses uncoated single crystal material operating at root attachment temperatures and notched conditions.

In the base and optional programs, candidate constitutive and life prediction models are being developed concurrently. Laboratory specimens, tested using a variety of mechanical and thermal load histories, will provide data for the final model selections. Finally, the selected models will be incorporated into a computer code.

The first year effort of the program involved materials selection, specimen fabrication, basic material tests, literature searches of appropriate constitutive and life prediction models, initial formulation of constitutive models, and initial constitutive and fatigue life tests. The results of the first year effort are reported in NASA CR-174952 (Reference 1).

The second year effort of the program involved constitutive testing of the selected overlay coating and primary single crystal (PWA 1480) materials, Level I fatigue life testing, development of "microscopic" and "macroscopic" single crystal constitutive models, selection of two coating constitutive models for further development, and initial coating and single crystal life model evaluations. The results of the second year effort are reported in NASA CR-179594 (Reference 2).

This interim report covers the period from February, 1986 to December, 1988. The results of the effort during that period include the following:

Base Program

o   Completed machining of specimens for the multiaxial experiments.

o   Evaluated candidate overlay coating constitutive and life models and selected an overlay coating constitutive model and an overlay coating life model for final development.

o   Selected the single crystal constitutive model.

o   Evaluated candidate single crystal life models applicable to coated gas turbine airfoil TMF conditions and selected two TMF life models for further development.

o   Completed aluminide coating constitutive tests.

o   Completed Level II coated single crystal uniaxial fatigue life tests.

Option 1

o   Completed finite element elastic stress analyses of each notched specimen design to select most appropriate secondary crystal orientation for the notched tests.

o   Initial smooth and notched fatigue life tests were completed.

o   Evaluated initial smooth and notched fatigue lives using concentrated elastic stress range criteria.

o   Determined crack initiation site for un-HIP'd specimens (i.e., specimens not Hot Isostatically Pressed).

4

SECTION 3.0

TASK I - MATERIAL/COATING SELECTION AND ACQUISITION

PWA 1480 and Alloy 185 were previously selected as the primary and secondary single crystal materials, respectively, to be evaluated in this program (Reference 1).

PWA 1480 was the first superalloy specifically designed for use in single crystal form and was developed with the goal of achieving an optimum balance of creep strength, thermal fatigue strength, and oxidation and hot corrosion resistance. PWA 1480 is the most widely used single crystal alloy in gas turbine engines today. PWA 1480 was certified for commercial use in the JT9D-7R4D/E engine in late 1981 and has since been certified for use in the JT9D-7R4G/H, PW2037, PW4000, and V2500 engines.

Two heats of PWA 1480 were procured for this program from the Howmet Turbine Components Corporation, Alloy Division, Dover, New Jersey. The primary heat, identified by Howmet as 200A14824, has been designated P9866. The secondary heat, identified by Howmet as 200B14773, has been designated P9867.

Alloy 185 exhibits greater creep anisotropy than PWA 1480 as a result of its higher hardener content compared to PWA 1480 and different structure. Consequently, its selection as the secondary single crystal material makes it possible to test the range of applicability of the constitutive and life models developed in the program (Reference 1).

A single heat of Alloy 185 was procured for this program from the Howmet Corporation, Alloy Division. This heat, designated by Howmet as 242A15847, has been designated P9921.

Nominal compositions for PWA 1480 and Alloy 185 along with actual compositions of the procured heats are available in Reference 2.

The directional solidification casting process was employed to cast cylindrical single crystal bars of both selected alloys with nominal 15.2 cm (6.0 in. length and 2.54 cm (1.0 in.) and 1.59 cm (0.625 in.) diameters. The primary growth direction was controlled to produce <001>, <111>, <011>, and <213> oriented bars. The castings were solution heat treated, followed by a rigorous evaluation to ensure that only quality castings were used for specimen fabrication (Reference 1).

Two coatings were selected for this program to be representative of those employed on actual turbine airfoils operating in gas turbine engines: PWA 286 overlay coating and PWA 273 outward diffusion aluminide (Reference 1). The general coating compositions and application processes along with typical coating microstructures are provided in Reference 2.

3.1 PRIMARY ALLOY (PWA 1480) AND COATING SPECIMEN FABRICATION

3.1.1 PWA 1480 Material Specimens

Fatigue test specimen geometries were chosen to allow test conditions comparable to those found in actual turbine airfoils. Figure 1 schematically illustrates the geometries for the hollow tube LCF/TMF (low cycle fatigue/thermomechanical fatigue) specimens. To take full advantage of external extensometry, a ridgeless specimen (Figure 1B) was developed early in the program to replace the internally ridged specimen (Figure 1A). A comparison study of internal and external extensometers was reported in Reference 2.

(A) OLD FATIGUE SPECIMEN DESIGN — TYPE 44C
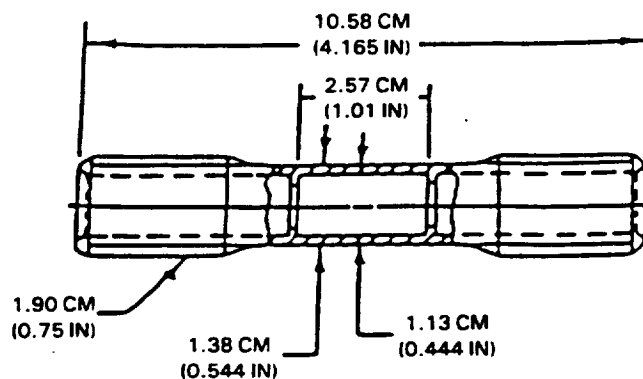
(B) NEW FATIGUE SPECIMEN DESIGN — TYPE 73C
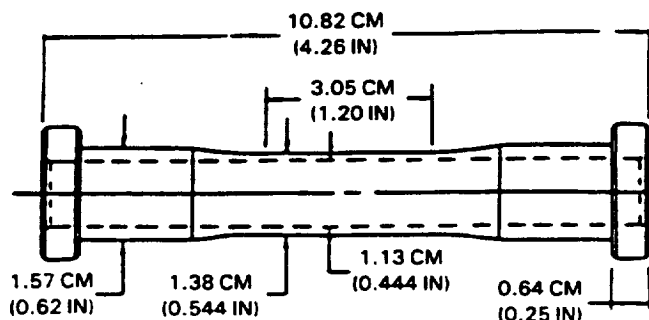
Figure 1   Geometries of Uniaxial Tubular Specimens for Fatigue Testing

The balance of uniaxial fatigue test specimens needed for the base program were machined according to Figure 1B and were coated, using the standard methods discussed in Reference 2, with either PWA 286 or PWA 273 coating. Multiaxial specimens were machined from 3.17 cm (1.25 in.) bars of heat P9867 material according to the geometry presented in Figure 2.
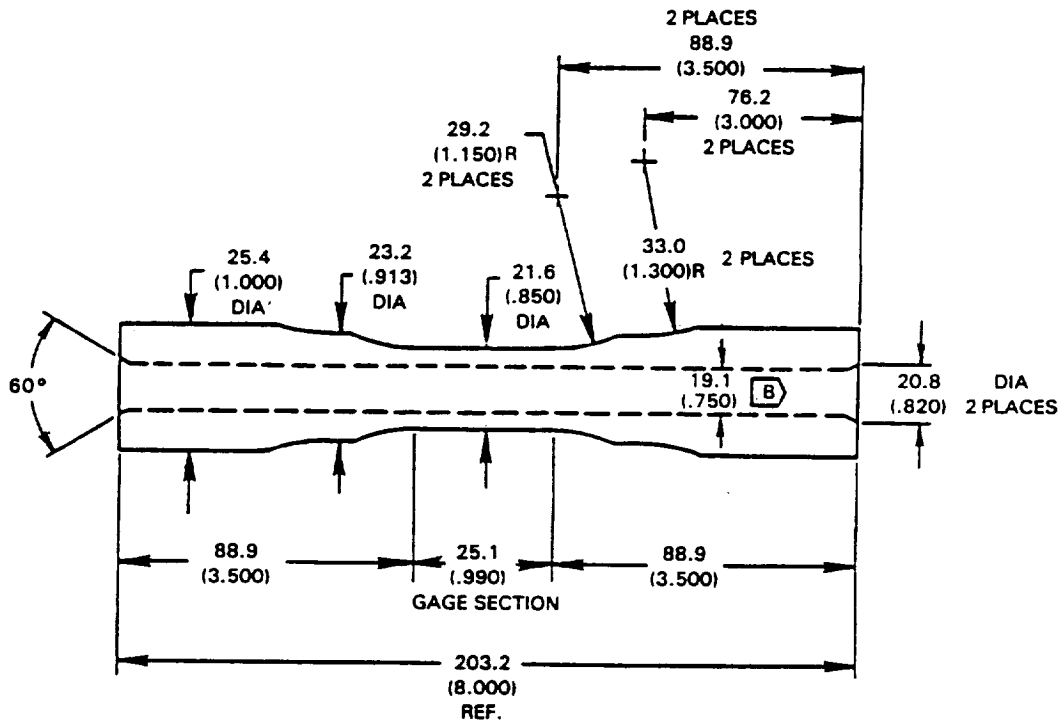
DIMENSION IN MM (in)

Figure 2   Biaxial Tension Torsion Specimen

All of the PWA 1480 specimens for physical, thermal, monotonic tensile and creep, and cyclic constitutive testing were fabricated in prior years (Reference 1).

3.1.2   PWA 286 and PWA 273 Coating Specimens

All bulk PWA 286 overlay coating specimens for constitutive behavior testing were fabricated in prior years (References 1 and 2).

The structure of diffusion coatings is much more complex than that of overlay coatings. The diffusion coating chemistry and microstructure vary from the coating surface to the substrate because of interdiffusion between the coating material and the substrate during the coating process, and, as a result, mechanical properties can not be effectively determined from homogeneous bulk specimens. To obtain diffusion coating behavior, the approach taken in this program was to coat two thicknesses of thin PWA 1480 substrates and test the

7

resulting composite structure. Theoretically, the effective coating properties can then be obtained by comparing the thicker specimen response to that of the thinner specimen.

Flat specimens for PWA 273 coating constitutive tests were fabricated by forming coating on both sides of the PWA 1480 substrate. PWA 1480 <100> substrates were fabricated from 2.54 cm (1.0 in.) diameter bars of heat P9867 material. The specimens were oriented such that the transverse direction was parallel to a secondary <010> direction. The nominal, before coating, substrate gage section thicknesses were: 0.25 mm (0.01 in.) and 0.13 mm (0.005 in.) as shown in Figure 3. Due to the fragile nature of these specimens, fixtures were constructed to hold the specimens during the coating process and subsequent diffusion heat treatment at 1079°C (1975°F) and aging at 871°C (1600°F). The 0.25 mm (0.10 in.) thick specimens were previously fabricated (Reference 2). However, as also reported in Reference 2, the thin substrate specimens severely deformed during the heat treatment process. During this reporting period, additional thin substrates were fabricated from the P9867 heat material to replace those destroyed during heat treatment. These specimens were coated and, by using a special fixture, successfully heat treated.

UNCOATED DIMENSIONS ~ CM (IN)
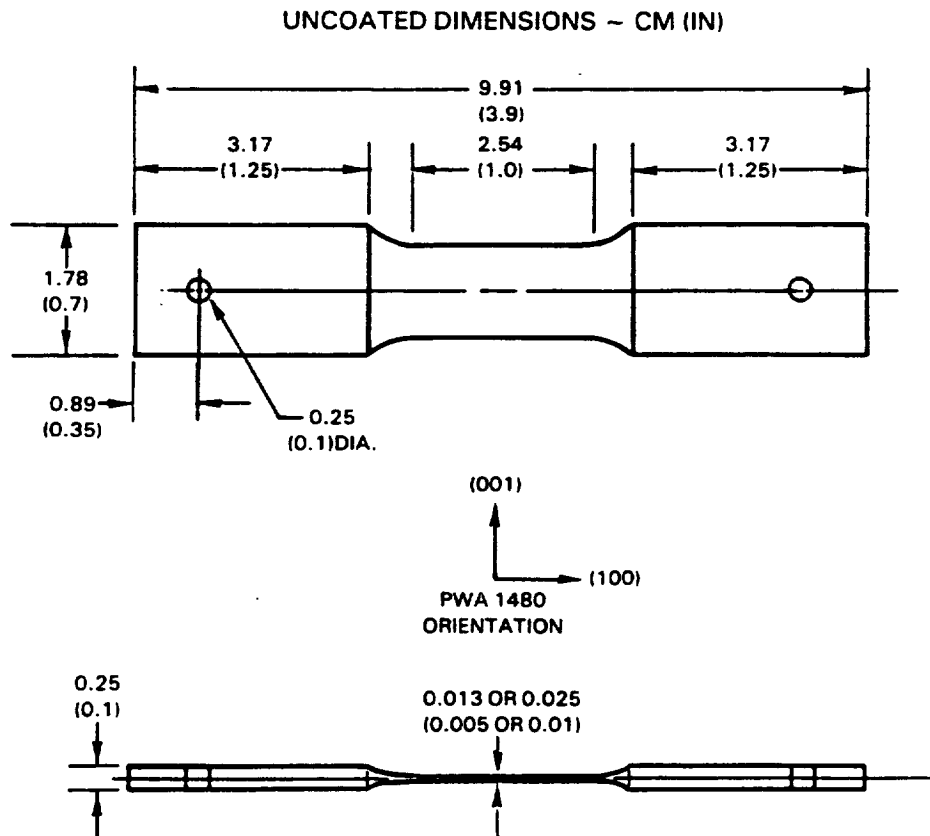
Figure 3 Substrate Design for Diffused Aluminide Coating Mechanical Property Tests

8

The 0.25 mm (0.010 in.) initial substrate thickness reduces to about 0.14 mm (0.0055 in.) after coating, while the 0.13 mm (0.005 in.) initial thickness reduces to about 0.02 mm (0.0008 in.) substrate thickness. The coating microstructure appearance of completed PWA 273 aluminide constitutive specimens is available in Reference 2.

3.2 ALTERNATE SINGLE CRYSTAL MATERIAL (ALLOY 185) SPECIMEN FABRICATION

Alloy 185 bars were cast using the single crystal directional solidification process. Bar sizes were consistent with the PWA 1480 bars (Reference 1). The bars were heat treated at 1316°C (2400°F) followed by a forced gas cool to refine and homogenize the gamma prime hardener without the onset of incipient melting. The same inspection procedure as was used for PWA 1480 cast bars was employed to ensure the quality of the Alloy 185 castings used for specimen fabrication.

3.3 PHYSICAL, THERMAL, AND MONOTONIC MECHANICAL PROPERTIES

Thermal-physical and monotonic mechanical property tests of PWA 1480 single crystal material and the two selected coatings (PWA 273 aluminide and PWA 286 overlay) were completed earlier and were reported in References 1 and 2.

Elastic constants for the primary single crystal material have been obtained by ultrasonic wave velocity measurements over the entire range of temperatures applicable to the base program and Option 1. The resulting "dynamic" stiffnesses are shown in Figure 4. Table 1 contains the dynamic stiffnesses, C_{ij}, and the dynamic compliances, S_{ij}, which are related by the following equations.

$$S11 = \left[\frac{C11 + C12}{(C11 - C12)(C11 + 2C12)} \right]$$

$$S12 = \left[\frac{- C12}{(C11 - C12)(C11 + 2C12)} \right]$$

$$S44 = \frac{1}{C44}$$
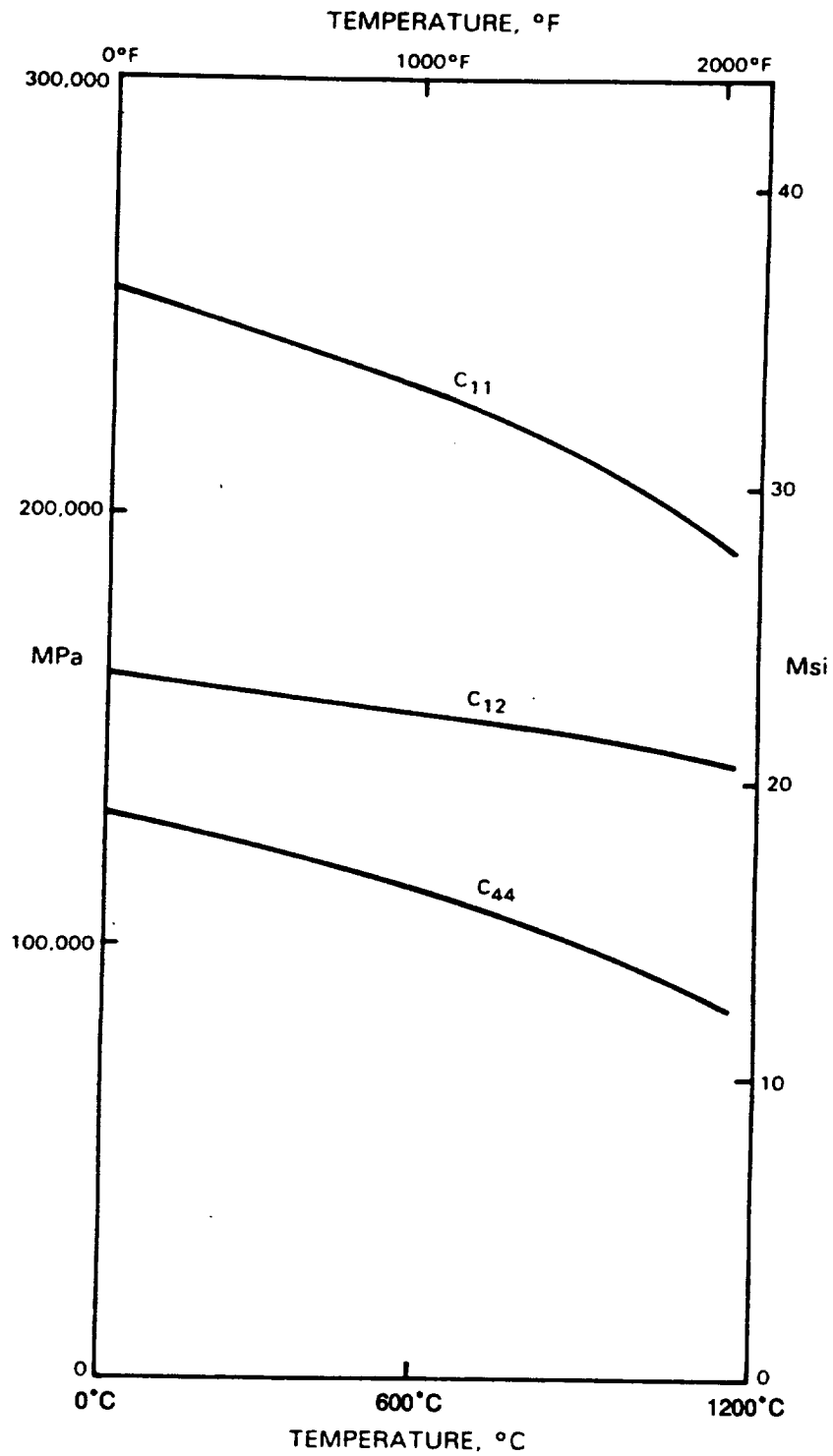
Figure 4 PWA 1480 Dynamic Stiffnesses Vs. Temperature

10

TABLE 1

DYNAMIC ELASTIC CONSTANTS
AND APPARENT MODULUS FOR UNIAXIAL BARS IN FOUR ORIENTATIONS

TEMP °F	CONSTANTS REFERRED TO CRYSTAL AXES						APPARENT MODULUS			
	C11 Msi	C12 Msi	C44 Msi	S11	S12	S44	<001> Msi	<101> Msi	<213> Msi	<111> Msi
				x 10⁻⁹ Psi⁻¹						
0.	36.5	23.6	19.0	55.6	-21.8	52.7	18.0	33.3	33.3	46.4
100.	36.3	23.6	18.7	56.5	-22.3	53.3	17.7	32.8	32.8	45.9
200.	36.0	23.4	18.5	56.9	-22.4	54.0	17.6	32.5	32.5	45.4
300.	35.7	23.2	18.3	57.4	-22.6	54.7	17.4	32.2	32.2	44.8
400.	35.4	23.1	18.0	58.0	-22.9	55.5	17.2	31.8	31.8	44.3
500.	35.1	22.9	17.8	58.9	-23.3	56.3	17.0	31.4	31.4	43.7
600.	34.8	22.8	17.5	59.7	-23.7	57.2	16.7	30.9	30.9	43.1
700.	34.5	22.7	17.2	60.8	-24.1	58.1	16.4	30.4	30.4	42.5
800.	34.1	22.6	16.9	61.9	-24.7	59.0	16.1	29.9	29.9	41.9
900.	33.8	22.4	16.6	63.0	-25.2	60.1	15.9	29.5	29.5	41.2
1000.	33.4	22.3	16.4	64.2	-25.7	61.1	15.6	29.0	29.0	40.6
1100.	33.0	22.1	16.1	65.5	-26.3	62.2	15.3	28.4	28.4	39.9
1200.	32.7	22.0	15.8	66.9	-26.9	63.4	15.0	27.9	27.9	39.3
1300.	32.3	21.9	15.5	68.6	-27.7	64.6	14.6	27.3	27.3	38.6
1400.	31.8	21.8	15.2	70.6	-28.7	65.9	14.2	26.7	26.7	37.9
1500.	31.4	21.7	14.8	72.9	-29.8	67.3	13.7	26.0	26.0	37.2
1600.	30.9	21.6	14.5	75.6	-31.0	68.9	13.2	25.3	25.3	36.4
1700.	30.4	21.4	14.1	78.5	-32.4	70.7	12.7	24.6	24.6	35.6
1800.	29.9	21.2	13.7	81.9	-34.0	72.8	12.2	23.7	23.7	34.6
1900.	29.2	21.0	13.3	86.0	-36.0	75.2	11.6	22.8	22.8	33.6
2000.	28.5	20.8	12.8	91.4	-38.6	78.1	10.9	21.8	21.8	32.5
2100.	27.8	20.7	12.3	99.4	-42.5	81.4	10.1	20.5	20.5	31.3
2200.	27.0	20.6	11.8	108.9	-47.1	85.0	9.2	19.2	19.2	30.1

1 MPa = 1.45 x 10⁻⁴ Msi = 145 Psi
C = 1.8 x (F-32)

Also included in Table 1 is the "apparent modulus" that would be obtained from a simple tensile test of a single crystal bar oriented in each of the four primary orientations being used in this program. The apparent modulus is obtained through the following equation.

$$\text{"E"} = \left\{ S11 - \left[2(S11 - S12) - S44 \right] F \right\}^{-1}$$

$$\text{where} \quad F = \sin^2\alpha \, \cos^2\alpha + \frac{\sin^4\alpha \, \sin^2 2\beta}{4}$$

The angles α and β define the tensile direction as shown in Figure 5.
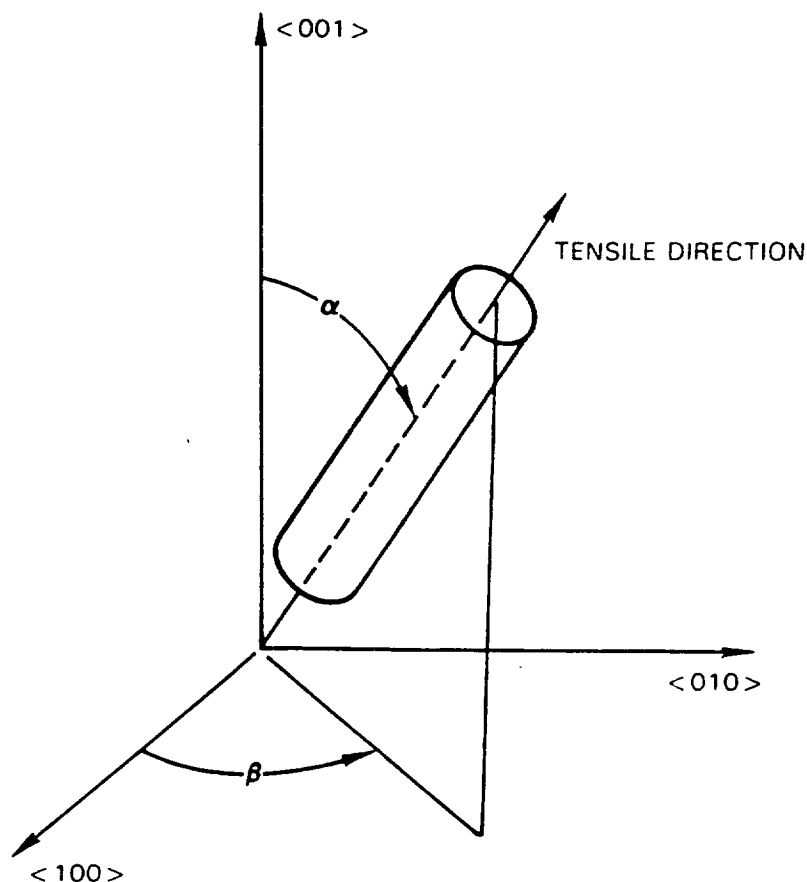
ANGLES α AND β DEFINE THE TENSILE DIRECTION

Figure 5   Definition of PWA 1480 Orientation Angles α and β

Ultrasonic wave velocity measurements were made using a Panametrics 5054 pulse-echo-overlap system with 1.27 cm (0.5 in.) diameter, 10 MHz Harisonic transducers. Both longitudinal and shear wave velocities were measured on an <001> primary orientation specimen while only shear wave velocities were taken on an <011> primary orientation specimen. The <001> specimen was machined from bar JB-160 and was 2.1 degrees from exact <001>. The <011> specimen was machined from bar KB-20 and was 0.9 degrees from exact <011>. Each specimen was finished machined to 1.27 cm (0.5 in.) diameter and a step was cut in the end of the bar 1.27 cm (0.5 in.) deep and approximately 60% through the diameter with the face of the step in a defined crystallographic direction. This step and the end of the specimen provided two reflecting surfaces for the ultrasonic waves. The orientation of the final step face and bar axis was confirmed by x-ray diffraction.

Figures 6 through 9 compare the apparent modulus obtained from "static" tensile testing to the apparent modulus from the dynamic constants. At higher temperatures and for certain orientations the "static" modulus is lower than the "dynamic" modulus. The orientation dependence appears to have at least some degree of correlation with the cube slip system shear stresses. The maximum resolved shear stresses and the number of slip systems with shear stresses within 10% of the maximum are given below.

Resolved Shear Stress (% of Applied Stress)

Tensile Direction	Octahedral Systems		Cube Systems	
	Maximum	# within 10%	Maximum	# within 10%
<001>	41%	8	0%	0
<213>	47%	1	46%	2
<011>	41%	4	35%	4
<111>	27%	6	47%	3

The dynamic elastic constants were used in the single crystal constitutive modeling effort.
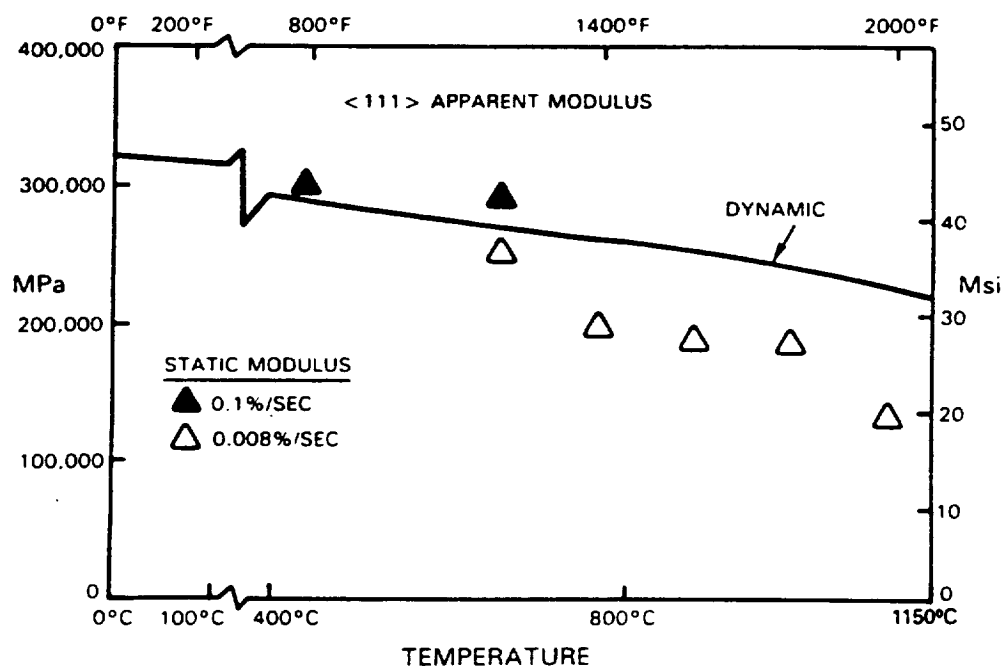
Figure 6   Comparison of <111> PWA 1480 Static and Dynamic Moduli

13
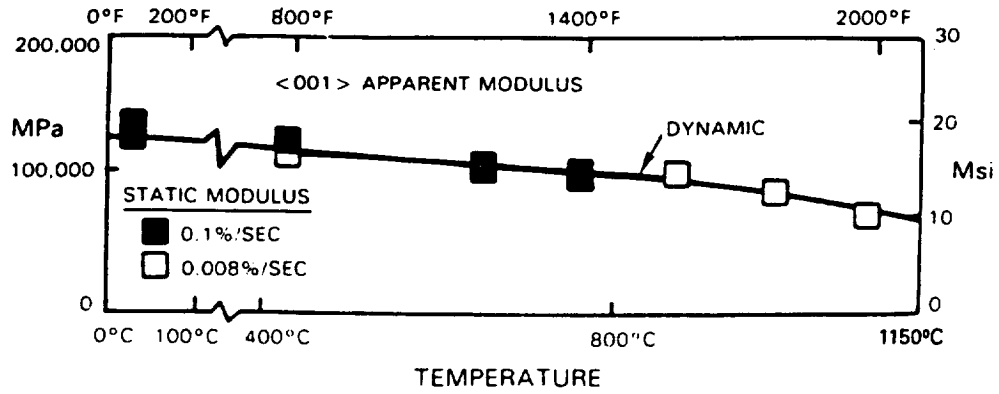
Figure 7   Comparison of <001> PWA 1480 Static and Dynamic Moduli
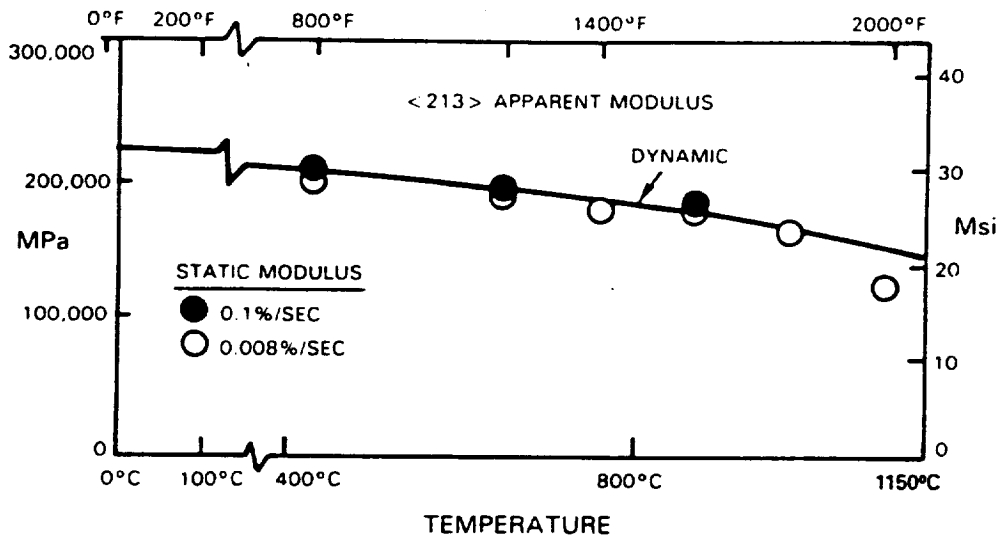
Figure 8   Comparison of <213> PWA 1480 Static and Dynamic Moduli
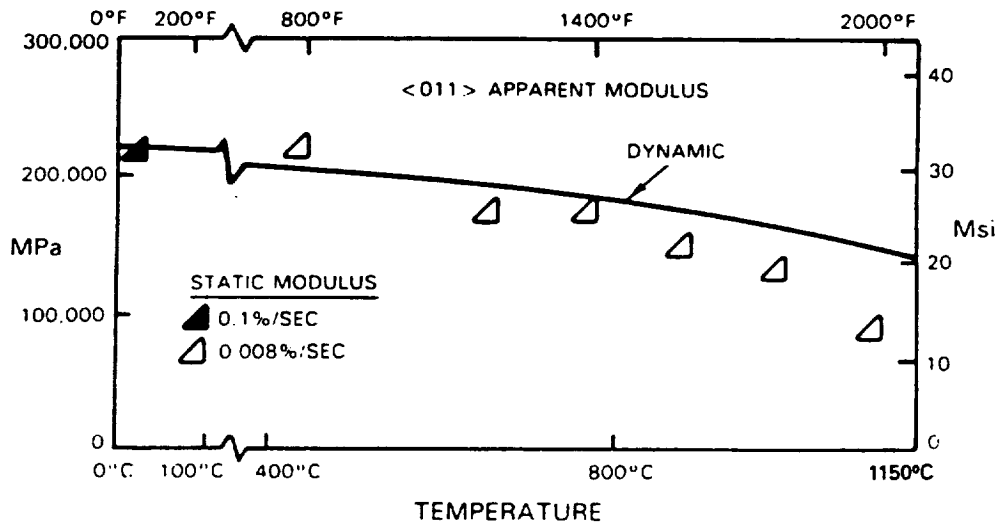
Figure 9   Comparison of <011> PWA 1480 Static and Dynamic Moduli

14

SECTION 4.0

TASK II – SELECTION OF CANDIDATE LIFE PREDICTION AND CONSTITUTIVE MODELS

4.1 SELECTION OF CONSTITUTIVE MODELS FOR COATINGS AND SINGLE CRYSTAL MATERIALS

Basic to life prediction for any structural component is the description of local stress-strain history. This necessitates availability of good constitutive models. As a gas turbine part is cycled through a wide range of stresses, strains, and temperatures, deformation and damage accumulate by a variety of mechanisms both in the single crystal alloy base material and the coating, all of which play a role in the component's ultimate failure. It is the goal of constitutive modeling to predict this stress-strain history so that the conditions at fatigue crack initiation are accurately known.

During the first year of this program, candidate constitutive models for the coatings and single crystal material were selected for evaluation (Reference 1). The selected models included:

1. Coatings

    a. Classical model (uncoupled plasticity and creep)
    b. Walker's model (unified viscoplastic)
    c. Simplified Walker's model (no equilibrium stress term)
    d. Moreno's Simplified Approach (hybrid model for Hastelloy X)
    e. Stowell equation (based on self-diffusion mechanism)

2. Single Crystal Material

    a. Classical Hill model (based on Von Mises yield function)
    b. Lee and Zaverl model (macroscopic viscoplastic model)
    c. Micromechanical Viscoplastic Formulation (extension of Walker's model to crystallographic deformation)

Detailed descriptions of these models and discussion of their selection are presented in Reference 1.

4.2 SELECTION OF LIFE PREDICTION MODELS

4.2.1 Literature Survey

In order to identify life prediction models which are applicable to coated anisotropic materials of gas turbine airfoils, a literature survey was conducted as part of the work reported in Reference 1. The survey resulted in an extensive listing of model concepts that have been used to match available data and meet specific needs of individual investigators.

Three broad classes of life models are available: phenomenological, cumulative damage, and crack growth.

A detailed discussion of individual model descriptions is presented in Appendix C of Reference 1.

4.2.2 Life Prediction Model Approach

Based on the literature survey, previous Pratt & Whitney experience, and specimen tests conducted under this program, it has been concluded that coatings have a role equally important with that of the base material in determining turbine airfoil crack initiation life. Coatings, applied to the airfoil surfaces to provide oxidation protection, were found to serve as primary crack initiation sites at relevant turbine operating conditions. Thus, coatings are a major determinant of cracking location and life. Base material cracks subsequently develop from a coating crack and propagate to failure.

Base material cracking underneath the coating can also be experienced on coated single crystal specimens. Base alloy initiated cracks typically occur when the base alloy is subjected to high stress levels and low strain levels such as generally happens under high temperature isothermal conditions for single crystal primary orientations which significantly deviate from <001>. Such orientations have high elastic modulus relative to <001> so that smaller strains introduce higher stresses. In some instances, coating cracks may be observed along with the base alloy initiated crack, but they do not influence the specimen's fatigue life.

The large variety of cracking modes that have been experienced on anisotropic material test specimens indicates that a complex life prediction approach is required to determine when such materials will fail due to fatigue. For coated surfaces, the approach must include the capability to account for coating cracking, coating affected cracking of the base alloy and crack propagation in the base alloy. Base material crack initiation is a competing failure mode to coating cracking and requires additional predictive capabilities. These include predicting crack initiation from three sources: macroscopic inelasticity, uncoated surface interaction with the environment, and microscopic defects (e.g., porosity).

The following overall life prediction approach is proposed:

$$Nf = Nc + Nsc + Nsp \qquad (1)$$

$$\text{or} \quad Nf = Nsi + Nsp, \text{ whichever is smaller,} \qquad (2)$$

where Nf = Total cycles to failure.

   Nc = Cycles to initiate a crack through the coating.

   Nsc = Cycles for coating crack to penetrate a small distance into the substrate (base alloy).

   Nsi = Cycles to initiate a substrate (base alloy) crack.

   Nsp = Cycles to propagate a substrate (base alloy) crack to failure.

In this program, crack initiation of coated nickel-based single crystal materials operating at relevant gas turbine airfoil conditions is addressed. As such, only the prediction of the cyclic life given by Nc and Nsc will be considered.

4.2.3 Candidate Life Prediction Models

Coating Life (Nc):

Coatings undergo substantial inelastic deformation during typical gas turbine engine operation and coating cracking appears strongly related to such deformation.

Two candidate models for coating cracking life prediction were selected for evaluation. These are the Coffin-Manson model which relates life to inelastic strain and an Ostergren hysteretic energy model. An important ingredient for these models is that terms may be added to account for environmental degradation of the coatings.

Coffin-Manson:

$$e_{inel} \cdot N^{B1} = C1 \tag{3}$$

Ostergren:

$$W_t \cdot N^{B2} = C2 \tag{4}$$

where
e_{inel} = inelastic strain range

W_t = tensile hysteretic energy

N = cracking life, including cycle frequency correction for environmental exposure

$B1, B2, C1, C2$ = material constants

Phenomenological models are particularly appropriate for coating life prediction because structural modeling and experimental capabilities for coatings significantly lag those for structural materials. Coating microstructure and composition change with time as the coating is exposed to the severe turbine operating environment. As a result, the coating properties which affect coating fatigue life, such as thermal expansion, ductility, and creep resistance, are altered. To accommodate such behavior, complex life prediction models typically require material property information documenting the change in each coating property. Obtaining such information is beyond the current capabilities of specimen fabrication and experimentation for coatings. Thus, simple models which are able to include environmental effects were chosen for this program.

Single Crystal Life (Nsc):

In order to extend isotropic material life prediction models to anisotropic materials such as single crystals, a method to account for material orientation effects is required. Similar to the methods for single crystal constitutive modeling, both macroscopic and micromechanical approaches are possible. The macroscopic approach describes anisotropy effects in terms of bulk material properties and observed loading response. The use of this approach generally assumes that the initiating crack orientation is known, usually normal to the applied load direction. The micromechanical approach utilizes material deformations at the slip level. Applied strains are resolved into components along the individual slip directions which depend on the material orientation. Fatigue life can than be related to the resulting slip plane stresses and strains.

Based on previous Pratt & Whitney experience and the fatigue data generated in this program, coated single crystal material initiates cracks normal to the loading direction. Crystallographic fatigue crack initiation, which would necessitate a micromechanical based model, was not observed for relevant gas turbine cyclic loading conditions. As a result, macroscopic based models were considered a good starting point from which to develop a single crystal life model.

At least one representative model from each class (phenomenological, cumulative damage, and crack growth) was selected for evaluation.

   1.   Coffin-Manson
   2.   Modified Strain Model
   3.   Hysteretic Energy Approach
   4.   Cyclic Damage Accumulation (CDA)
   5.   Crack Tip Opening Displacement (CTOD)

Other models may be also be evaluated depending on the observed fatigue life trends.

The Coffin-Manson model formulation (see the section on Coating Life models) was chosen based on the qualitative observation from the isothermal constitutive behavior tests. In those tests, a reasonable approximation of the remaining "cyclic" life was determined by summing the inelastic strain range from each cycle and comparing that quantity to the available tensile elongation ductility obtained from monotonic tensile tests.

The modified strain model has been successfully used at Pratt & Whitney to correlate thermomechanical fatigue (TMF) life of coated PWA 1480 for out-of-phase strain-temperature test conditions. The model relates fatigue life to the product of strain range and elastic modulus.

18

$$Nsc = A \cdot (E \cdot e_{range})^{-B} \qquad (5)$$

where: e_{range} = mechanical strain range (elastic and inelastic)

E = elastic modulus along the loading direction

A, B = material constants

A hysteretic energy approach was used by DeLuca and Cowles (Reference 3) and further developed by Heine, Warren, and Cowles (Reference 4) to correlate 50% specimen load drop TMF life of PWA 1480.

$$Nsc = A \cdot W_{eff}^{-B} \qquad (6)$$

where:
$$W_{eff} = S_t \cdot e_{inel} \cdot (dS_{\langle 111 \rangle} / E) \qquad (7)$$

S_t = maximum tensile stress

e_{inel} = inelastic strain range

$dS_{\langle 111 \rangle}$ = maximum normal octahedral slip plane stress range

E = elastic modulus along loading direction

A, B = material constants

The CDA model is currently under development for isotropic Ni-based superalloy materials in a companion contract, NAS3-23288 (References 5 and 6). Its formulation is based on the notions that 1) absolute levels of damage are difficult to calculate, thus the damage should be ratioed to a reference fatigue condition and 2) the fatigue capability of a material is intimately tied to its available ductility which is exhausted on a cycle by cycle basis. The CDA model formulation used for PWA 1480 single crystal material is given in Reference 6, section 7.5.2:

$$N_{SC} = \int_0^1 \left[\frac{\overline{\epsilon}_p}{\left(\left.\dfrac{dD}{dN}\right]_{Ref}\right) F(\sigma_t,\, \Delta\sigma)} \right] G\left(\frac{N}{N_{SC}}\right) df_\epsilon \tag{8}$$

where
$$F(\sigma_t, \Delta\sigma) = \left(\frac{\sigma_t}{\sigma_{tRef}}\right) \left(\frac{\Delta_\sigma}{\Delta\sigma_{Ref}}\right) + \left[\left(\frac{\Delta\sigma_{Ref}}{\Delta\sigma}\right)\left(\frac{\sigma_t}{\sigma_{tRef}}\right)\right]^{B^1} \left[\left(\frac{t}{t_{Ref}}\right)^{C^1} - 1\right] \tag{9}$$

$$G\left(\frac{N}{N_{SC}}\right) = (1-LF)(M+1)\left[1 - \left(\frac{N}{N_{SC}}\right)\right]^m + LF \tag{10}$$

$$\left.\frac{dD}{dN}\right]_{Ref} = A\, \Delta\epsilon^{B} \tag{11}$$

The CTOD model was chosen based on the notion that coating crack propagation into the single crystal substrate is controlled by conventional linear elastic crack growth mechanisms. The isotropic form of CTOD was chosen to simplify the analysis.

$$N_{SC} = A\, (\text{CTOD})^{-B} \tag{12}$$

where:
$$\text{CTOD} = (K_I^2) / (E \cdot S_y) \tag{13}$$

K_I = mode I stress intensity factor

E = elastic modulus along the loading direction

S_y = yield stress

A, B = material constants

20

SECTION 5.0

TASK III - LEVEL I EXPERIMENTS

5.1 COATING CONSTITUTIVE TESTS

Cyclic stress relaxation tests were conducted to determine the constitutive behavior for the coating systems selected in this program. A typical test cycle is presented in Figure 10.

CYCLIC RELAXATION TEST

IS MIN STRAIN HOLD

STRESS

5 MIN STRAIN HOLD

$\Delta\epsilon_3$

STRAIN

RECORD STRESS, STRAIN, TIME

CYCLE	STRAIN INCREMENT
1	.1%
2	.2
3	.3
4	.4
5	.6
6	.8
7	1.0
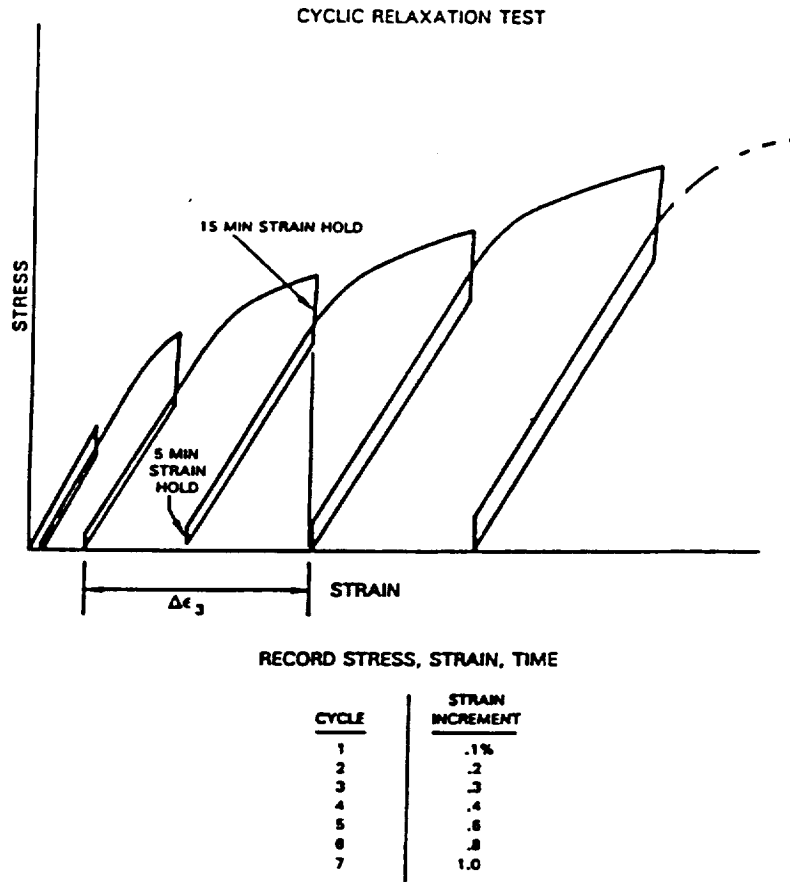
Figure 10   Representative Stress Relaxation Test Used to Obtain Coating Behavior

In order to obtain data from coating specimens, significant development of testing techniques was required, including rig control improvements and extensometry development. Manual specimen loading was not adequate for maintaining constant strain rates. Also, maintaining constant strain hold periods during stress relaxation was difficult. For these reasons, computer controls were installed, making use of a test software package developed in a separate Pratt & Whitney program. Another concern was the method for obtaining deflection measurements from the PWA 273 specimens. Such a thin specimen could not support the extensometer hardware. Two externally supported extensometry setups were subsequently developed in another Pratt & Whitney program. The first extensometer concentrated on minimizing the extensometer loads on the specimen and resulted in the counter-balanced lever type extensometer shown in

21

Figure 11. This extensometer was successfully used to gather data on the 0.25 mm (0.010 in.) thick specimens up to roughly 982°C (1800°F). Unfortunately, at higher temperatures (or low loads), this extensometer tended to produce an irregular response due to motion at the pivot points. In the second extensometer setup, the pivot points were eliminated and the deflections were measured directly using an MTS extensometer (Figure 12). Specially designed double quartz rods were used to balance side forces on the specimen normally caused by the spring loaded extensometer rods.
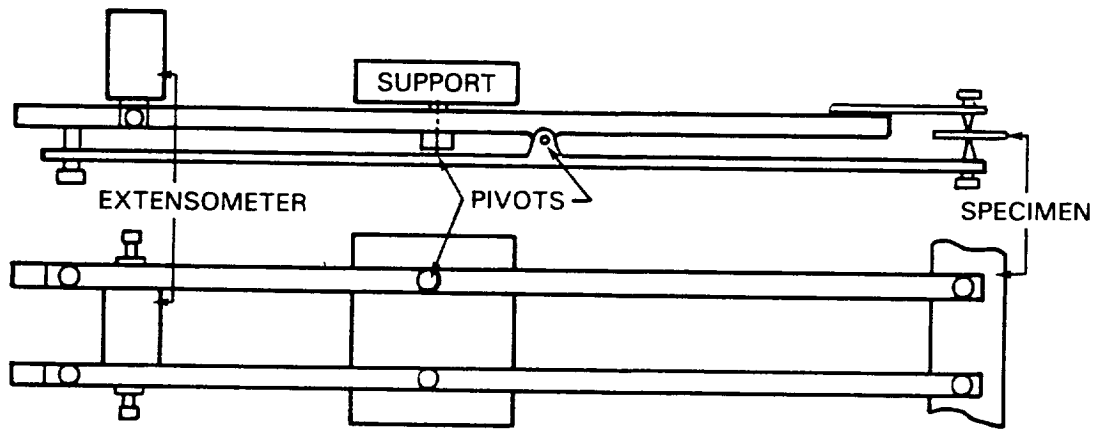
Figure 11 Schematic of Extensometer Arrangement Used to Obtain Deflection Data From Initial 0.25 mm (0.01 in.) Thick Aluminide Coating Constitutive Specimens
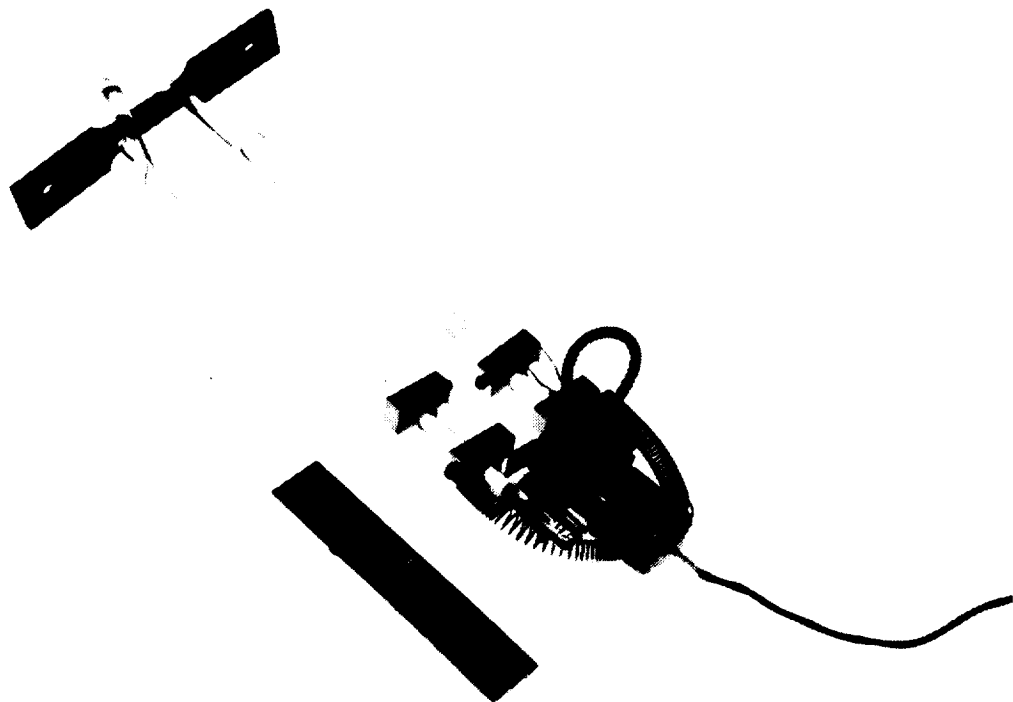
Figure 12 Extensometer Setup Used to Obtain Deflection Data From 0.13 mm (0.005 in.) and High Temperature 0.25 mm (0.01 in.) Aluminide Coating Constitutive Specimens

22

PWA 286 overlay coating constitutive tests were completed previously and reported in References 1 and 2.

Testing of PWA 273 aluminide coating to determine constitutive properties was completed during this period. Tested specimens were either 0.25 mm (0.010 in.) or 0.13 mm (0.005 in.) thick PWA 1480 strips coated on both sides with PWA 273 coating. Two thicknesses were tested so that the effective coating behavior may be estimated by extrapolating constitutive model constants (obtained at each thickness) to zero substrate thickness. A summary of test conditions is given in Table 2.

TABLE 2

SUMMARY OF PWA 273 ALUMINIDE COATING
CONSTITUTIVE TESTS

Spec ID	Nom. Gage Thickness mm (in)	Temperature °C (°F)
55-2 Uncoated	0.13 (0.005)	427 (800)
78-2	0.25 (0.010)	" "
78-3	0.25 (0.010)	593 (1100)
53-3	0.25 (0.010)	649 (1200)
75-2	0.25 (0.010)	760 (1400)
75-4	" "	" "
55-1	0.13 (0.005)	816 (1500)
75-3	0.25 (0.010)	" "
55-3	0.13 (0.005)	871 (1600)
53-1	" "	" "
53-4	0.25 (0.010)	" "
56-2	0.13 (0.005)	927 (1700)
07-4	0.25 (0.010)	" "
56-3	0.13 (0.005)	982 (1800)
75-1	0.25 (0.010)	" "
07-3	" "	" "
56-4	0.13 (0.005)	1038 (1900)
55-4	0.13 (0.005)	1093 (2000)
01-4	0.25 (0.010)	" "
01-1 Uncoated	" "	" "

23

5.2 SINGLE CRYSTAL CONSTITUTIVE TESTS

Five cyclic constitutive tests were conducted to supplement the constitutive behavior database for PWA 1480. These tests were designed to extend the temperature range available for the constitutive modeling effort up to 1149°C (2100°F) which corresponds to the highest temperature used in the fatigue tests.

5.3 SINGLE CRYSTAL FATIGUE TESTS

5.3.1 Test Facility

The test facility used for isothermal and thermomechanical fatigue (TMF) tests consists of a servo-controlled, closed loop hydraulic testing machine with MTS controllers, a low frequency (10 kHz) 20 kW TOCCO induction heater, and an Ircon model 7000 radiation pyrometer, calibrated over a temperature range of 260°C to 1371°C (500°F to 2500°F), for temperature measurement. Induction heating was selected to accommodate MTS external extensometry and to provide adequate heating rates. The quartz rods of the MTS extensometer, which define a 2.54 cm (1.0 in.) gage section, are spring loaded against the specimen and did not show any signs of slippage during testing. A typical test setup is illustrated in Figures 13 and 14.
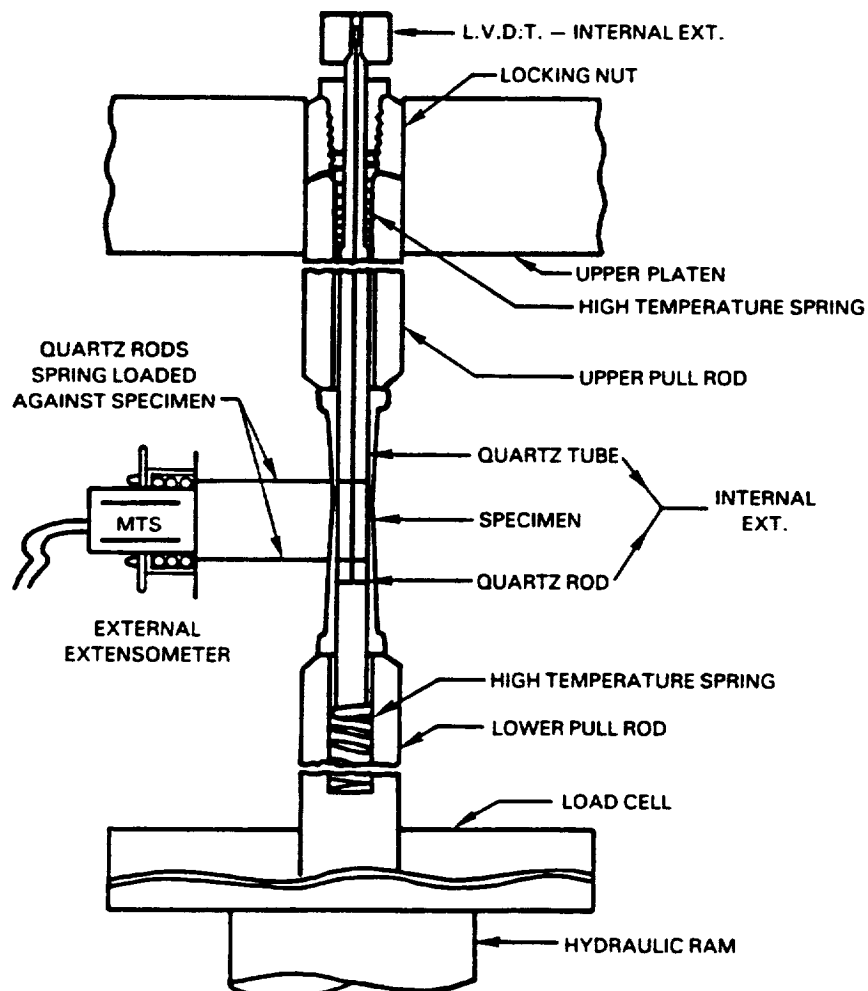
Figure 13 Extensometry Setup for Fatigue Testing

24
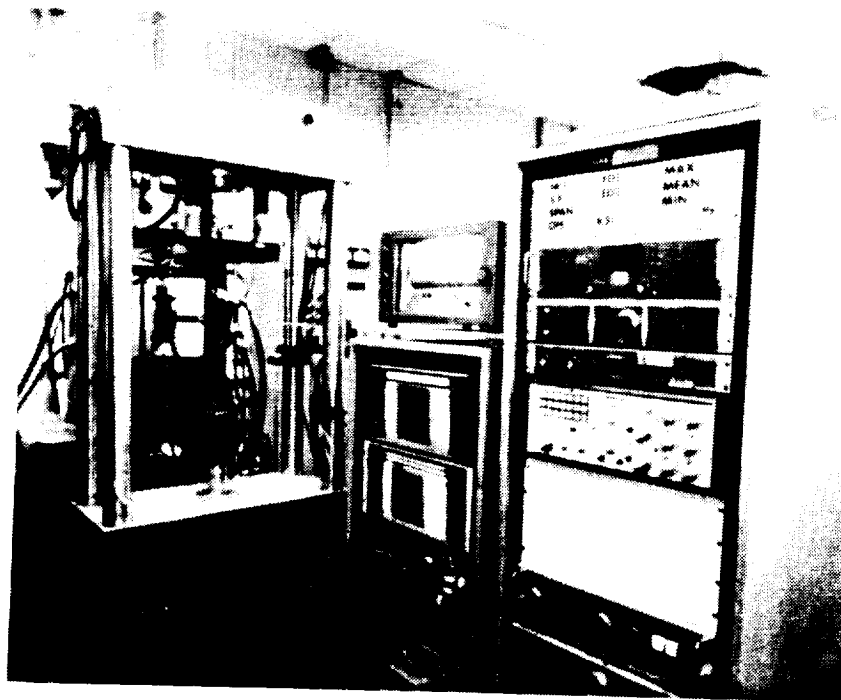
Figure 14   Thermomechanical Fatigue Test Rig

The internal and external extensometer setup shown in Figure 13 was used during initial fatigue tests to compare the two extensometers and gain experience with the external extensometer. The external extensometer was proven to provide better deflection measurements and was chosen as the sole deflection measurement device. A summary of the internal and external comparison study is given in Reference 2.

5.3.2 Fatigue Tests

Isothermal fatigue and TMF tests were conducted to define crack initiation life of coated PWA 1480 single crystal material and to provide data for initial life prediction model evaluations. All fatigue tests used the specimen geometry shown in Figures 1A or 1B. The latter design (denoted as 73C) relied on an MTS extensometer for deflection measurement. Where necessary, the recorded deflections obtained from the internal extensometer in the 44C design were corrected by 2-D finite element analysis to be consistent with the MTS extensometry.

25

Level I tests were limited to key variables considered relevant to creep-fatigue life prediction. The variables included crystallographic orientation, coating, strain range, mean strain, strain rate, strain hold periods, and temperature. Tests were conducted using strain controlled conditions. A summary of Level I fatigue lives and specimen responses is presented in Appendices A and B.

The onset of coating cracking and crack propagation was monitored during each test by taking a series of acetate film surface replicas. Metallographic inspection of the tested specimens was performed at the conclusion of each test in order to interpret the replica data, characterize cracking patterns, and identify crack initiation sites. Specimen load, strain, and temperature histories were monitored during the course of testing to provide information useful for the modeling efforts.

In general, both PWA 286 overlay and PWA 273 diffusion aluminide coated specimens were found to develop coating cracks substantially before specimen failure. Subsequent metallographic inspection of failed specimens indicated that, in many specimens, the coating cracks had progressed into the PWA 1480 substrate and directly caused failure. However, in other specimens, the coating cracks did not extend into the PWA 1480 substrate, and the failure resulted from a competing crack which had initiated near to, or at, the uncoated ID of the specimen. In all cases, PWA 273 aluminide coating initiated cracks propagated into the PWA 1480 substrate. PWA 286 overlay coated specimens, however, did not propagate coating cracks into the PWA 1480 when the specimen was subjected to tensile stresses at high temperatures (1038°C isothermal or in-phase TMF). In such instances, ID cracks caused specimen failure, even though the overlay coating cracks developed early in the isothermal tests. Overlay coating cracks propagated into the PWA 1480 during low temperature isothermal LCF or out-of-phase TMF tests. Representative coating crack microphotographs are presented in Figure 15. In some other coated specimens, principly the <111> PWA 1480 coated specimens, subsurface crack initiation was observed.

Typical isothermal and TMF specimen hysteresis loops and representative dislocation networks produced during TMF are presented in Reference 2.

26

(A)   JB-6   A385
                                      100X

(B)   JB-9   A400
                                      100X

(C)   JB-39   250X
             LONGITUDINAL   A281

(D)   JB-81   A366
                                      100X
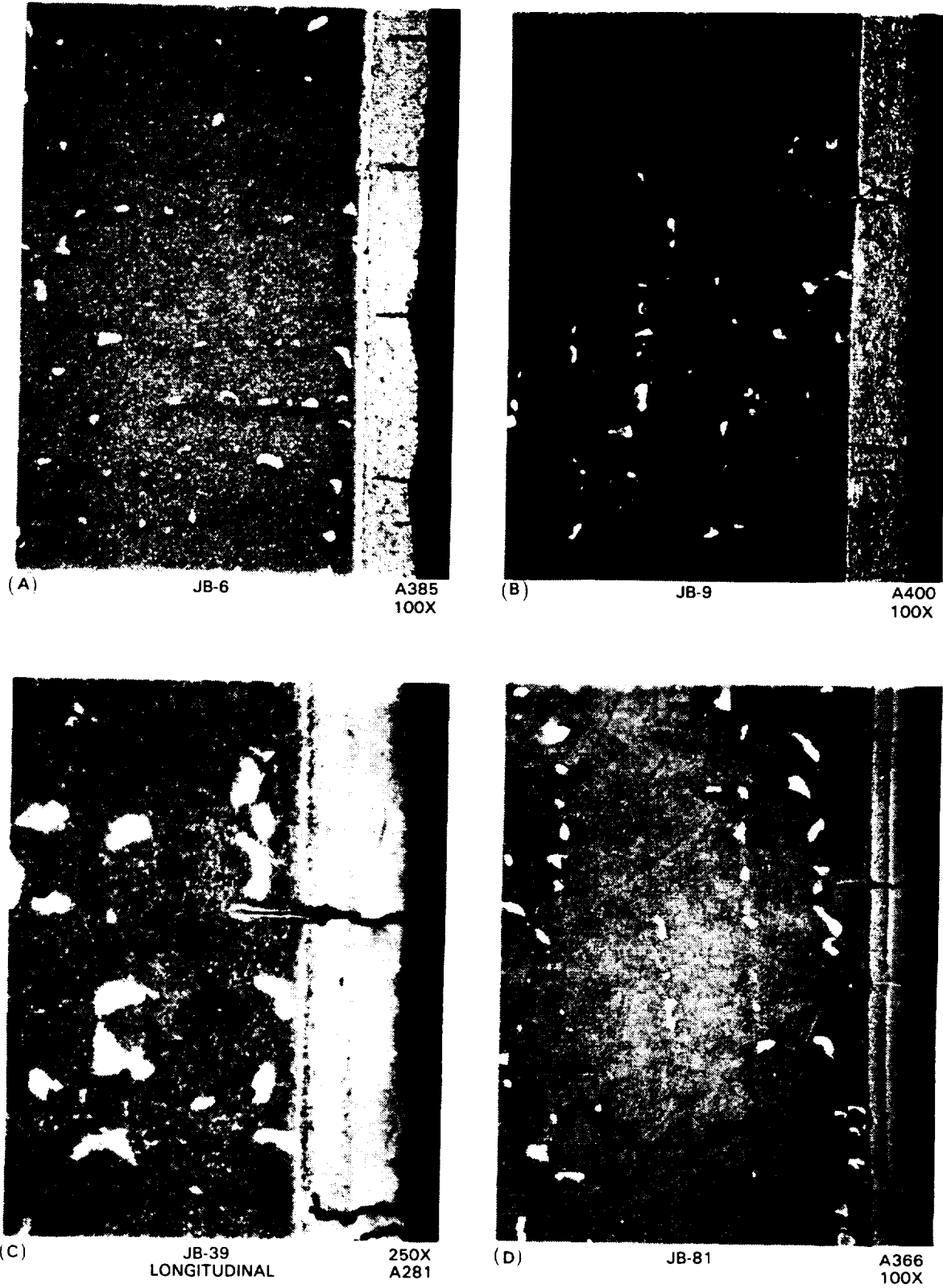
Figure 15   Representative Coating Cracks: (A) PWA 286, 1038°C (1900°F) LCF;
             (B) PWA 286, 427°C to 1038°C (900°F to 1900°F) Out-of-Phase TMF;
             (C) PWA 273, 1038°C (1900°F) LCF; and (D) PWA 273, 427°C to 1038°C
             (800°F to 1900°F) TMF

27

To bookkeep all the observed crack initiation modes, the following nomenclature was adopted for identifying where the crack which led to specimen failure had initiated:

          c   = Coating
          cs = Coating diffusion zone
          sc = Coating-substrate interfacial region
          s   = Substrate (subsurface)
          ID = Uncoated ID surface of the specimen
          IDc = Uncoated ID surface of the specimen; coating cracks
                observed along the OD surface
          IDs = Substrate (subsurface) initiation near the uncoated ID
                surface
          d   = Test discontinued with no observed cracks
          dc = Test discontinued with coating cracks observed along
                the OD surface
          dcs = Test discontinued with cracks along the OD surface
                which initiated at the coating diffusion zone
          dsc = Test discontinued with cracks along the OD surface
                which initiated at the coating-substrate interfacial
                region

Examples of c, cs, sc, and s failure modes are presented in Figures 16 to 19.
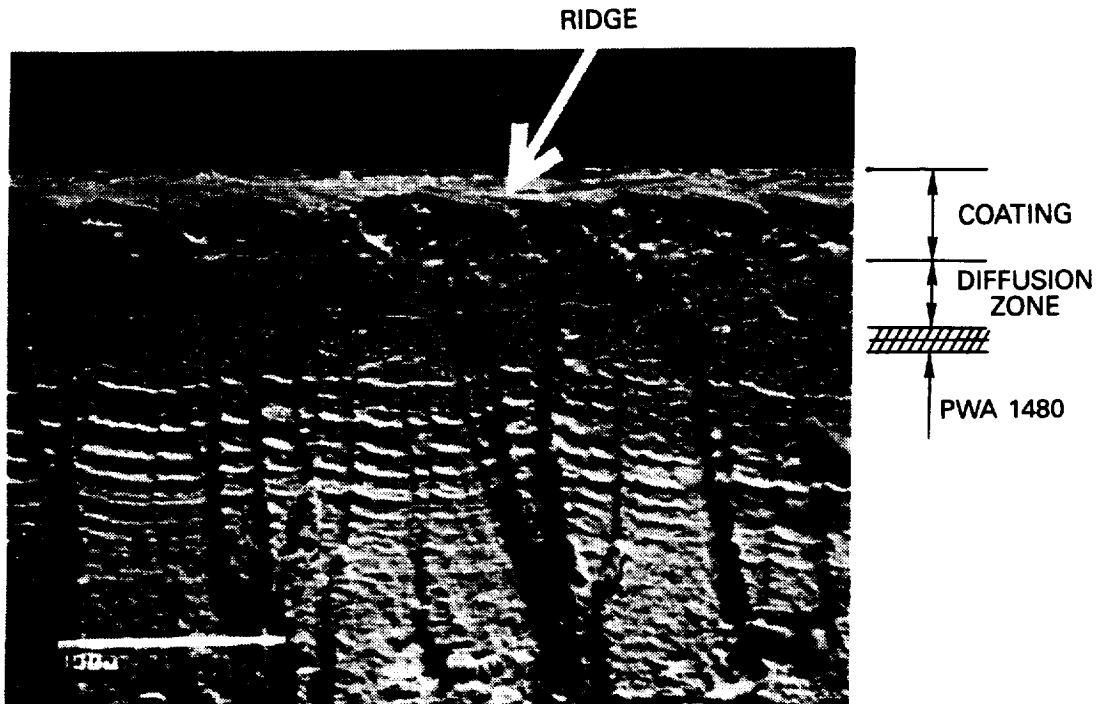
RIDGE

Figure 16   Backscatter Electron Image of Primary Crack Initiation Region In
             Specimen MB-1 After Fatigue Testing at 427-1038°C (800-1900°F),
             ±0.2%, 1 cpm, Out-of-Phase for 749 Cycles. Initiation occurred at
             ridge inside coating layer. Failure mode = "C".
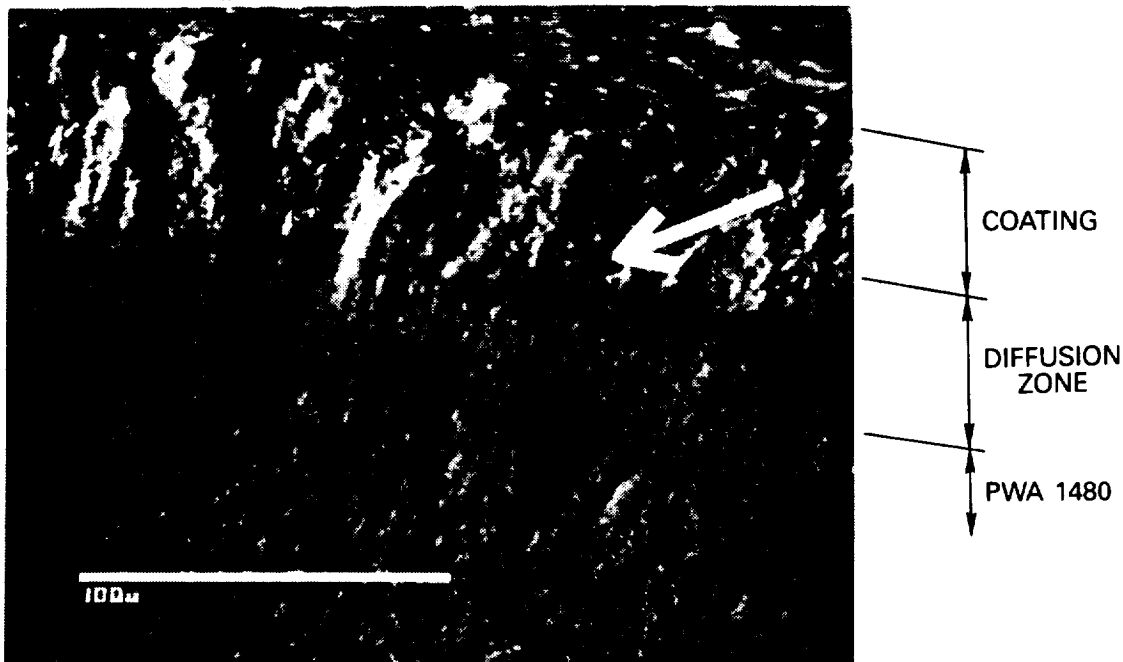
Figure 17   Backscatter Electron Image of Primary Crack Initiation Region In
Specimen MB-21 After Fatigue Testing at 927°C (1700°F), +0.25%, 10
cpm for 11648 cycles. Arrow indicates initiation site. Failure mode
= "CS".
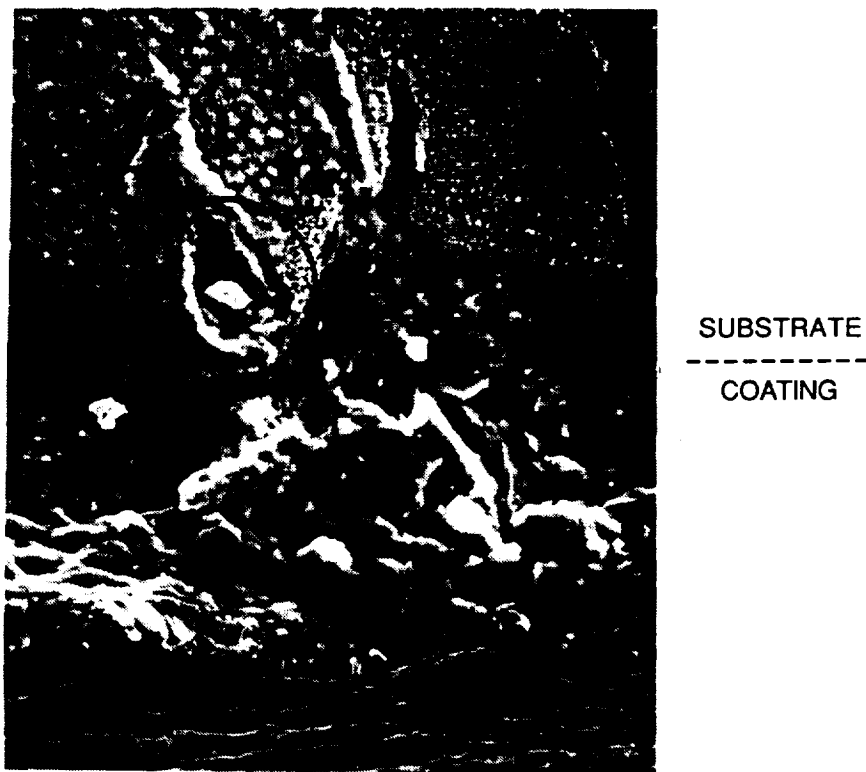
500X

Figure 18   Secondary Electron Image of Primary OD Surface Crack In Specimen
LB-156 After Fatigue Testing at 427-1038°C (800-1900°F), +0.15%, 1
cpm, Clockwise Baseball Cycle for 1639 Cycles. Initiation occurred
at coating-substrate interfacial region. Failure mode = "SC".

29
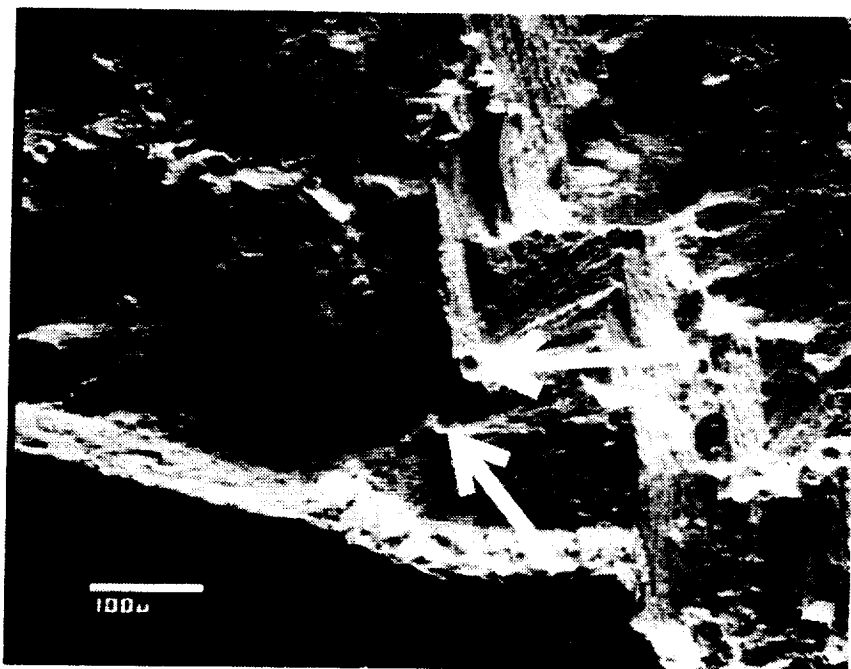
Figure 19   Backscatter Electron Image of Primary Crack Initiation Region In Specimen LB-180 After Fatigue Testing at 927°C (1700°F), +0.25%, 10 cpm for 3941 Cycles. Arrows indicate porosity initiation sites in PWA 1480. Failure mode = "S".

Level I tests indicated that creep-fatigue life is dependent on several factors: 1) the presence of a coating, 2) the coating composition and microstructure, 3) single crystal orientation, and 4) the cyclic strain-temperature-time relationship (i.e., the cyclic loading history). And, of those variables encompassed by cyclic loading history, mean strain appeared to be the least significant. Observations made during the Level I experiments reinforced the need for constitutive and life models for coating materials and verified the chosen life approach (Section 4.2.2).

Two critical experiments are noteworthy. The first experiment investigated the importance of cyclic load history, and the second studied the effect of thermal cycling on coated TMF life.

PWA 273 aluminide coated <111> PWA 1480 specimens LB-21 and LB-156 were TMF tested using the "baseball" cycle shown in Figure 20. The only difference in test conditions between the two specimens was that specimen LB-21 was cycled in a counter-clockwise (ccw) direction whereas LB-156 was cycled in a clockwise (cw) direction. Stabilized hysteresis loops for both specimens are presented in Figures 21 and 22. Though the same strain-temperature cycle was used in both tests, the crack initiation and failure lives of the two specimens varied significantly. Specimen LB-156 (cw cycle) crack initiation and failure lives were 370-510 and 1639 cycles while the lives for specimen LB-21 were 5200-6500 and 6689 cycles. Cyclic history was thus shown to have a strong effect on fatigue life.
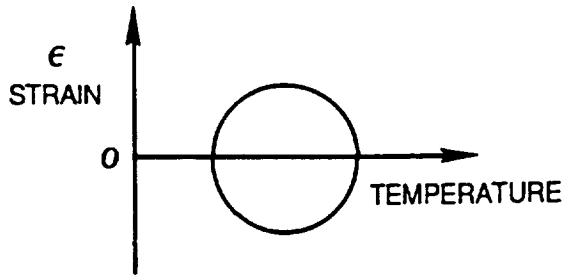
Figure 20 Schematic of Mechanical Strain Vs. Temperature Cycle Used In TMF Testing of Specimens LB-21 and LB-156. This cycle type is called a "baseball" cycle.

1 KSI = 6.895 MPa
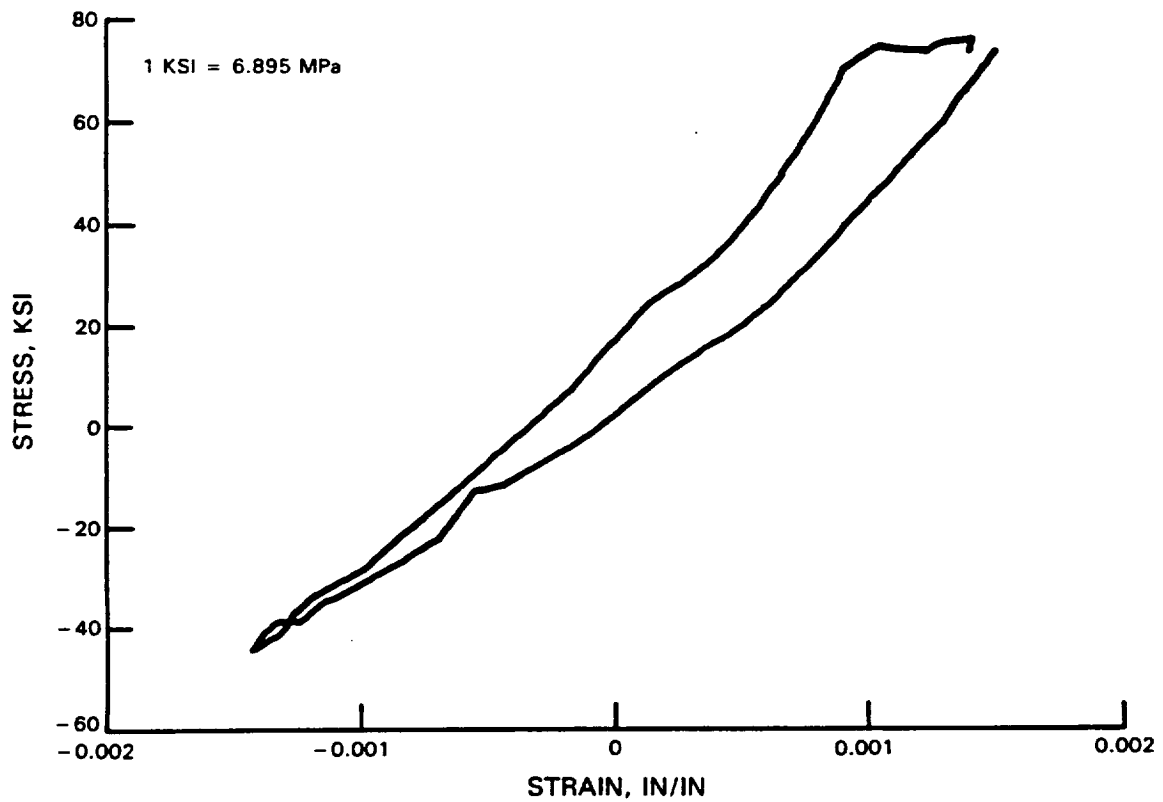
Figure 21 Stress Vs. Mechanical Strain Response of Specimen LB-156 – Clockwise "Baseball" TMF Cycle

31
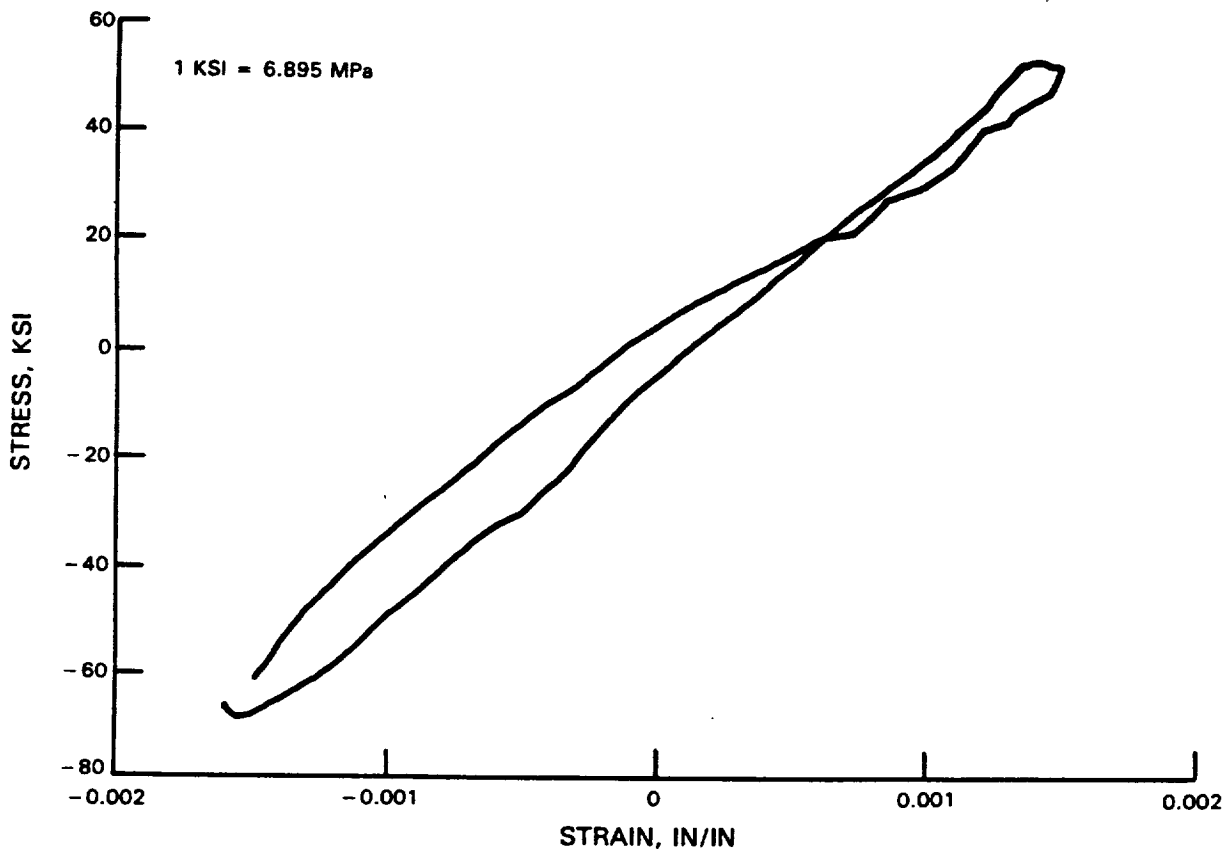
Figure 22   Stress Vs. Mechanical Strain Response of Specimen LB-21 -
Counter-Clockwise "Baseball" TMF Cycle

PWA 286 overlay coated <001> PWA 1480 specimens JB-102 and JB-104 established
the dominant role coatings play in fatigue crack initiation. Specimen JB-102
was isothermally fatigued at 427°C (800°F), +0.3% strain at 8 cpm. Specimen
JB-104 was subjected to +0.3% strain at virtually the same temperature, but
was also subjected to a thermal cycle up to 1038°C (1900°F) at zero strain
(this TMF cycle is referred to as a T-cycle). The associated crack initiation
and failure lives of these two specimens were >41578 and >41578 for JB-102 and
6000 and 6032 for JB-104. Testing of specimen JB-102 was discontinued after
41578 cycles with no observed cracks in the gage section. The imposed thermal
cycle dramatically reduced the fatigue lives. A comparison of specimen
hysteresis loops from JB-102 and JB-104 gave no indication that the lives
would be different. In fact, the hysteresis loops were identical. However,
one-dimensional, two-bar analysis of the T-cycle clearly shows why temperature
cycling is "damaging" to the coating. Due to its thermal growth and stress
relaxation properties, the coating produced higher tensile stress and
inelastic flow when temperature was cycled. Coating hysteresis loops for the
427°C (800°F) isothermal test and the T-cycle TMF test are presented in Figure
23 and a schematic of the two-bar analysis technique is presented in Figure 24.

32
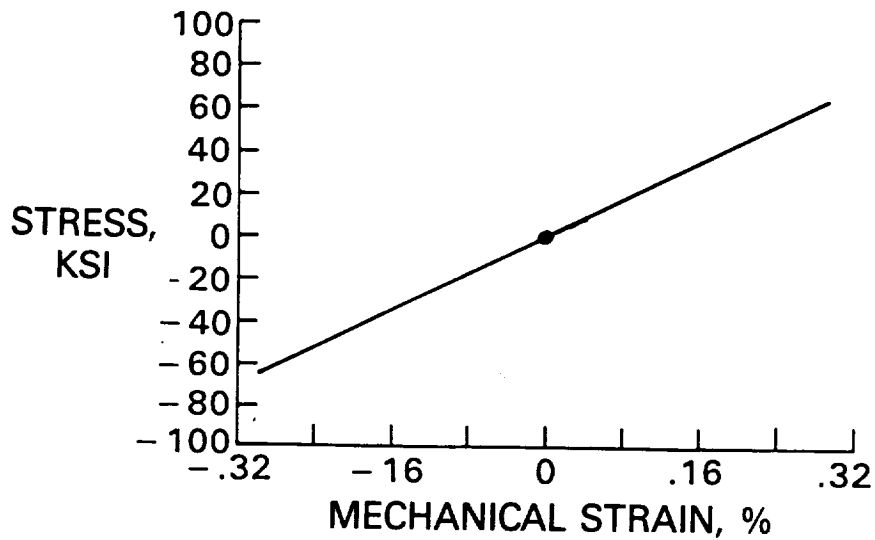
(A)
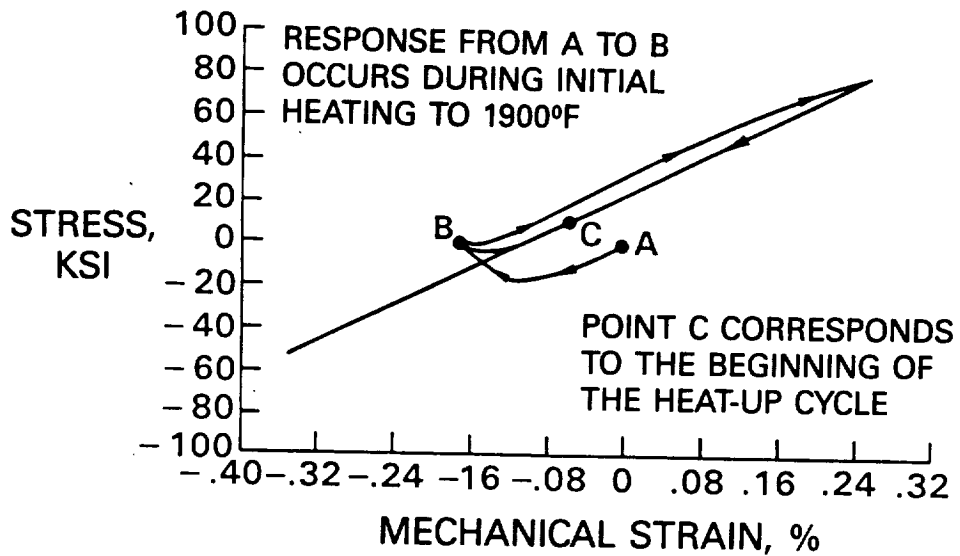
(B)

Figure 23   Two-Bar Mechanism Simulation of PWA 286 Overlay Coating During: a)
Isothermal Testing at 427°C (800°F), +0.3%, 8 cpm. B) T-cycle TMF
testing at 427-1038°C (800-1900°F), +0.3%, 0.5 cpm.

33

P(t)

$P_c + P_s = P(t)$

$\delta_c = \delta_s$

COATING

SUBSTRATE
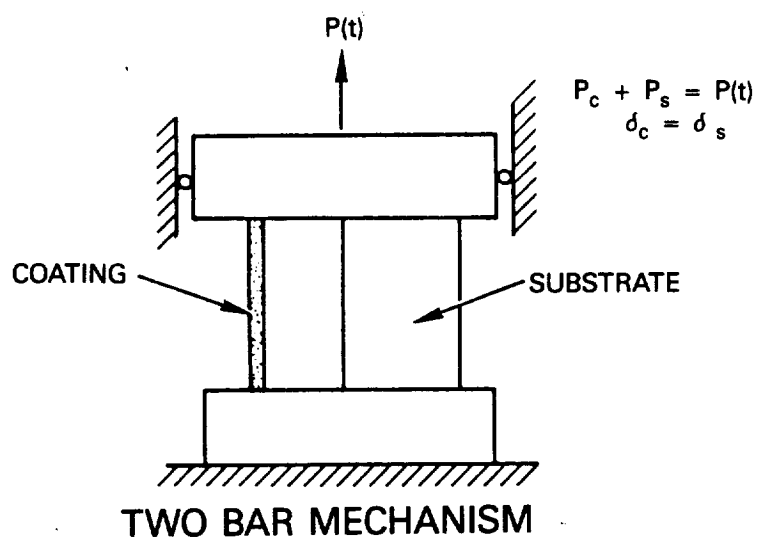
TWO BAR MECHANISM

Figure 24   Schematic of the Two Bar Mechanism

SECTION 6.0

TASK IV - CORRELATION OF MODELS WITH LEVEL I EXPERIMENTS

6.1 COATING CONSTITUTIVE MODEL

From previous Pratt & Whitney experience and the Level I fatigue experiments, it was clear that coatings play a major role in the crack initiation life of coated single crystal material (Nc + Nsc). As such, coating constitutive models are needed to predict the coating behavior.

To streamline the coating constitutive model development process, the overlay coating (PWA 286) was chosen as the model development vehicle. The final overlay coating model formulation may then be applied to the aluminide diffusion coating (PWA 273).

6.1.1 PWA 286 Overlay Coating

The results from the evaluation of the four candidate constitutive models (see Section 4.1) were presented in Reference 2. Based on that effort, two models were selected for further development: Moreno's Simplified Approach (Reference 7) and Walker's Unified Viscoplastic Formulation developed for Hastelloy X (Reference 8).

Final coating constitutive model selection was based on the second series of overlay coating stress relaxation experiments conducted at the United Technologies Research Center (UTRC) and reported in Reference 2. The results of these experiments were considered superior to the first series of tests which were reported in Reference 1. However, the data used at 427°C (800°F) was from the first series of experiments, not the second, because the second series specimen at 427°C (800°F) broke at the specimen grip before any inelastic activity was observed.

The Walker model utilized in the analysis, presented in one-dimensional form below, was the differential form of the Hastelloy X model discussed in Reference 8.

$$e = sig/E + e_{in} \tag{14}$$

$$\dot{e}_{in} = ((sig-omega)/K) ** n \tag{15}$$

$$K = K1 - K2*exp(-n7*R) \tag{16}$$

$$\dot{omega} = (n1+n2)*\dot{e}_{in} + e_{in}* \frac{dn1}{dT} * \dot{T} - (omega-omega0-n1*e_{in})*(\dot{G} - \frac{dn2}{n2*dT} * \dot{T}) \tag{17}$$

$$\dot{G} = (n3+n4*exp(-n5*R)) * \dot{R} + n6*(omega) ** (m-1) \tag{18}$$

35

$$\dot{R} = abs(\dot{e}_{in})$$ (19)

Material constants: E,omega0,n,m,n1,n2,n3,n4,n5,n6,n7,K1,K2,
depend on temperature, T.

Interpolation and extrapolation of model constants was performed to produce consistent tensile behavior throughout a 427-1204°C (800-2200°F) temperature range. A summary of regressed Walker model constants for unexposed, bulk HIP PWA 286 overlay coating is presented in Table 3.

TABLE 3   6.895 kPa = 1 psi

SUMMARY OF WALKER AND MORENO CONSTITUTIVE MODEL REGRESSED
TEMPERATURE DEPENDENT CONSTANTS FOR UNEXPOSED, BULK HIP PWA 286

	427°C (800°F)	538°C (1000°F)	649°C (1200°F)	760°C (1400°F)	871°C (1600°F)	1093°C (2000°F)
E, psi	0.2180E8	0.2133E8	0.1902E8	0.1550E8	0.9502E7	0.1500E7

WALKER

	427°C (800°F)	538°C (1000°F)	649°C (1200°F)	760°C (1400°F)	871°C (1600°F)	1093°C (2000°F)
n	0.5143E2	0.2070E2	0.3300E1	0.2130E1	0.1705E1	0.1345E1
n1, psi	0.	0.	0.	0.	0.	0.
n2, psi	0.3130E8	0.3130E8	0.3017E8	0.1334E8	0.3467E7	0.7292E5
n3	0.5000E3	0.7000E3	0.9000E3	0.1000E4	0.8786E3	0.2516E3
n4	0.	0.	0.	0.	0.	0.
n5	0.	0.	0.	0.	0.	0.
n6	0.1488E-8	0.3162E-7	0.3162E-6	0.1110E-5	0.2109E-5	0.3437E-5
n7	0.	0.	0.	0.	0.	0.
K1, psi	0.9548E5	0.1240E6	0.1253E7	0.2488E7	0.1543E7	0.3950E6
K2, psi	0.	0.	0.	0.	0.	0.
m	0.1200E1	0.1320E1	0.1492E1	0.1788E1	0.2042E1	0.2202E1
omega0, psi	0.	0.	0.	0.	0.	0.

MORENO

	427°C (800°F)	538°C (1000°F)	649°C (1200°F)	760°C (1400°F)	871°C (1600°F)	1093°C (2000°F)
n	0.5143E2	0.2070E2	0.3300E1	0.2130E1	0.1705E1	0.1345E1
K, psi	0.1600E6	0.1971E6	0.3230E7	0.3765E7	0.2080E7	0.5077E6
Sy, psi	0.1150E6	0.1047E6	0.9000E5	0.4680E5	0.1700E5	0.9770E3
Ep, psi	0.1700E7	0.1606E7	0.4863E6	0.4786E5	0.2240E4	0.1000E1

The Moreno model was a modified version of the model presented in Reference 7. Instead of using a set of rules to determine back stress, a simple continuously evolving back stress formulation was used. The set of equations describing the Moreno model utilized in this analysis is presented below:

If sig - omega $\geq$ Sy   and $\dot{T} \leq 0$; $\dot{sig} = Ep * \dot{e}$ (20)

36

$$e_{in} = e - sig/E \qquad (21)$$

If $sig - omega \geq Sy$ and $\dot{T} > 0$; $\dot{sig} = \dot{Sy}$ $\qquad (22)$

$$e_{in} = e - sig/E \qquad (23)$$

If $sig - omega < Sy$; $sig = E * (e - e_{in})$ $\qquad (24)$

$$\dot{e}_{in} = (sig / K) ** n \qquad (25)$$

$$\dot{omega} = Ep * \dot{e}_{in} + e_{in} * \frac{dEp}{dT} * dT \qquad (26)$$

Material Constants: E, Ep, n, K, and Sy depend on temperature, T.

The technique used to obtain the material constants for the Moreno model was also different than that of Reference 7. In this instance, monotonic tensile and creep information for the PWA 286 coating was either unavailable or incomplete. Constant determination for the Moreno model subsequently involved regressing the isothermal stress relaxation tests using the formulation given above. The material constant 'n' in the Moreno model creep law was assumed to be equivalent to the exponent 'n' in the Walker model flow rule. A summary of regressed material constants for the Moreno model is presented in Table 3.

Because the response of PWA 286 coating at moderate to elevated temperatures is primarily controlled by time dependent inelastic processes, for temperatures greater than 649°C (1200°F), only the creep law equation was used to regress the stress relaxation data. Material constants Ep and Sy at the higher temperatures were obtained by extrapolation from the lower temperature values after the creep law equation was fit.

Correlation of the 649°C (1200°F) stress relaxation test from the second test series by the Walker and Moreno models is presented in Figure 25. Overall, the Walker model correlates this data set better than the Moreno model and is able to fit the positive stress relaxation trend. The inability of the Moreno model to fit the observed positive stress relaxation is a result of the assumed back stress growth law. Even if the back stress term would appear in the creep law equation, no change in the correlation would result because the back stress is too small to produce the desired effect. Reformulating the back stress equation was considered, but it was felt that such an action would only produce a model similar to the Walker model.

37

···DATA —CORRELATION

WALKER

1 KSI = 6.895 MPa

MORENO

1 KSI = 6.895 MPa
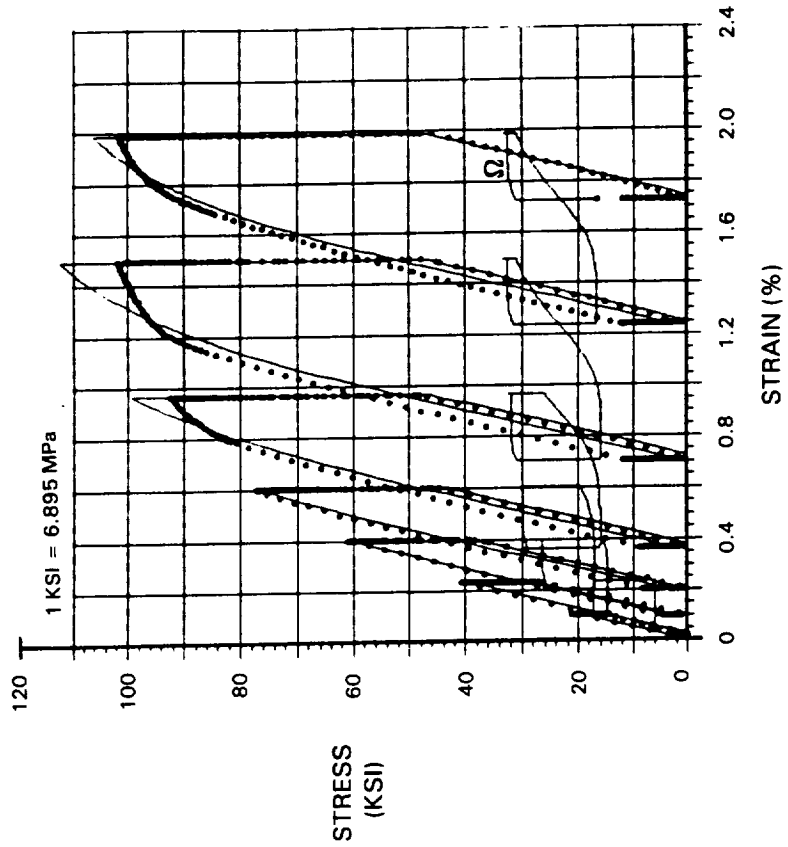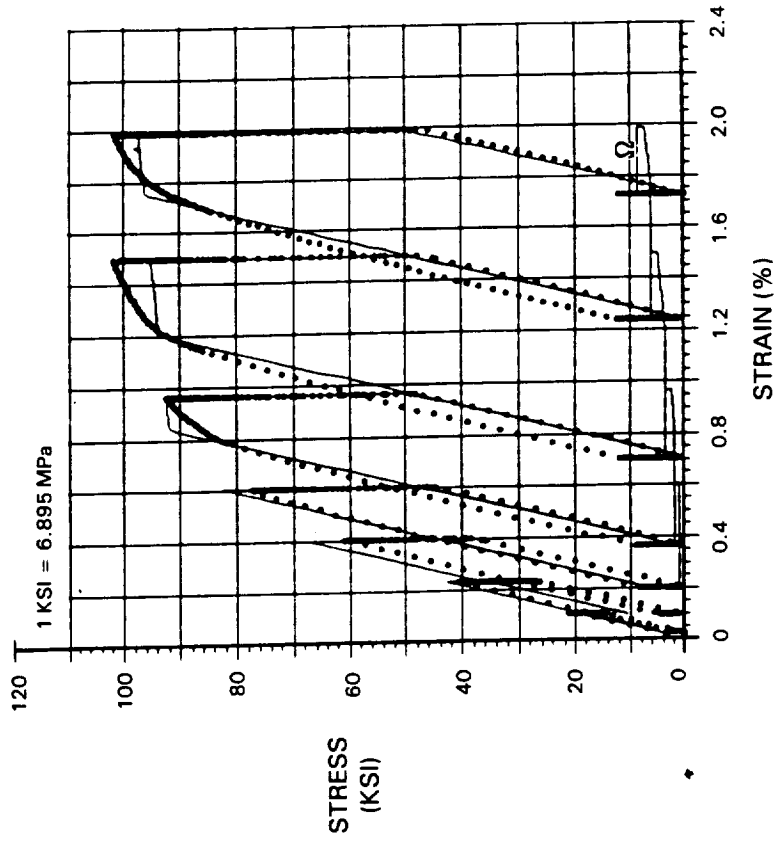
Figure 25 Walker and Moreno Model Correlation of 649°C (1200°F) Isothermal
Stress Relaxation Test

38

Walker and Moreno model prediction of the response of an unexposed, bulk HIP PWA 286 coating specimen tested using an out-of-phase TMF waveform is presented in Figure 26. Again, the Walker model is better able to duplicate the observed behavior, although the Moreno model is able to represent the gross material response. Both models still overpredict the maximum tensile stress, however, the Walker model is able to predict the graceful tensile yielding trend. Note that the second cycle maximum compressive stress is also overpredicted. This was not expected since both models fit the baseline relaxation rates rather well.
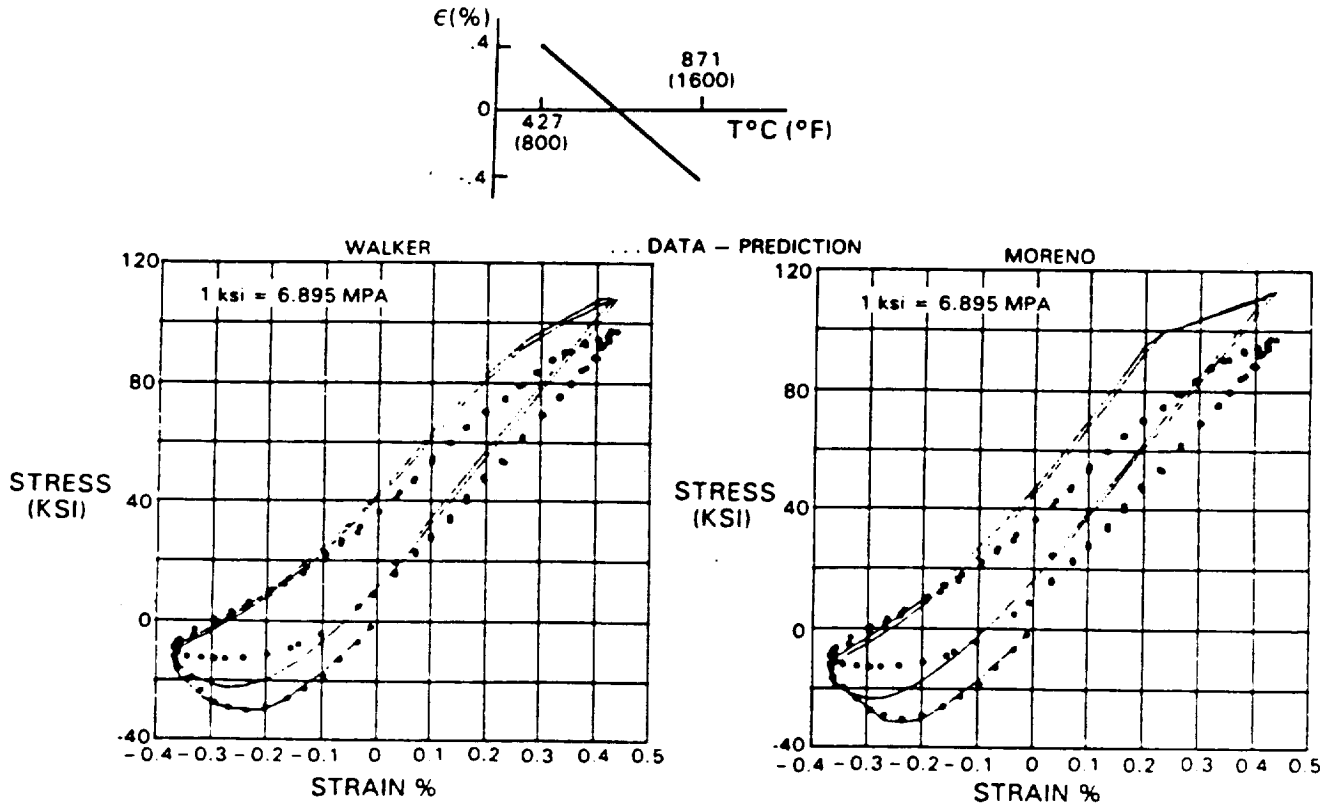
Figure 26   Walker and Moreno Model Prediction of Out-of-Phase TMF Test

A summary of predicted secondary creep rates versus data is presented in Table 4. The secondary creep rates were generally overpredicted by both models. Coatings do not elongate in gas turbine applications because the substrate material constrains the coating creep extension. As such, the inability to predict long term creep rates should not restrict the models. Walker model predicted creep strain versus creep data is presented in Figure 27. Note that the primary creep regime (i.e., for times less than 15 min.) is fairly well duplicated by the Walker model. Times up to 15 min. are consistent with the maximum strain hold time present in the baseline stress relaxation experiments.

39

TABLE 4

UNEXPOSED, BULK HIP PWA 286 CREEP RATES
DATA VS. PREDICTION

| | | | Secondary Creep Rate (in/in/hr) | |
| | | | ----Predicted---- | |
Temp °C (°F)	Stress MPa (ksi)	Data	Walker	Moreno
649 (1200)	68.9 (10)	0.266E-4	0.305E-4	0.188E-4
649 (1200)	103.4 (15)	0.173E-3	0.574E-4	0.718E-4
760 (1400)	20.7 (3)	0.139E-3	0.256E-3	0.905E-3
760 (1400)	34.5 (5)	0.388E-3	0.732E-3	0.268E-2
871 (1600)	6.9 (1)	0.461E-4	0.171E-2	0.792E-2
871 (1600)	20.7 (3)	0.103E-1	0.179E-1	0.516E-1
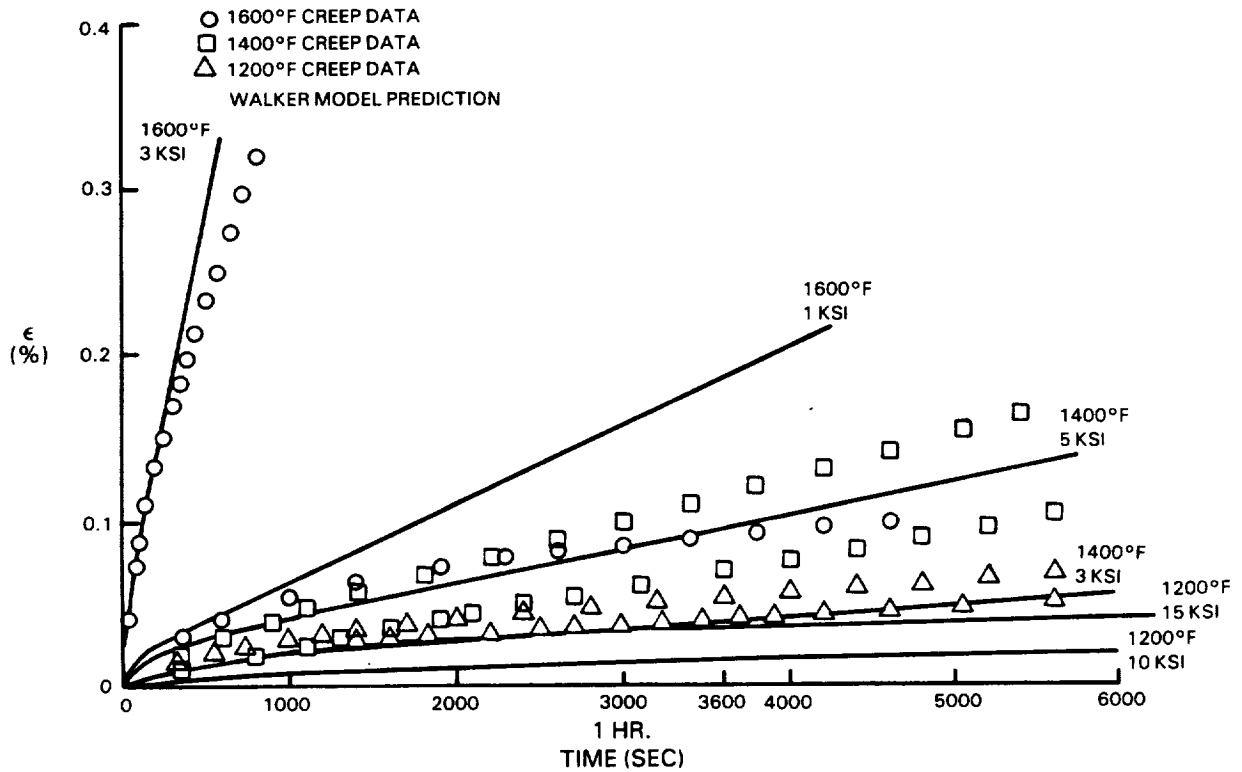
Figure 27 Walker Model Prediction of Monotonic Creep Behavior of Unexposed, Bulk HIP PWA 286.

Based on overall correlation and prediction capabilities as well as ease of incorporation into a finite element code, the Walker model was chosen as the final coating constitutive model.

6.1.2 PWA 273 Aluminide Coating

Walker model constant regression for the aluminide coating is pending the reduction of the aluminide coating constitutive behavior test data.

6.2 SINGLE CRYSTAL CONSTITUTIVE MODEL

Two separate unified constitutive models for single crystal PWA 1480 were formulated and developed. The first model, the "microscopic model," computes the inelastic quantities on the crystallographic slip systems. Development of this slip system based model began at Pratt & Whitney in 1982 and was part of a large company effort to develop constitutive models. The development has continued since 1982 through the combined efforts of Pratt & Whitney's personnel and consultants under the company program and in a complementary NASA grant, NAG-512. This model achieves the required directional properties as a consequence of summing the slip system strains which have been resolved onto the global coordinate system. The second model, the "macroscopic model," uses global stresses and strains directly and employs anisotropic tensors operating on global inelastic quantities to achieve the required directional properties.

The two models offer a trade between accuracy and physical significance and computing time requirements. The microscopic model is more accurate and is more physically significant in its formulation than the macroscopic model. However, the macroscopic model is more computationally efficient because integration of the evolutionary equations is required only for the six global stress/strain quantities rather than for each of the 18 slip systems.

A discussion of model formulations and correlation of PWA 1480 isothermal hysteresis loop data was reported in Reference 2.

6.3 COATED SINGLE CRYSTAL LIFE PREDICTION MODELING

Fatigue life for coated single crystal materials was defined as follows (see Section 4.2):

$$Nf = Nc + Nsc + Nsp \tag{27}$$

$$\text{or} \quad Nf = \quad Nsi + Nsp, \quad \text{whichever is smaller,} \tag{28}$$

where Nf = Total cycles to failure.

Nc = Cycles to initiate a crack through the coating.

Nsc = Cycles for coating crack to penetrate a small distance into the substrate (base alloy).

Nsi = Cycles to initiate a substrate (base alloy) crack.

Nsp = Cycles to propagate a substrate (base alloy) crack to failure.

41

The choice of coating crack initiation (Nc) was based on experimental observations and the practical limitation of the acetate film inspection technique. Acetate replicas of surface cracks during TMF tests and the post-test crack morphology exams together indicate that coating cracks rapidly penetrate through the coating. Also, crack depths less than 1/2 to 1 coating thickness are difficult to replicate and are considered near the limit of acetate film replica resolution.

Substrate cracking (Nsc or Nsi) will include short crack behavior. For engineering purposes, a crack size which is easily inspected in a component is desirable. This translates to a surface crack size of about 0.76 mm (0.031 in.). Thus, the depth of penetration into the substrate was selected to be 0.254 mm (0.010 in.) so that the overall surface crack length would approximate 0.76 mm (0.031 in.) for a 2.0 aspect ratio thumbnail crack in a specimen with a 0.127 mm (0.005 in.) coating.

Modeling of substrate crack propagation life (Nsp) will not be addressed in this program.

6.3.1 Coating Life Models

Two phenomenological based candidate life models were chosen for the coating life modeling effort: Coffin-Manson and Ostergren (i.e., hysteretic energy approaches). Like the coating constitutive modeling effort, PWA 286 overlay coating was used as the model development vehicle. The selected model may then be applied to the PWA 273 aluminide coating.

PWA 286 Overlay Coating

For the initial model evaluations, the coating life (Nc) was assumed to be adequately defined by a surface crack length of 0.254 mm (0.010 in.) which is roughly equivalent to twice the nominal PWA 286 overlay coating thickness. Surface crack lengths were determined from the acetate replica data taken during each test.

The database used to correlate overlay coating cracking life included 427, 760, 927, and 1038°C (800, 1400, 1700, and 1900°F) isothermal data and 427-1038°C and 427-1149°C (800-1900°F and 800-2100°F) TMF data, some of which was acquired in Level II experiments.

Four models were evaluated: Coffin-Manson, Ostergren, Tensile Energy Approach based on Teff (i.e., an Ostergren model which uses the concept of an "effective" temperature, Teff), and Tensile Hysteretic Energy (i.e., an Ostergren model which used an integrated energy over the tensile portion of the hysteresis loop).

Parameters such as inelastic strain range, inelastic strain range based on Teff (Teff=(Tmin+Tmax)/2), tensile stress, stress range, and tensile hysteretic energy were considered in the life correlations. All the parameters were obtained from an analysis utilizing a two-bar mechanism such as shown in Figure 24. Tensile hysteretic energy was obtained by integrating around the tensile portion of the hysteresis loop. These correlations are presented in

Figure 28. A band of ±2X in life was drawn about the TMF data to ease model to model comparisons.
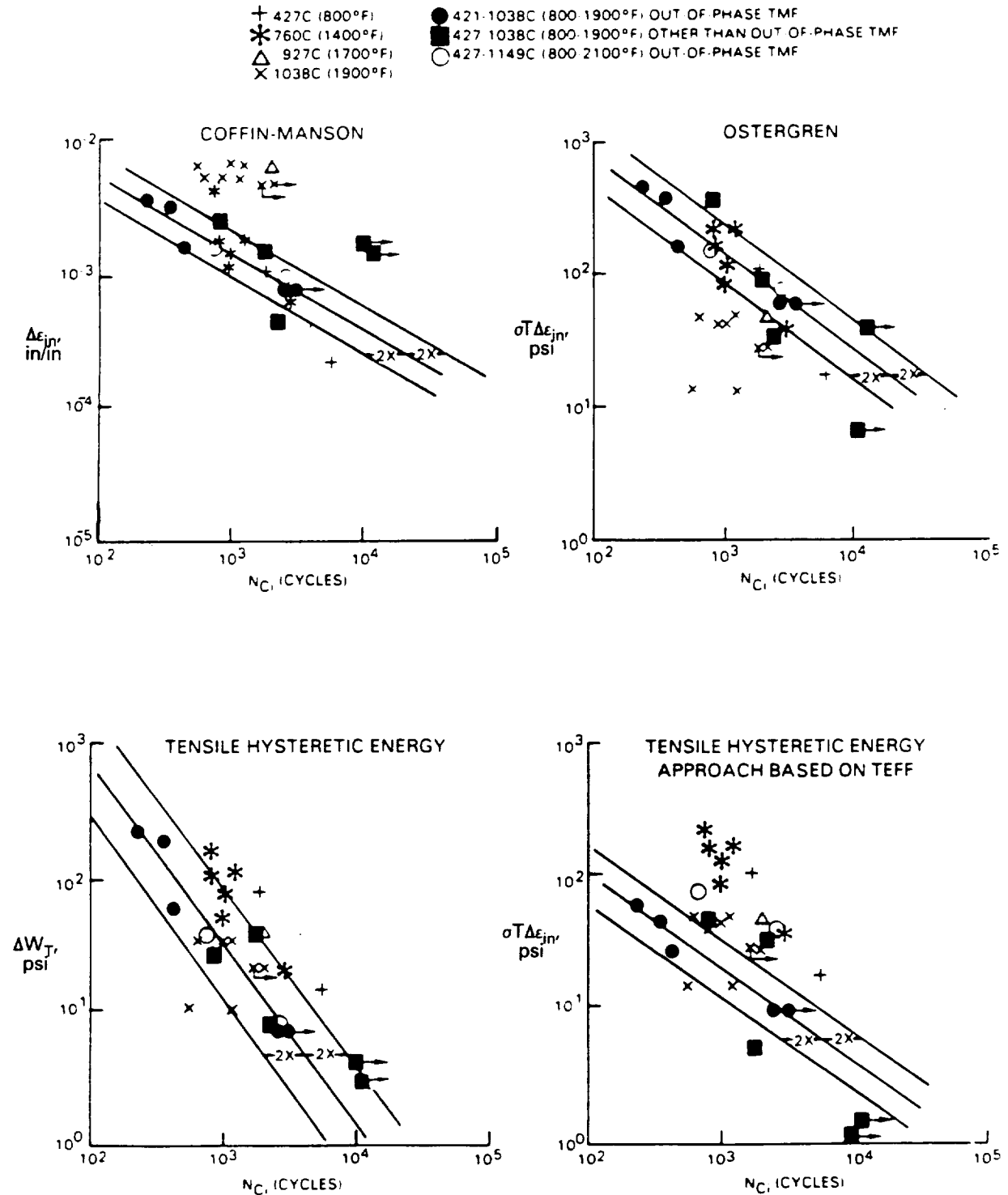
Figure 28 PWA 286 Overlay Coating Cracking Life Correlations

43

From Figure 28, it is clear that none of the parameters correlate the lives within a +2X life band. However, of the four models, tensile hysteretic energy appears to be the best. Unfortunately, this model in its current form is unable to correlate strain rate (frequency) effects. For example, consider the response of the coating at 1038°C (1900°F). At high strain rates, the hysteresis loops are narrow resulting in low tensile hysteretic energy (small inelastic strain), and, at low strain rates, the hysteresis loops are wide which also results in low tensile hysteretic energy (small tensile stress). Thus, the same life is predicted for a slow and fast cyclic rate test, but the observed lives can be much different. A representative plot of tensile hysteretic energy vs. cyclic frequency is presented in Figure 29. The frequency at which the maximum tensile energy occurs is a function of temperature and strain range, and, therefore, the tensile energy must be modified to account for temperature- and time-dependent damage effects to produce accurate life predictions.
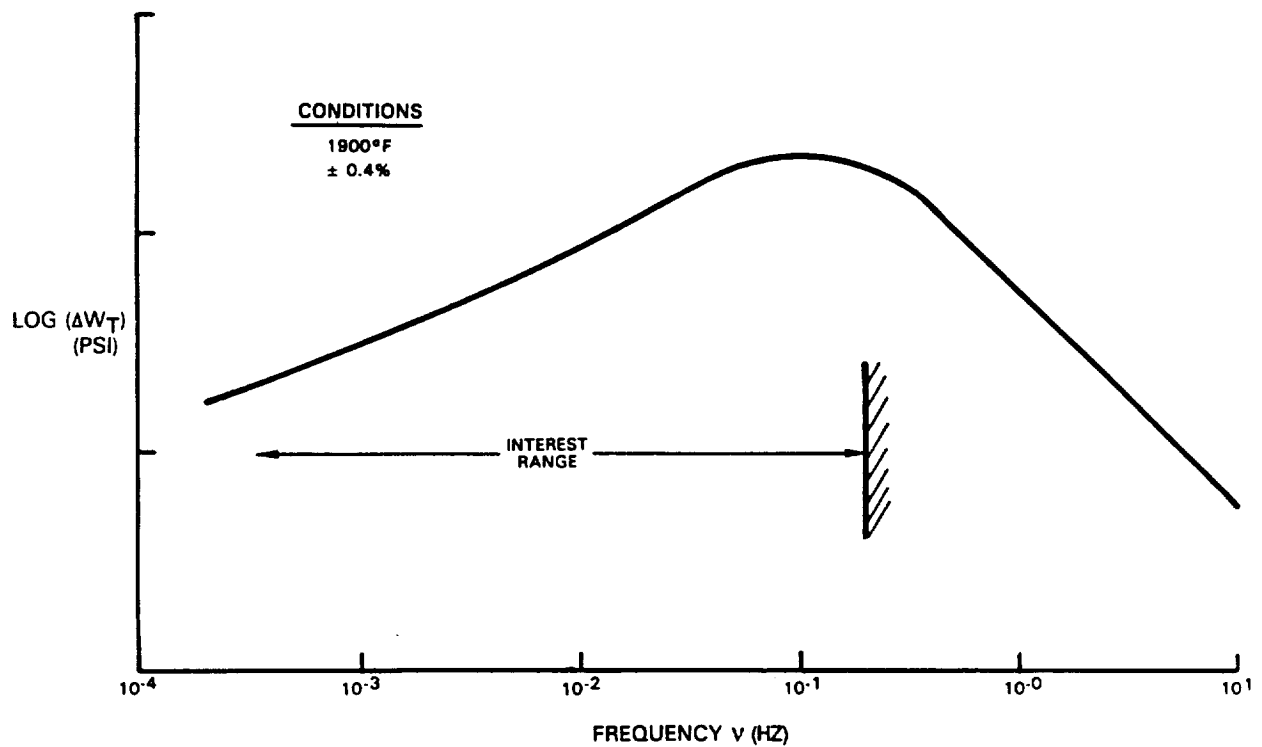
Figure 29   Representative Response of Tensile Hysteretic Energy With Respect to Frequency

Based on the results of the model evaluations, the tensile hysteretic energy model was selected for final development.

PWA 273 Aluminide Coating

A literature survey was conducted on diffusion coated failure mechanisms (References 9 to 11). Reported failures were caused by two general types of crack initiation events, either surface initiation in the coating or subsurface initiation in the coating diffusion zone.

Observations from the Level I tests confirmed that crack initiation may occur below the OD surface of the coating, and, as a result, specific nomenclature was adopted to classify each type of initiation event (see Section 5.3.2).

Due to the complexity of the observed PWA 273 aluminide crack initiation processes, application of the tensile hysteretic energy life model to this coating was deferred until the completion of the Level II experiments.

6.3.2 Single Crystal Life Models (Coated)

Five life models were applied to an isothermal data base consisting of PWA 273 coated PWA 1480 crack initiation lives at 927°C (1700°F).

1) Coffin-Manson: $N = A \, \Delta\epsilon_{in}^{B}$

2) Crack Tip Opening Displacement (CTOD): $N = A(\sigma_t^2/E\sigma_y)^B$

3) Modified Strain: $N = A(\Delta\epsilon \, E/2)^B$

4) Ostergren: $N = A(\sigma_t \Delta\epsilon_{in})^B$

5) Hysteretic Energy Approach (Ref. 2): $N = A\left[\sigma_t \Delta\epsilon_{in} \, \dfrac{\Delta\sigma_{[111]}}{E}\right]^B$

where:

σ_t = Specimen tensile stress

σ_y = 0.2% PWA 1480 yield stress

$\Delta\epsilon_{in}$ = Specimen inelastic strain range

E = PWA 1480 elastic modulus parallel to specimen loading direction

$\Delta\epsilon$ = Specimen total (mechanical) strain range

$\Delta\sigma_{[111]}$ = PWA 1480 resolved octahedral normal stress range

The model correlations are presented in Figures 30 to 34, respectively.

45
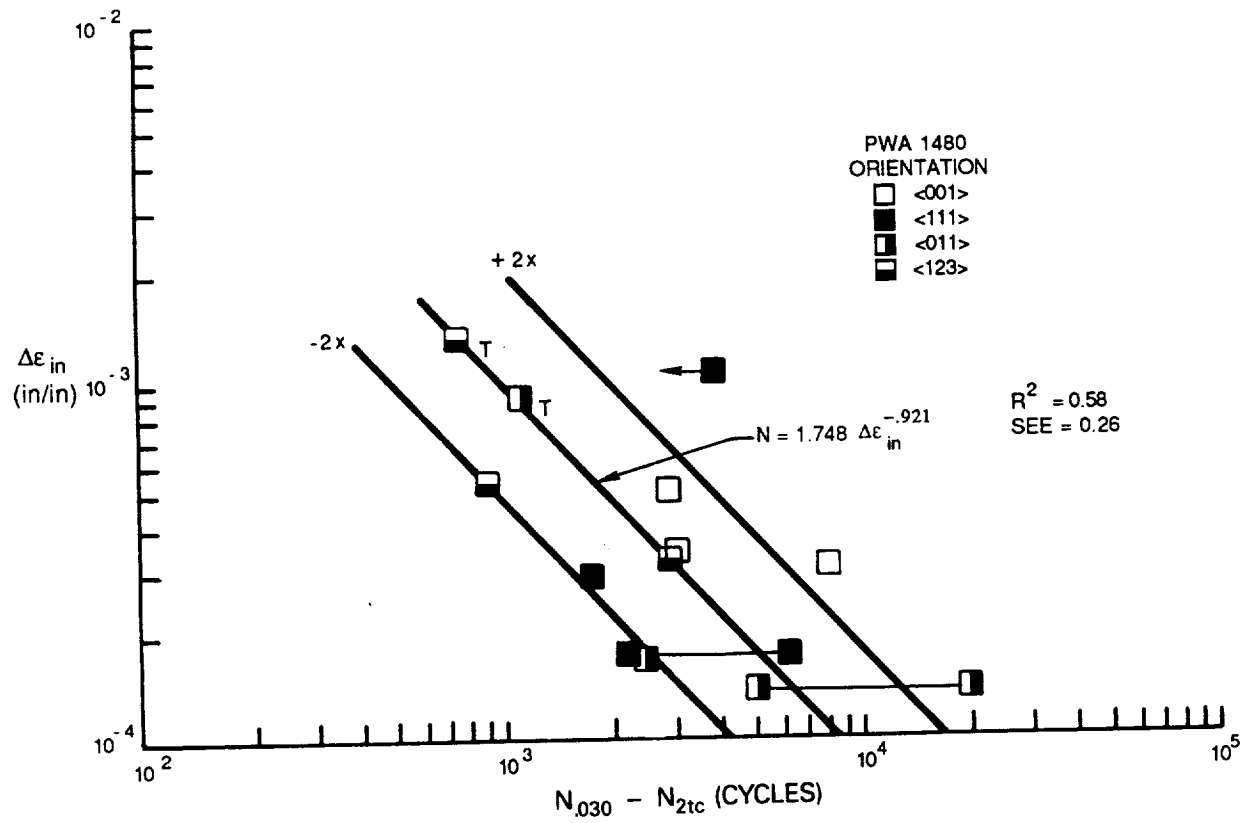
Figure 30   Inelastic Strain Correlation of PWA 1480 Cracking Lives at 927°C (1700°)
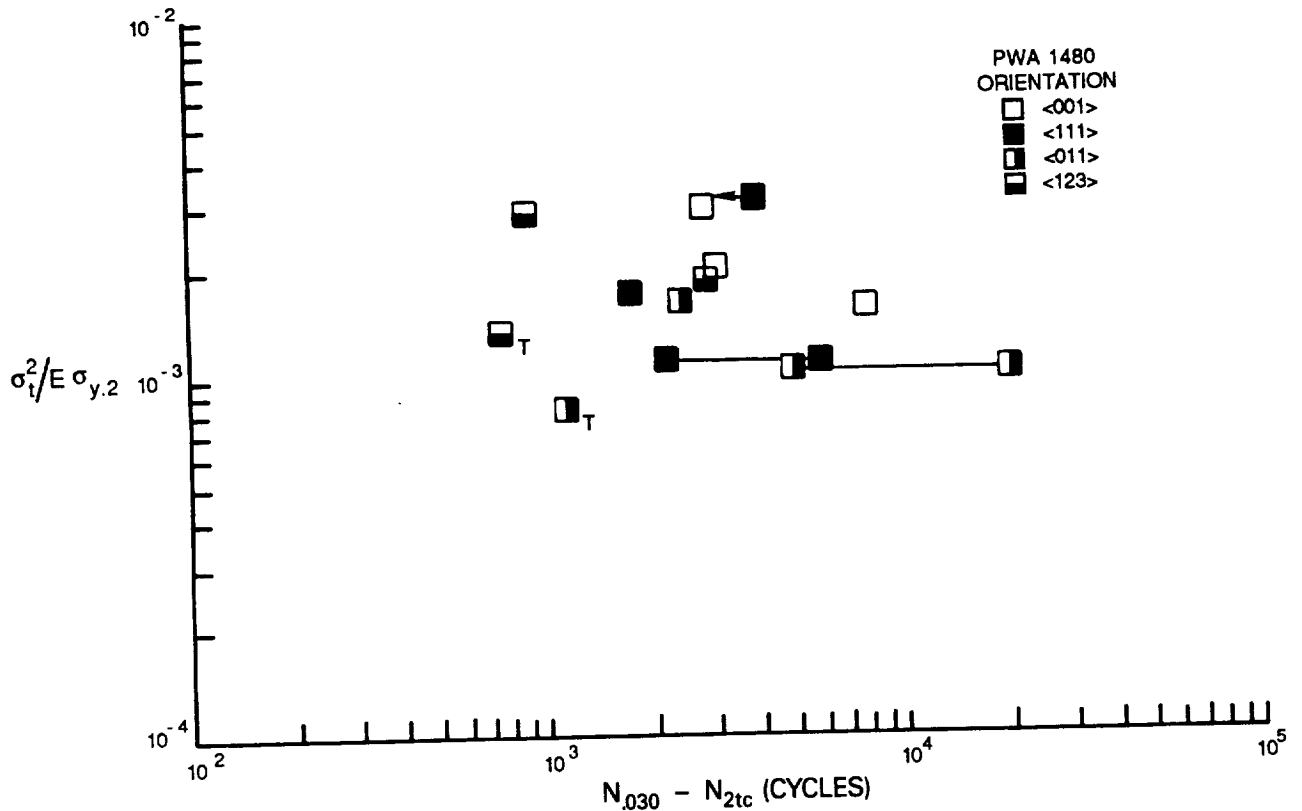
Figure 31   CTOD Correlation of PWA 1480 Cracking Lives at 927°C (1700°F)

46
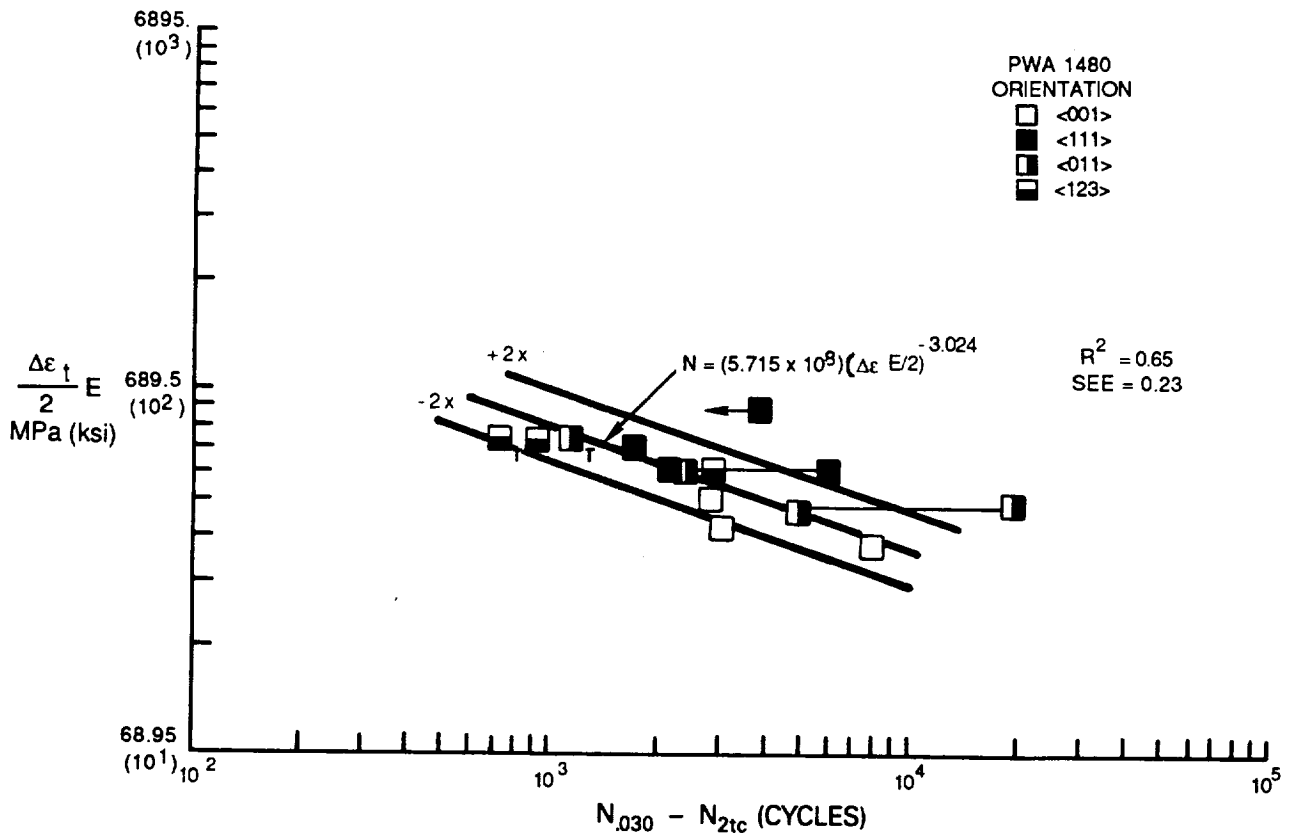
Figure 32   Modified Strain Correlation of PWA 1480 Cracking Lives at 927°C (1700°F)
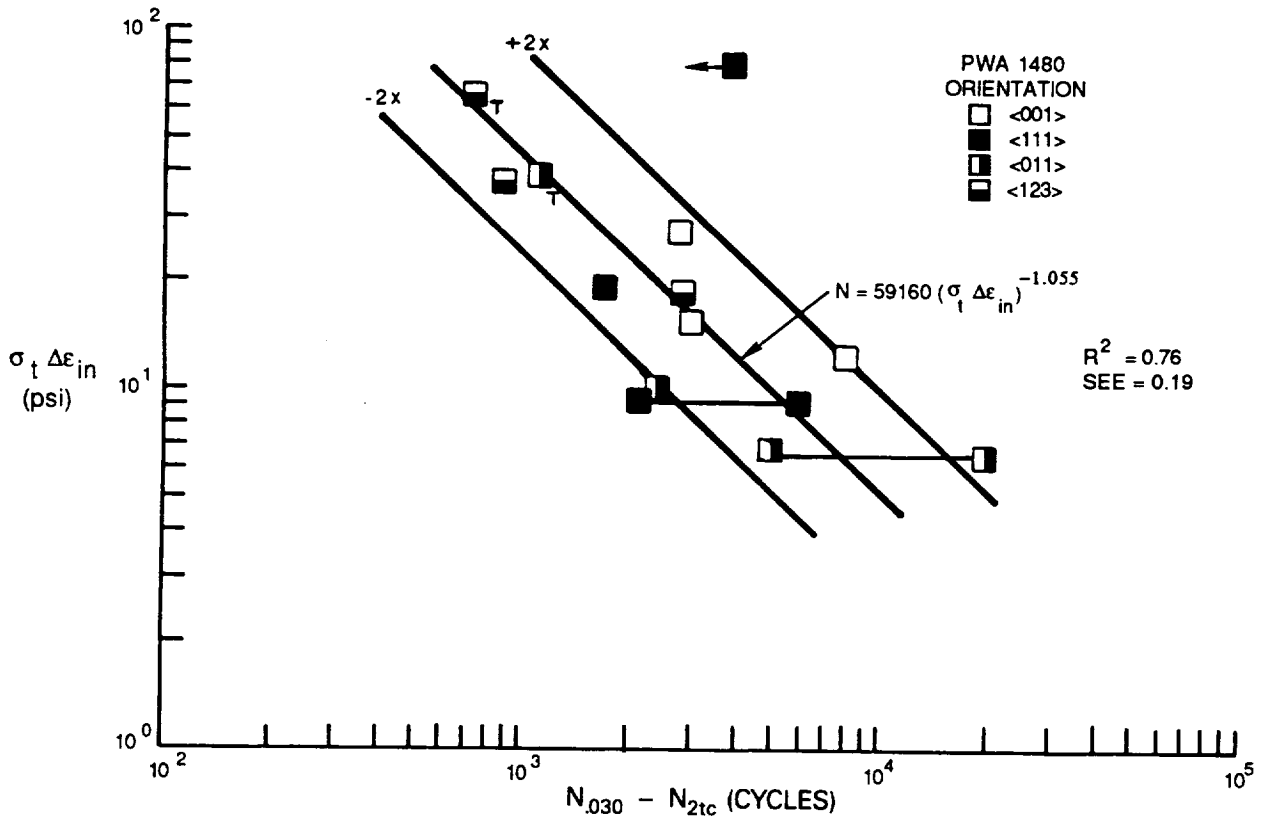
Figure 33   Ostergren Model Correlation of PWA 1480 Cracking Lives at 927°C (1700°F)
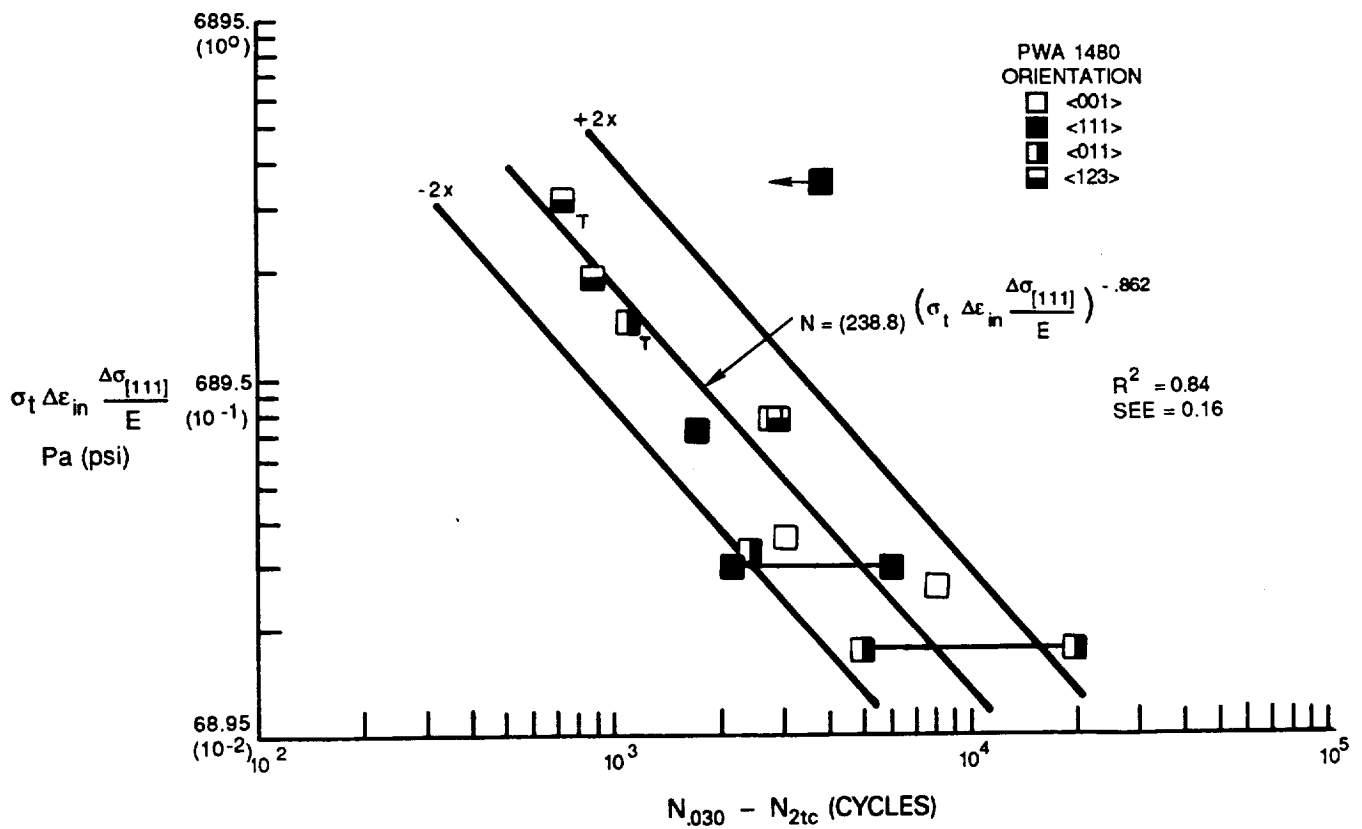
Figure 34 Modified Hysteretic Energy Model Correlation of PWA 1480 Cracking Lives at 927°C (1700°F)

Because fractographic analyses of these specimens were incomplete at the time these correlations were conducted, PWA 1480 crack initiation life was assumed to be adequately described by the number of cycles to produce a 0.76 mm (0.030 in.) surface crack minus the coating life determined at two times the coating thickness (i.e., N.030-N2tc). It was felt that this assumption was reasonable based on the observed thumbnail-like specimen crack geometry.

Of the five models considered, the Hysteretic Energy Approach, Ostergren, and Coffin-Manson models are the most promising for correlating isothermal fatigue life data when measureable inelastic strains are present.

This program, however, emphasizes life prediction of TMF cycles. As such, selection of two life prediction models for PWA 1480 was deferred until sufficient TMF life data from all four orientations was available from the Level II experiments. Meanwhile, the remainder of the PWA 1480 life model development effort in this task was devoted to developing a process by which accurate PWA 1480 life data may be obtained from the tested specimens.

PWA 1480 Single Crystal Life Determination

Specimen failures caused by cracking were observed at several locations depending on the test temperatures and loads and specimen orientation. A description of each failure location is presented below:

gag = Specimen failed inside the 2.54 cm (1.0 in.) extensometer monitored gage section.
but = Specimen failed at the specimen buttonhead grip fillet.
ext = Specimen failed from crack which initiated underneath the MTS extensometer quartz rods.
IDr = Specimen failed from the ID surface near the ID ridge region (44C specimen design only).
gagr = Specimen failed inside the monitored gage section near the ID ridge region (44C specimen design only).
ogag = Specimen failed outside the monitored gage section, but within the constant cross-section portion of the specimen.

"IDr" and "gagr" type of failures were limited to certain 44C specimen tests conducted in the Level I experiments. Only cracks which initiated along the OD surface, away from the extensometer rods, and inside the constant cross-section portion of the specimen were considered useful for life prediction modeling of Nc and Nsc. Other cracks which appeared outside this restriction were not evaluated.

Several methods were identified and used to obtain PWA 1480 crack initiation life, Nsc or Nsi, from the coated specimens. A particular method was chosen for each specimen based on its observed cracking behavior. A synopsis of when and how each method was applied is presented below. Slight modifications to these basic methods were considered when specimen information was limited.

Case 1 - "Classical" Cracking

In this case, crack geometry is typically thumbnail in nature and OD surface replicas can be used to establish PWA 1480 crack initiation life. This type of crack geometry is shown in Figure 35A.
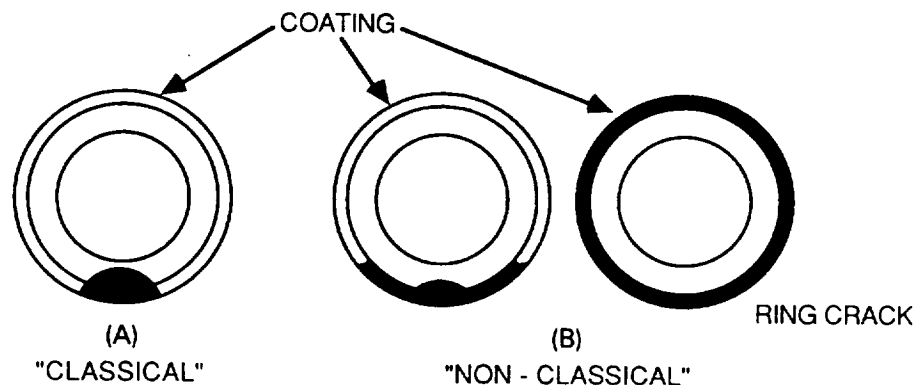
Figure 35   Types of O.D. Initiated Cracking Observed From Coated PWA 1480 Specimens

49

Method 1 - Obtain crack aspect ratio (length/depth) from fractographic analysis.
- Enter surface crack length versus cycle number curve at crack length of: (crack aspect ratio)*(crack depth); Crack depth = coating thickness + 0.254 mm (0.010 in.).
- Replica data may be prudently extrapolated.
- See Figure 36.
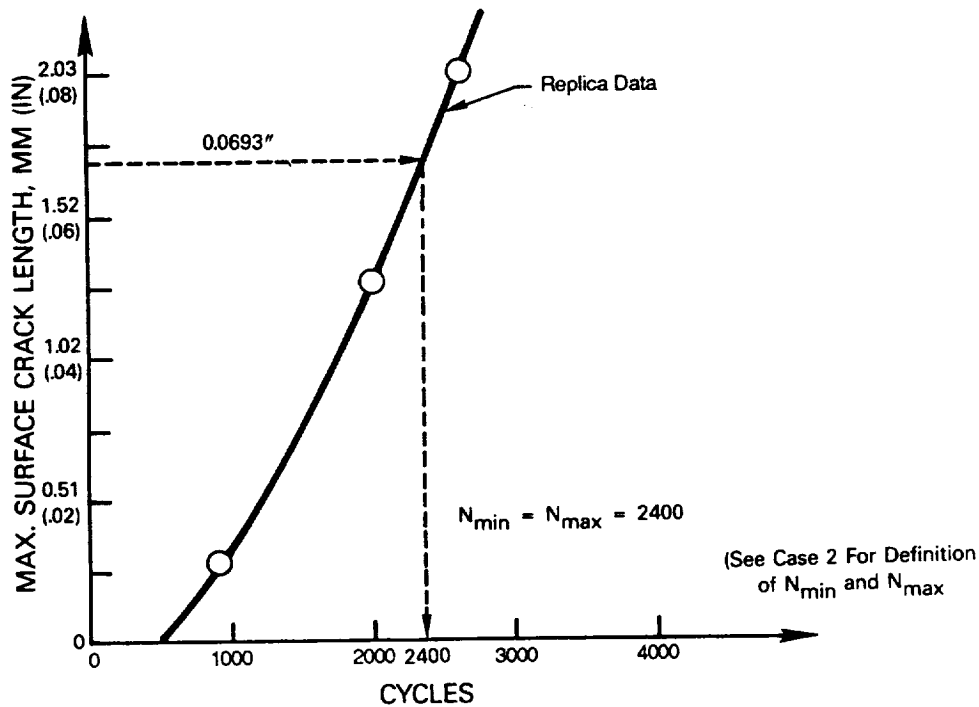
Figure 36 Method 1 Application to Specimen JB-121. Crack aspect ratio = 4.5; desired crack length = 4.5 (0.0154 in.) = 0.0693 in.

Case 2 - "Non-classical" Cracking

Coating cracks grow along specimen circumference and minimally penetrate into the substrate or appear as "ring" cracks. These types of cracks are shown in Figure 35B. Long OD surface cracks observed on replicas are, therefore, not indicative of substrate cracking. As such, it was considered reasonable to determine lower and upper bounds on life (Nmin and Nmax) between which the actual life lies.

N_{min} = Lower life bound = Nc + Nsc (lower bound)
N_{max} = Upper life bound = Nc + Nsc (upper bound)
Nc = Coating Life

50

Method 2 : For a primary gage section crack that penetrates less than 0.254 mm (0.010 in.) into the substrate.

- Set Nmin = cycle number which generated the small crack.
- Obtain estimate of substrate crack aspect ratio from fractographic analysis.
- Draw a straight line from the replica data curve at the point where Nc occurs through the known crack length (crack aspect ratio * known crack depth), Nmin point.
- Extrapolate the straight line to the desired crack length and pick off Nmax.
- See Figure 37.
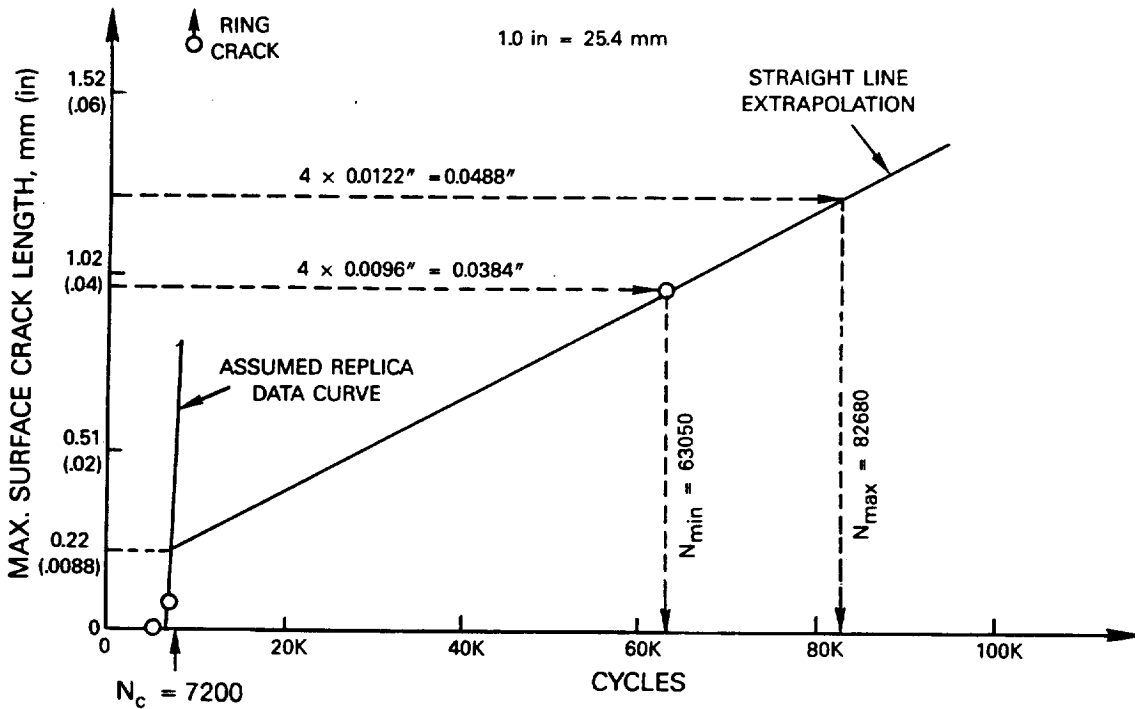
Figure 37 Method 2 Application to Specimen JB-103. Coating Initiation Appeared As a Ring Crack. Estimated substrate crack aspect ratio = 4.0. N_c was determined at 4 x (coating thickness) = 4(0.0022 in.) = 0.0088 in. Maximum crack penetration = 0.0096 in. at 63050 cycles. Desired crack length = 4.0 (0.010 in. + 0.0022 in.) = 0.0488 in.

Method 3 : For a primary gauge section crack that penetrates more than 0.254 mm (0.010 in.) into the substrate.

- Determine number of cycles (typically Nf) to a known crack depth and crack aspect ratio by using fracture photos.
- Plot the known crack surface length (crack aspect ratio * known crack depth), cycle number point together with the specimen replica data.

51

- Extrapolate replica data curve beyond the last replica data point. Note: This extrapolated curve will rarely pass through the known crack size, cycle point.
- Draw a straight line from the replica data curve at the point where Nc occurs to the known crack size, cycle point.
- Pick Nmin off the straight line at a surface crack length equal to the (crack aspect ratio)*(desired crack depth).
- If Nmin is less than would be obtained by using the extrapolated replica data curve, redetermine Nmin from the extrapolated replica data curve.
- Translate extrapolated replica data curve so that it passes through the known crack size, cycle point.
- Pick Nmax off the translated replica data curve in the same manner as Nmin was picked.
- See Figures 38 and 39.
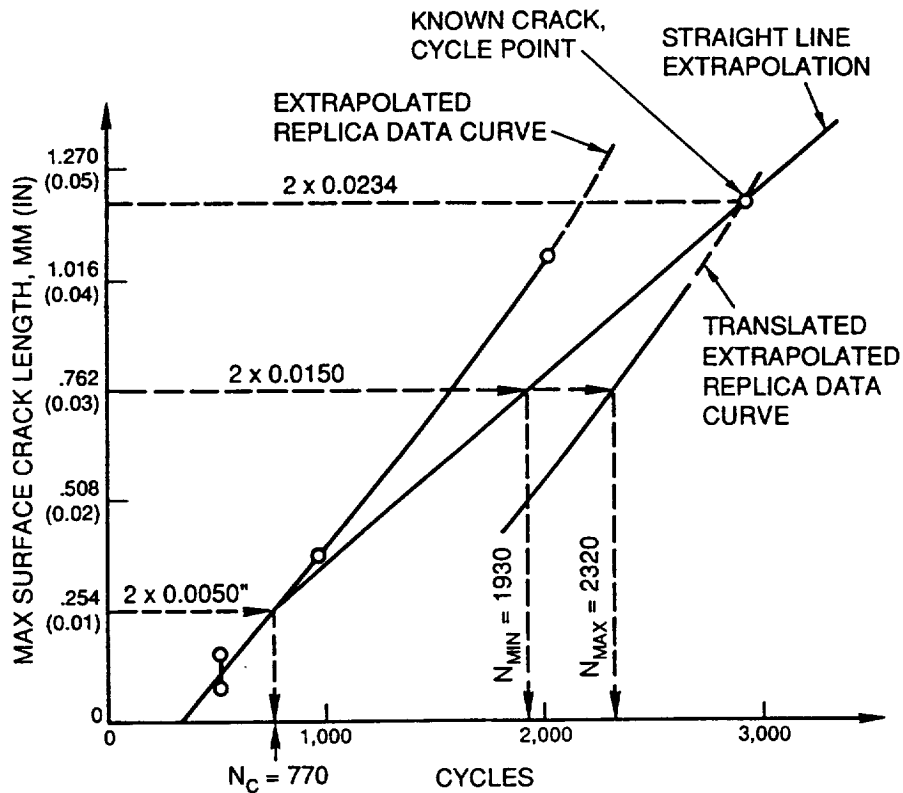
Figure 38 Method 3 Application to Specimen JB-89. Estimated crack aspect ratio = 2.0. N_c was determined at 2 x (coating thickness) = 2 x (0.0050 in.) = 0.0100 in. Maximum crack penetration = 0.0234 in. at 2912 cycles (N_f). Desired crack length = 2 (0.0150 in.) = 0.0300 in. From straight line extrapolation, N_{min} = 1930 cycles. From translated extrapolated replica data curve, N_{max} = 2320 cycles.

52
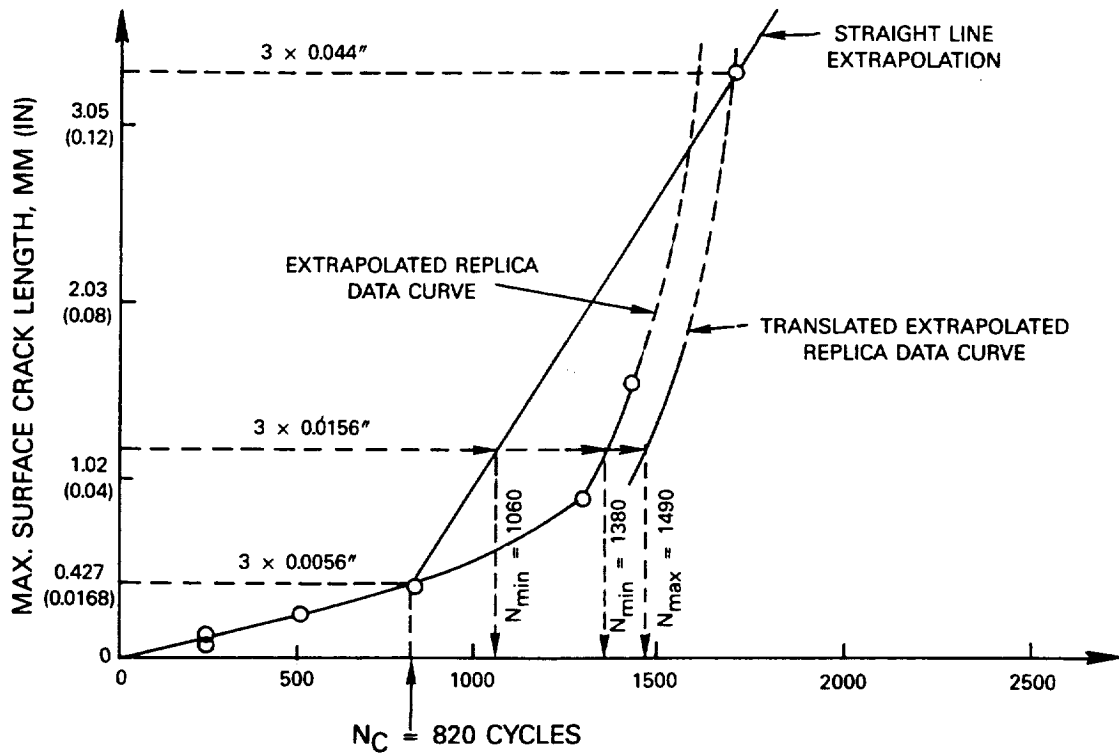
Figure 39 Method 3 Application to Specimen JB-21. Estimated crack aspect
ratio = 3.0. N_c was determined at 3 x (coating thickness) = 3
(0.0056 in.) = 0.0168 in. Maximum crack penetration = 0.044 in. at
1847 cycles (N_f). Desired crack length = 3 (0.0156 in.) = 0.0468
in. From straight line extrapolation, N_{min} = 1060 cycles, but
N_{min} = 1380 cycles from replica data. Use N_{min} = 1380 cycles.
From translated extrapolated replica data curve, N_{max} = 1490
cycles.

Method 4 : Check of Nmax obtained by methods 2 and 3.

- Using plot of specimen stress range versus cycle number, determine
  cycle number at which load range drop initiates (Nld), see
  Reference 12.
- If Nld < Nmax ; Nmax = Nld.
- See Figure 40.

53
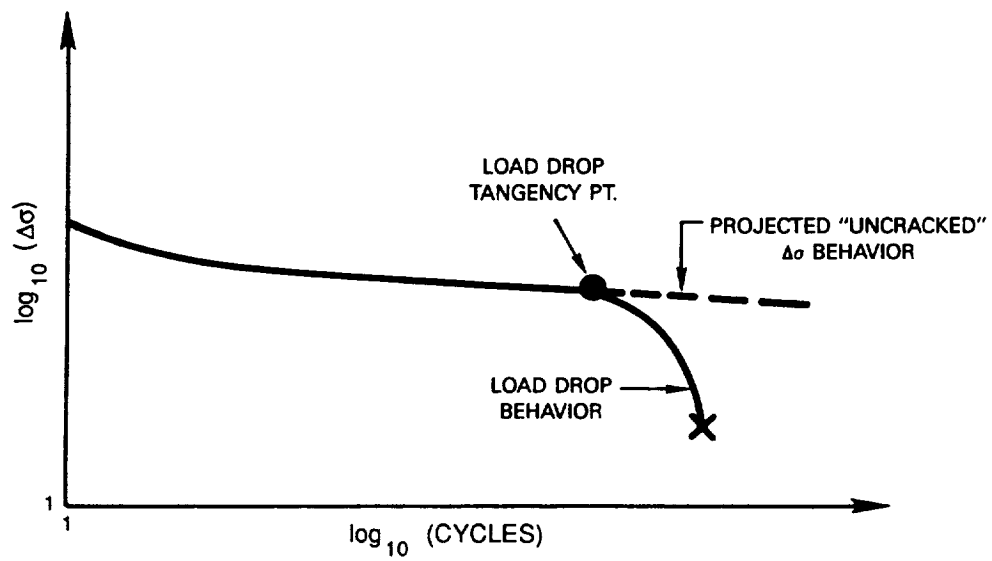
Figure 40 Method 4 check of N_{max} Calculation. It is assumed that a crack which has penetrated into the PWA 1480 at least 0.010 in. exists at the load drop tangency point.

54

SECTION 7.0

TASK V - LEVEL II SINGLE CRYSTAL EXPERIMENTS

Isothermal fatigue and TMF tests were conducted to define the crack initiation life of coated PWA 1480 single crystal material to verify Level I data trends and to increase the database for life model selection and development.

All fatigue tests used the specimen geometry shown in Figure 1B.

The test facility used for Level II experiments was identical to that used in the Level I experiments (see Section 5.3).

The specimen and fatigue test variables considered for Level II experiments included thermal exposure in addition to those variables considered in the Level I tests (see Section 5.3).

The onset of coating cracking and crack propagation was monitored during each test by taking a series of acetate film surface replicas. Metallographic inspection of the tested specimens was performed at the conclusion of each test in order to interpret the replica data, characterize cracking patterns, and identify crack initiation sites. Specimen load, strain, and temperature histories were monitored during the course of testing to provide information useful for the modeling efforts.

7.1 UNIAXIAL FATIGUE TESTS

A summary of Level II uniaxial fatigue lives and specimen responses is presented in Appendices A and B.

Overall, Level II tests confirmed that coated PWA 1480 single crystal creep-fatigue life is dependent on several factors: 1) the presence of a coating, 2) the coating composition and microstructure, 3) single crystal orientation, and 4) the cyclic strain-temperature-time relationship (i.e., the cyclic loading history). In addition, thermal exposure effects were shown to be important.

The effect of cyclic history on coated TMF life was confirmed during Level II experiments. PWA 286 overlay coated <111> PWA 1480 specimens LB-32 and LB-29 were TMF tested using the "baseball" cycle shown in Figure 20 to verify the data trend observed from aluminide coated specimens LB-21 and LB-156. Specimen LB-32 was cycled in a counter-clockwise (ccw) direction and LB-29 was cycled in a clockwise (cw) direction. Stabilized hysteresis loops for LB-29 and LB-32 were practically identical to those presented in Figures 21 and 22 for specimens LB-156 and LB-21, respectively. Specimen LB-29 (cw cycle) crack initiation and failure lives were 2600-3200 and 3773 cycles while the crack initiation life for specimen LB-32 was >11852 cycles. At 11852 cycles no cracks were observed on LB-32 and the test was discontinued.

55

PWA 286 overlay coated <111> PWA 1480 specimens LB-26 and LB-30 confirmed the importance coatings play in fatigue crack initiation. Specimen LB-30 was isothermally fatigued at 427°C (800°F), +0.25% strain at 10 cpm. Specimen LB-26 was TMF tested at +0.25% strain using the "T-cycle" strain-temperature cycle described in Section 5.3.2. The associated crack initiation and failure lives of these two specimens were >7130 and 7130 for LB-30 and >3260 and 3532 for LB-26. Specimen LB-30 failed at the specimen buttonhead grip fillet at 7130 cycles and no cracks were observed in the gage section. Specimen LB-26 failed from a crack underneath the extensometer quartz rods and small cracks were observed in the gage section which penetrated the coating at 2560 cycles and minimally penetrated into the PWA 1480 substrate.

A spallation failure mode in which the coating is liberated from the substrate may occur when the coating undergoes severe compressive deformation. Specimen JB-102 was TMF tested using a counter-clockwise baseball cycle at 427-1038°C (800-1900°F), +0.4%, 1 cpm. Note that this specimen previously ran roughly 41000 cycles at 800F, +0.3%, 8 cpm. Although JB-102 failed from a crack which initiated at the uncoated ID surface, the coating surface was littered with cracks which were inclined roughly 45 deg. to the loading axis. A transverse coating micrograph is presented in Figure 41. Acute coating rumpling and cracks propagating parallel to the interface are the dominant features. The coating cracks were apparently due to shear not tensile forces. Severe compressive nonlinear coating behavior was predicted by the PWA 286 overlay coating constitutive model, thus activating the shear failure mode. In addition, the predicted level of coating compressive stress introduces a tensile radial stress component at the coating-substrate interface. It is believed that this radial stress influenced the crack trajectory, forcing it to turn along the interface. Final fracture was crystallographic in nature indicating that the PWA 1480 load levels were not generally relevant to gas turbine airfoils. However, the interesting failure of JB-102 indicates that multiple failure modes are possible in coatings. This places limits on the realistic extrapolation capability of the coating life models being developed for cracks normal to the loading direction (i.e., typical mode I cracks).

Numerous coated non-<001> oriented PWA 1480 specimens tested under isothermal conditions failed from porosity adjacent to the coating or uncoated ID surface. Examples of crack initiation sites from such specimens are presented in Figures 42 to 44. Contrary to that experience, out-of-phase TMF tests produced failures which originated from coating cracks in a manner consistent with Pratt & Whitney's experience with coated single crystal airfoils. Typical TMF failures are presented in Figures 45 to 47. Therefore, in keeping with the main intent of this program, i.e., to develop models relevant to gas turbine airfoils, the TMF testing effort was substantially increased and the isothermal fatigue testing effort was reduced accordingly.

Figure 41 Transverse Micrograph of Specimen JB-102 Showing Coating Crack Morphology

50X

200X

Figure 42   Secondary Electron Image of PWA 273 Aluminide Coated <111> PWA 1480
Specimen LB-124 After Isothermal LCF Testing At 760°C (1400°F),
+0.3%, 0.5 cpm for 1372 cycles. Arrow indicates location of
subsurface PWA 1480 porosity where crack initiation occurred.

Figure 43   Optical Microscopy Image of PWA 286 Overlay Coated <011> PWA 1480
Specimen KB-65 After Isothermal LCF Testing At 927°C (1700°F),
+0.25%, 1 cpm for 6624 cycles. Arrow indicates location of
subsurface PWA 1480 porosity where crack initiation occurred.

58

Figure 44   Optical Microscopy Image of PWA 286 Overlay Coated <213> PWA 1480
Specimen MB-38 After Isothermal LCF At 1038°C (1900°F), ±0.25%, 10
cpm for 8253 Cycles. Arrow indicates location of subsurface PWA
1480 porosity where crack initiation occurred.

Figure 45 Optical Microscopy Image of PWA 286 Overlay Coated <111> PWA 1480 Specimen LB-181 After Out-of-Phase TMF Testing At 427-1038°C (800-1900°F), ±0.125%, 1 cpm for 7675 Cycles. Arrow indicates typical coating initiated crack.
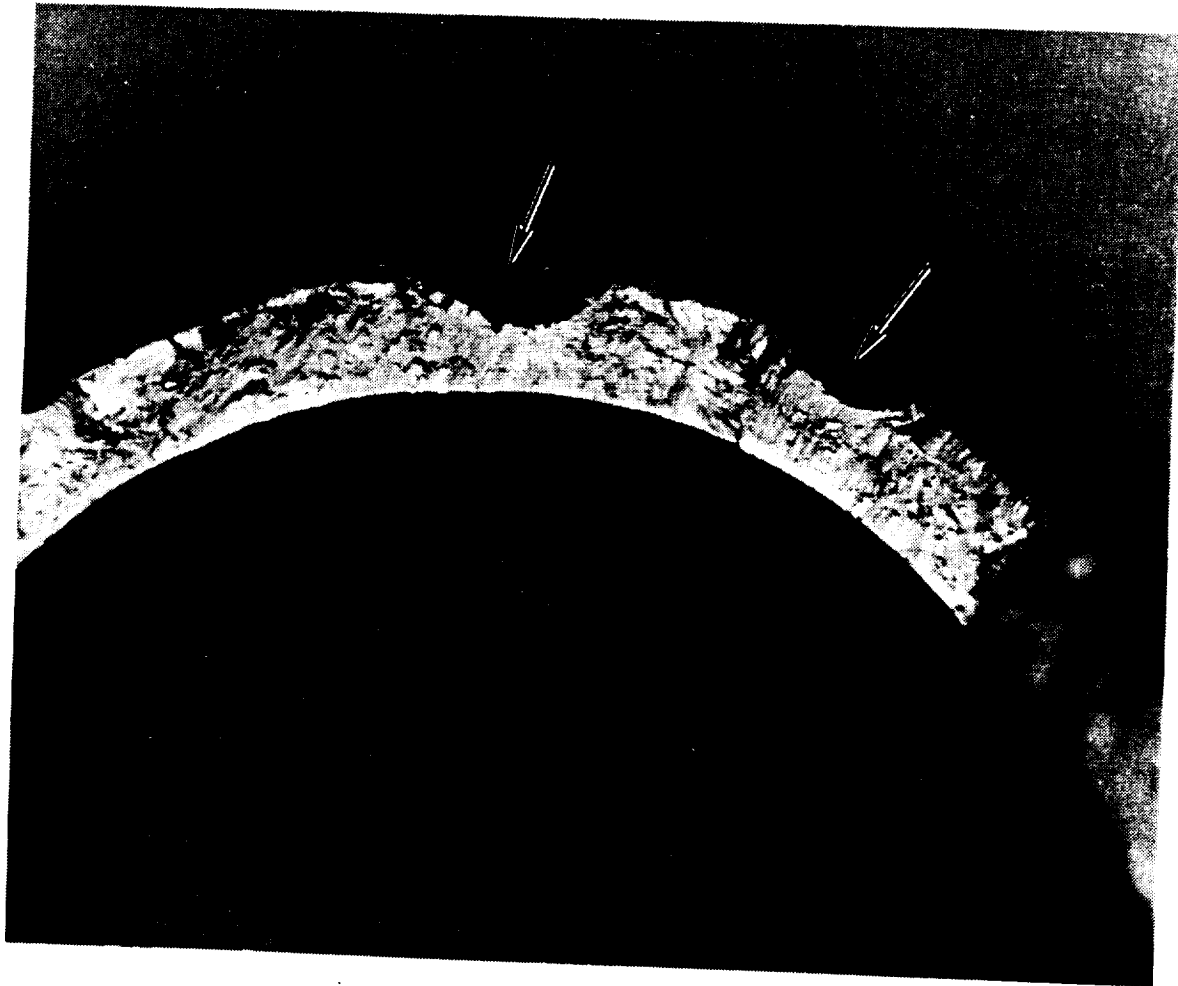
Figure 46   Optical Microscopy Image of PWA 286 Overlay Coated <011> PWA 1480 Specimen KB-24 After Out-of-Phase TMF Testing AT 427-1038°C (800-1900°F) ±0.15%, 1 cpm for 5927 cycles. Arrow indicates typical coating initiated crack.
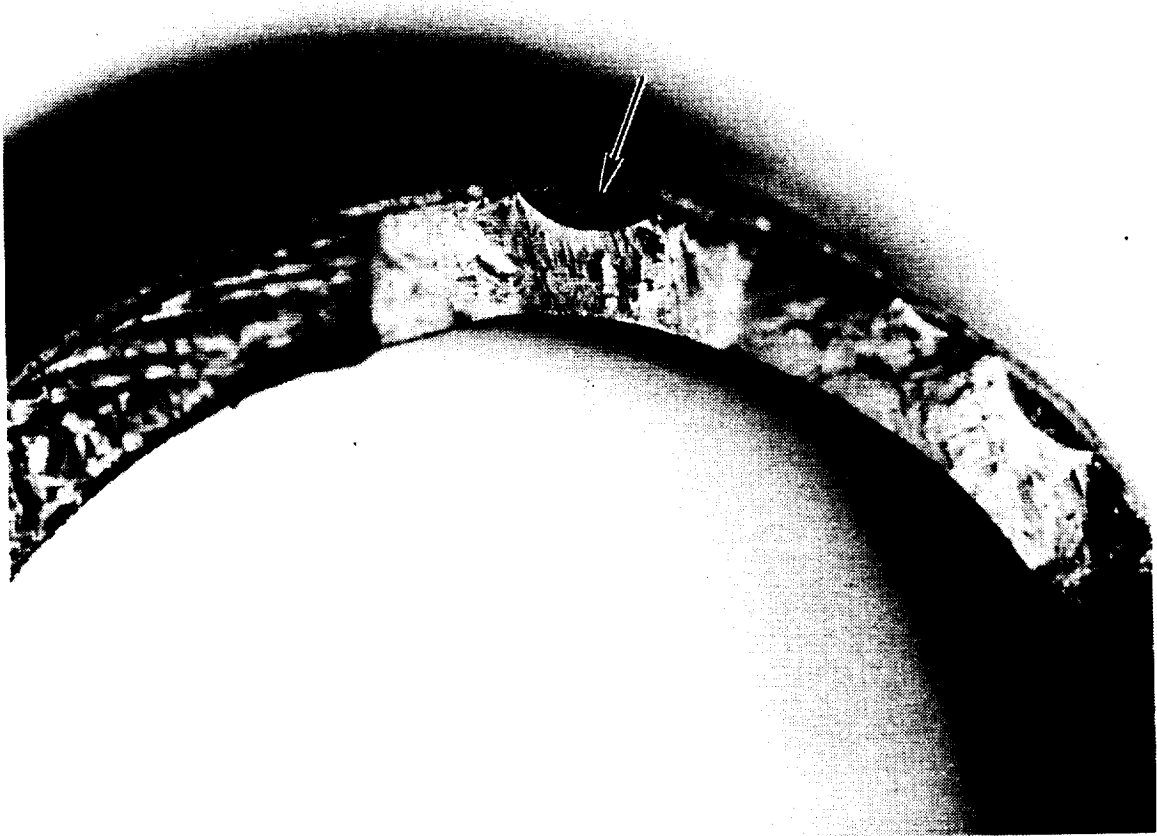
Figure 47 Optical Microscopy Image of PWA 286 Overlay Coated <213> PWA 1480 Specimen MB-17 After Out-of-Phase TMF Testing At 427-1038°C (800-1900°F), ±0.125%, 1 cpm for 7294 Cycles. Arrow indicates typical coating initiated crack.

7.2 EFFECT OF THERMAL EXPOSURE ON FATIGUE LIFE

A total of 12 coated PWA 1480 specimens were pre-exposed 100 hours at 1093°C (2000°F) before testing to determine the significance of thermal exposure on coated fatigue life. A summary of these test results are included in Appendices A and B.

7.2.1 Coating Materials

TMF coating lives for the pre-exposed specimens is presented in Figures 48 and 49. PWA 286 overlay coating out-of-phase TMF life was not significantly affected by the pre-exposure. Baseline PWA 273 aluminide TMF data is limited, however, the life trend suggests that pre-exposure is detrimental.
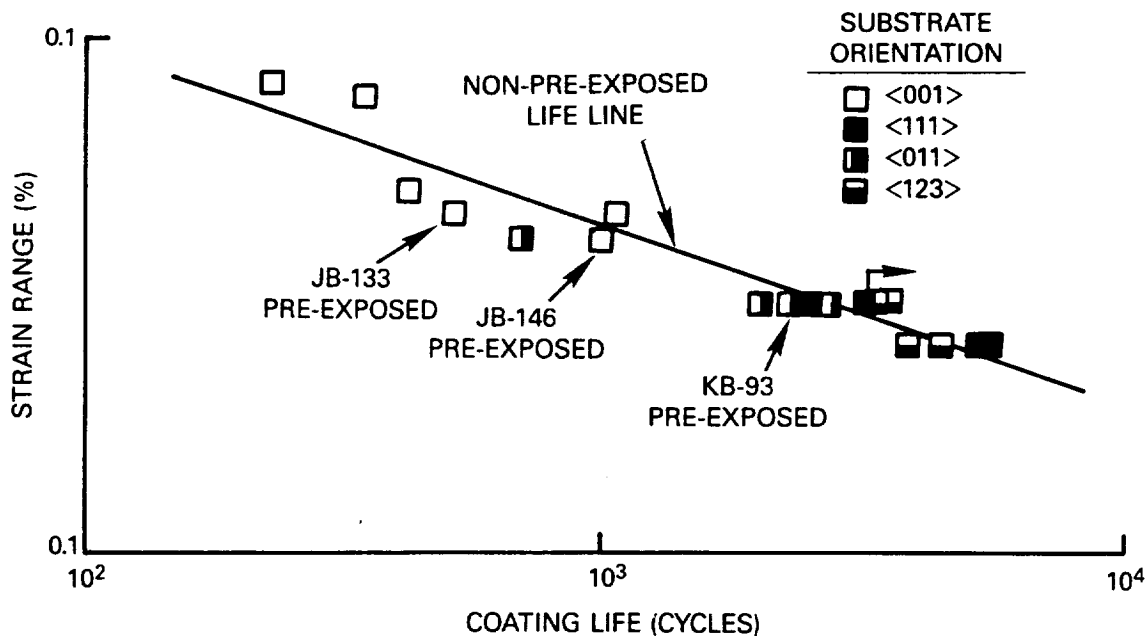
Figure 48   Strain Range Vs. Coating Life for PWA 286 Overlay Coated PWA 1480.
All tests are 427-1038°C (800-1900°F), 1 cpm, Out-of-Phase TMF.
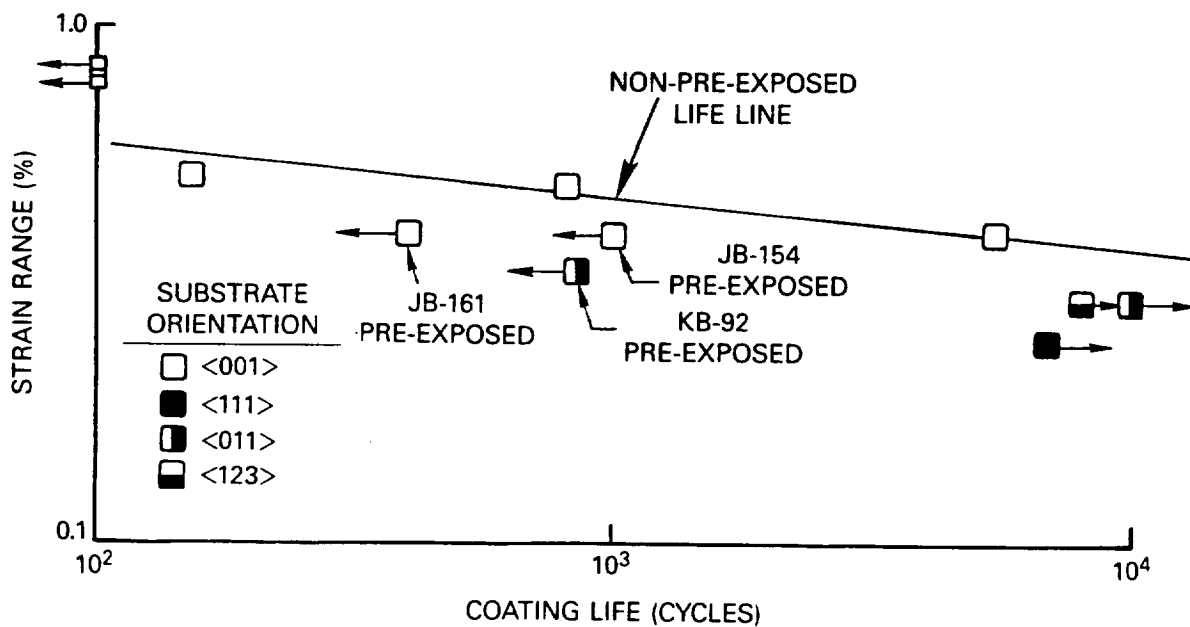
Figure 49   Strain Range Vs. Coating Life for PWA 273 Aluminide Coated PWA
1480. All tests are 427-1038°C (800-1900°F), 1 cpm, Out-of-Phase
TMF.

Insufficient information exists from which to conclude what specific physical mechanism causes the observed life trends. It is speculated, however, that the composition and microstructure evolution which occurs as a result of high temperature exposure is the main cause.

Coatings, by their very nature, are not stable alloys. High temperature exposure causes diffusion of aluminum towards the surface for oxidation protection and into the substrate. Depletion of aluminum precipitates formation of gamma prime and/or gamma matrix in the coating, principly at coating grain boundaries. Coating micrographs from pre-exposed specimens JB-133 and JB-154 are compared to non-pre-exposed micros from specimens JB-147 and JB-98 in Figures 50 and 51. As a result of these coating compositional and microstructural changes which occur during exposure, coating constitutive behavior and properties such as ductility and coefficient of thermal expansion are different than those obtained from virgin specimens.

One factor which may play a significant role is thermal expansion (see Figure 52). A NiCoCrAlY overlay coating is composed of aluminum rich beta (NiAl) and the heavier elemental gamma phases. This is a much more stable composition and microstructure than in an aluminide which is initially composed of the beta phase. As diffusion occurs, more gamma phase is formed in both coatings, but the potential gradient for diffusion is higher in the aluminide than the overlay. Since gamma phase is generated, it is anticipated that the coefficient of thermal expansion increases for both coatings, but more rapidly in the aluminide. This suggests that the life of an aluminide is more sensitive to exposure than that of an overlay.

An increase in coating coefficient of thermal expansion is detrimental to coating life in cases when tensile straining is occurring during cooling (i.e., out-of-phase TMF). In such cases, higher tensile strains (or stresses) are produced. Aluminides, which have limited ductility at low temperatures, would be sensitive to such cases. For discussion purposes, hysteretic energies for the aluminide coating were generated using the PWA 286 overlay coating constitutive model with the aluminide coefficient of thermal expansion (i.e., unexposed coating coefficient of thermal expansion). The resulting life relationship for 427-1038°C (800-1900°F) out-of-phase TMF is presented in Figure 53. As shown in this figure, arbitrarily increasing the coefficient of thermal expansion by 10% produces a significant increase in hysteretic energy and nearly a 7X life reduction.

64

MAG: 500X

b)
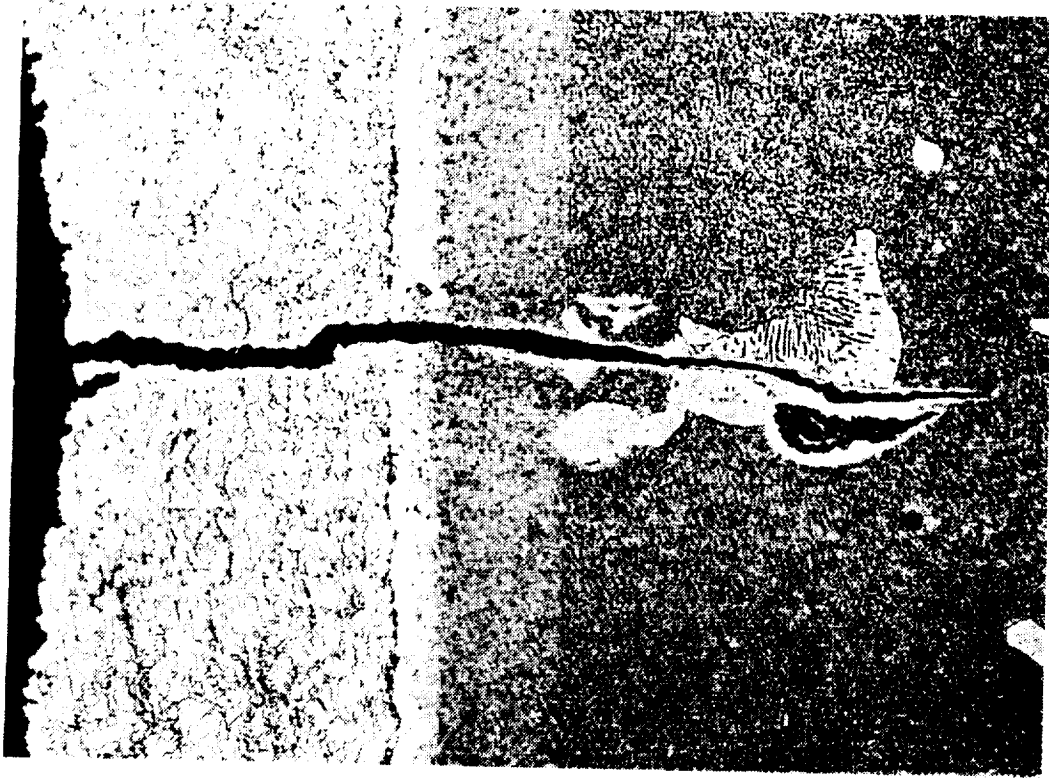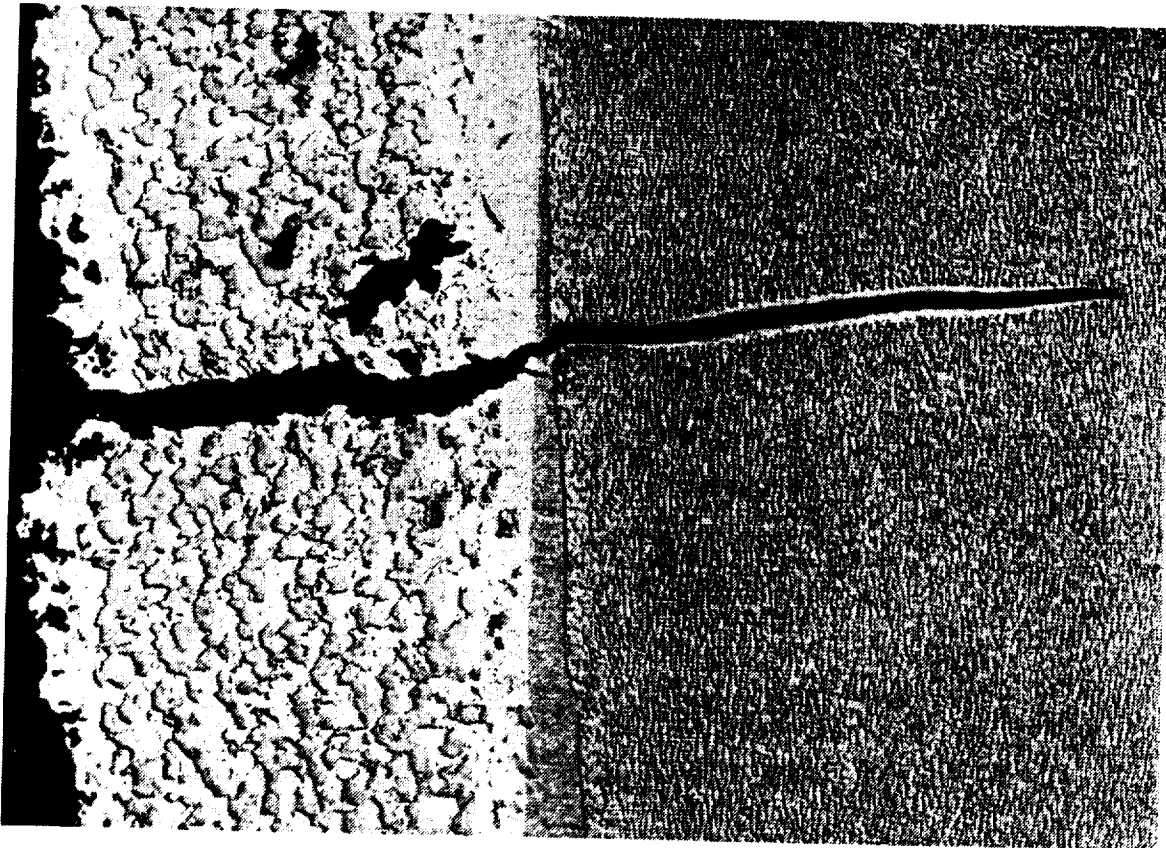
MAG: 500X

a)

Figure 50 Overlay Coating Microstructure of a) Pre-exposed Specimen JB-133 and b) Non-pre-exposed Specimen JB-147 TMF Tested at 427-1038°C (800-1900°F), ±0.225%, 1 cpm, Out-of-Phase

65

MAG: 500X

b)
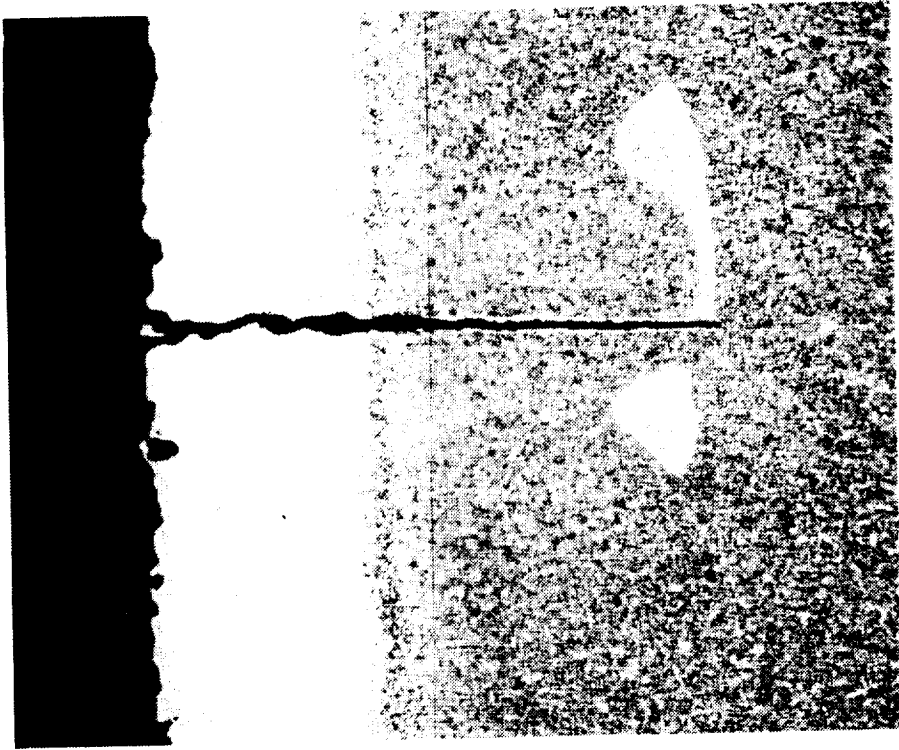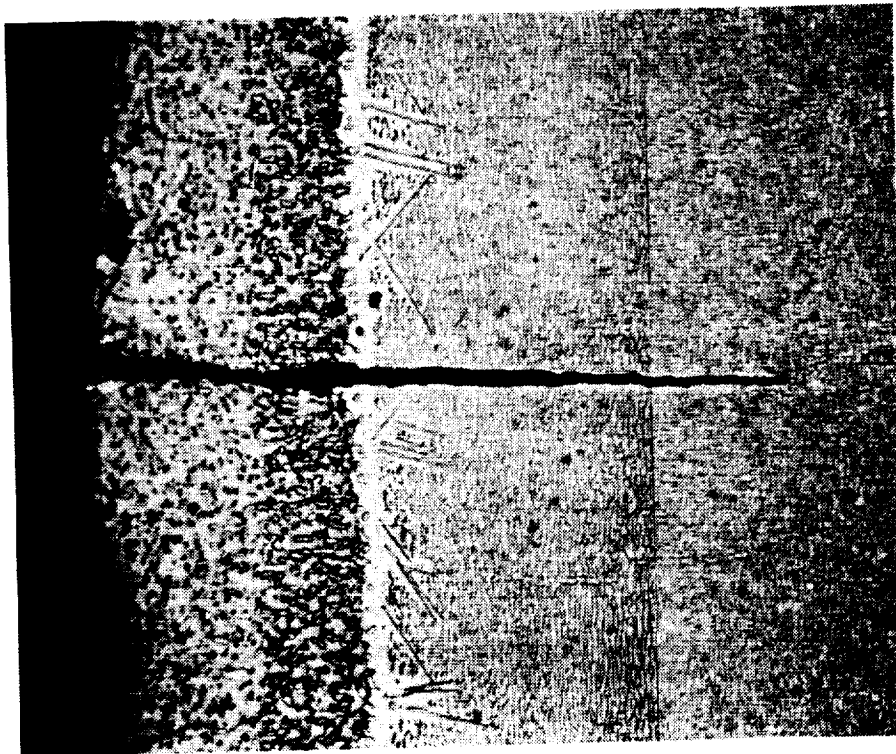
MAG: 500X

a)

Figure 51 Aluminide Coating Microstructure of a) Pre-exposed Specimen JB-154
and b) Non-pre-exposed Specimen JB-98 TMF Tested at 427-1038°C
(800-1900°F), ±0.2%, 1 cpm, Out-of-Phase

66
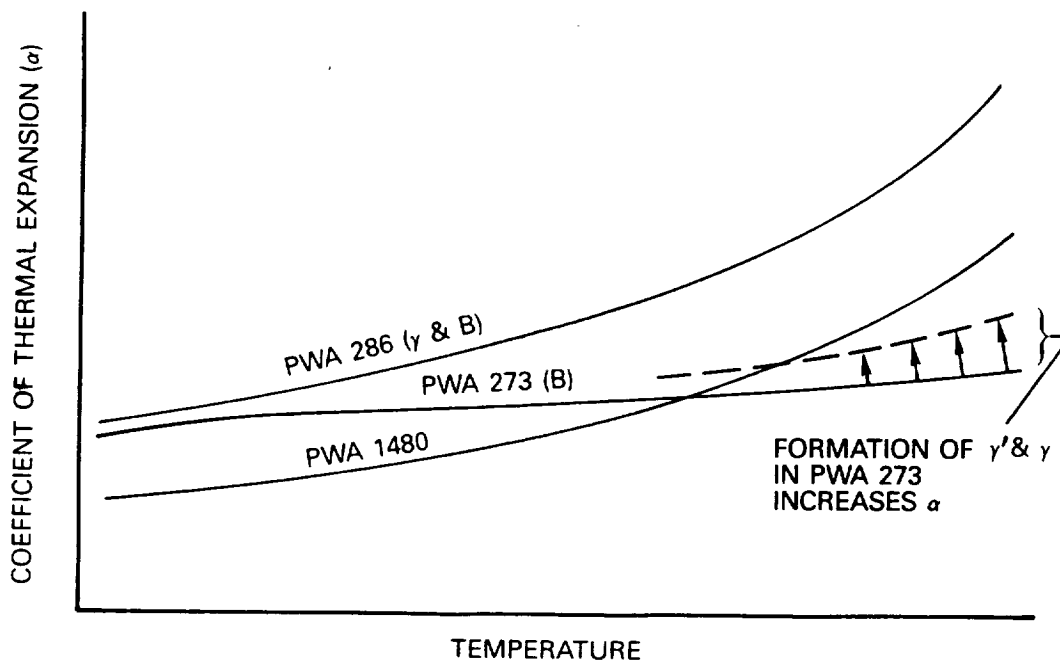
Figure 52   Coefficient of Thermal Expansion Vs. Temperature Trends
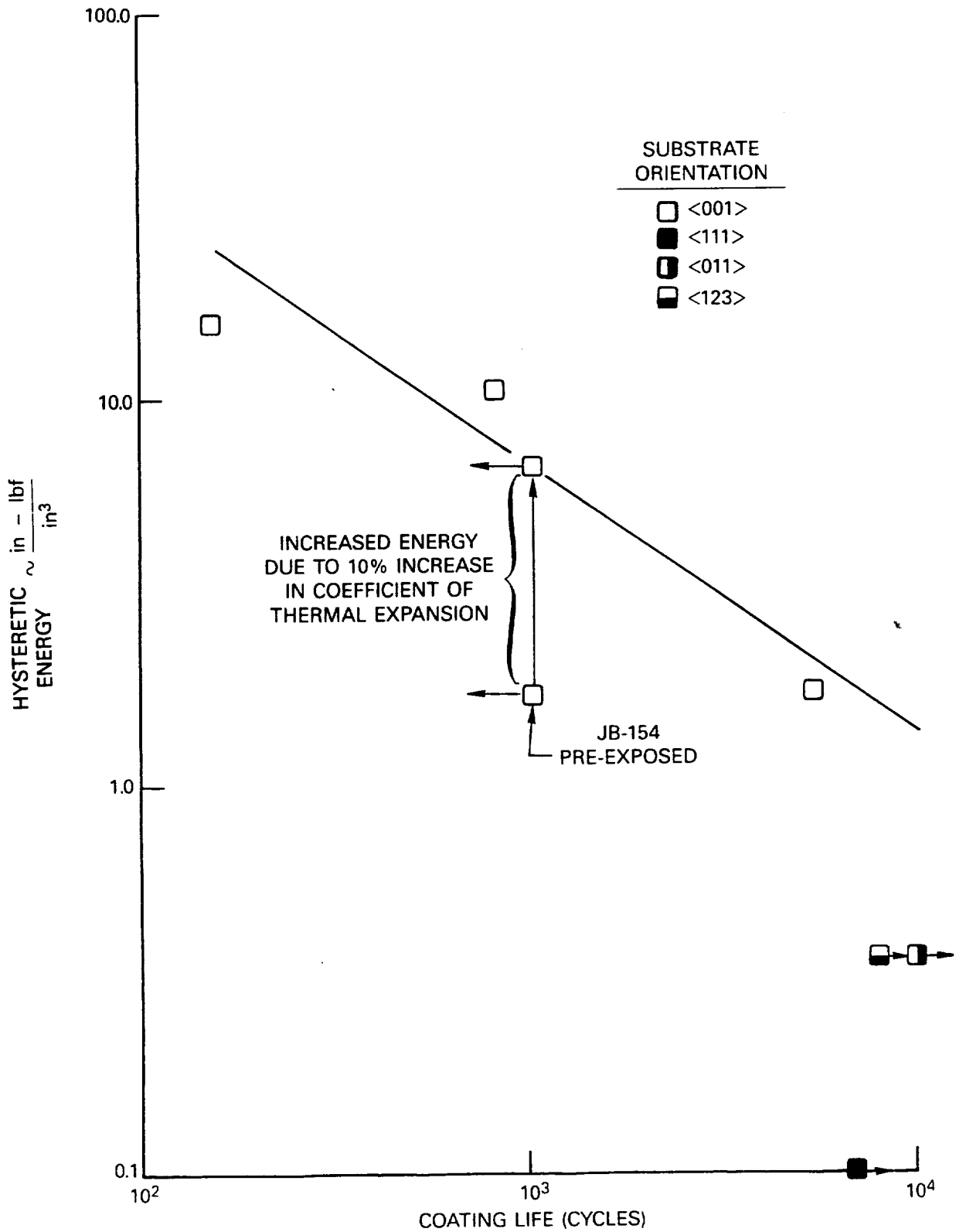
Figure 53   Hysteretic Energy Vs. Coating Life for PWA 273 Aluminide Coated PWA 1480. All tests are 427-1038°C (800-1900°F), 1 cpm, Out-of-Phase TMF.

7.2.2 PWA 1480 Single Crystal Material

The crack initiation (Nsc) and propagation (Nsp) lives for the pre-exposed specimens subjected to TMF are compared to TMF tested non-pre-exposed specimens in Figures 54 and 55, respectively. In general, the pre-exposure was found to be somewhat more detrimental to the propagation life than the crack initiation life. This observation suggests that the crack propagation rate of PWA 1480 (associated with Nsp) is more sensitive to thermal exposure than PWA 1480 crack initiation. However, the shorter pre-exposed specimen propagation lives were generally associated with crack geometries which generate high values of stress intensities. Thus, it is felt that pre-exposure had little overall effect on PWA 1480 TMF life.
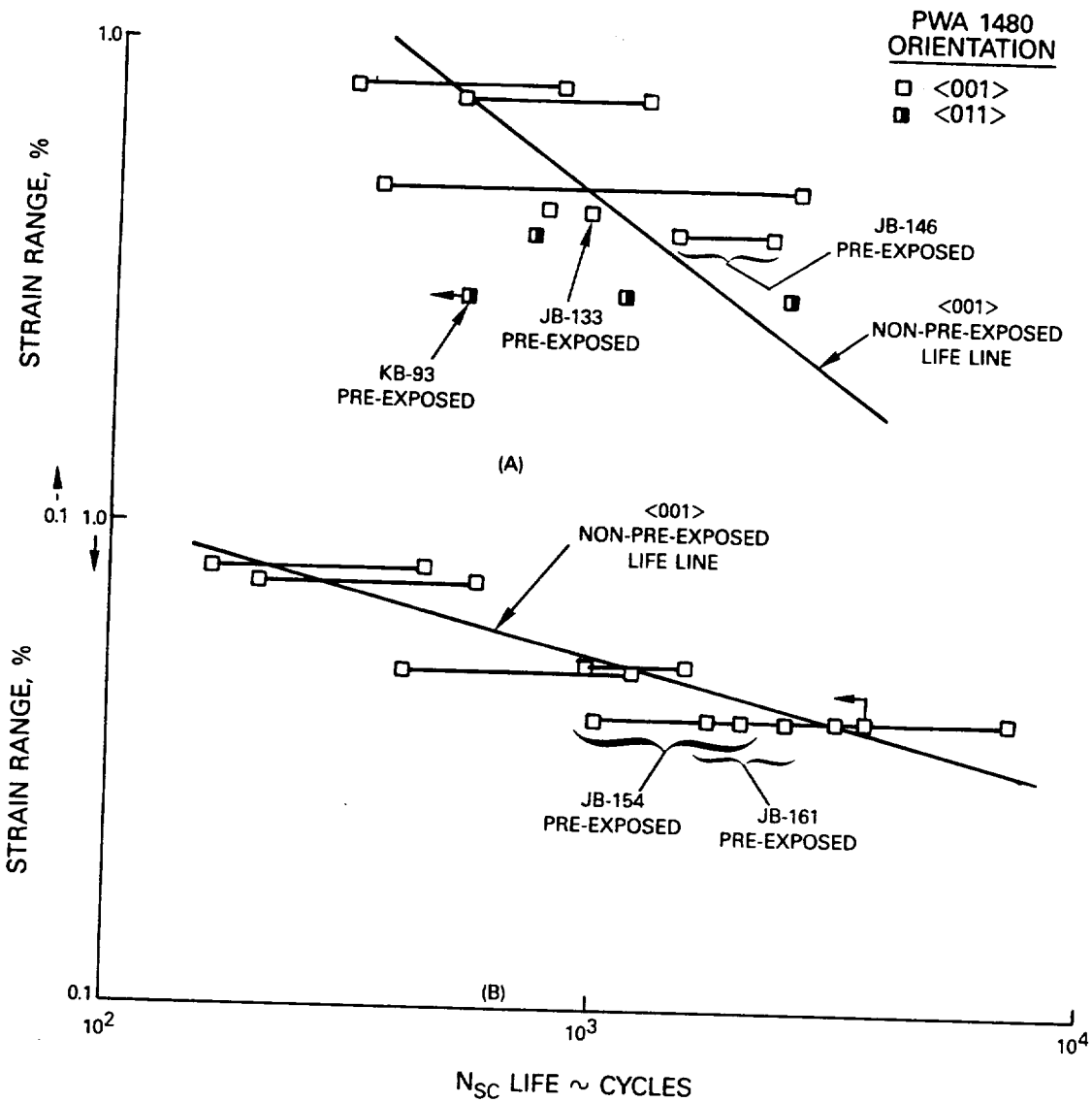
Figure 54   Strain Range Vs. PWA 1480 Crack Initiation Life (Nsc) for A) Overlay Coated Specimens and B) Aluminide Coated Specimens Subjected to 427-1038°C (800-1900°F), 1 cpm, Out-of-Phase TMF
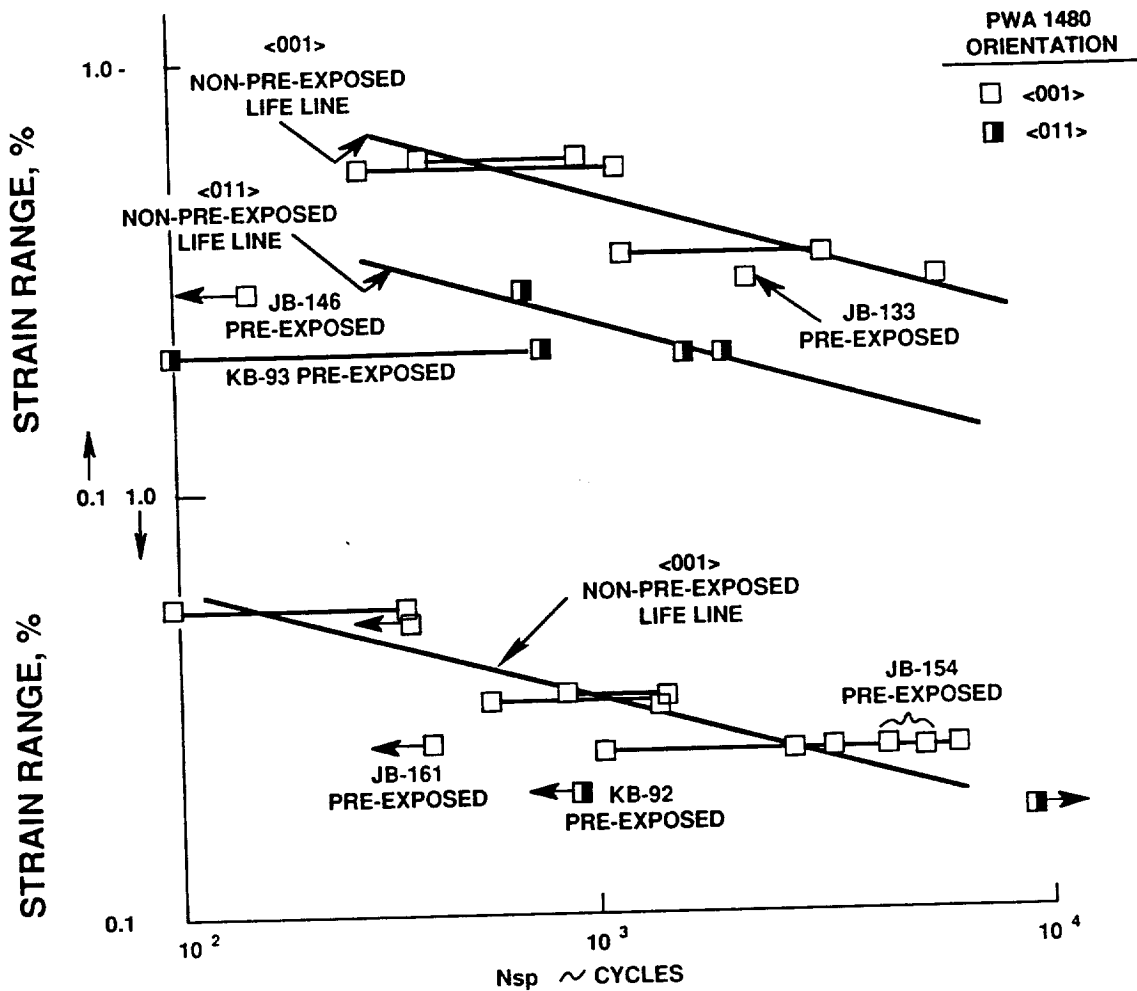
Figure 55 Strain Range Vs. PWA 1480 Propagation Life (N_{sp}) for A) Overlay Coated Specimens and B) Aluminide Coated Specimens Subjected to 427-1038°C (800-1900°F), 1 cpm, Out-of-Phase TMF

Microstructure changes also occur in gamma prime strengthened Ni-based superalloys. During high temperature exposure, the initially cuboidal gamma prime agglomerates (i.e., it can grow in size and lose its cuboidal shape). As reported by Cetel and Duhl in Reference 13, gamma prime size is optimized for the best combination of low temperature yield and high temperature creep strengths. They indicated, however, that gamma prime size can increase from an initial value of about 0.3 to 1.0 microns during severe thermal exposure. Tensile tests conducted at 593°C (1100°F) on <001> PWA 1480 specimens with varying gamma prime sizes indicated as much as a 20% drop in yield strength for the largest gamma prime sizes. Earlier, Shah and Duhl (Reference 14) reported similar compression yield strength trends for <001> and <111> PWA 1480 specimens of various gamma prime sizes. Comparison of the <001> and <111> data indicated that the yield strength reduction was much more pronounced in the <111> orientation and occurred over a wider temperature range than the

70

<001> orientation. Beyond 760°C (1400°F), there was little effect of gamma prime size on the yield strength of the <001> orientation which normally deforms by octahedral slip. This was attributed to the activated cube cross-slip model developed for "L12" compounds (References 15 and 16), provided that gamma prime shearing is the primary strengthening mechanism. For the <111> orientation which deforms by octahedral and cube slip, thermally activated cross-slip is irrelevant and gamma prime size is the controlling parameter. Thus, the <111> yield strength reduction with increasing gamma prime size occurs more uniformly across the temperature range.

7.3 MULTIAXIAL FATIGUE TESTS

Tension-torsion tests are planned for several coated specimens of two primary orientations for the PWA 1480 material. These tests are designed to verify the multiaxial capability of the constitutive and life models.

SECTION 8.0

TASK VI – FINAL SELECTION OF LIFE PREDICTION AND CONSTITUTIVE MODELS

8.1 COATING CONSTITUTIVE MODEL

To streamline the coating constitutive model development process, the overlay coating (PWA 286) was chosen as the model development vehicle. The final overlay coating model formulation may then be applied to the aluminide diffusion coating (PWA 273).

8.1.1 PWA 286 Overlay Coating

Poisson's ratio for PWA 286 was assumed equivalent to Hastelloy X. Based on the observed inelastic flow similarity between PWA 286 and Hastelloy X, Poisson's ratio for PWA 286 was obtained from Reference 8.

Checkout of the MARC (Reference 17) user subroutine HYPELA was completed for isothermal cases and MARC element types 7 and 21 (3D "brick" elements). As part of the checkout process, a study of the "reference" stiffness matrix concept (Reference 18) was conducted. A detailed description of the "reference" stiffness matrix concept is presented in Section 8.2. Results indicated that reassembly of the stiffness matrix is necessary for this material. In fact, cases in which the temperature was not equivalent to the reference temperature (temperature at which the reference stiffness matrix was formed) failed to converge.

Every convergence strategy available in the MARC version K.1 was considered, but none was successful. Evidently, this material's stiffness variation across the relevant temperature range is too great to use the reference stiffness matrix concept. Presumably, after a few attempts, an adequately small MARC increment size could be chosen to obtain convergence. However, the associated cost of conducting coated component analyses in such a manner is probably higher than the cost to reassemble the stiffness matrix.

A check on the effective inelastic strain increment size was included in the PWA 286 MARC HYPELA routine to prevent non-convergence during stress relaxation. Previously, PWA 286 HYPELA subincrement step size determination was based solely on mechanical strain, temperature, or time MARC increments only. During isothermal stress relaxation, however, strain and temperature increments are zero and the number of subincrements obtained from the time increment criterion is too small. This results in MARC convergence failure. Currently, when the effective inelastic strain increment size limit is exceeded, the number of subincrements is recalculated and the MARC increment is recycled through the subincrement loop. The effective inelastic strain increment size limit and the maximum number of subincrements allowed are user defined variables.

8.1.2 PWA 273 Aluminide Coating

Walker model constant regression for the aluminide coating is pending the reduction of the aluminide coating constitutive behavior test data.

8.2 SINGLE CRYSTAL CONSTITUTIVE MODEL

The micromechanical model rather than the macroscopic model was selected for final development. A preliminary version of the micromechanical model has been documented and delivered per NASA request along with a MARC test case for NASA's use in evaluating the model.

Effort concentrated on incorporating the slip system based constitutive model into the MARC finite element program with particular emphasis on nonisothermal loading.

Generally, if the temperature at any part of a structure experiences a temperature change from one increment to the next, the structural stiffness matrix is reformulated with the elastic constants at the new temperature. This is a time consuming task and has been circumvented by measures introduced in previous NASA sponsored constitutive modeling contracts (Reference 18). In brief, these measures set flags in appropriate MARC subroutines so that the structural stiffness matrix is formulated and inverted only once using elastic constants from a "reference temperature" and then include all elastic stress changes due to temperature variations (as well as actual inelastic stress increments) in the inelastic stress increment vector, G, supplied by the HYPELA subroutine. This method was incorporated into the slip system model HYPELA code.

In addition, a provision has been made for elastic behavior of selected elements in a structure. Such a feature was provided in the constitutive model for B1900+Hf in a previous NASA contract (Reference 19), and it was shown to be very desirable for analysis of large complicated structures that may have regions of confined inelasticity or regions where only "average" stiffnesses contribute to structural loads (e.g. internal pedestals in a turbine blade). For the elastic elements, the inelastic calculations are bypassed so that the contribution to the G vector (the inelastic stress increment) due to material inelasticity is zero. However, the contribution to G due to an elastic modulus change from the reference stiffness temperature will be included.

To improve low temperature model predictions, the low temperature model response was reformulated based on the observed rate independent material behavior. As temperature decreases below approximately 760°C (1400°F), PWA 1480 material becomes increasingly rate independent. This poses a fundamental difficulty for viscoplastic models which are formulated to be rate dependent. In the present model, the low temperature rate independence effectively imposes a severe constraint on the model constants, causing, for example, the exponent of the overstress to be very high for the octahedral systems. To overcome these concerns, the applied strain rates will be "transformed" to effective strain rates before being used with the same set of evolutionary equations. The transformation will be such that applied strain rates are preserved at high temperatures, while a constant (reference) strain rate will be achieved at low temperatures. In a transition temperature regime (approximately 649°C (1200°F) to 760°C (1400°F)), the effective strain rate transitions between the two limits. Symbolically, the transformation is:

73

$$E \text{ eff} = A \times E \text{ actual} + B$$

where
$$E \text{ eff} = \text{the effective strain rate}$$
$$E \text{ actual} = \text{the applied strain rate}$$

and the limits on the constants A and B are as follows:

Low Temperature Limit	Constant	High Temperature Limit
0	A	1
E ref	B	0

A routine was subsequently added to the HYPELA code that produces rate independent behavior at low temperatures. The model constants were fit to isothermal stress-strain data at temperatures of 760°C (1400°F) and above. At 649°C (1200°F) and below, the model constants were fit to monotonic tensile data. Because the thermal mechanical fatigue cycles of interest in this contract are nominally elastic below 649°C (1200°F) it was judged that this assumption would not severely affect the use of the model in the base program.

Another feature was added to the model to effect a controlled cycle-by-cycle relaxation of nonisothermal loops. It is a characteristic of viscoplastic models containing a back stress that over many cycles of loading the entire hysteresis loop will relax in stress until the back stress is approximately symmetric about zero global stress. The rate of relaxation of the loop is usually uncontrolled in that it is not explicitly modeled in the evolutionary equations for the state variables. Such is the case with the model developed in this program. That is, the model was formulated and the constants were fit to reproduce the stress-strain loop shape; long term cyclic evolution is not modeled. A mechanism has been included in the back stress evolutionary equations that will permit the user to exercise some measure of control over loop relaxation for nonisothermal simulations.

The micromechanical HYPELA code was checked out using simple one element test cases. An out-of-phase thermal mechanical fatigue cycle, similar to that conducted on specimen LB-34, was used as one of the test cases. Figure 56 compares the test case strain-temperature cycle to that imposed on specimen LB-34. In each cycle the strain-time variation is sinusoidal over a period of 60 seconds. The MARC test case results and the experimental results from LB-34 are shown in Figure 57.

No obvious incompatabilities with the MARC code were observed in the test cases. In spite of the relatively large load steps in some portions of the TMF cycle, convergence was achieved without recycling. The load increments are shown in Figures 56 and 57. Additional test cases, using even larger load increments and a strain hold period at the high temperature end of the cycle also executed well. The test case load increments are expected to be larger than those that would be employed in a transient analysis of a turbine airfoil. For example, in a previous NASA HOST contract (Reference 19), the load increments corresponded to 10°C (50°F) temperature increments.

74
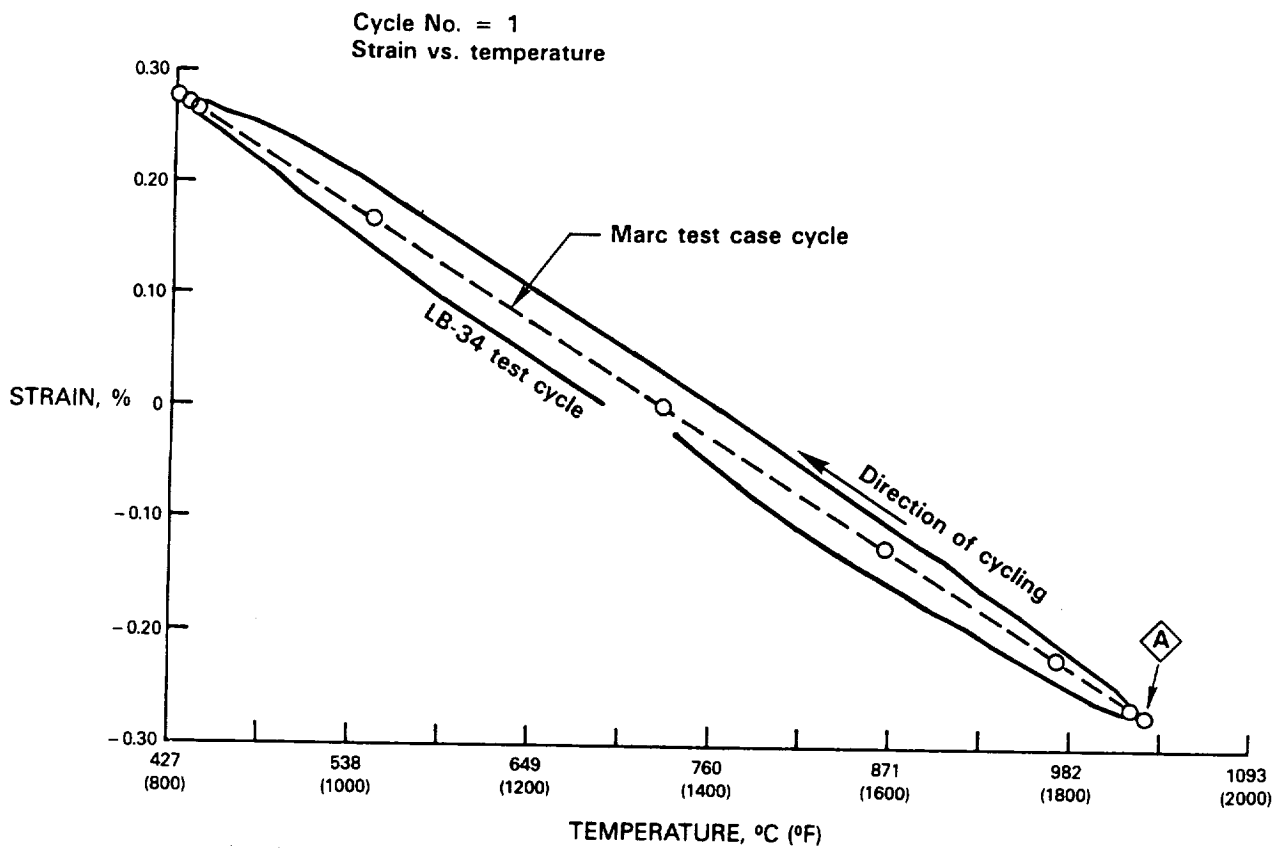
Figure 56 Strain Vs. Temperature Waveforms of LB-34 Compared to the One Used In the Test Case

75
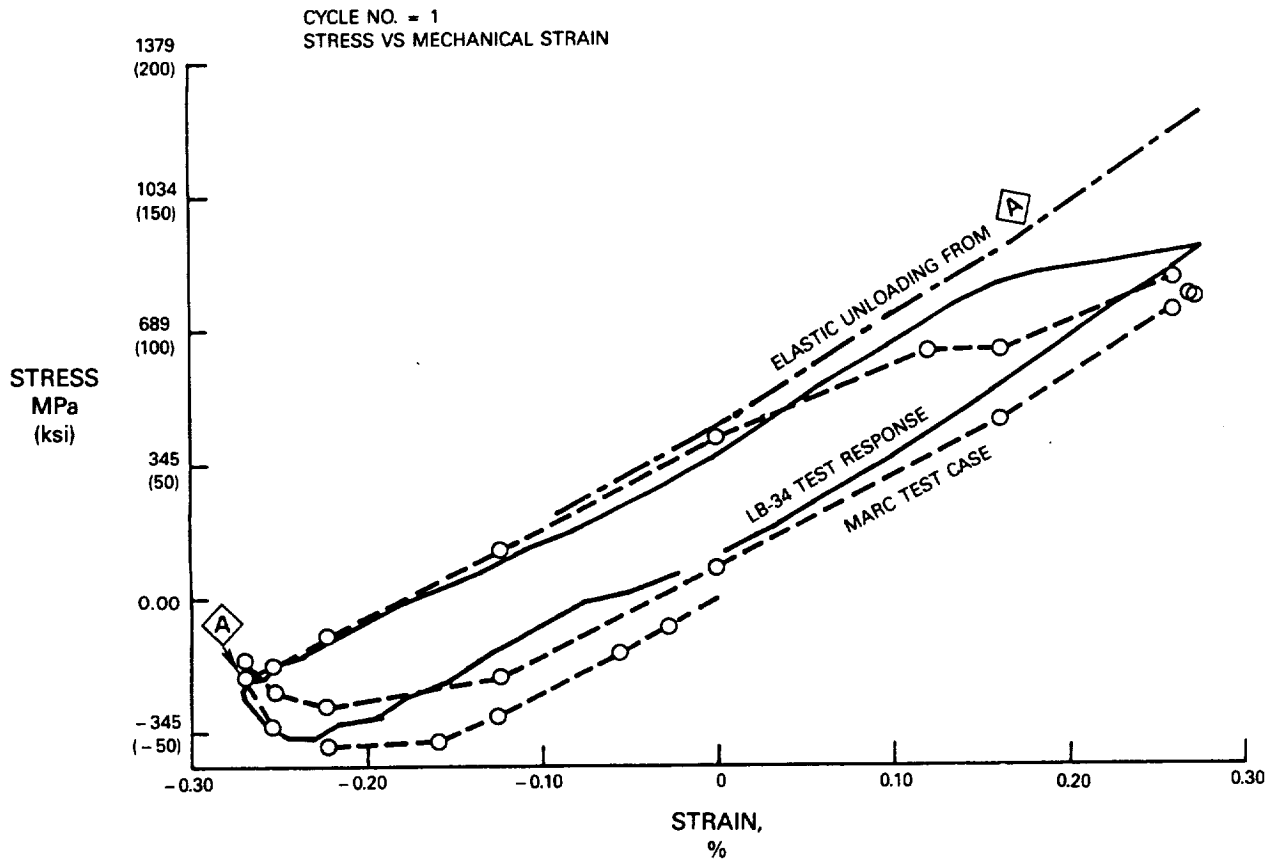
Figure 57   Predicted Vs. Actual Behavior of Specimen LB-34

8.3   COATED SINGLE CRYSTAL LIFE PREDICTION MODELING

Fatigue life for coated single crystal materials was defined in Section 6.3.

8.3.1   Coating Life Models

The tensile hysteretic energy life model was selected for the coating life modeling effort based on initial model evaluations (see Section 6.3.1). Like the coating constitutive modeling effort, PWA 286 overlay coating was used as the model development vehicle. The selected model may then be applied to the PWA 273 aluminide coating.

PWA 286 Overlay Coating

Inspection of the tensile hysteretic energy correlation of the isothermal fatigue data presented in Section 6.3.1 showed the data to be segregated by temperature and cycle frequency (Figure 28). In general, the segregation was greatest for 1038°C (1900°F) (hottest temperature) and 1 cpm (longest cycle time) conditions, indicating a need for temperature- and time-dependent damage correction to the stress/strain damage measured by tensile hysteretic energy. Based on this, a term similar in form to that used by Ostergren for time dependent damage (Reference 20) was included in the life prediction model:

$$Nc = C * W_t^{-B} * Freq^m \qquad (29)$$

where: Nc = Coating cracking life
           W_t = tensile hysteretic energy for the coating
           $Freq$ = correction for temperature- and time-dependent damage
           C, B, m = material dependent constants

In this case, however, Ostergrens' time dependent damage term, Freq, was extended to include temperature effects by introducing a temperature dependent damage rate which, in combination with the time, describes damage (equation 30. The damage rate is formulated by an equation usually applied to thermally activated processes, such as oxidation and diffusion (equation 32). Since 'Freq' is defined as a correction for temperature- and time-dependent damage, Freq < or = 1.0 by definition. A change from Ostergrens' model is that compressive hold time contributes to damage, but at a reduced rate.

$$Freq = \frac{1.0}{\frac{r(T)}{r(To)} * (t - to)} \qquad (30)$$

or,

$$Freq = \frac{1.0}{\frac{r(T)}{r(To)} * t - Do} \qquad (31)$$

$$r(T) = r_o \exp(-Q/T) \qquad (32)$$

where: T = cycle temperature (K or R)
           To = threshold temperature for temperature dependent damage, assumed to be 1088K (1960R)
           t = total cycle time (min), including 100% of tensile hold and 30% of compressive hold times, if any.
           to = incubation time (min)
           Do = "incubation damage"
           Q = effective activation energy for temperature- and time-dependent damage

77

Figure 28 data after correction for temperature/time damage are presented in Figure 58. Model constants were determined from the data as follows:

Constant:	Value:	Source:
C	44450.	Fit of 927 and 1038°C (1700 and 1900°F) isothermal data
B	-.820	Fit of 760°C (1400°F) isothermal data (unaffected by temperature and time correction)
m	.414	Fit of 1038°C (1900°F) isothermal data for three test frequencies
To	1960.	Assumed
Q	51100.	Fit of 927 and 1038°C (1700 and 1900°F) isothermal data
Do	9.985	Fit of 1038°C (1900°F) isothermal data for three test frequencies

Application of the cycle temperature/time correction to variable temperature (TMF) conditions is possible by summing (or integrating) damage increments for all temperatures in the TMF cycle.

$$Freq = \frac{1.0}{\sum_{cycle} \frac{r(Ti)}{r(To)} * ti - Do} \qquad (33)$$

where: Ti = individual temperature levels in the cycle (K or R)
ti = time at Ti (min), including 100% of tensile hold and 30% of compressive hold times in the cycle, if any.

The overlay coating life model was subsequently applied to an expanded data set. A plot of predicted vs. actual lives is presented in Figure 59. All the lives were collapsed within a factor of about 2.5. Generally, the worst predicted test lives were limited to 1149°C (2100°F) maximum temperature TMF tests. Prediction of those tests may improve when 1149°C (2100°F) isothermal tests are included in the data set used to determine model constants.

78
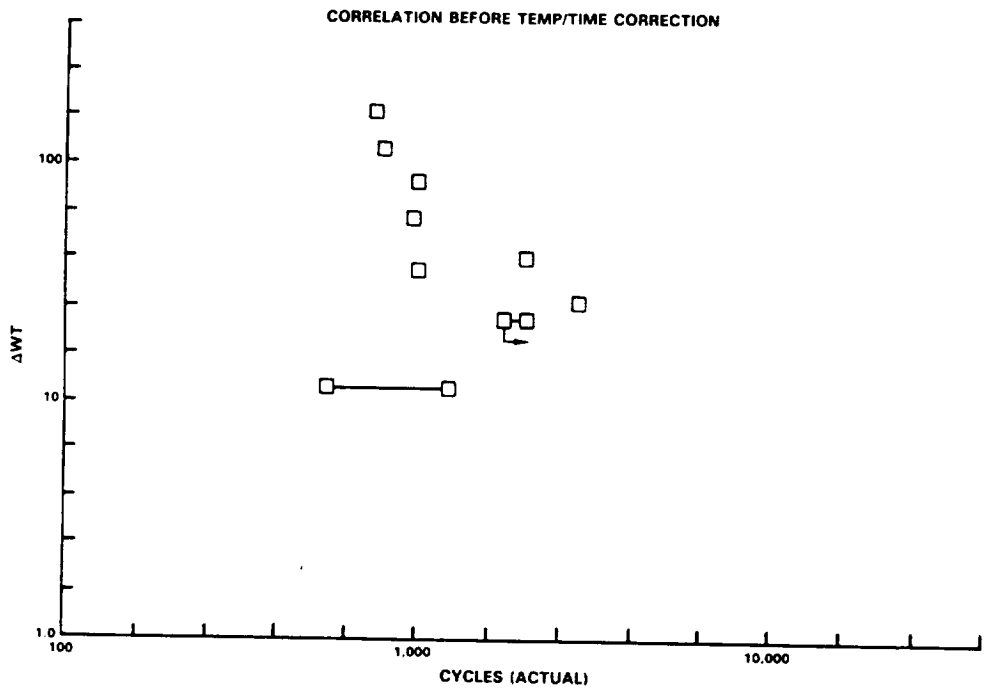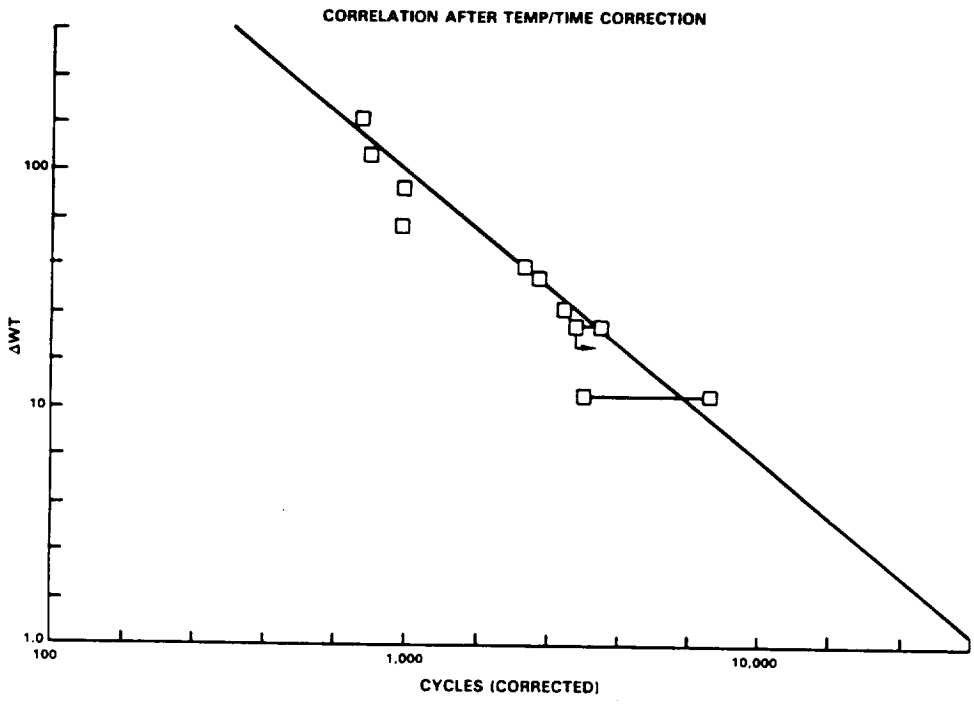
Figure 58 PWA 286 Coating Fatigue Life Model: (a) Correlation Before Temperature/Time Correction (b) Correlation After Temperature/Time Correction

79

ISOTHERMAL LCF
427, 760, 927, 1038°C
(800, 1400, 1700, 1900°F)

TMF
427-1038 or 427-1149°C
(800-1900 or 800-2100°F)
VARIOUS ϵ-T CYCLES

$$N_c = 44450 \cdot \Delta W_t^{-.82} \cdot \nu^{.414}$$

PREDICTED LIFE ~ CYCLES

ACTUAL LIFE ~ CYCLES
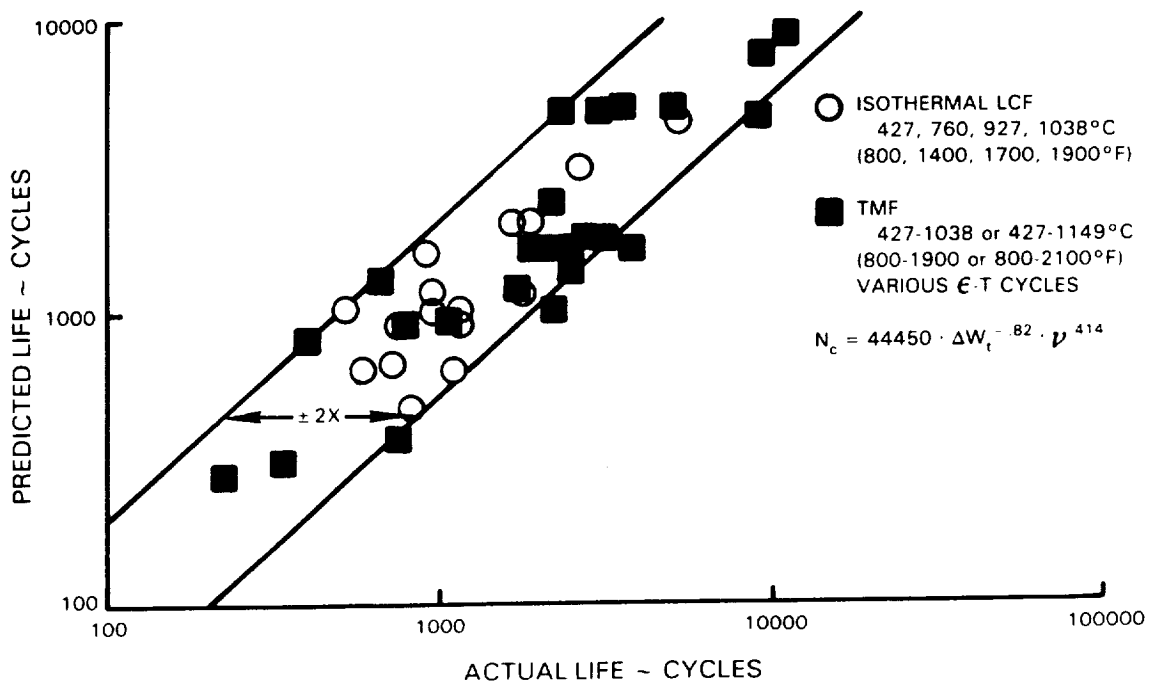
Figure 59 PWA 286 Coating Model Prediction of Isothermal LCF and TMF Life.
Note: All hysteresis loops were predicted using the PWA 286
constitutive model incorporated into a two-bar mechanism.

Effects of Thermal Exposure

The proposed coating life model lumps exposure effects during cycling into a
temperature- and time-dependent term. Presuming that similar compositional and
microstructural events occur whether pre-exposed or exposed during cycling,
the temperature- and time-dependent term may be correlated from data of either
type. However, since airfoils are exposed during cycling, data from cyclic
tests is preferred. Exposure may be incorporated into a TMF test by using hold
times at maximum temperature.

Future Developments

Additional coating life model enhancements are proposed which incorporate
multiaxial and hold time damage calculations. These formulas are required for
general model application.

It is well known that biaxial loads are introduced into the coating of a
coated specimen during thermal cycling due to coating/substrate thermal growth
mismatch. This biaxial loading contribution to coating damage cannot be
ignored. For example, MARC finite element analysis of a simple two element
structure was performed to obtain the coating hysteretic response to a
uniaxial, out-of-phase TMF test conducted at 427-1038°C (800-1900°F), ±0.15%,
and 1 cpm. The predicted hysteresis loop from the finite element analysis is
compared to the predicted loop from a one-dimensional analysis in Figure 60.

80
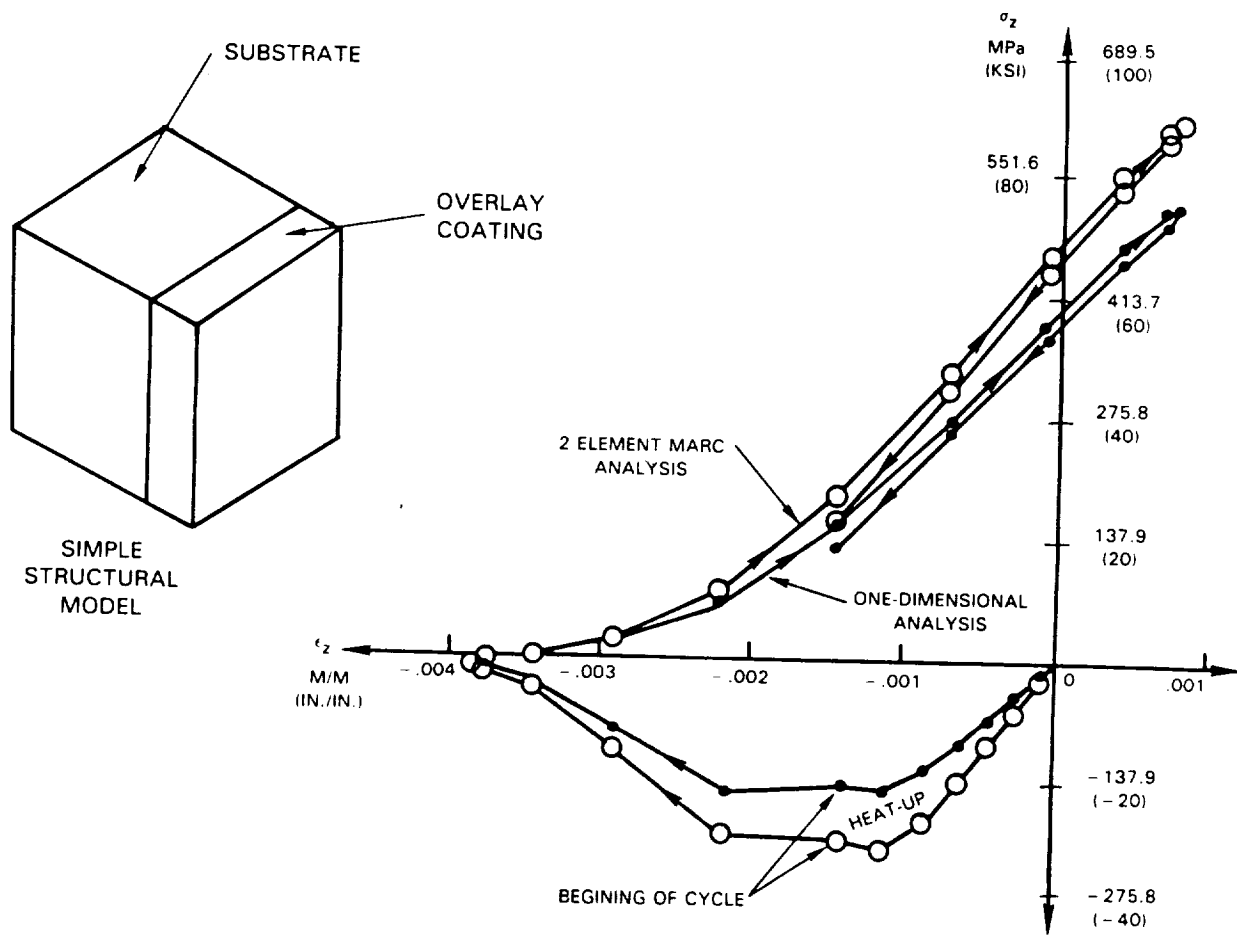
Figure 60   Predicted PWA 286 Coating Response to 427-1038°C (800-1900°F)
±0.15%, 1 cpm, Out-of-Phase Uniaxial TMF Test. A hypothetical
material with elastic moduli equivalent to <001> PWA 1480 was
assumed for the substrate.

To study the impact of biaxial loading on coating life, the coating hysteretic
energy was obtained from the finite element analysis results by the method
proposed by Garud (Reference 21), except only the tensile energy was
accumulated. For this condition, biaxial coating loads increased the tensile
energy 70% which would reduce the calculated life by a factor of about 1.5
using the current life model constants.

In the current life model, hold times are treated independent from the
transient portions of a given cycle. It is easy to distinguish hold times in
uniaxial fatigue tests, but for engine conditions, some judgement is required.

Judgements inevitably lead to inconsistent model application among different
users. In an effort to reduce model application inconsistencies, an expression
has been formulated which describes a hold time as a cyclic condition during
which a negligible mechanical strain change occurs. Integration of the
temperature- and time-dependent (i.e. frequency) term of the model uses an
effective time increment, dteff, which is defined as:

$$dteff = F * dt ,$$

(34)

81

where dt is the actual time increment and

$$F = 1 + (a - b * tanh(s) - 1) * exp(-c * abs(\dot{\epsilon}))$$ (35)

s = flow stress (sig-omega)

$\dot{\epsilon}$ = mechanical strain rate

a,b,c = constants

a = average of tension and compression hold time factors

b = a - tension hold time factor

Using the model hold time factors reported previously, a = 0.65 and b = -0.35. The function, F, is presented in Figure 61 for c = 10000.
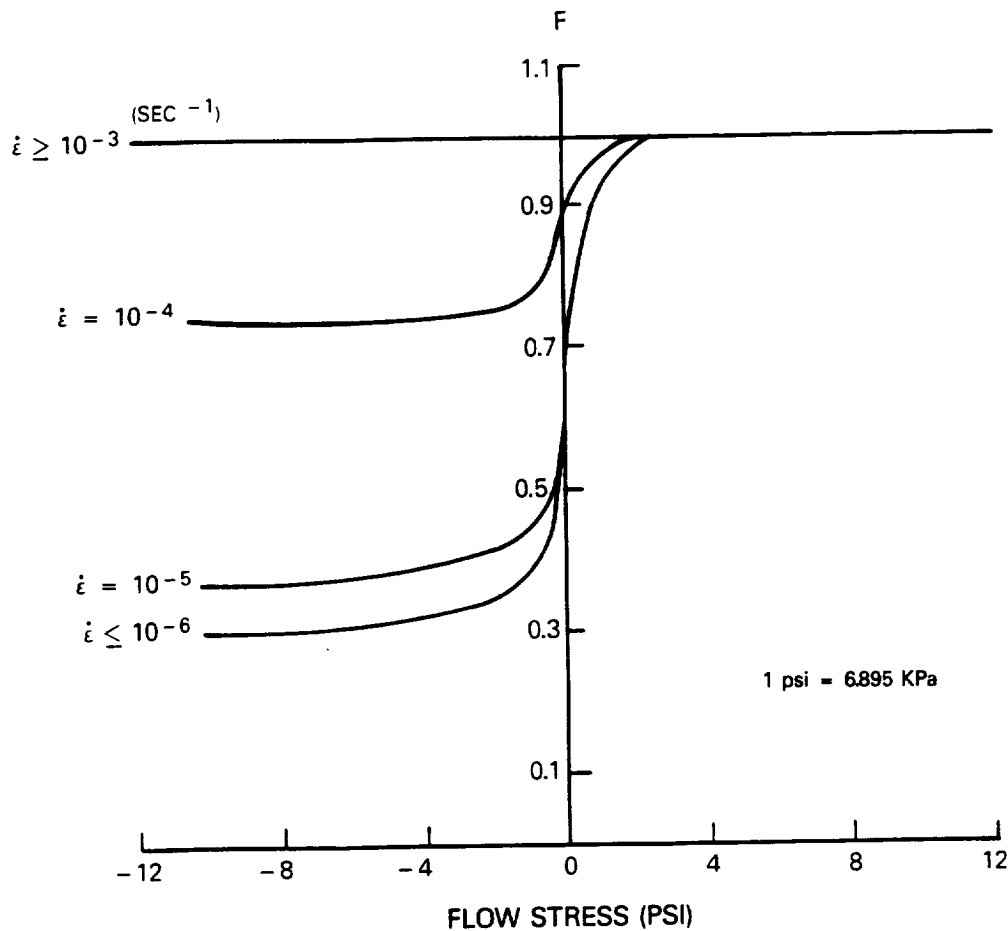
Figure 61   Hold Time Function, F, for C = 10000. For compression holds F = 0.30 and for tension holds F = 1.0.

PWA 273 Aluminide Coating

A review of cyclic data indicated that additional aluminide coated TMF tests are required to obtain cyclic thermal exposure data useful for determining the temperature- and time-dependent term constants. Isothermal fatigue test lives are not impacted by a change in coefficient of thermal expansion and are, therefore, of limited value for obtaining thermal exposure effects life data.

See Section 7.2 for a discussion of the effect of thermal expansion on aluminide coating life. Supplemental TMF tests are planned to obtain the required data.

8.3.2 Single Crystal Life Models (Coated)

Six candidate TMF life prediction models were assessed based on their ability to predict the life associated with growing a coating crack 0.254 mm (0.010 in.) deep into PWA 1480 (Nsc). The six models were:

1) Cyclic Damage Accumulation (CDA)

2) Modified Strain Range

3) Crack Tip Opening Displacement ("CTOD")

4) Crack Tip Opening Displacement using variable yield strength ("CTODgp")

5) Hysteretic Energy Approach

6) Maximum Tensile Stress

The data used in this study were obtained from PWA 286 coated PWA 1480 cylindrical tube specimens subjected to various TMF cycles. Most of the TMF cycles were of the out-of-phase type which was considered typical for gas turbine airfoils. The baseline TMF data used to obtain model constants is presented in Table 5, and the verification TMF data used to assess the predictive capability of each model is presented in Table 6.

TABLE 5

BASELINE TMF DATA SET

Spec ID	Nom. <hkl>	Max. Temp (F)	Strain Range (%)	Cycle Type	Stress Range (Ksi)	Tensile Stress (Ksi)	Initiation Life, Nsc (Cycles)
JB-147	<001>	1900	0.45	out-of-phase	64.5	51.9	1160
JB-10	"	"	0.50	" " "	78.0	56.1	440-2600
JB-9	"	"	0.76	" " "	109.5	84.8	500-1300
JB-80	"	"	0.80	" " "	120.3	105.8	440-870

Notes: 1) Minimum temperature for all cycles was 427°C (800°F).
2) Stress range and tensile stress were determined at half the distance (in cycles) from coating cracking life, Nc, and substrate plus coating cracking life, Nc + Nsc.
3) Stresses were corrected for coating load share based on a 1-D analysis.
4) 1038°C = 1900°F

TABLE 6

VERIFICATION TMF DATA SET

Spec ID	Nom. <hkl>	Max. Temp (F)	Strain Range (%)	Cycle Type	Stress Range (Ksi)	Tensile Stress (Ksi)	Initiation Life, Nsc (Cycles)
JB-121	<001>	"	0.45	out-of-phase	58.9	48.3	1470
JB-137	"	"	"	" " "	61.0	51.5	1250
JB-104	"	"	0.60	T-cycle	95.1	48.7	3712
JB-21	"	"	0.80	Z-cycle	120.5	91.9	550-657
JB-111	"	2100	0.35	out-of-phase	44.3	42.6	2200-4300
JB-89	"	"	0.50	" " "	67.6	65.9	1100-1600
JB-133	"	1900	0.45	" " "	67.6	52.8	1130
LB-170	<111>	1900	0.25	out-of-phase	85.7	92.1	1210
LB-181	"	"	"	" " "	94.7	101.9	1140
LB-27	"	"	0.30	" " "	119.5	99.8	350
LB-29	"	"	"	baseball,cw	109.3	61.3	700-1300
LB-26	"	"	0.50	T-cycle	201.4	99.0	>1210
LB-216	"	2100	0.23	out-of-phase	85.8	78.2	840
LB-239	"	"	0.25	" " "	90.8	87.0	800
KB-32	<011>	1900	0.30	out-of-phase	77.0	54.2	2190
KB-24	"	"	"	" " "	80.1	80.1	1250
KB-34	"	"	0.40	" " "	117.2	96.6	780
KB-48	"	2100	0.25	" " "	65.2	65.7	>1180
KB-52	"	"	"	" " "	65.0	58.8	1100

TABLE 6 (Continued)

Spec ID	Nom. <hkl>	Max. Temp (F)	Strain Range (%)	Cycle Type	Stress Range (Ksi)	Tensile Stress (Ksi)	Initiation Life, Nsc (Cycles)
MB-17	<123>	1900	0.25	out-of-phase	74.6	80.8	2680
MB-23	"	"	"	" " "	56.8	45.5	3130
MB-22	"	"	0.30	" " "	91.0	81.1	<1912
MB-8	"	"	"	" " "	81.9	73.3	1830
MB-19	"	"	"	" " "	66.0	56.0	<3200
MB-35	"	2100	0.23	" " "	70.8	70.5	1140
MB-37	"	"	0.25	" " "	74.0	74.1	1070

Notes: 1) Minimum temperature for all cycles was 427°C (800°F).
2) Stress range and tensile stress were determined at half the distance (in cycles) from coating cracking life, Nc, and substrate plus coating cracking life, Nc + Nsc.
3) Stresses were corrected for coating load share based on a 1-D analysis.
4) 1038°C = 1900°F ; 1149°C = 2100°F

Cyclic Damage Accumulation (CDA)

The CDA model is currently under development for isotropic Ni-based superalloy materials in a companion contract, NAS3-23288. Its formulation is based on the notions that 1) absolute levels of damage are difficult to calculate, thus the damage should be ratioed to a reference fatigue condition and 2) the fatigue capability of a material is intimately tied to its available ductility which is exhausted on a cycle by cycle basis. The available ductility was linked to tensile ductility or primary creep strain depending on the temperature (low T - tensile ; high T - primary creep). Furthermore, since primary creep strain is a function of stress level, the available ductility was calculated at high temperatures by using the maximum stress developed in the first cycle. For further information on the CDA model refer to References 5 and 6. The CDA model formulation used for PWA 1480 single crystal material is given in Reference 6, section 7.5.2:

$$N_{SC} = \int_0^1 \left[\frac{\bar{\epsilon}_p}{\left(\dfrac{dD}{dN}\right)_{Ref} F(\sigma_t, \Delta\sigma)} \right] G\left(\frac{N}{N_{SC}}\right) df_\epsilon \qquad (36)$$

C-2

$$\text{where} \quad F(\sigma_t, \Delta\sigma) = \left(\frac{\sigma_t}{\sigma_{tRef}}\right)\left(\frac{\Delta_\sigma}{\Delta\sigma_{Ref}}\right) + \left[\left(\frac{\Delta\sigma_{Ref}}{\Delta\sigma}\right)\left(\frac{\sigma_t}{\sigma_{tRef}}\right)\right]^{B^1}\left[\left(\frac{t}{t_{Ref}}\right)^{C^1} - 1\right] \quad (37)$$

$$G\left(\frac{N}{N_{SC}}\right) = (1-LF)(M+1)\left[1-\left(\frac{N}{N_{SC}}\right)\right]^m + LF \quad (38)$$

$$\frac{dD}{dN}\bigg]_{Ref} = A\,\Delta\epsilon^B \quad (39)$$

All the TMF cycles under consideration generated first cycle maximum stresses at temperatures below 816°C (1500°F) where PWA 1480 does not exhibit significant creep behavior. As such, a constant (tensile ductility) was assumed for the available ductility in the PWA 1480 model analysis. For the same reason, it was assumed that the time-dependent portion of the CDA model played an insignificant role in the damage process. Equation 36 was thus reduced to the following:

$$N_{SC} = \int_0^1 \left[\frac{\bar{\epsilon}_p}{\left(\dfrac{dD}{dN}\bigg]_{Ref}\right)\left(\dfrac{\sigma_t}{\sigma_{tRef}}\right)\left(\dfrac{\Delta\sigma}{\Delta\sigma_{Ref}}\right)}\right] G\left(\frac{N}{N_{SC}}\right) df_\epsilon \quad (40)$$

The reference fatigue stresses were viewed as constants and removed from inside the integration. And, since no block loadings were included in the TMF database, the function G, designed to capture block loading effects, was set equal to unity.

86

$$N_{SC} = Q \int_{C}^{1} \left[\frac{\overline{\epsilon}_p}{\left(\left[\dfrac{dD}{dN}\right]_{Ref} \right) \sigma_t \Delta\sigma} \right] df_\epsilon$$

(41)

where $Q = \sigma_{t_{Ref}} \Delta\sigma_{Ref}$

Substituting the equation for the reference damage rate and integrating yields:

$$N_{SC} = P\Delta\epsilon^{-B} \sigma_t^{a} \Delta\sigma^{b}$$

(42)

where $P = Q\overline{\epsilon}_p/A$

(43)

Finally, per recommendation of the Reference 6 P&W program manager, R.S. Nelson, the function for tensile stress was changed from a power law to an exponential:

$$N_{SC} = P\Delta\epsilon^{-B}\Delta\sigma^{b}10^{(\sigma_t/c)}$$

(44)

Modified Strain Range

The modified strain range model formulation was based on the notion that damage accumulates as a function of a pseudo-stress range obtained from the product of elastic modulus and strain range. This model was successfully used at P&W to correlate the 50% load drop life of single crystal TMF specimens having various primary orientations and an out-of-phase TMF cycle type. The modified strain range model equation used in this study was:

$$N_{SC} = A(E \cdot \Delta\epsilon)^{-B}$$

(45)

The elastic modulus used for the TMF cycles was associated with the temperature at maximum strain.

"Crack Tip Opening Displacement" ("CTOD")

The "CTOD" model was chosen based on the theory that coating crack propagation into the SC substate is controlled by conventional linear elastic crack growth mechanisms. The isotropic form of CTOD was chosen to simplify the analysis.

87

For mode I crack growth:

$$CTOD = \frac{K_I^2}{E\sigma_{y.2}}$$ (46)

where $\quad K_I = \beta\sigma_t\sqrt{\pi a}$ (47)

Substituting the expression for stress intensity factor, K_I, into the CTOD equation yields:

$$CTOD = \frac{\beta^2\sigma_t^2\pi a}{E\sigma_{y.2}}$$ (48)

Assuming σ_t is constant throughout the life span of Nsc and the effect of geometry is small yields the following life relationship:

$$N_{SC} = A \text{ "CTOD"}^{-B}$$ (49)

where the quotes signify that crack geometry effects were neglected.

Modulus, E, and 0.2% yield stress, $\sigma_{y.2}$, were determined at the temperature corresponding to the stress, σ_t.

"Crack Tip Opening Displacement - GP" ("CTODgp")

The "CTODgp" model is identical to the "CTOD" model discussed above with the exception that the 0.2% yield stress, $\sigma_{y.2}$, was varied as a function of gamma prime size. To study the impact of gamma prime size on PWA 1480 initiation life, an empirical formula which describes yield strength as a function of orientation and exposure was developed based on the information in References 13 and 14.

Hysteretic Energy Approach

A hysteretic energy approach was used by DeLuca and Cowles (Reference 3) and further developed by Heine, Warren, and Cowles (Reference 4) to correlate 50% load drop TMF life of PWA 1480.

$$N_{SC} = A \, W_{eff}^{-B} \tag{50}$$

$$\text{where} \quad W_{eff} = \sigma_t \Delta\epsilon_{in} \frac{\Delta\sigma_{[111]}}{E} \tag{51}$$

$$\Delta\sigma_{[111]} = \text{Max. normal octahedral slip plane stress range}$$

Inelastic strain range, $\Delta\epsilon_{in}$, was determined by using the incremented strain technique discussed in Reference 4. The modulus, E, was taken to be the dynamic modulus at the temperature associated with the stress, σ_t.

Maximum Tensile Stress

CDA correlation of all PWA 286 coated <001> PWA 1480 TMF data indicated that the only statistically significant parameter was maximum tensile stress, σ_t. Based on that analysis, a maximum tensile stress model was also assessed. The form of this model is simply:

$$N_{SC} = A\sigma_t^{-B} \tag{52}$$

Each model was assessed based on its overall capability in correlating the baseline data and predicting orientation, maximum cycle temperature, and strain-temperature waveform shape effects on TMF life. Model capability was assumed to be adequately measured by the Weibull slope, Beta, obtained by Weibullizing the ratio of calculated life to actual life.

The results of the Weibull analysis are presented in Figure 62. In general, little difference was observed between five of the six models. The only model which appeared significantly less capable was the modified strain range model. The capability of another model, "CTODgp", was virtually identical to that of the "CTOD" model.

89
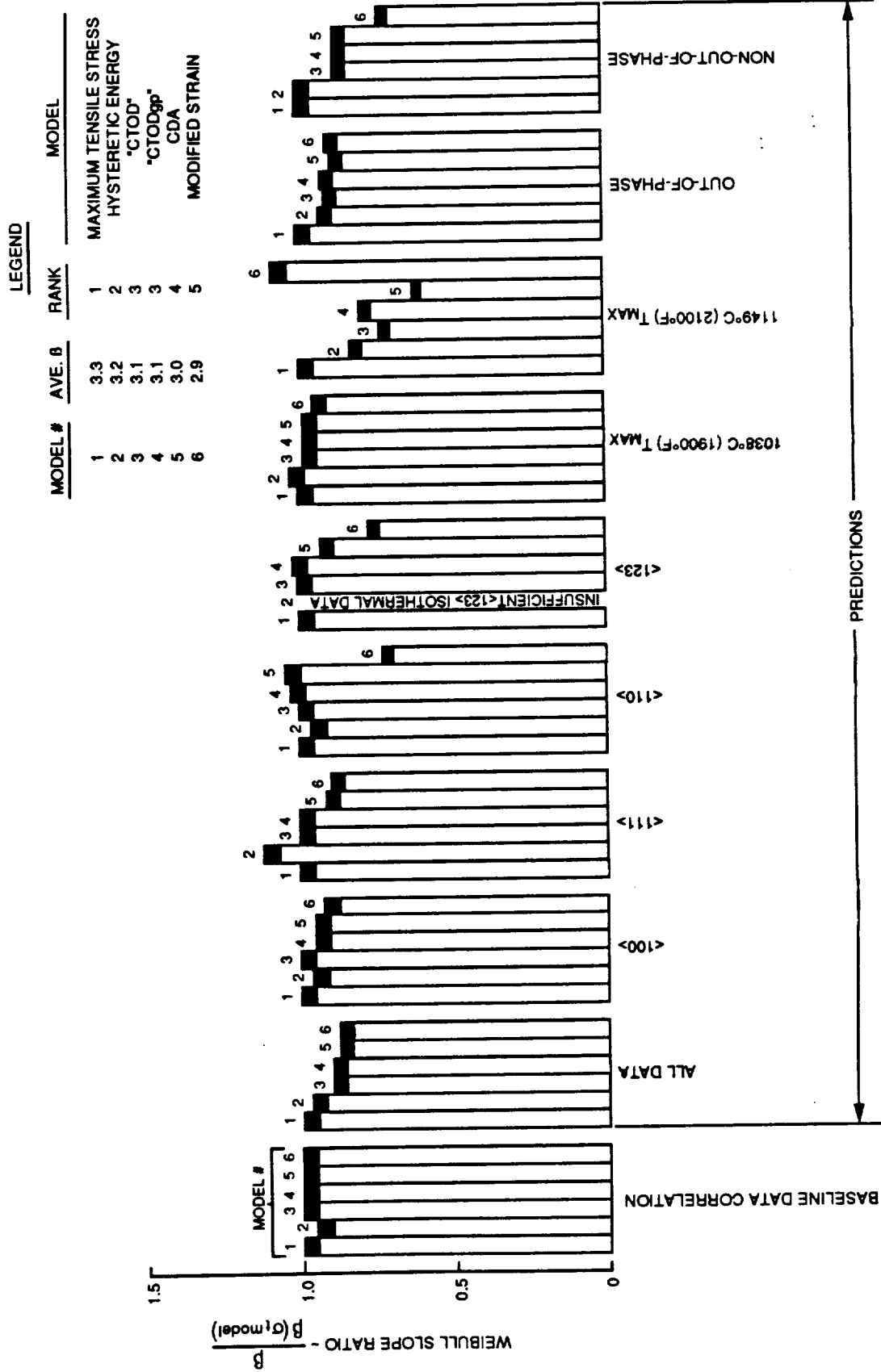
Figure 62 Results of Life Prediction Model Comparisons Using Weibull Slope

Although the hysteretic energy approach predicted the PWA 1480 TMF test specimen lives well, this approach will be sensitive to changes in inelastic strain magnitude which are difficult to measure and practically impossible to calculate. PWA 1480 TMF hysteresis loops are nominally elastic in the life regime relevant to gas turbine airfoils. The incremented inelastic strain technique given in Reference 4 provides a consistent means to calculate inelastic strain ranges for simple TMF cycles, but specific rules governing how the strain-temperature cycle is broken into straight line segments is ambiguous for general TMF cycles such as a baseball cycle (Note: An out-of-phase strain-temperature cycle was assumed for LB-29 in the life predictions). A hand calculation has shown that the calculated inelastic strain of an out-of-phase TMF cycle can vary significantly depending on how many segments are chosen to breakup the cycle.

Of the six models evaluated, the "CTOD" and maximum tensile stress models were selected for further development. The maximum tensile stress model was expanded into the maximum mode I stress intensity factor, Kmax, and "CTOD" was replaced by the true form of crack tip opening displacement, CTOD.

$$N_{SC} = A_1 \, K_{max}^{-B_1} \tag{53}$$

$$\text{and} \quad N_{SC} = A_2 \, CTOD^{-B_2} \tag{54}$$

Crack geometry effects were determined using the formulations given in Reference 22. The correction factor applicable to the TMF specimen geometry used in this program is presented in Figure 63. As a check, the results from Reference 23 were compared to the Reference 22 extrapolation (shown at an aspect ratio of about 42 in Figure 63) for the condition of a circumferential crack geometry. The two methods are in excellent agreement.

Correlation of PWA 1480 crack initiation life (Nsc) versus Kmax and CTOD using all <001> TMF data is presented in Figure 64. Prediction of all non-<001> TMF data by Kmax and CTOD is presented in Figures 65 and 66, respectively.
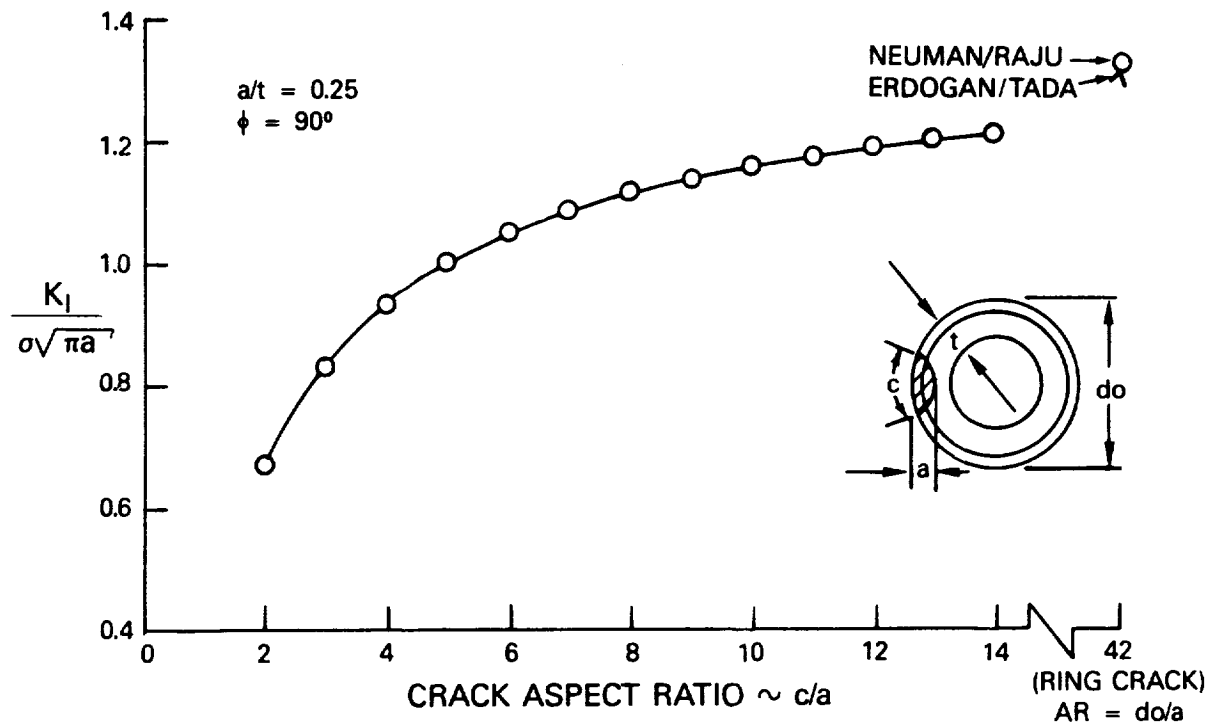
Figure 63 Mode I Stress Intensity Correction Factor
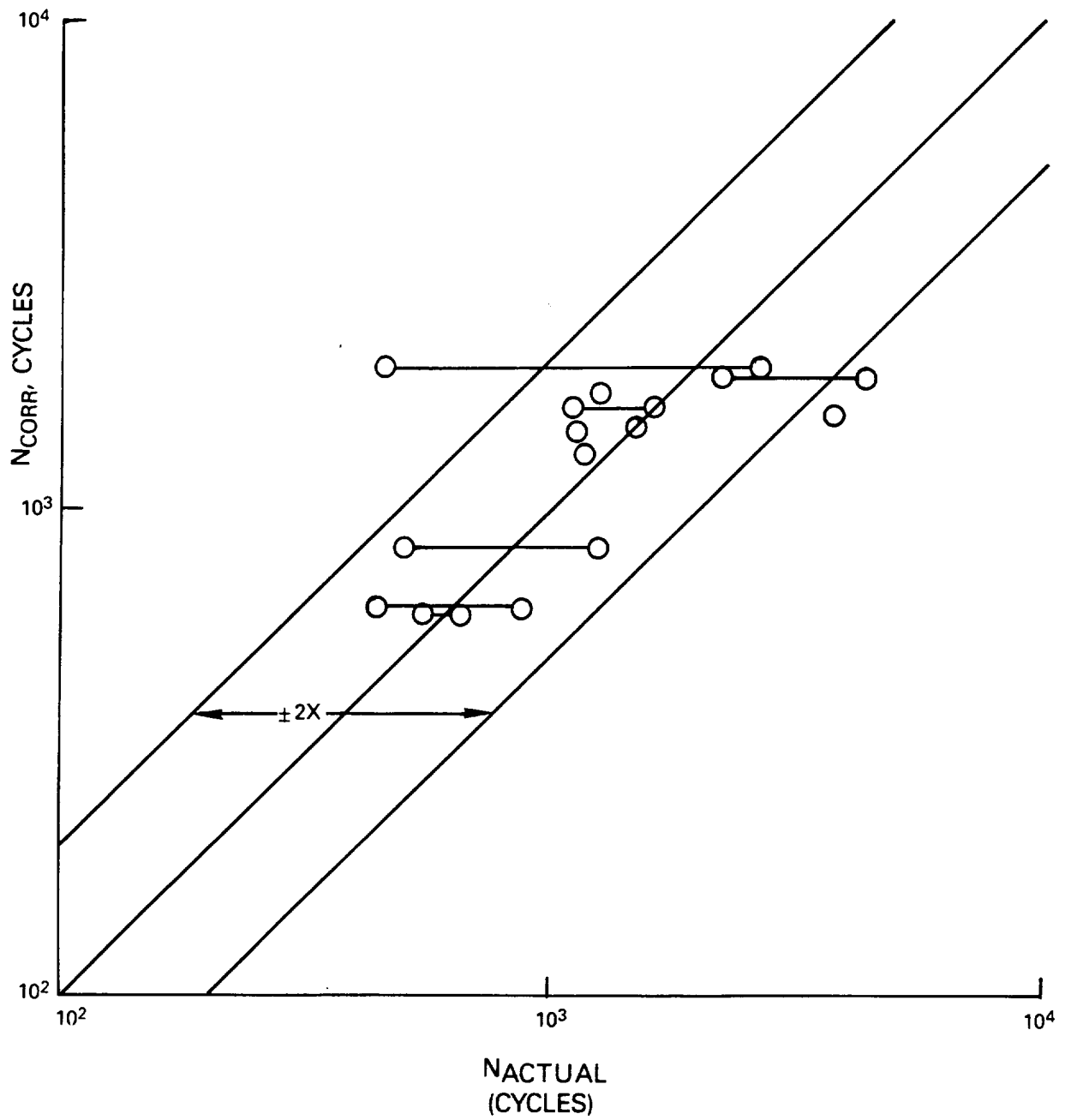
Figure 64 K_{max} and CTOD Correlation of All <001> TMF Data
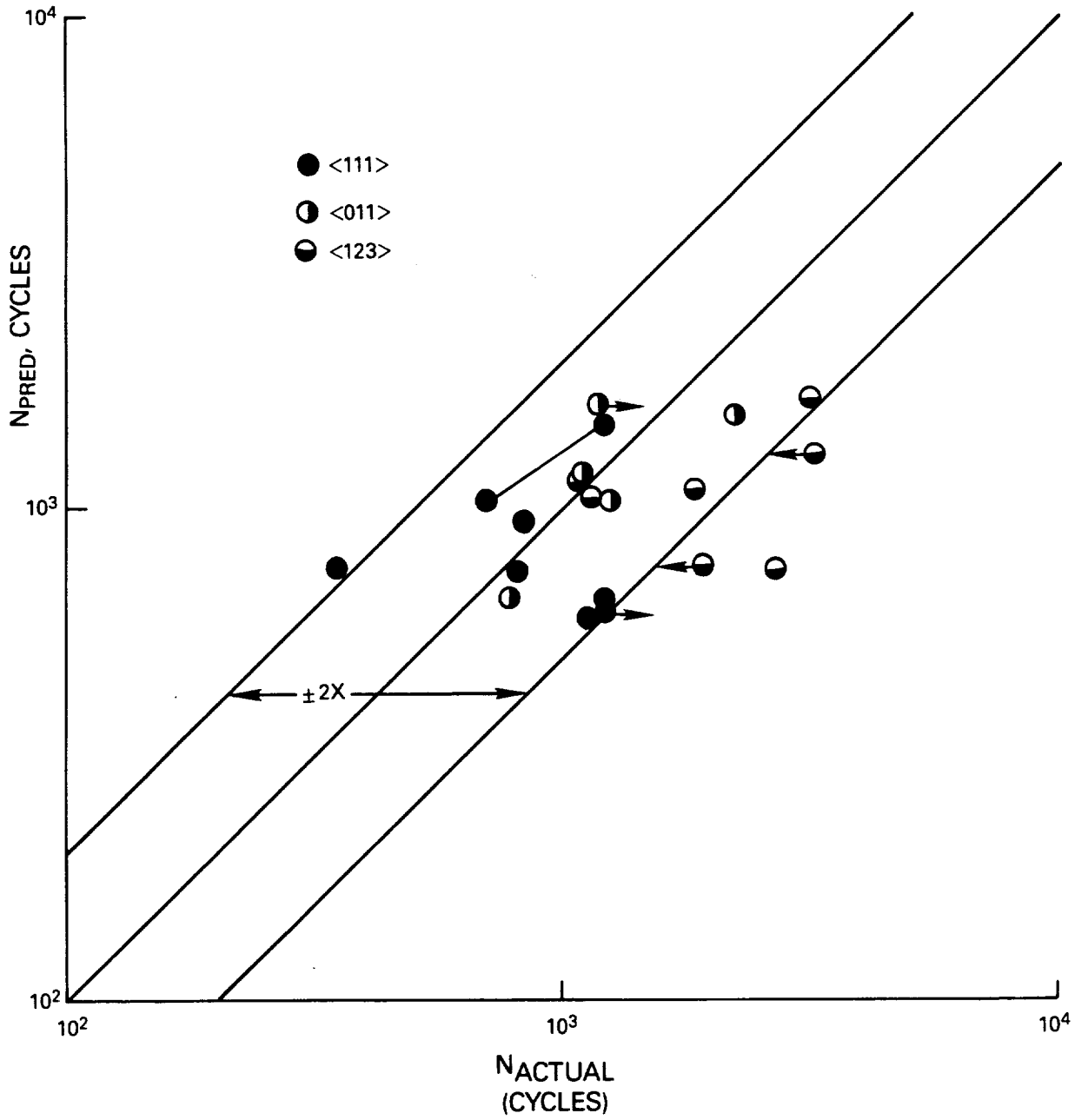
Figure 65 K_{max} Prediction of Non-<001> TMF Data
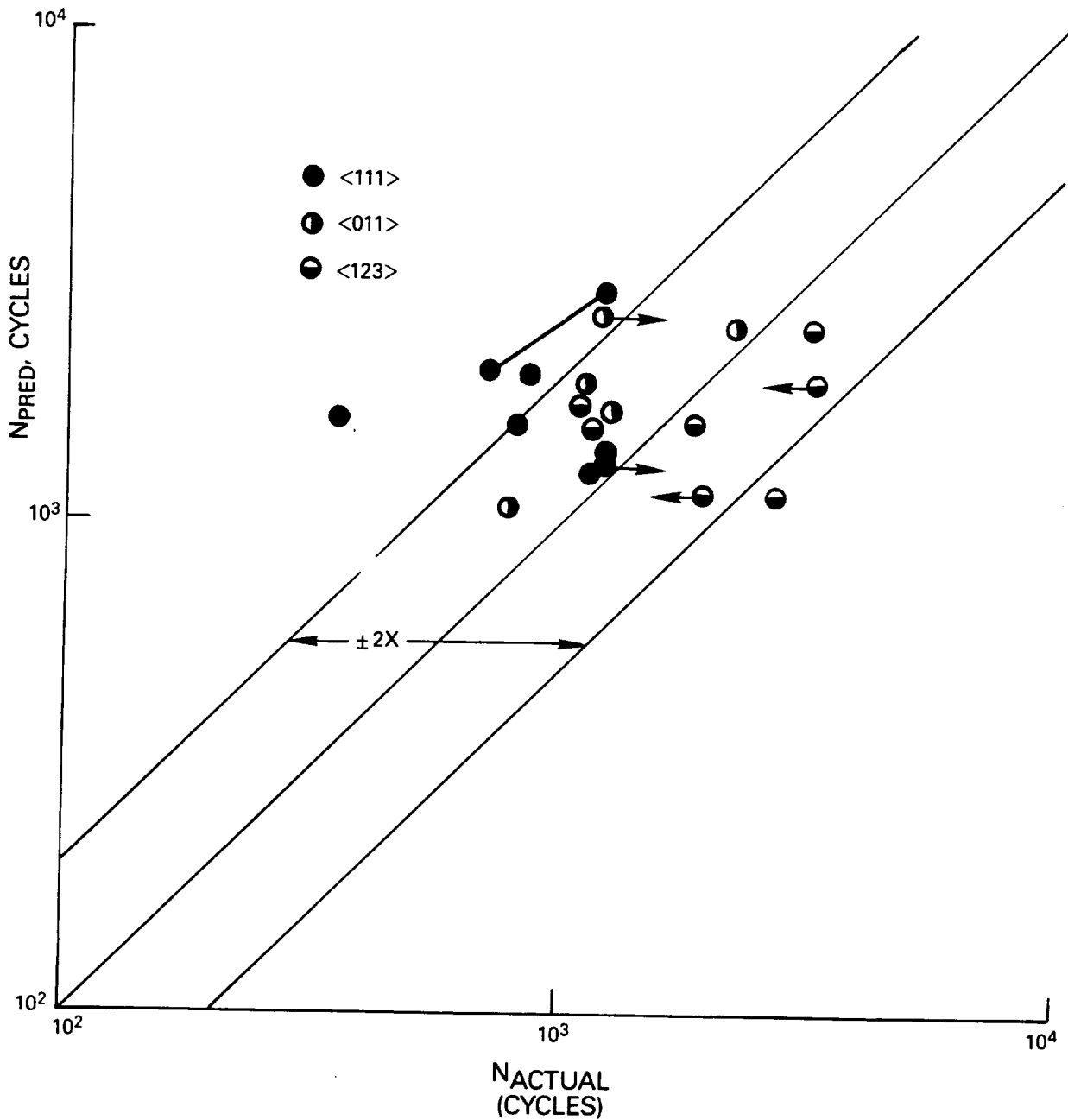
Figure 66 CTOD Prediction of Non-<001> TMF Data

The lives quoted in Tables 5 and 6 were determined by assuming a constant coating thickness of 0.13 mm (0.005 in.). Actual coating thicknesses for PWA 286 overlay coating typically range from 0.01 mm to 0.015 mm (0.004 to 0.006 inches). Subsequently, all life data contained in Appendices A and B were updated to reflect actual coating thicknesses. The decision between Kmax and CTOD for the final PWA 1480 life model will be made using the updated data and the results from PWA 273 aluminide coated TMF life prediction.

95

8.4 COMPUTER SOFTWARE DEVELOPMENT

Conducting an analysis of a coated airfoil is considered impractical for general design applications due to the increased model complexity and the small increments needed to converge the coating constitutive model (i.e., overwhelming engineering and computer costs). Instead, an alternative method is being developed. One which uses a simplified structural analysis to simulate airfoil critical locations and drive the life prediction models. This simplified structural model will have the capability to model the general multiaxial loading conditions of a smooth flat surface. Boundary conditions for the simplified structural model would be obtained from an uncoated airfoil elastic or inelastic analysis.

Integration of all constitutive and life models and development of a simplified structural analysis technique was initiated. The software flowchart is shown in Figure 67. It is intended that all the software developed in this program remain modular to permit future model additions or alterations.

DESCRIPTION

CONTAINS SUMMARY OF CYCLIC CONDITIONS AND HISTORY

GENERATES ε_{ij}, T INCREMENTS SUITABLE FOR NONLINEAR ANALYSIS AND SIMPLIFIED STRUCTURAL MODEL MESH AND BOUNDARY CONDITIONS

CONDUCTS NONLINEAR ANALYSIS OF MULTI-LAYERED STRUCTURES

CALCULATES REQUIRED PARAMETERS FOR LIFE PREDICTION MODELS

CALCULATES CYCLIC LIFE
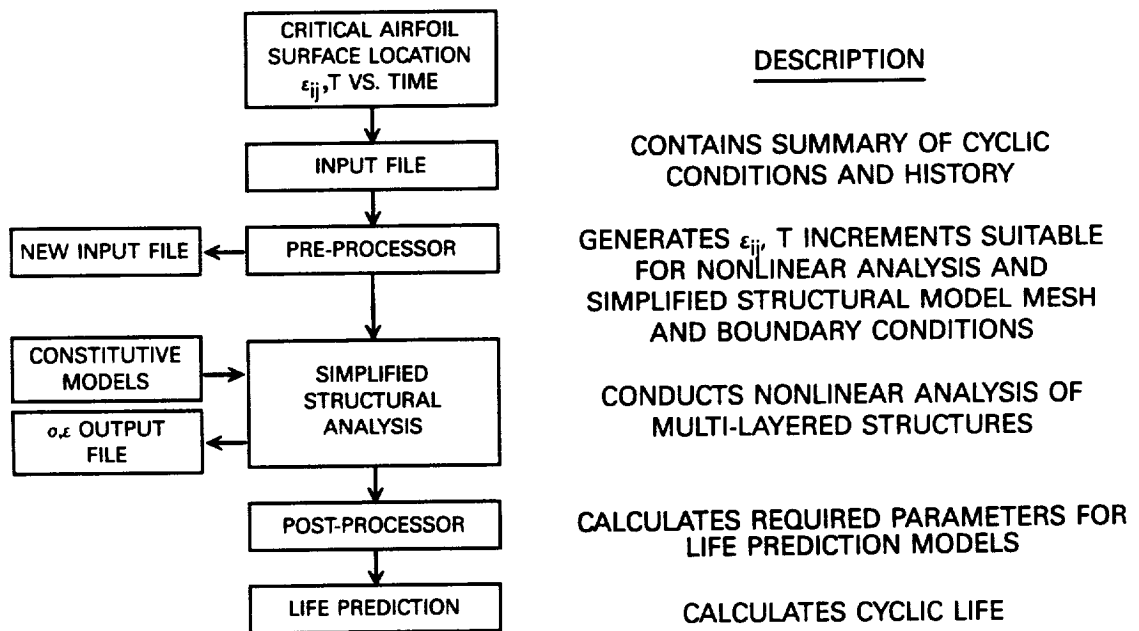
Figure 67 Computer Software Flowchart for Implementation of the Constitutive and Life Models

SECTION 9.0

TASK VII - SUBCOMPONENT VERIFICATION FOR PRIMARY SC MATERIAL

9.1 TEST SPECIMEN AND CYCLE

The specimen geometry selected for the verification test is shown in Figure 1B. Specimen orientation and coating chosen were <001> and PWA 286 overlay (specimen JB-135). The test envelope chosen was 427-1038°C (800-1900°F) with a strain range of 0.45% and strain ratio (V-ratio) of -1.

The verification test TMF cycle was defined based on the nonlinear airfoil analysis conducted by T. Meyer in support of NASA contract NAS3-23925 (Reference 19). Specifically, the predicted airfoil leading edge strain-temperature history presented by Meyer for an entire transient flight cycle was normalized and used to calculate test parameters. Maximum and minimum temperatures and strain range were selected to approximate the airfoil loading history. The predicted airfoil versus test strain-temperature histories are compared in Figure 68 and a description of the airfoil transient flight cycle is presented in Table 7. Constant loading conditions which occur in the airfoil during climb and cruise were modeled by holding constant strain. Test strain versus time and temperature versus time cycles are presented in Figures 69 and 70, respectively.
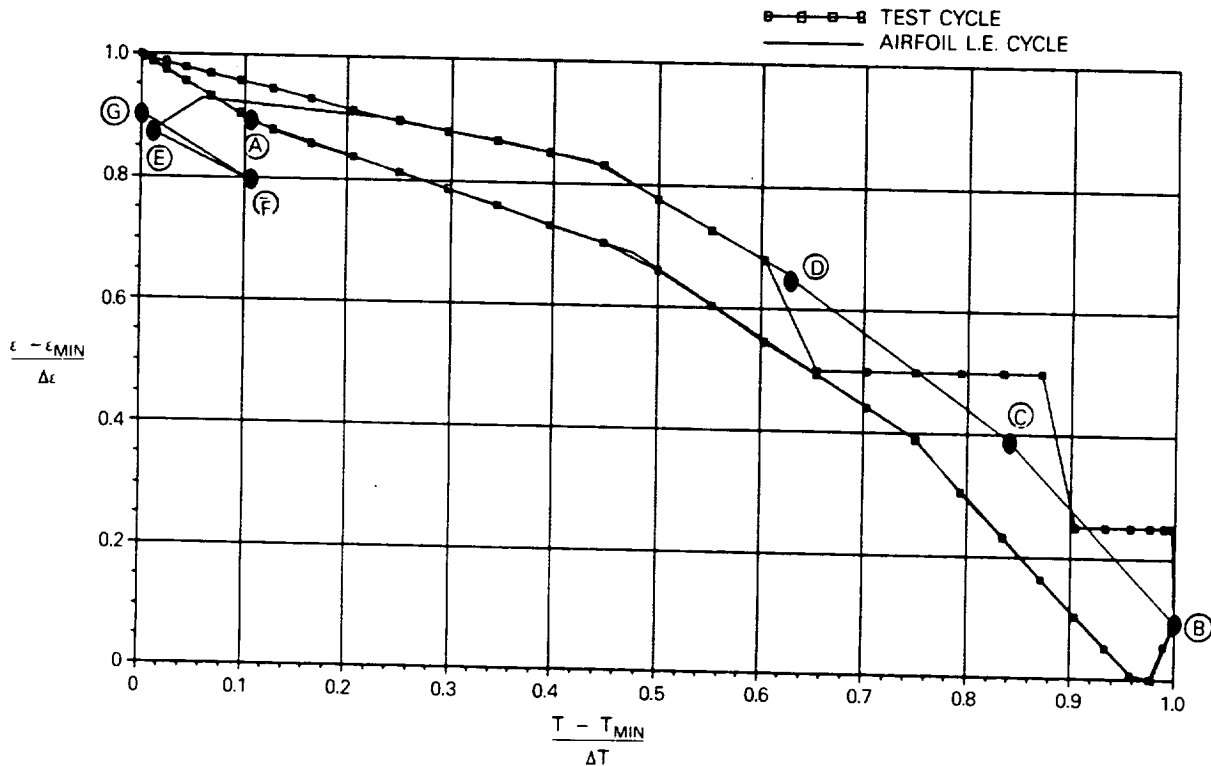
Figure 68   Normalized Strain Vs. Normalized Temperature Comparison of Airfoil Leading Edge and Verification Test Cycles. See Table 7 for Description of Points A through G.

TABLE 7

DESCRIPTION OF AIRFOIL LEADING EDGE TRANSIENT FLIGHT CYCLE

Point Number	Strain (in/in)	Temp (F)	Comment
A	-0.00041	930	Steady state ground idle
B	-0.00339	1966	End of takeoff
C	-0.00228	1779	End of climb
D	-0.00129	1535	End of cruise
E	-0.00047	818	Decent
F	-0.00077	929	Steady state ground idle
G	-0.00036	805	Shutdown (200 rpm)
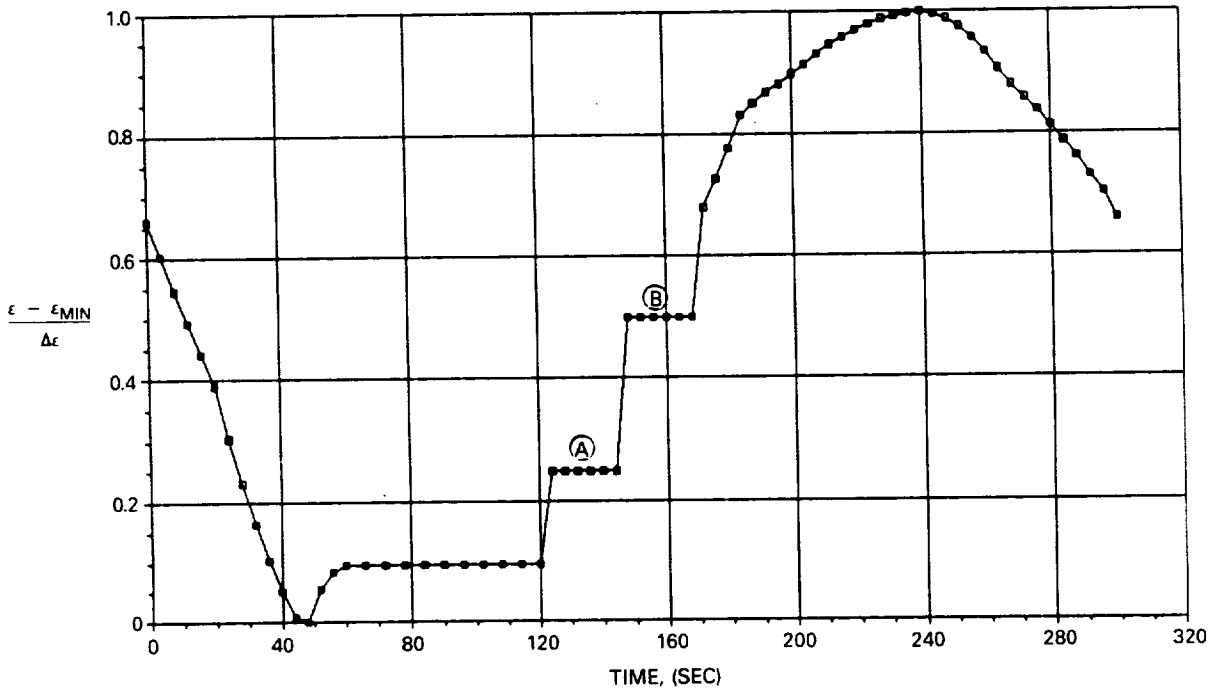
Figure 69   Normalized Strain Vs. Time for Verification Test. Strain holds labelled A and B are designed to simulate climb and cruise holds.
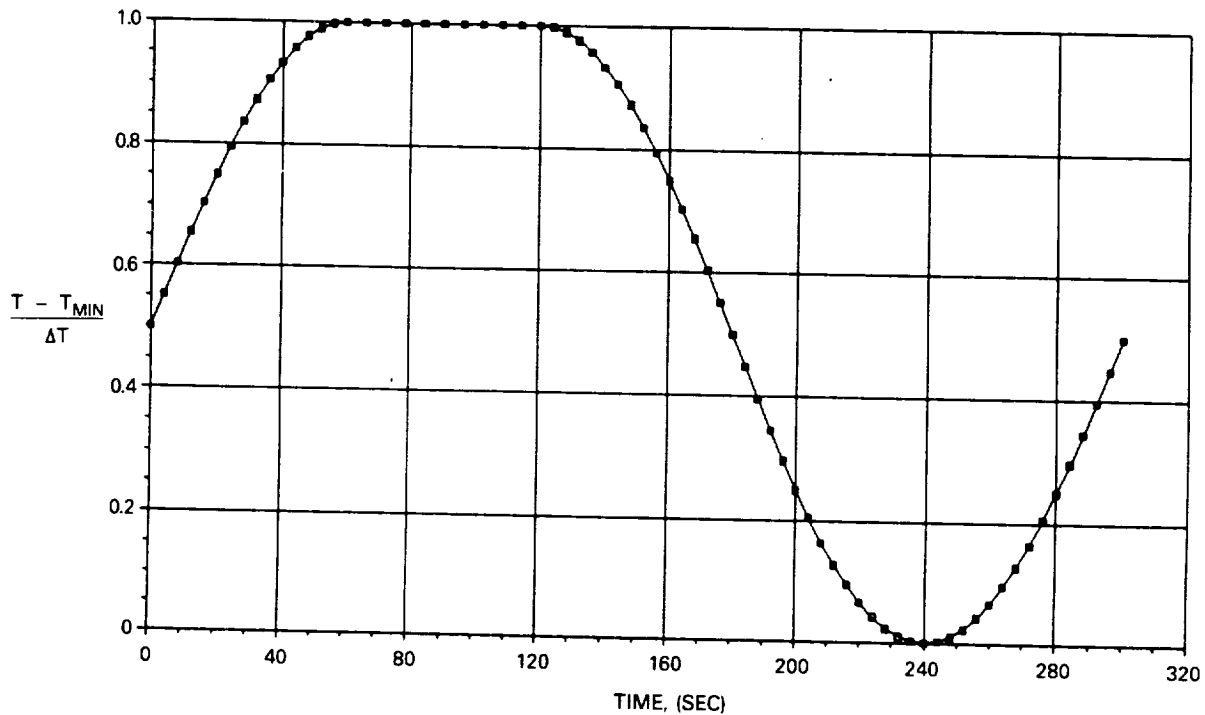
Figure 70 Normalized Temperature Vs. Time for Verification Test. Hold at maximum temperature is designed to simulate steady state takeoff.

9.2 VERIFICATION TEST RESULTS

The results from specimen JB-135 are included in Appendices A and B and the strain-temperature and initial hysteresis loops are presented in Figures 71 and 72. Cracking was typical of an overlay coated PWA 1480 specimen. Coating cracks initiated at multiple sites throughout the specimen gage section. Failure was caused by linkup of multiple, coating generated, cracks which had initiated at slightly different levels along the specimen OD. The general appearance of the fracture surface of JB-135 is presented in Figure 73.
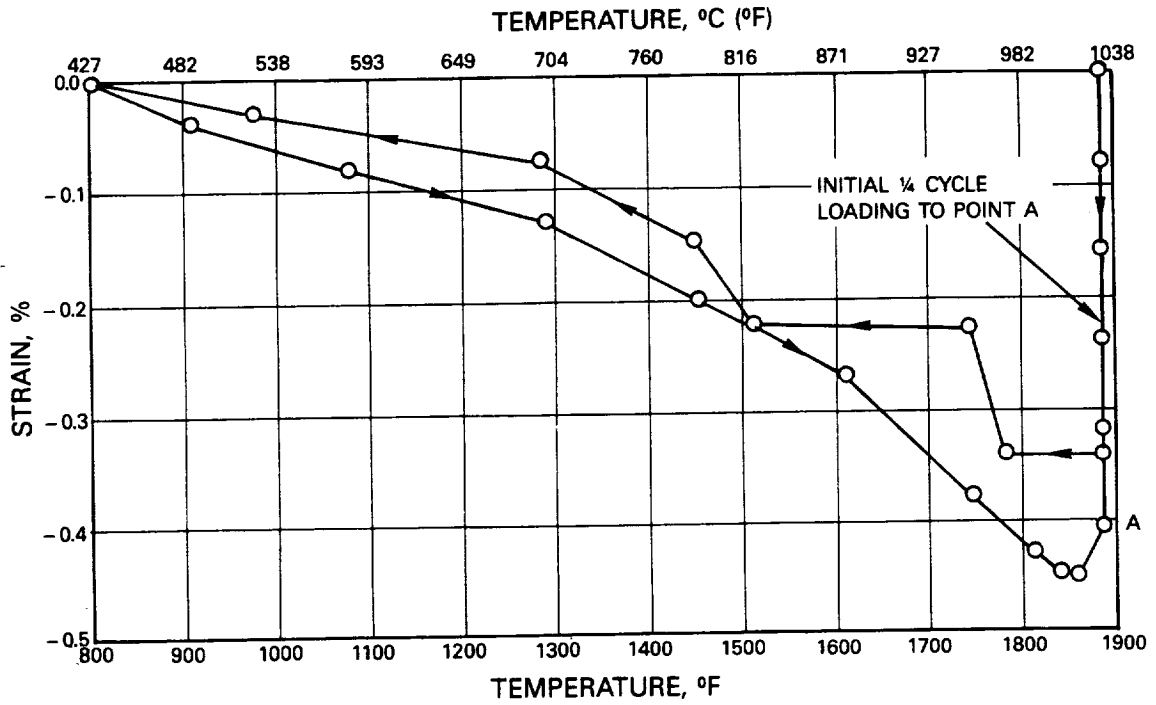
Figure 71   Experimental Strain-Temperature History for Verification TMF Test
of Specimen JB-135. T_{max} = 1029°C (1885°F).
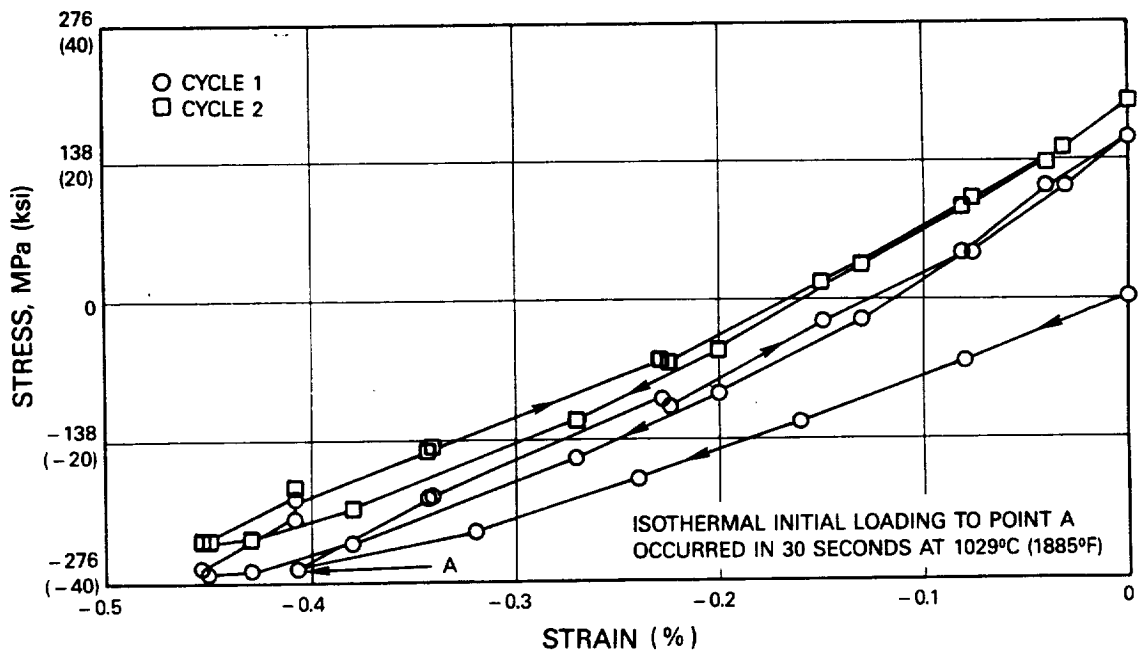
Figure 72   Initial Hysteresis Loops for Specimen JB-135

100
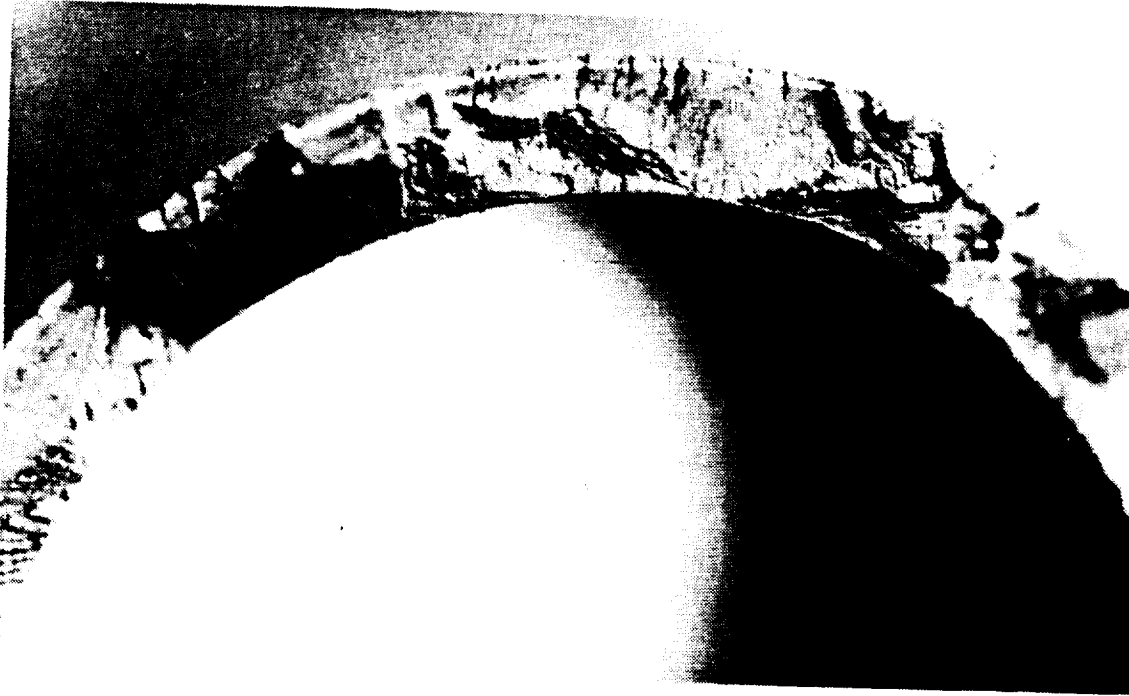
(A)
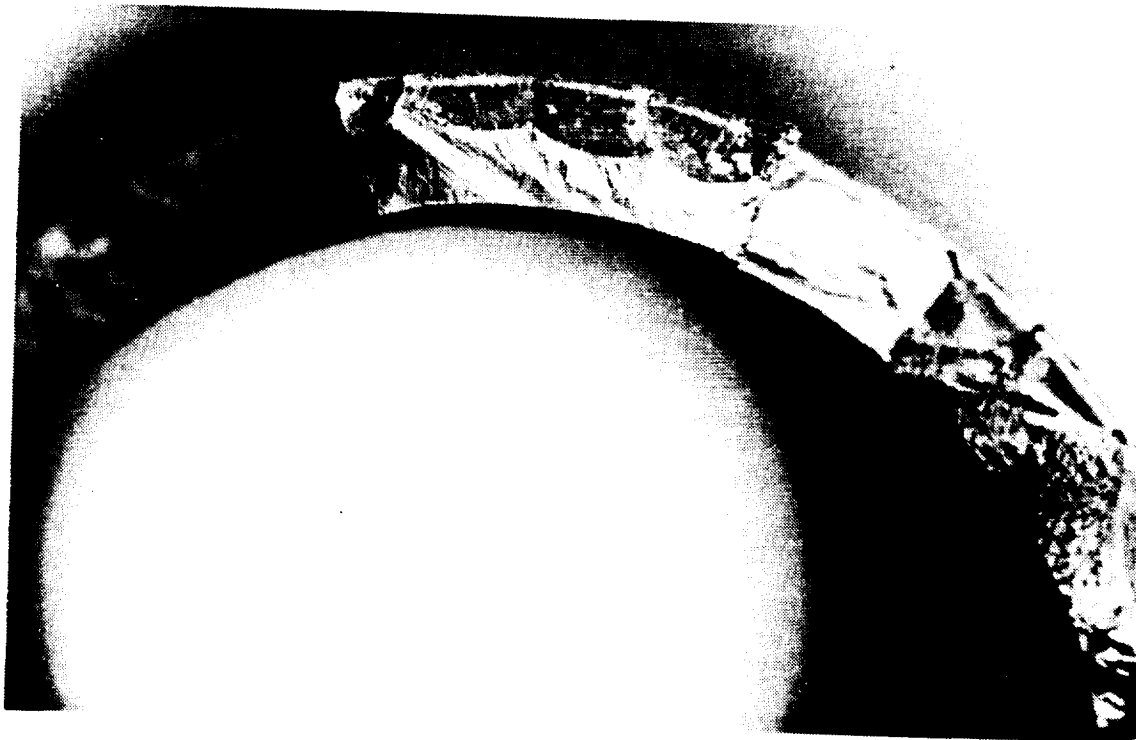
(B)

Figure 73 Fracture Surface Appearance of Verification TMF Test Specimen
JB-135 After Testing At 427-1038°C (800-1900°F), 0 to -0.45%, Using
the Airfoil Cycle Defined In Figures 68-70 for 5059 Cycles.
(A) Appearance of major fatigue crack region and (B) Typical
appearance of secondary fatigue cracks.

TASK VIII – ALTERNATE SC MATERIAL CHARACTERIZATION FOR AIRFOILS

10.1 TEST SPECIMEN FABRICATION

Eighteen (18) solid bar and ten (10) cylindrical tube specimens were fabricated to support Tasks VIII and IX. A summary of the fabricated specimens is presented in Table 8 and specimen geometries are shown in Figures 74 (solid) and 1B (tube).

TABLE 8

SUMMARY OF ALLOY 185 SPECIMENS

Specimen Design	Specimen Type	Orientation	Coating	Number
LED 41784	solid bar	<001>	none	4
		<111>	none	2
M26	solid bar	<001>	none	7
		<111>	none	5
73C	cylindrical tube	<001>	PWA 286	7
		<111>	PWA 286	3

A) TENSILE AND CREEP TEST SPECIMEN (M26)
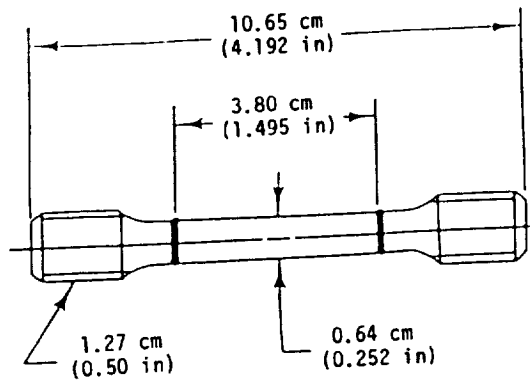
B) CYCLIC CONSTITUTIVE TEST SPECIMEN (LED 41784)
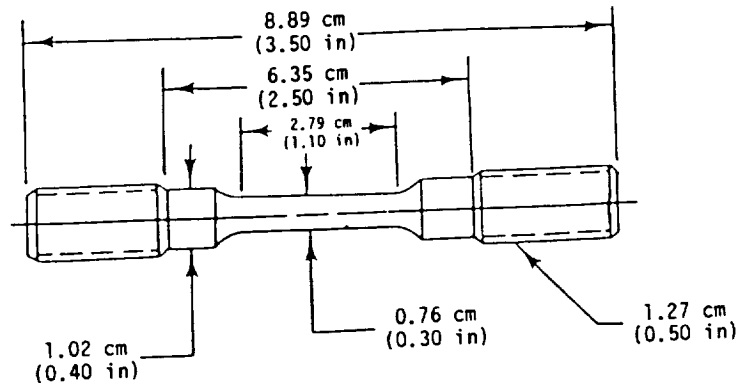
Figure 74   Specimen Designs for Alloy 185 Single Crystal Property Tests

10.2 MONOTONIC TESTS

10.2.1 Alloy 185 Tensile Tests

All tensile tests of Alloy 185 were completed. A summary of test results is presented in Table 9.

TABLE 9

SUMMARY OF UNCOATED ALLOY 185 TENSILE TESTS

Test Strain Rate = 0.005 / min

Temp C(F)	Spec. ID	Orient	E x 10⁻³ MPa(KSI)	0.2% Yield MPa(KSI)	Ultimate MPa(KSI)	Elong. %	RA %
RT	HJA-5	<001>	139.3 (20.2)	757.8 (109.9)	1025.3 (148.7)	7.0	5.5
427 (800)	HJA-7	<001>	133.1 (19.3)	886.0 (128.5)	1057.7 (153.4)	6.3	4.7
760 (1400)	HJA-9	<001>	117.2 (17.0)	1008.0 (146.2)	1070.8 (155.3)	6.0	7.0
982 (1800)	HJB-3	<001>	90.8 (13.0)	711.8 (101.9)	714.6 (102.3)	18.0	18.2
1093 (2000)	HJB-17	<001>	71.9 (10.3)	440.8 (63.1)	458.9 (65.7)	29.3	36.5
427 (800)	HLB-29	<111>	266.1 (38.6)	950.1 (137.8)	1474.1 (213.8)	9.6	7.8
760 (1400)	HLB-33	<111>	246.1 (35.7)	852.9 (123.7)	1070.8 (155.3)	25.0	15.3
1093 (2000)	HLB-35	<111>	131.9 (19.1)	455.1 (66.0)	466.1 (67.6)	19.0	17.0

10.2.2 Alloy 185 Creep Tests

All creep tests of Alloy 185 were completed. A summary of test results is presented in Table 10.

103

TABLE 10

SUMMARY OF UNCOATED ALLOY 185 CREEP TESTS

Temp C(F)	Spec. ID	Orient	Stress MPa (KSI)	Percent of 0.2% Yield	Life (hr)	Creep Rate (1/min)	Elong %	RA %
982 (1800)	HJA-1	<001>	193.1 (28.0)	27.5	165.1	9.23E-7	16.0	22.5
1093 (2000)	HJA-3	<001>	68.9 (10.0)	15.8	1080.2	2.24E-8	-	-
Uploaded @ 1080.2 hrs.			103.4 (15.0)	23.8	+131.8	5.07E-7	6.0	23.8
982 (1800)	HLA-10	<111>	248.2 (36.0)	NA	142.3	6.84E-7	9.3	11.6
1093 (2000)	HLB-27	<111>	172.4 (25.0)	37.9	64.2	1.35E-6	3.3	3.2

10.3 FATIGUE TESTS

Baseline PWA 286 overlay coated Alloy 185 TMF experiments were conducted during this reporting period. The results from optical fracture surface inspection are given below:

1) <001> HJB-4 427-1038°C (800-1900°F), +0.15%, 1 cpm, Out-of-phase Coating initiated cracking. Multiple sites observed along fracture surface. Coating cracks appeared early during the test and grew along the specimen circumference with little growth into the substrate. This resulted in substrate cracks which were long and shallow.

2) <001> HJB-1 427-1038°C (800-1900°F), +0.25%, 1 cpm, Out-of-phase Mixed mode (ID and OD surface initiation) cracking was observed. The predominant mode was OD coating initiated cracking. Multiple coating cracks were observed along the fracture surface.

3) <001> HJB-8 427-1038°C (800-1900°F), +0.35%, 1 cpm, Out-of-phase Coating initiated cracking. Some small ID surface cracks were also observed. Coating cracks appeared early and formed long, shallow substrate cracks similar in nature to specimen HJB-4.

Life and stress history summaries for the Alloy 185 tests are presented in Appendix C.

In general, TMF cracking of overlay coated <001> Alloy 185 was similar in nature to that of overlay coated PWA 1480 (i.e., multiple coating initiated substrate cracks). Typical fracture surface appearance is presented in Figure 75. Initiation life (Nsc) of coated Alloy 185 is compared to coated PWA 1480 in Figure 76. As expected, PWA 1480 is the superior alloy.
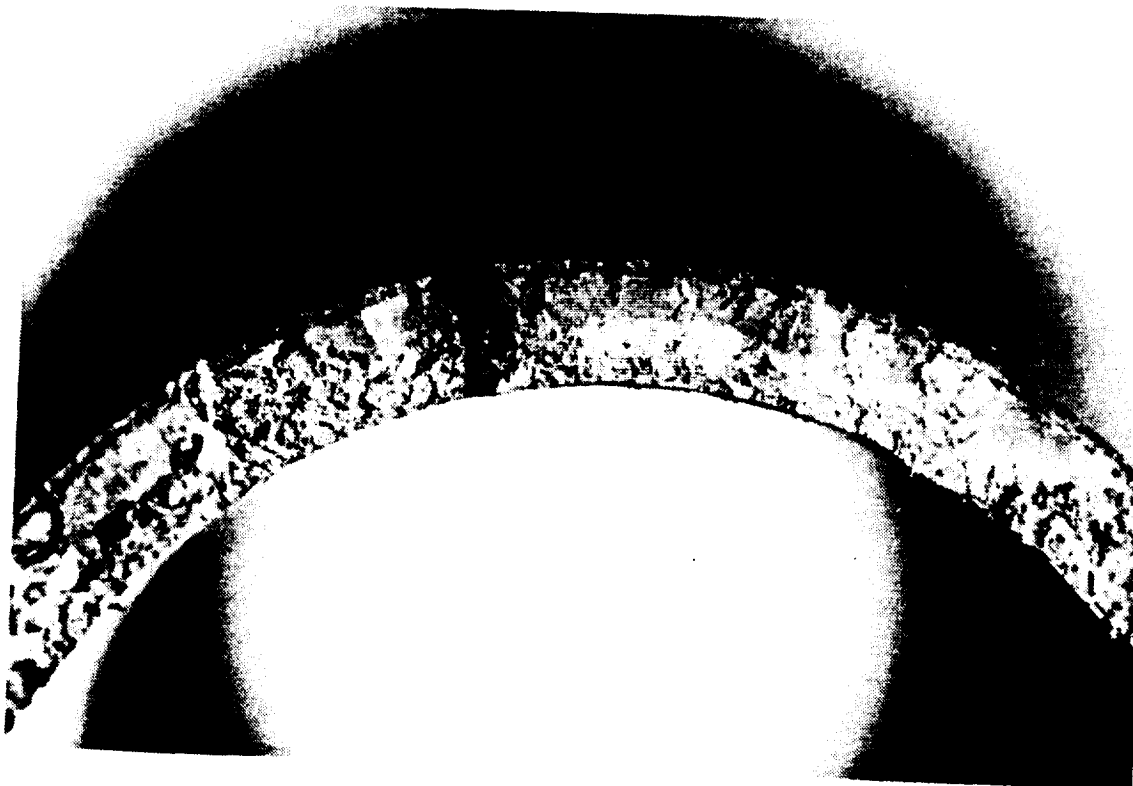
Figure 75   Typical Fracture Surface Features of PWA 286 Coated Alloy 185 Subjected to 428-1038°C (800-1900°F) Out-of-Phase TMF Testing.
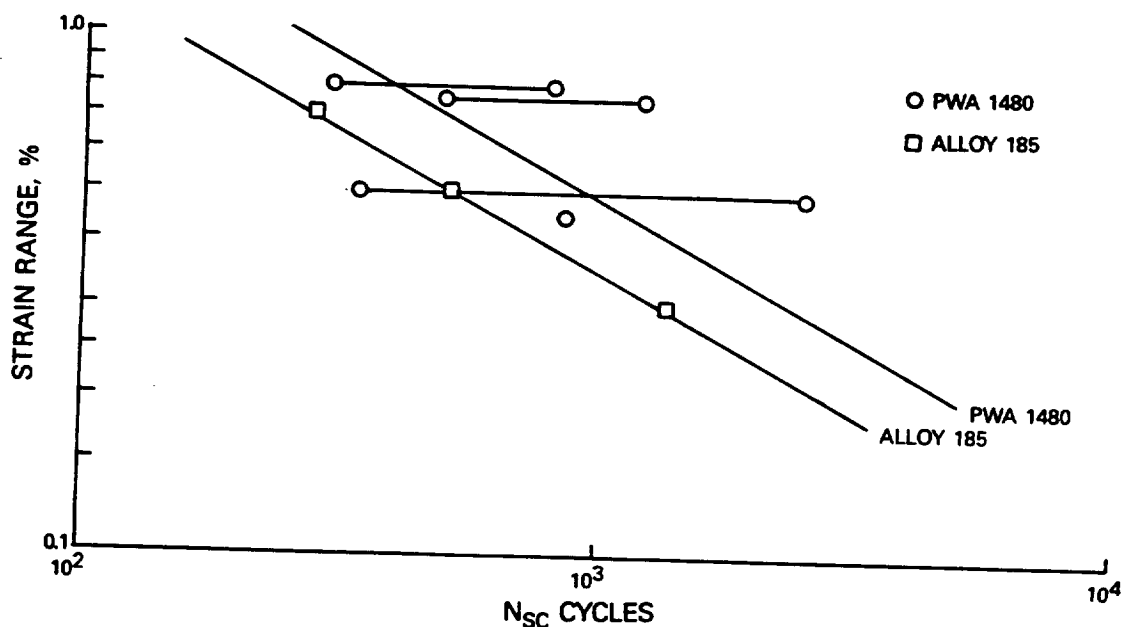
Figure 76   Comparison of PWA 1480 and Alloy 185 Overlay Coated 427-1038°C (800-1900°F) Out-of-Phase TMF Tests

SECTION 11.0

TASK XII – SPECIMEN PREPARATION

11.1 SPECIMEN DESIGN AND PREPARATION

The initial smooth section strain controlled fatigue tests showed a propensity to fail in the threaded section outside the monitored gage section. The smooth specimen geometry was subsequently redesigned. The new design has a smaller gage section diameter (0.63 cm versus 0.76 cm, 0.25 in. versus 0.30 in.) and finer threads. As part of the new design, slight sockets were placed in the gage section to receive the ends of the extensometer to prohibit extensometer slipping. These sockets did not cause premature fatigue crack initiation. The original and new smooth specimen geometries are shown in Figure 77.
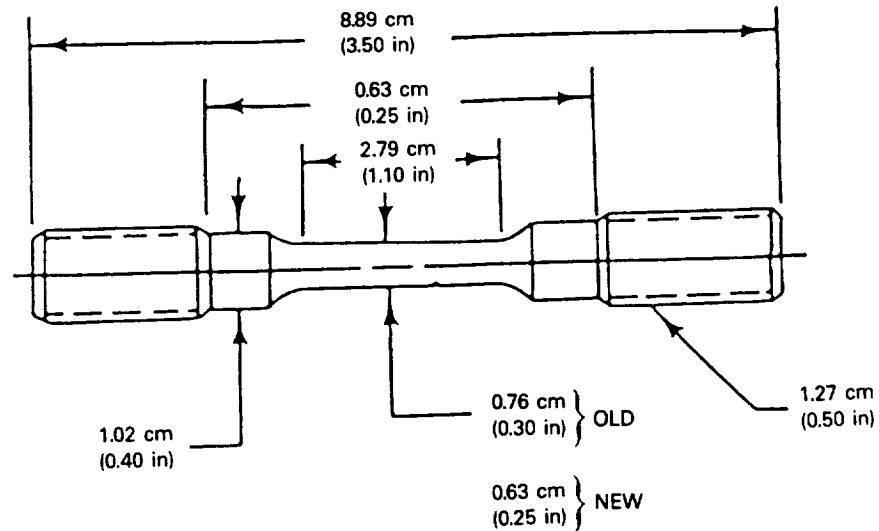
Figure 77   Smooth, Uniaxial Specimen, LED 41784

Specimen designs also were completed for the rectangular section, notched specimens. See Figures 78 through 80.

To facilitate SEM (Scanning Electron Microscope) inspection of the notch slip behavior, selected notched specimens were polished to about 4 rms surface finish.

Criteria used in designing the notched specimens and selecting their primary and secondary orientations (see Figure 81) included testability, parametric variation of possible deformation and fatigue life variables, and applicability of two dimensional analyses.

106
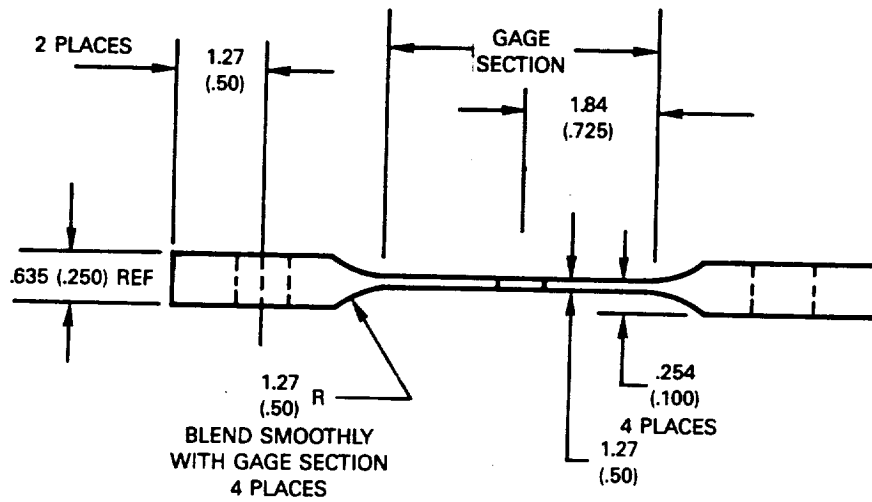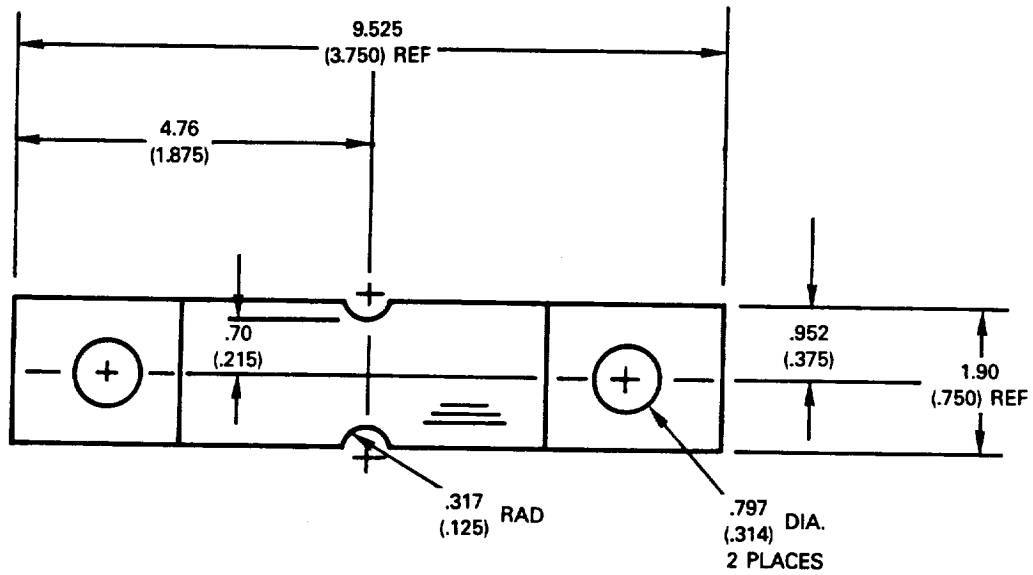
Figure 78 Thin Mild Notched Fatigue Specimen - cm (in.)

107

14.60
(5.750) REF

7.302
(2.875)

A

.317
(.125) RAD
2 PLACES, DO NOT
BREAK EDGES

3.213
(1.265)

5.08
(2.00) RAD,
4 PLACES

2.54
(1.00)

2.54
(1.00) RAD, 4 PLACES

GAGE
SECTION
5.08
(2.00)
4 PLACES

.875

.508
(.200)

.952
(.375)

.698
(.275)
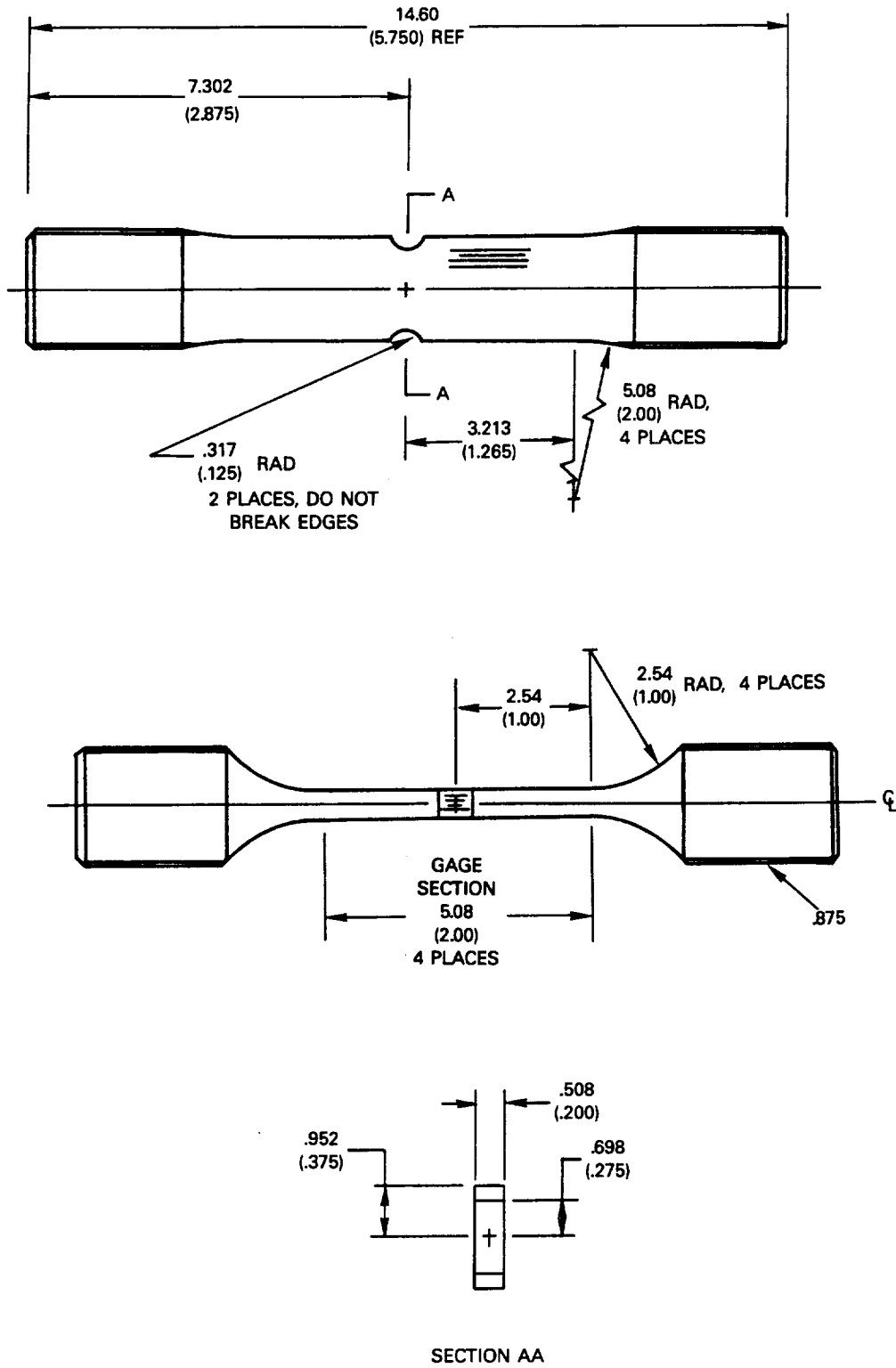
SECTION AA

Figure 79   Thick Mild Notched Fatigue Specimen – cm (in.)

108
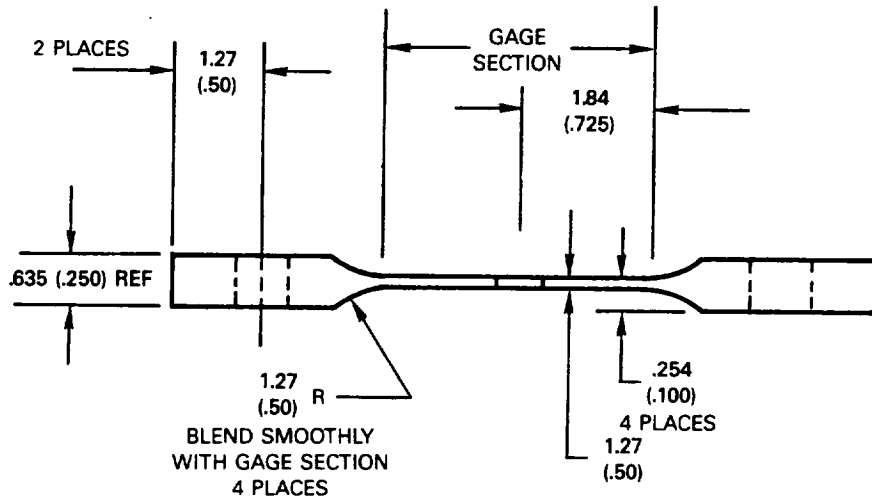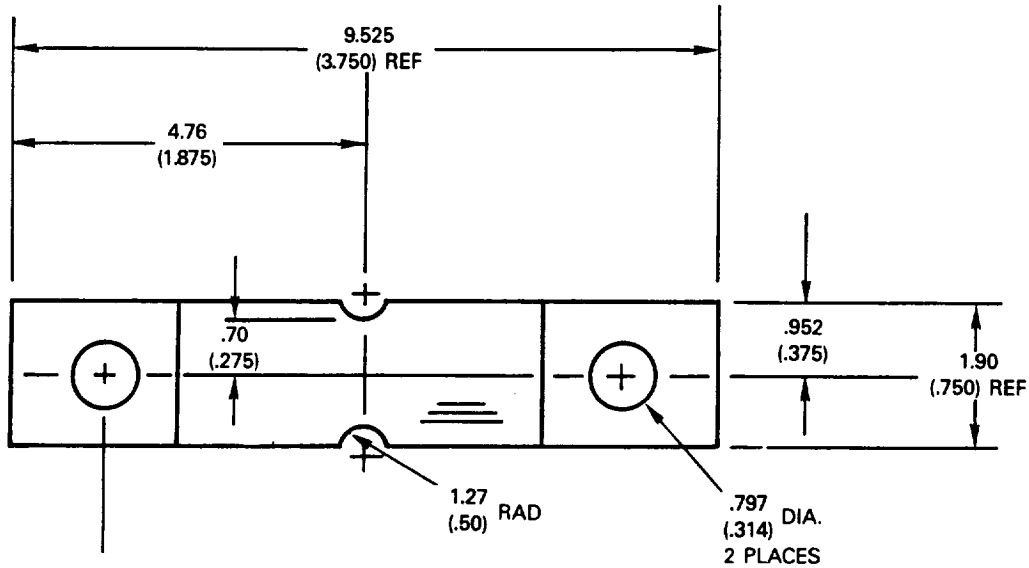
Figure 80   Thin Sharp Notched Fatigue Specimen — cm (in.)

a)   Testability

A common concern in fatigue testing is designing the specimen so that failure is likely to occur in the test section rather than in the grip region. The specimens shown in Figures 78 through 80 were designed so that the ratio of the test section concentrated stresses to the grip section concentrated stresses were consistent with other successful specimen designs used at Pratt & Whitney.

P S
~ ~
<101> <10̄1̄>
<101> <1√2̄1̄>

P S
~ ~
<00̄1̄> <100>
<100> <210>

P S
~ ~
<213> <45̄1̄>

P S
~ ~
<1̄11> <011̄>

P
~

S
~

O

O
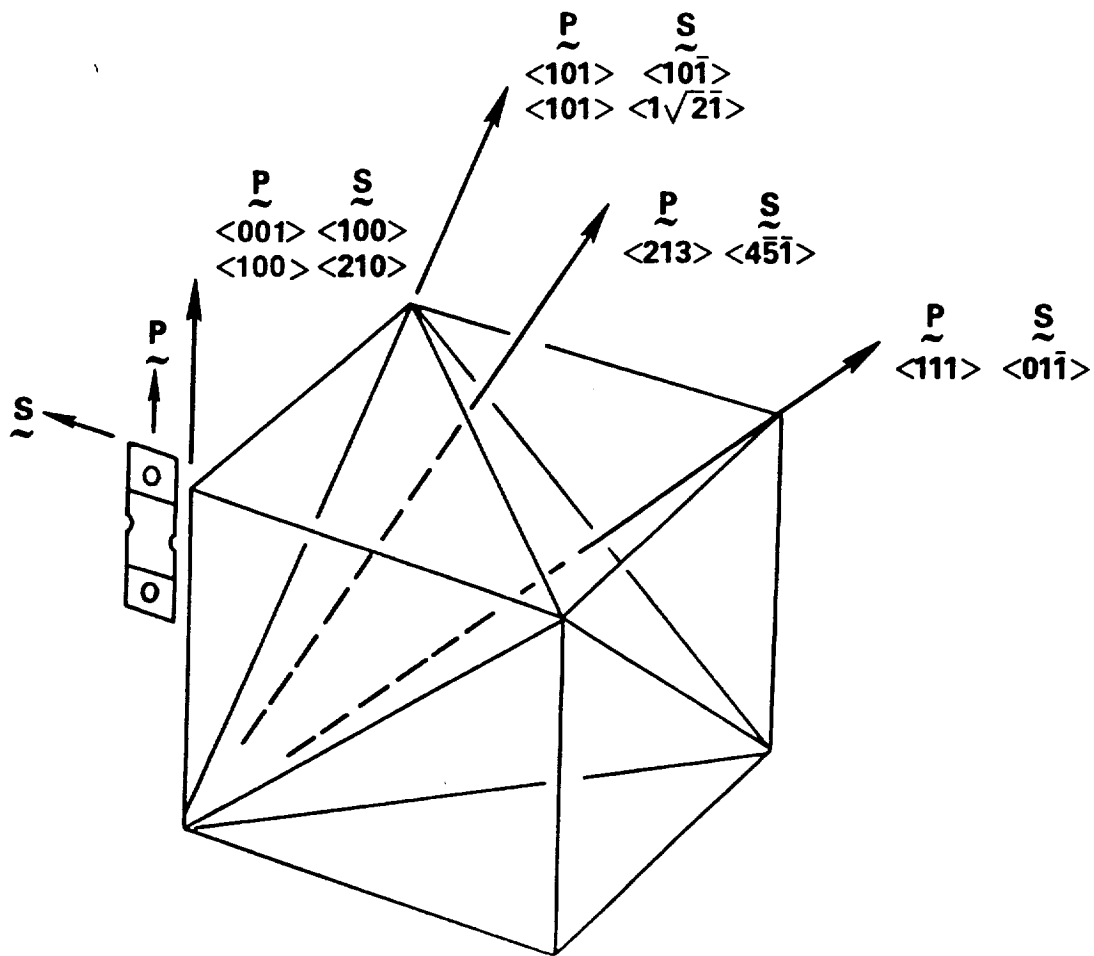
Figure 81   Notched Specimens In Six Crystal Orientations Will be Tested

An additional test concern with anisotropic materials is the introduction of bending moments and torques during tensile loading. This is the result of the coupling of shear and normal stress terms in the elastic stiffness matrix. Examination of the stiffness matrices and three dimensional finite element analyses for each of the primary orientations has shown this to be a concern only for the <011> and <213> primary orientations. The effect can be eliminated in the <011> specimens so long as the secondary orientations are 0.0 or 45.0 degrees (see Figure 82). Consequently these two secondary orientations were selected for testing. The effect cannot be eliminated for the <213> primary orientation specimens, however, a secondary orientation can be selected to minimize the distortions. The secondary orientation selected for the <213> specimens is such that the plane of the specimen lies in the <111> plane.
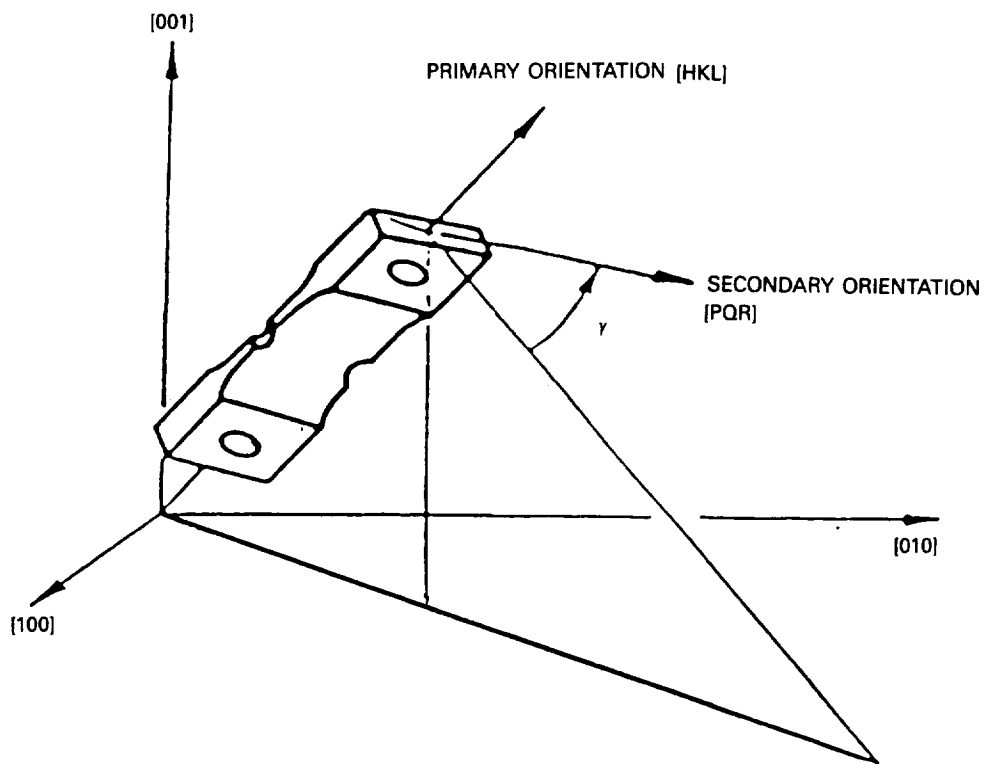
Figure 82   Definition of Secondary Orientation Angle, γ

b) Deformation and Fatigue Variables

The specimens were designed to include two notch acuities and the effect of transverse (plane strain) stresses. The stress concentrations (Kt) are 1.8 for the mild notch and 2.3 for the sharp notch if the primary orientation is <001>. Three dimensional analyses have shown that the Kt depends upon primary orientation but is only weakly dependent upon secondary orientation. The maximum octahedral slip system shear stress is dependent upon both primary and secondary orientations but does not have the same dependency as Kt. Consequently, the maximum slip system stress and the maximum principal stress (Kt) are not in constant ratios. The orientations chosen represent a "matrix" of principal stresses and slip system stresses which should facilitate identifying the critical quantities for deformation and fatigue.

The orientations have been selected so that slip traces would be visible on the lateral face of the specimens and so that the slip step height in the notch varies as much as possible. The slip step height may be important for fatigue crack initiation especially for HIP'd (Hot Isostatic Pressed) single crystals.

111

Finally, the three dimensional analyses show that the number of highly loaded slip systems (i.e., the propensity for multiple slip) varies considerably for the primary orientations to be tested. This may also be important for fatigue crack initiation and growth since it effects the degree of reversability of slip and local material hardening/softening.

c) Applicability of 2D Analyses

For an arbitrarily oriented anisotropic material, three dimensional structural analysis would be required due to the coupling of normal and shear stress and strain quantities. However, for certain combinations of material, geometric and loading axes this coupling is reduced making it possible to apply the assumptions of plane stress or plane strain. While it is not presumed that the plane stress or plane strain assumption is valid for calculating deformation or fatigue parameters in the notch, it is prudent to select orientations amenable to two dimensional analysis when possible. All orientations selected, except the <213> specimen, have such orientations. The elastic stiffness/compliance matrices are such that all out-of-plane quantities are uncoupled from the in-plane quantities and can be expressed by a simple set of ancillary equations. Furthermore, in the plane of the analysis, the direct stress and strain quantities are not coupled to the shear quantities.

11.2 PHYSICAL, THERMAL, AND MONOTONIC MECHANICAL PROPERTIES

Thirteen (13) monotonic tensile tests were conducted to supplement the tensile tests conducted in the Base Program.

Table 11 summarizes the results of these tests along with previously generated uncoated monotonic data. The reduction in area was not reported because many of the final cross sections at the lower temperatures were either highly elliptical due to coarse slip on octahedral planes or were multi-planar (also on the octahedral slip planes). Figure 83 is a plot of the 0.2% offset yield strength.

A subset of the tensile data was examined for ovalization of the cross section at failure to better understand the deformation. Specimens from the Base Program and from the Option 1 Program were measured. Specimens tested in the Base Program had 0.63 cm (0.25 in.) gage section diameters and were tested at 0.0083 %/sec while the Option 1 specimens had 0.76 cm (0.30 in.) gage section diameters and were tested at 0.10 %/sec strain rate. Table 12 and Figure 84 show the data obtained from these specimens. The ovalization of the cross section is characterized by the ratio of minimum and maximum diameter in the gage section at failure. The tensile elongations are shown for convenience.

Some degree of ovalization was observed for all orientations except the <001> orientation. There does not appear to be a clear trend in the data for the "off-axis" orientations. It is possible however that trends are masked by the fact that the data set contains two different strain rates. In addition, it is possible that those specimens having larger elongations may have more fully developed ovalization. Early tensile failure could then have prevented full ovalization.

TABLE 11

PWA 1480 MONOTONIC TENSILE DATA

Temp °C(°F)	Spec ID	<hkl>	Modulus MPa	(Msi)	0.2% Offset MPa	(Ksi)	UTS MPa	(Ksi)	EL %
21 (70)	JB49	001	123.4	(17.9)	1013.0	(146.9)	**	**	**
	JJB17	001	123.4	(17.9)	1011.7	(146.7)	1219.3	(176.8)	7.2
	JJB28	001	130.3	(18.9)	993.1	(144.0)	1090.3	(158.1)	8.2
	JJB21	001	128.3	(18.6)	1024.1	(148.5)	1195.2	(173.3)	5.6
	JKB5B	011	220.0	(31.9)	980.7	(142.2)	1033.8	(149.9)	13.0
	KB20	011	217.9	(31.6)	958.4	(139.0)	***	***	***
427 (800)	JA16*	001	113.8	(16.5)	989.4	(143.5)	1118.4	(162.2)	5.7
	KA2*	011	221.3	(32.1)	921.9	(133.7)	957.0	(138.8)	14.3
	LA36*	111	239.3	(34.7)	897.0	(130.1)	1393.5	(202.1)	11.7
	JLB18A	111	300.7	(43.6)	844.8	(122.5)	1395.9	(202.4)	13.5
	MA1*	123	198.6	(28.8)	837.7	(121.5)	1218.3	(176.7)	19.1
	JMB2A	123	210.3	(30.5)	799.3	(115.9)	932.4	(135.2)	5.3
649 (1200)	KA3*	011	176.5	(25.6)	929.4	(134.8)	1081.1	(156.8)	4.7
	LA51*	111	253.7	(36.8)	849.5	(123.2)	1245.2	(180.6)	23.7
	JLB14B	111	293.8	(42.6)	944.8	(137.0)	1175.2	(170.4)	4.2
	MA3*	123	193.7	(28.1)	824.0	(119.5)	1082.5	(157.0)	22.7
	JMB2B	123	193.8	(28.1)	793.1	(115.0)	1023.4	(148.4)	7.4
	JMB4B	123	189.0	(27.4)	773.1	(112.1)	944.8	(137.0)	8.8
760 (1400)	JA34*	001	101.4	(14.7)	1177.0	(170.7)	1324.5	(192.1)	14.1
	JJB22	001	100.7	(14.6)	1186.9	(172.1)	1271.7	(184.4)	12.8
	KA4*	011	174.4	(25.3)	948.1	(137.5)	1108.7	(160.8)	10.5
	LA52*	111	200.0	(29.0)	879.8	(127.6)	1093.5	(158.6)	22.1
	MA4*	123	180.0	(26.1)	891.5	(129.3)	985.3	(142.9)	17.8
871 (1600)	JA36*	001	102.0	(14.8)	715.0	(103.7)	1021.1	(148.1)	13.7
	KA6*	011	149.6	(21.7)	786.0	(114.0)	910.1	(132.0)	13.1
	LA53*	111	190.3	(27.6)	696.4	(101.0)	819.8	(118.9)	19.1
	MA5*	123	179.3	(26.0)	626.1	(90.8)	764.7	(110.9)	18.0
	JMB4A	123	183.4	(26.6)	842.8	(122.2)	884.8	(128.3)	9.4
982 (1800)	JA37*	001	88.3	(12.8)	452.3	(65.6)	695.0	(100.8)	23.0
	KA8*	011	133.1	(19.3)	519.9	(75.4)	628.8	(91.2)	16.7
	LA54*	111	189.6	(27.5)	427.5	(62.0)	557.8	(80.9)	22.2
	MA6*	123	164.8	(23.9)	431.6	(62.6)	539.9	(78.3)	25.9
1093 (2000)	JA38*	001	72.4	(10.5)	275.1	(39.9)	371.6	(53.9)	30.0
	KA9*	011	91.7	(13.3)	315.8	(45.8)	385.4	(55.9)	18.7
	LA55*	111	132.4	(19.2)	259.9	(37.7)	328.9	(47.7)	41.7
	MA9*	123	125.5	(18.2)	273.0	(39.6)	319.2	(46.3)	24.9

* Tests conducted at a strain rate of 0.0083 %/sec. All other tests were conducted at a strain rate of 0.1000 %/sec.
** Tube specimen. Interrupted tensile test @ 1.37%
*** Tube specimen. Interrupted tensile test @ 0.67%
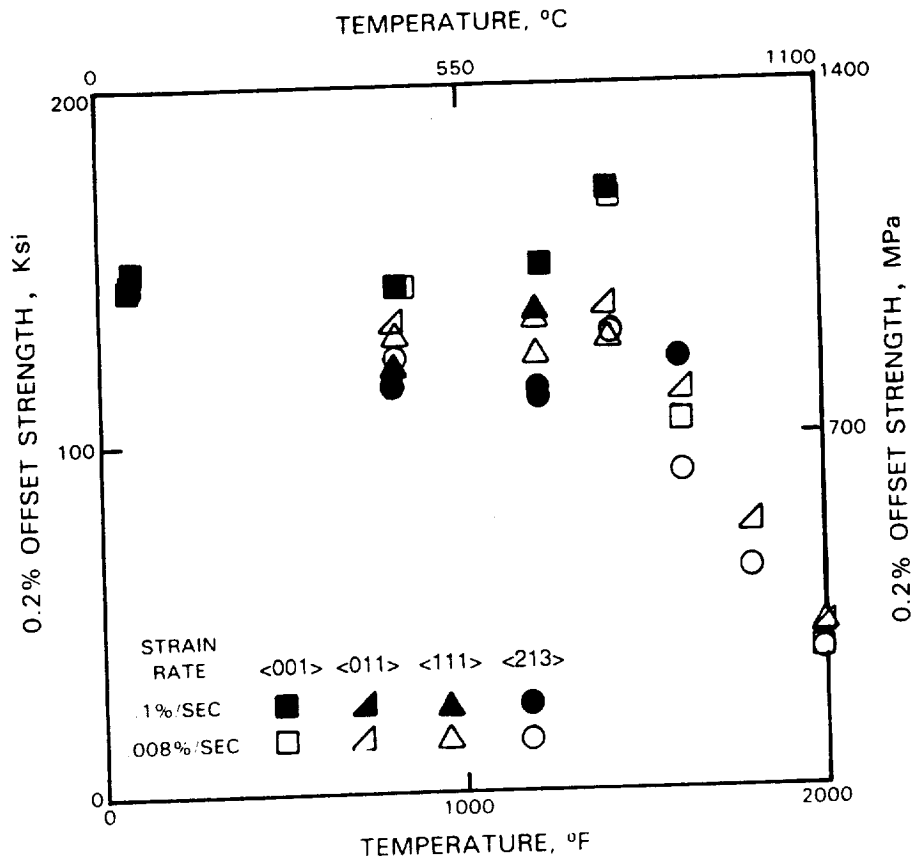
Figure 83   PWA 1480 0.2% Yield Strength Vs. Temperature

TABLE 12

TENSILE SPECIMEN OVALIZATION

Spec ID	Orientation	Temp °C(°F)	Elongation (%)	Dmin/Dmax
JJB-18	<001>	427 (800)	3.8	0.98
KA-2*	<011>	427 (800)	14.3	0.74
JLB-18A	<111>	427 (800)	13.5	0.89
MA-1	<123>	427 (800)	19.1	0.90
JJB-24	<001>	649 (1200)	5.6	0.98
KA-3*	<011>	649 (1200)	4.7	0.96
JLB-14B	<111>	649 (1200)	4.2	0.92
JMB-4B	<123>	649 (1200)	8.8	0.91
MA-3*	<123>	649 (1200)	22.7	0.79
JA-37*	<001>	982 (1800)	23.0	1.00
KA-8*	<011>	982 (1800)	16.7	0.80
MA-6*	<123>	982 (1800)	25.9	0.95

* 0.63 cm (0.25 in.) diameter specimens tested at 0.0083 %/sec.
  All others were 0.76 cm (0.30 in.) diameter tested at 0.1 %/sec.
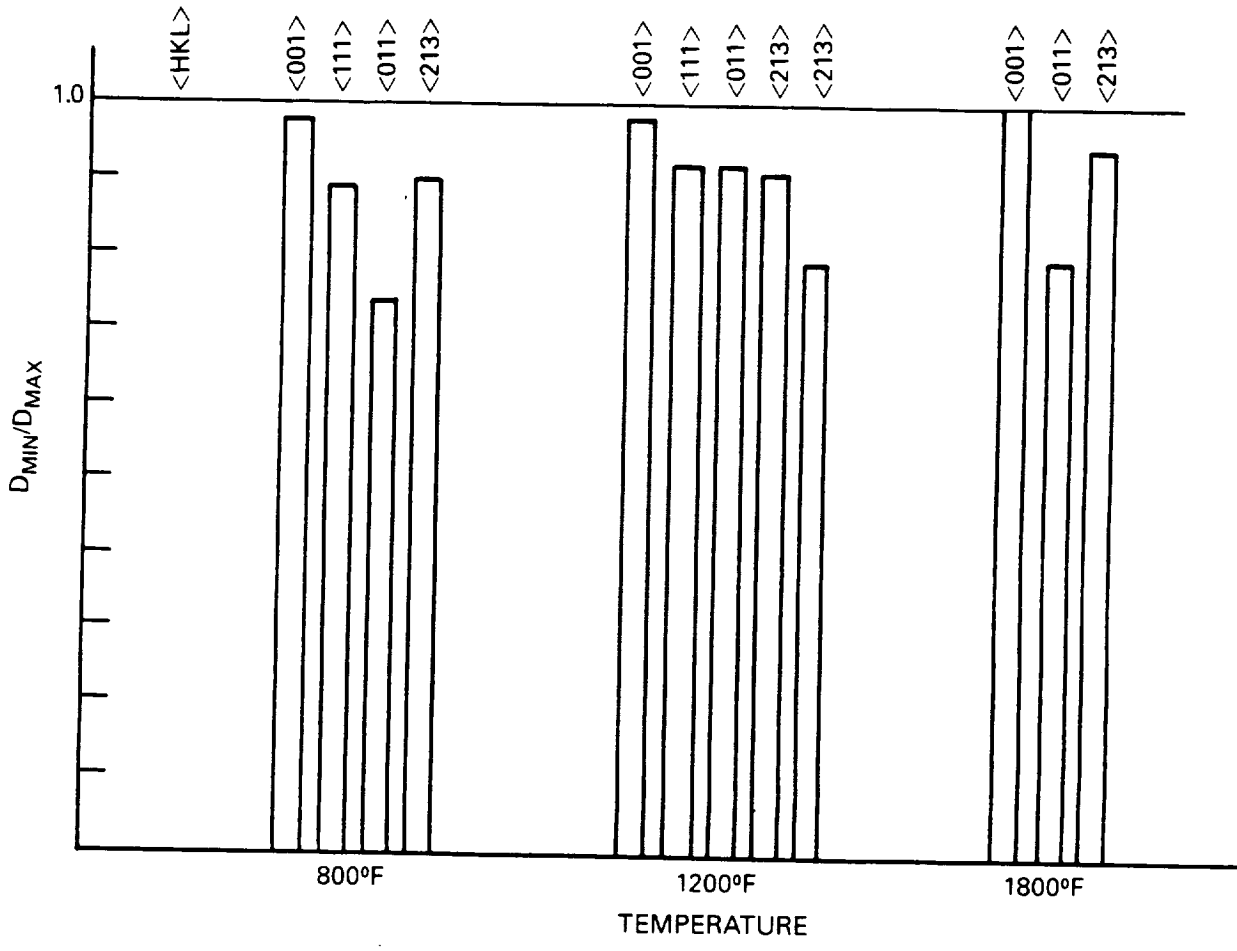
Figure 84   Ovalization of PWA 1480 Tensile Specimens

SECTION 12.0

TASK XIII - SELECTION OF CANDIDATE CONSTITUTIVE AND LIFE PREDICTION MODELS

12.1 SPECIMEN STRUCTURAL ANALYSIS

Three dimensional elastic structural analyses of the Option 1 specimen designs were conducted for use in the life prediction models. MARC finite element and BEST3D boundary element (which is currently being developed under NASA contract NAS3-23697) codes were used in this effort. Post processing routines were written to obtain slip system quantities that may be required during the life model development effort.

Figure 85 shows the typical BEST3D mesh used in the analyses and Table 13 summarizes the results. Stress values were normalized by the net section stress to give a stress concentration factor. Table 13 also includes the results for an isotropic material using the same BEST3D mesh. Figures 86 through 88 show the variation of the principal stress on the surface of the notch and the maximum octahedral slip system shear stress for a net section stress of 689 MPa (100 Ksi). A curve was fit through the BEST3D nodal points based on a more refined two dimensional boundary element analysis.

The finite element analyses were conducted using the K.3 version of the MARC program. This version of the MARC program calculates stresses at nodal points and they have been found to agree well with BEST3D boundary element results. The MARC analysis was chosen for all future analysis in the program because of its widespread use in industry and its nonlinear material capability. Figure 89 shows the finite element meshes used for each of the specimens. Prior to the anisotropic analyses, an isotropic material analysis was conducted to evaluate the accuracy that could be expected from the mesh being used. Results were within 3% of handbook solutions for the geometries. Figure 90 shows the results of the anisotropic stress analyses. The stresses shown are normalized to net section stress and correspond to the maximum values whether they are mid-plane or locations near the lateral surface of the specimen. It is only in the <213> and the <111> primary orientations that restrained out-of-plane warping leads to peak stresses near the lateral surface. In all other orientations, the peak stresses occur at the mid-plane. (It is interesting to note that fatigue initiation sites in the <111> primary oriented specimens did not appear to be at the lateral surface, indicating that the actual restraints during testing may not be as severe as those modeled by restrained lateral motion.) The principle stresses shown in Figure 90 are parallel to the contour of the notch at the angular location indicated. The slip system shear stress shown (also normalized to net section stress) is that corresponding to the octahedral slip system having the highest shear stress. All six components of global stress were used in determining the slip system shear stress.
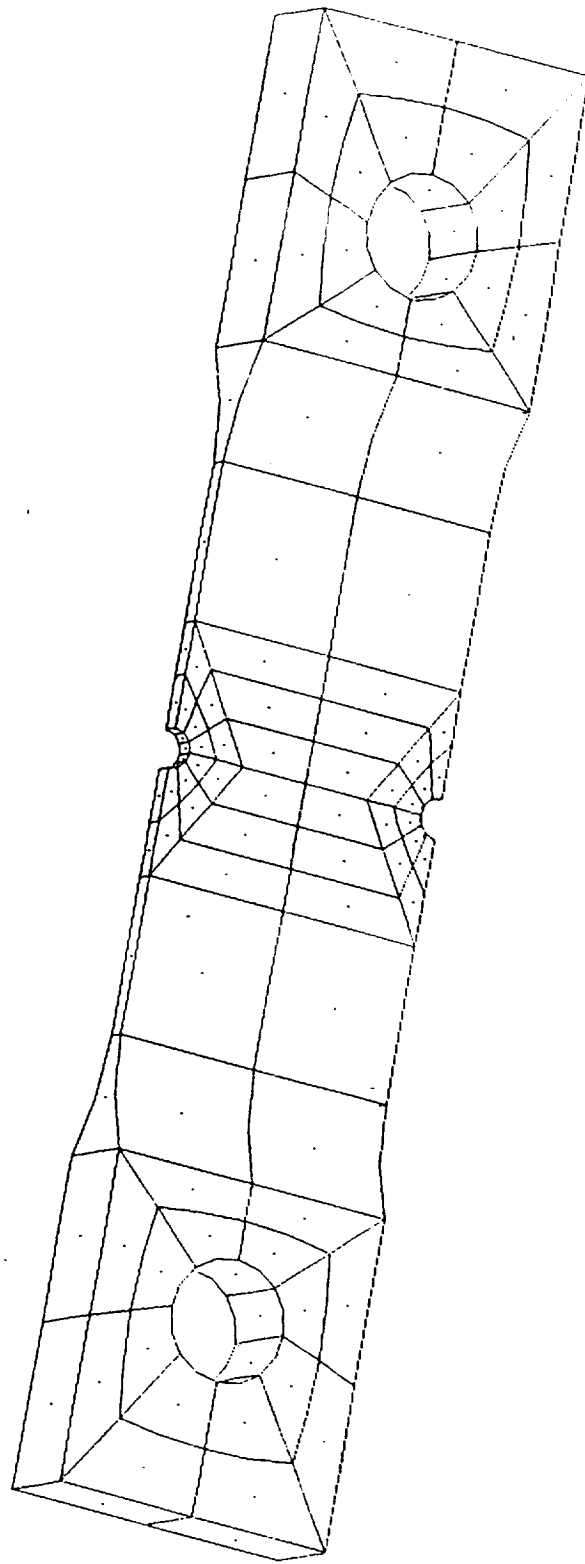
Figure 85 Boundary Element Mesh

TABLE 13

BEST3D ELASTIC ANALYSIS RESULTS FOR NOTCHED SPECIMENS

Specimen Type	Material and Orientation	Location in Notch (degrees)	Stress Concentration Kt	
Thin Sharp Notch	Isotropic	0.	2.59	
(TM3387)	Single Crystal <001><100>	0. 15.	2.14 2.26	
Thin Mild Notch	Isotropic	0.	2.00	
(TM3487)	Single Crystal <001><100>	0. 30.	1.64 1.73	
Thick Mild Notch	Isotropic	0.	2.06	
(LED3587)	Single Crystal <001><100>	0. 30.	1.74 1.79	} mid plane
		0. 30.	1.50 1.58	} lateral surface

Notes: 1. Angular location in the notch measured from the minimum section

2. Kt = principal stress / net section stress

118
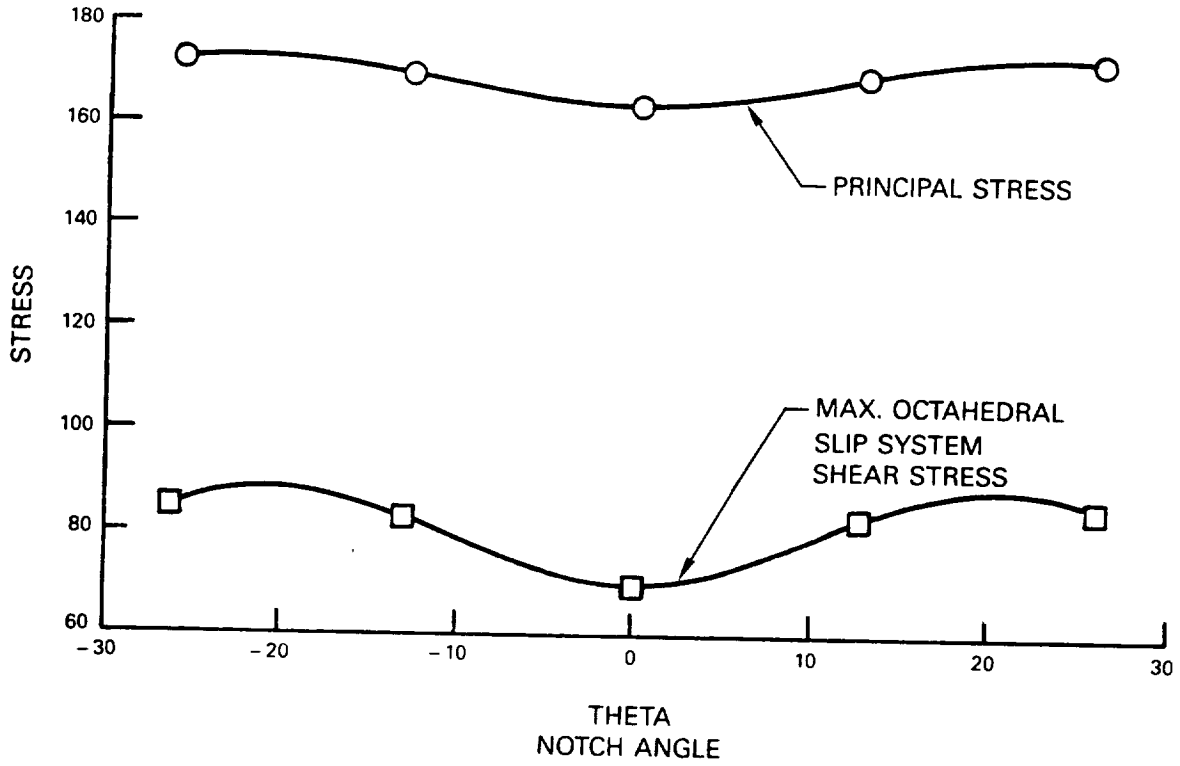
Figure 86   Stress Variation In the Thin Sharp Notch Specimen for 100 Ksi Nominal Stress
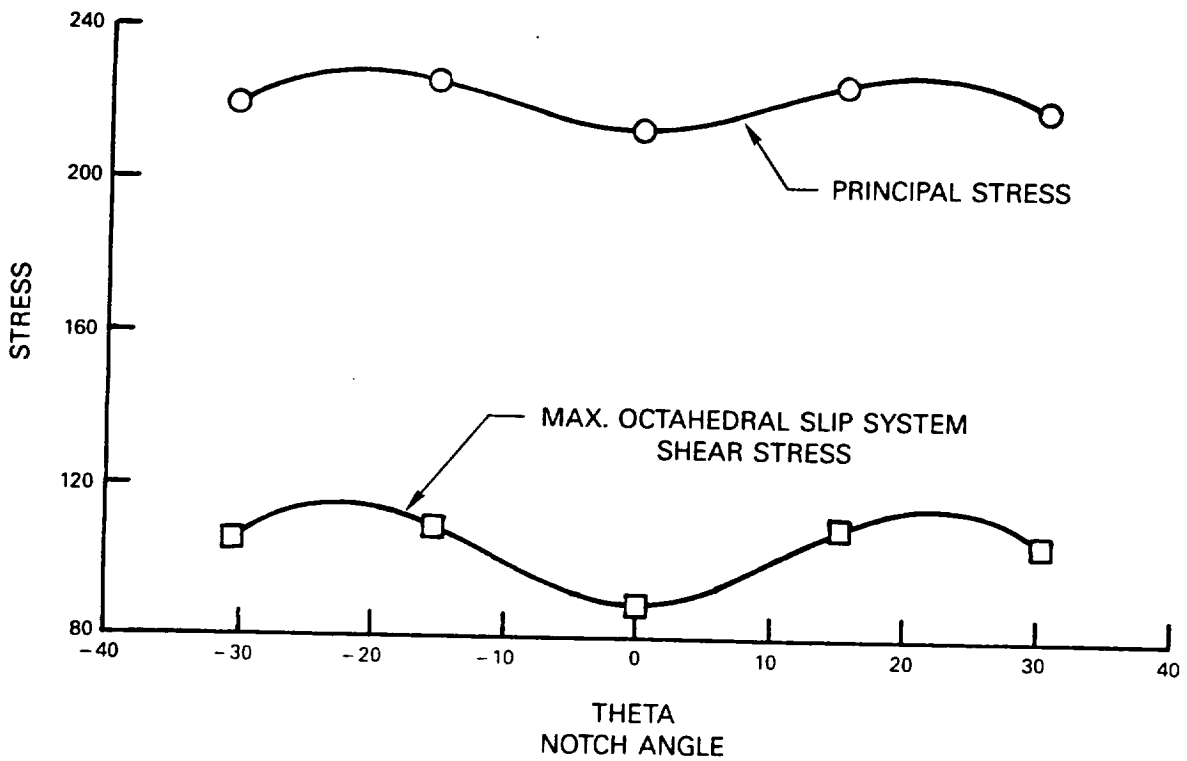
Figure 87   Stress Variation In the Thin Mild Notch Specimen for 100 Ksi Nominal Stress

119
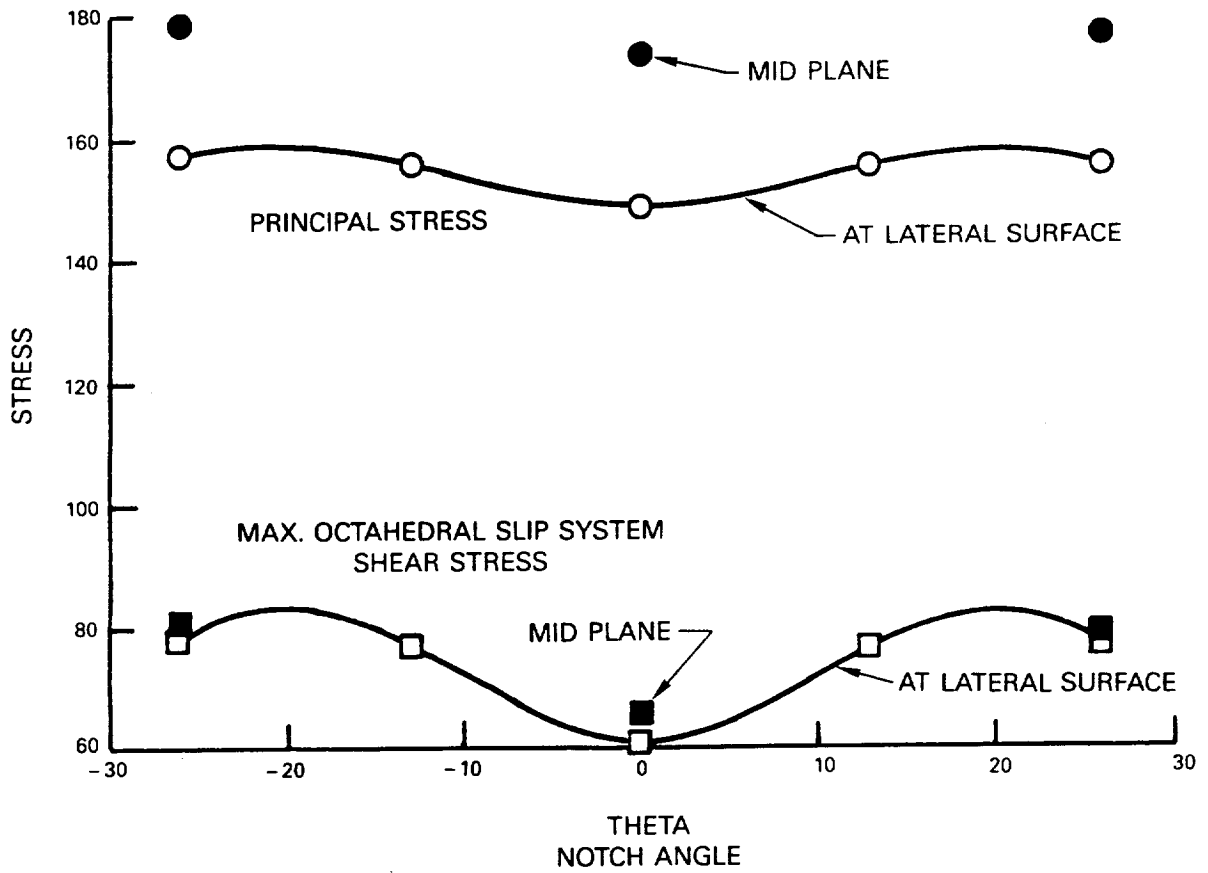
Figure 88 Stress Variation In the Thick Mild Notch Specimen for 100 Ksi Nominal Stress

- THIN, MILD NOTCHED SPECIMEN; TM3487
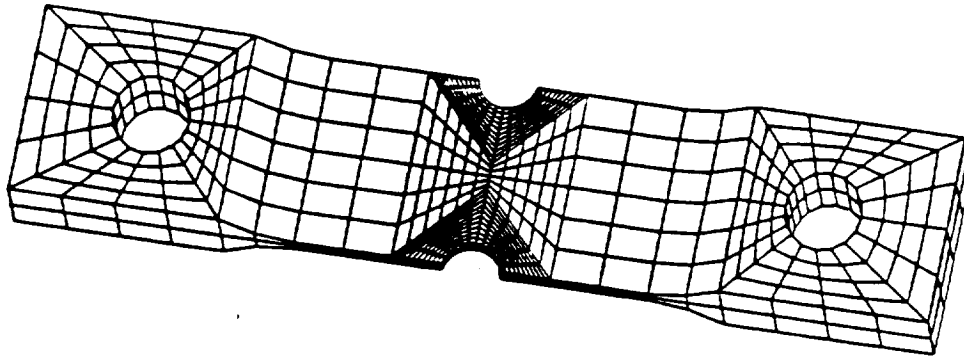
- THIN, SHARP NOTCHED SPECIMEN; TM3387
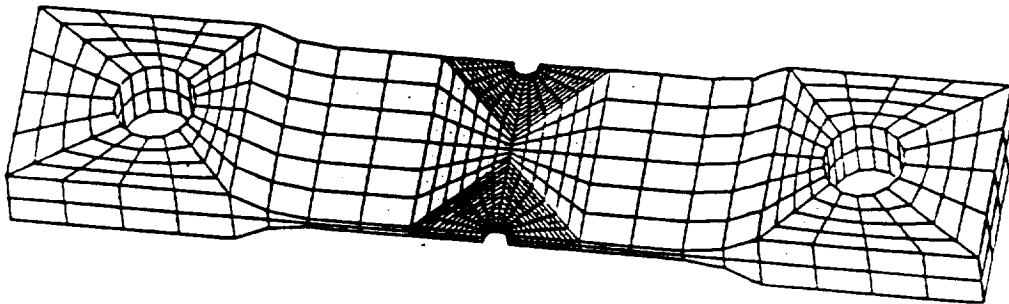
- THICK, MILD NOTCHED SPECIMEN; LED3587
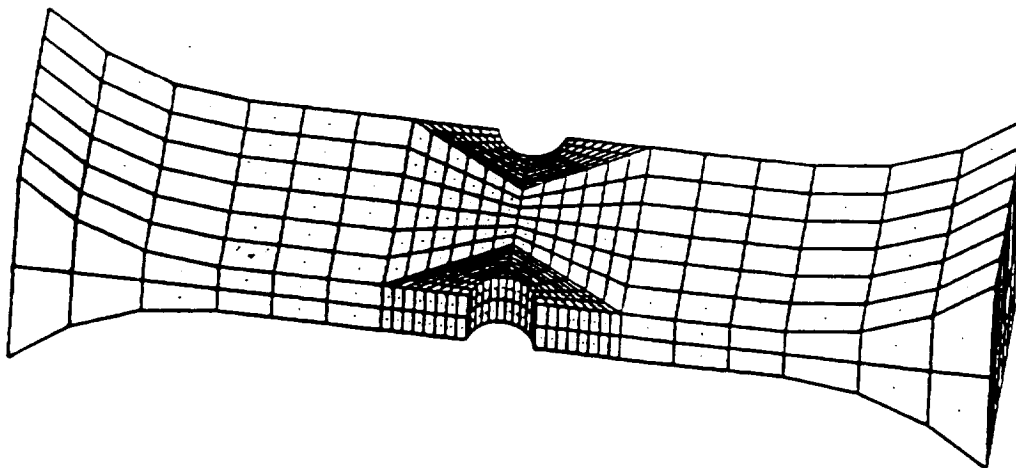
Figure 89   MARC Finite Element Meshes

121

		TM3387 THIN, SHARP NOTCHED		TM3487 THIN, MILD NOTCHED		LED3587 THICK, MILD NOTCHED	
ORIENTATION PRIMARY	SECONDARY	Kt	θ	Kt	θ	Kt	θ
(001)	(100)	2.48	0°	1.78	26°	1.89	26°
(001)	(210)	2.37	0°	1.70	26°	1.83	26°
(011)	(01-1)	3.20	0°	2.58	0°	2.90	0°
(011)	($\sqrt{21}$-1)	3.04	0°	2.48	0°	2.43	0°
(111)	(01-1)	2.95	0°	2.46	0°	2.54	0°
(123)	(5-41)	2.85	0°	2.25	0°	2.27	0°

PRINCIPAL STRESSES

		TM3387 THIN, SHARP NOTCHED		TM3487 THIN, MILD NOTCHED		LED3587 THICK, MILD NOTCHED	
ORIENTATION PRIMARY	SECONDARY	Kt	θ	Kt	θ	Kt	θ
(001)	(100)	1.06	23	0.87	21	0.87	21
(001)	(210)	1.06	23	0.87	22	0.82	22
(011)	(01-1)	1.12	0	0.89	0	0.92	0
(011)	($\sqrt{21}$-1)	1.02	0	0.90	0	0.87	13
(111)	(01-1)	0.81	16	0.84	10	0.73	13
(123)	(5-41)	0.96	0	0.87	0	0.88	0

SLIP SYSTEM SHEAR STRESSES ON MOST HIGHLY STRESSED OCTAHEDRAL SLIP SYSTEM

Figure 90 MARC Finite Element Stress Analysis Results

12.2 CANDIDATE CONSTITUTIVE MODELS

The slip system based constitutive model developed in the Base Program will serve as the starting point for model development for the low temperature notched regions. A major difficulty with this model and all "unified" material models is that the basic mathematical formulation is strain rate dependent and so has difficulty in reproducing rate independent behavior at low

temperatures. This difficulty has been overcome by incorporating a subroutine in the model which changes the applied time increment to one which will result in a constant reference strain rate for low temperatures. The transition between rate dependence and rate independence occurs gradually between 816°C (1500°F) and 704°C (1300°F).

The fatigue data obtained to date indicates that the total stress excursions in the notches is less than twice the 0.2% yield strength for low cycle fatigue lives greater than approximately 1000 cycles. See Figures 83 and 91. This conclusion is based on elastic finite element analyses of the specimens which should produce an upper bound on the stress range. This indicates that large cyclic inelastic strains are not likely to be encountered in the notches. In addition, only small cyclic inelastic strains were observed in strain controlled fatigue tests whose lives were greater than approximately 1000 cycles. In contrast, significant inelasticity is expected during the initial loading portion of the fatigue cycle. So the efforts in the constitutive model development will first focus on the monotonic response of the material. This will be important for determining the mean stress in the notches.
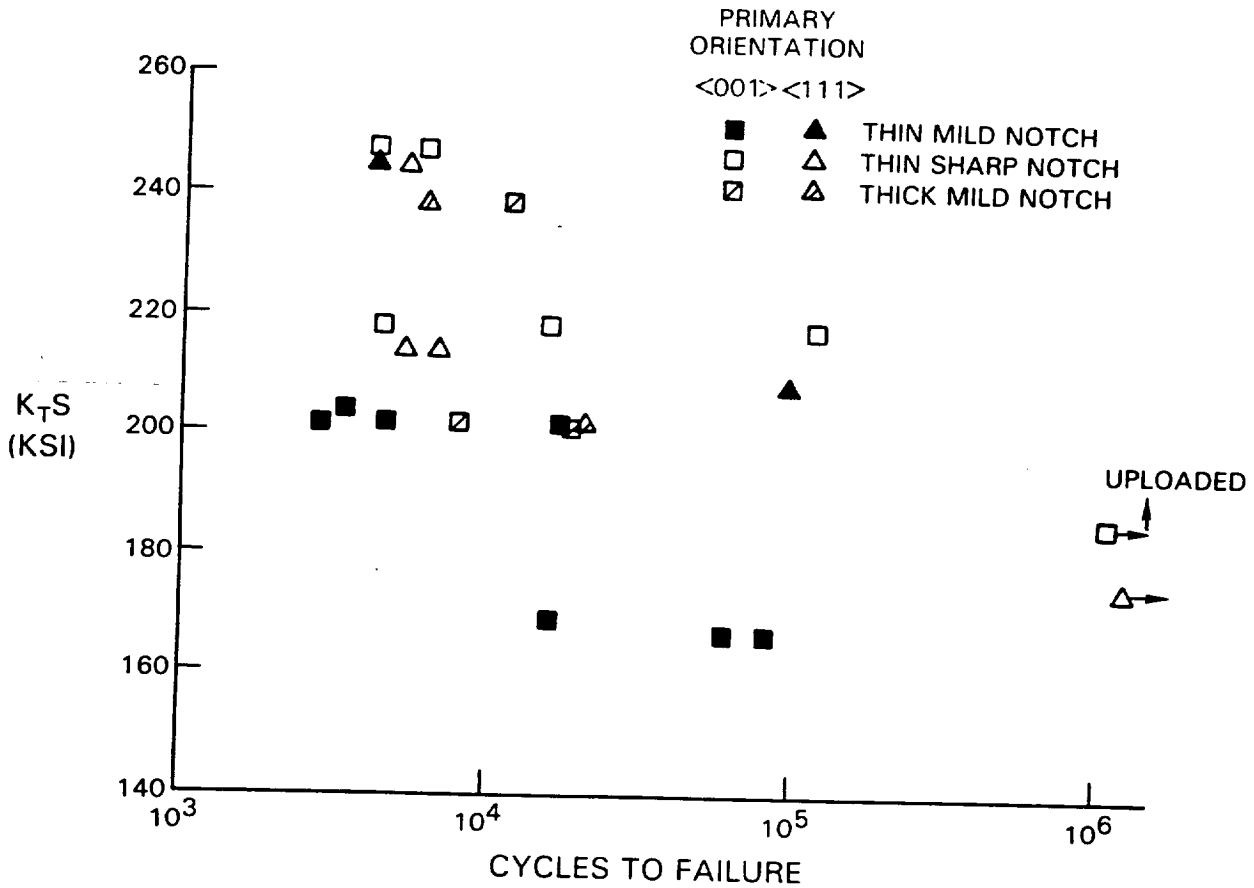
Figure 91   649°C (1200°F) Notched LCF Un-HIP'd PWA 1480 Life Results

123

12.3 CANDIDATE LIFE PREDICTION MODELS

Candidate life prediction models are being identified. These include the simple macroscopic approach of correlating life with maximum principal stress. A second possible approach has been identified from a previous Government sponsored program, "Fatigue and Fracture of Advanced Blade Materials", AFWAL-TR-84-4167 (Reference 3). In that program, a correlating parameter, W_{eff}, was reported for uniaxial fatigue tests:

$$W_{eff} = \Delta W \frac{\sigma_{\langle 111 \rangle}}{E} \tag{55}$$

where ΔW = the tensile hysteretic energy

$\sigma_{\langle 111 \rangle}$ = the maximum stress normal to an octahedral plane

E = the apparent modulus of the uniaxial specimen.

This second approach was evaluated in the base portion of this program for use in modeling elevated temperature airfoil conditions.

The correlations reported in AFWAL-TR-84-4167 and the Base Program were encouraging but additional effort is required to extend the approach to predominantly elastic loading conditions and to multiaxial situations.

Elastic stress range was used as a starting point in developing a life model. Figure 91 shows the initial 649°C (1200°F) notched failure data plotted against concentrated elastic stress in the notch. The elastic stress range was obtained from the finite element specimen analyses discussed previously. Figure 91 shows that there is a first order correlation of the data based on this parameter, especially at higher stress levels. However, there are clear trends with specimen type and possibly orientation.

124

SECTION 13.0

TASK XIV - CYCLIC LIFE AND CONSTITUTIVE BEHAVIOR

13.1 TEST FACILITY

The tests for Option 1 are being conducted on two MTS servohydraulic test machines available at United Technologies Research Center. Strain controlled tests employ standard MTS extensometry and are controlled by a DEC computer running MTS BASIC. Special purpose control and data acquisition programs provide control for constitutive and strain controlled fatigue tests. Load controlled fatigue tests are controlled by the standard function generators supplied with each system. Specimens are heated with standard resistance furnaces.

13.2 CYCLIC LIFE TESTS.

13.2.1 Specimen Inspection Technique

A sensitive die penetrant has been used to inspect for cracks but without success in spite of frequent inspections. The inspection technique is capable of detecting cracks as small as 0.25 mm (0.010 in.). Inspection intervals are as frequent as 2000 cycles. More frequent inspections are impractical due to the large number of tests to be conducted and the life regime being tested (5000 to 100000 cycles).

All subsequent efforts to find developing fatigue cracks have failed. Scanning Electron Microscopy has shown that the steady fatigue crack zone is confined to a very small surface crack length which in many cases is near the detection limits of standard wink zyglo techniques. Consequently, inspections for crack initiation were suspended. The remaining specimens will be cycled to failure.

13.2.2 Fatigue Tests

Initial smooth and notched fatigue tests have been completed. The majority of the tests were conducted at 649°C (1200°F) although a few tests were conducted at 760°C (1400°F) and 871°C (1600°F). A summary of specimen geometries, test conditions, and lives is presented in Tables 14a through 14g. In Tables 14a and 14b, the strain and stress limits correspond to the tenth fatigue cycle. Virtually no cyclic relaxation was observed at 649°C (1200°F). In Tables 14c through 14g, Smax. refers to the net section stress. R is the ratio of the minimum stress to the maximum nominal stress in the fatigue cycle. The stress concentration factor is also shown corresponding to the maximum principal stress location in the notch. Finally, the concentrated elastic stress range is shown for each specimen.

125

TABLE 14a

SMOOTH SPECIMEN LOW CYCLE FATIGUE

PWA 1480. No-HIP
Strain Rate = 0.4% Per Sec.

Spec. No.	Orient.	Temp. (°F)	Strain % Max.	Strain % Min.	Stress (KSI) Max.	Stress (KSI) Min.	Life (Cycles)
JJB49	(001)	1200	1.509	0.014	158.0	−76.5	1326
JJB43	(001)	1200	1.120	0.020	149.0	−35.0	4414
JJB50	(001)	1200	1.202	0.008	159.5	−39.3	5673
JJB45	(001)	1200	1.740	0.270	165.5	−61.0	1593
JLB58	(111)	1200	0.809	0.008	138.1	−138.8	1016
JLB56	(111)	1200	0.600	0.000	120.0	−104.0	3410
JLB66	(111)	1200	0.591	0.015	126.1	−105.0	7356
JLB57	(111)	1200	0.960	0.150	148.3	−150.3	843
JLB59	(111)	1200	1.205	0.625	132.9	− 91.5	7904
JLB60	(111)	1200	1.219	−0.603	171.7	−168.7	26
JLB61	(111)	1200	0.291	−0.284	119.7	−118.4	7101
JMB29	(213)	1200	1.212	0.000	130.6	−140.6	79
JMB41	(213)	1200	0.795	0.013	122.9	−120.4	4175
JMB35	(213)	1200	0.600	0.000	113.7	− 48.8	114789
JMB32	(213)	1200	0.602	0.008	117.7	− 61.5	45640+
JMB36	(213)	1200	0.601	0.005	132.8	− 6.5	34676
JJB41	(001)	1400	1.120	0.030	153.0	− 13.0	4912
JJB46	(001)	1600	1.160	0.000	119.7	− 28.0	5431
JLB64	(111)	1600	0.602	0.007	116.9	− 79.4	3354
JMB39	(213)	1600	1.170	0.005	133.1	−113.0	350

TABLE 14b

SMOOTH SPECIMEN LOW CYCLE FATIGUE

PWA 1480. No-HIP
Strain Rate = 0.4% Per Sec.

Spec. No.	Orient.	Temp. (°F)	Strain % Max.	Min.	Stress (KSI) Max.	Min.	Life
JJB74	(001)	1200	1.814	0.015	186.8	-100.6	1471
JJB75B	(001)	1200	1.508	0.011	180.0	- 68.0	2964
JJB79	(001)	1200	1.202	0.010	167.8	- 31.9	20051
JJB80	(001)	1200	1.103	0.021	160.2	- 19.7	32448
JLB25B	(111)	1200	0.811	0.003	145.5	-144.2	1166
JLB25A	(111)	1200	0.590	0.014	137.2	-101.3	27410
JLB26A	(111)	1200	0.492	0.019	125.1	- 70.7	325570
JKB13A	(011)	1200	0.902	0.016	126.4	-112.2	1806
JKB13B	(011)	1200	0.890	0.027	131.1	-110.5	737
JJB78	(001)	1600	1.164	0.007	133.1	- 26.9	12413
JJB81	(001)	1600	1.160	0.011	134.4	- 24.9	13174
JLB26B	(111)	1600	0.598	0.007	123.9	- 82.1	4269

127

TABLE 14c

THIN MILD NOTCHED LOW CYCLE FATIGUE

PWA 1480. No-HIP 1 CPS, Load Control

Spec. No.	Orient. P	S	KT	Temp. (°F)	SMAX (KSI)	R	KTΔS (KSI)	Life
JB26B	(001)	(010)	1.78	1200	115	0.05	194.5	2860
JB132A	(001)	(010)	1.78	1200	115	0.05	194.5	4721
JB18A	(001)	(010)	1.78	1200	115	0.05	194.5	17227
JB30A	(001)	(010)	1.78	1200	115	0.50	102.4	1122917
JB30B	(001)	(010)	1.78	1200	95	0.05	160.6	62119
JB18B	(001)	(010)	1.78	1200	95	0.05	160.6	84626
JJB48A	(001)	(210)	1.70	1200	115	0.05	185.7	3434
JJB48B	(001)	(210)	1.70	1200	95	0.05	153.4	16427
JJB56B	(001)	(210)	1.70	1200	95	0.05	153.4	85040
JLB69B	(111)	(01-1)	1.70	1200	100	0.05	232.8	4178
JLB69A	(111)	(01-1)	1.70	1200	85	0.05	198.6	97870
JB26A	(001)	(100)	1.78	1400	115	0.05	194.5	2476
JB132B	(001)	(100)	1.78	1600	115	0.05	194.5	1128
JB58B	(001)	(100)	1.78	1600	95	0.05	160.6	3402
JLB70A	(111)	(01-1)	2.45	1600	100	0.05	232.8	930
JLB70B	(111)	(01-1)	2.45	1600	85	0.05	198.6	1952

128

TABLE 14d

THIN SHARP NOTCHED LOW CYCLE FATIGUE

PWA 1480. No-HIP, Load Control, 1 CPS

Spec. No.	Orient. P	S	KT	Temp. (°F)	SMAX (KSI)	R	KTΔS (KSI)	Life
830-4B	(001)	(100)	2.48	1200	100	0.05	235.6	4190
JJB4B	(001)	(100)	2.48	1200	100	0.05	235.6	5157
789-3B	(001)	(100)	2.48	1200	88	0.05	207.3	16015
789-4A	(001)	(100)	2.48	1200	88	0.05	207.3	117596
JJB4A	(001)	(100)	2.48	1200	75	0.05	176.7	1,070,000+ *
JLB73A	(111)	(01-1)	2.94	1200	83	0.05	232.6	5286
JLB73B	(111)	(01-1)	2.94	1200	73	0.05	204.6	5154
JLB74A	(111)	(01-1)	2.94	1200	73	0.05	204.6	6888
JLB74B	(111)	(01-1)	2.94	1200	57	0.05	159.7	1,250,000+

+ Indicates suspended test
* Subsequently cycled at KTΔS = 235.6 KSI for 4485 cycles to failure

TABLE 14e

THICK MILD NOTCHED LOW CYCLE FATIGUE

PWA 1480. No-HIP, Load Control, 1 CPS

Spec. No.	Orient. P	S	KT	Temp. (°F)	SMAX (KSI)	R	KTΔS (KSI)	Life
789-2	(001)	(100)	2.08	1200	115	0.05	227.2	12048
830-2	(001)	(100)	2.08	1200	97.3	0.05	192.3	8253
830-3	(001)	(100)	2.08	1200	97.3	0.05	192.3	17232
JLB75	(111)	(01-1)	2.54	1200	94.2	0.05	227.3	6343
JLB76	(111)	(01-1)	2.54	1200	79.5	0.05	191.8	20918

TABLE 14f

THIN MILD NOTCHED LOW CYCLE FATIGUE

PWA 1480. No-HIP, Load Control, 1 CPS

Spec. No.	Orient. P	S	KT	Temp. (°F)	SMAX (KSI)	R	KTΔS (KSI)	Life
JJB82A	(001)	(100)	1.78	1200	115	0.05	194.5	413610
JJB82B	(001)	(100)	1.78	1200	115	0.05	194.5	327143
JJB84A	(001)	(100)	1.78	1200	95	0.05	160.6	1,060,620+
JJB104	(001)	(210)	1.70	1200	95	0.05	153.4	1,334,290+

+ Indicates suspended test.

TABLE 14g

THIN SHARP NOTCHED LOW CYCLE FATIGUE

PWA 1480. HIP, Load Control, 1 CPS

Spec. No.	Orient. P	S	KT	Temp. (°F)	SMAX (KSI)	R	KTΔS (KSI)	Life
JJB95A	(001)	(100)	2.48	1200	100	0.05	248.0	48190

Initial smooth section strain controlled fatigue tests showed a propensity to fail in the threaded section outside the monitored gage section. The smooth specimen geometry was subsequently redesigned (see Section 11.1).

In general, cracks were found to initiate from casting micropores in un-HIP'd material and at locations corresponding to the maximum principal stress rather than the maximum principal strain. For the orientations tested to date this initiation site also coincides with the maximum slip system shear stress, so that it is not possible to conclude which of these two parameters is more important. Figure 92 is an overall view of a <001><100> specimen cycled between 41 and 793 MPa (6 and 115 ksi) nominal stress at 760°C (1400°F). Life to failure was 2976 cycles. Fatigue cracks initiated in both notches near the maximum stress location and, in the latter stage of growth, progressed along a <111> plane intersecting the specimen surface at an angle of 48 degrees from a line connecting the notch centers. For a perfectly aligned <001><100> specimen, the slip system with the highest shear stress intersects the specimen surface at 45 degrees from a line connecting the notch centers. Figure 93 shows the initiation sites in the primary crack in more detail. Cracks initiated from two separate pores which were located at angles of 22 and 30 degrees from the minimum specimen dimension. The maximum stress location in this orientation is calculated to be 23 degrees from the notch bottom. The crack planes near the initiation sites were perpendicular to the maximum stress direction rather than along a single <111> plane.
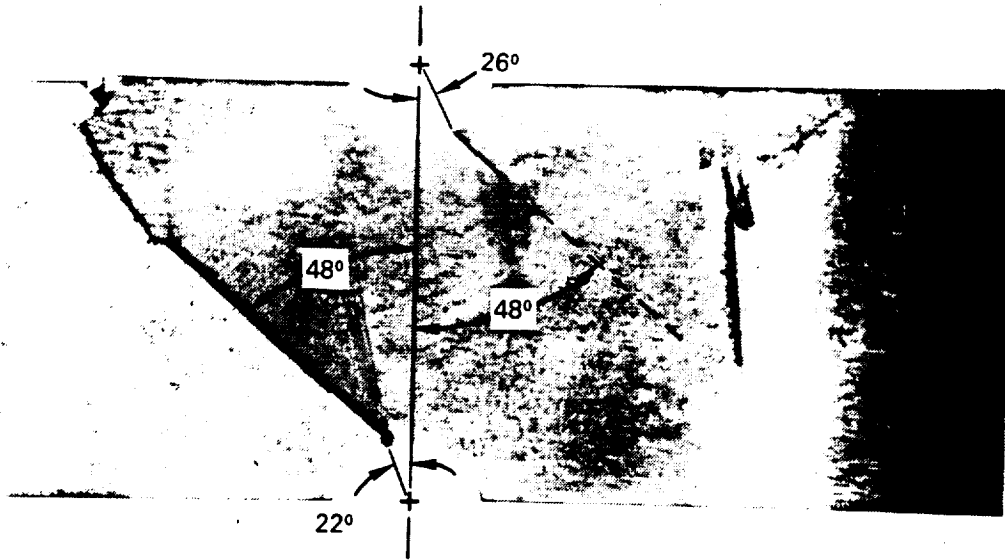
Figure 92 Fatigue Cracks In <001><100> Mild Notched Specimen
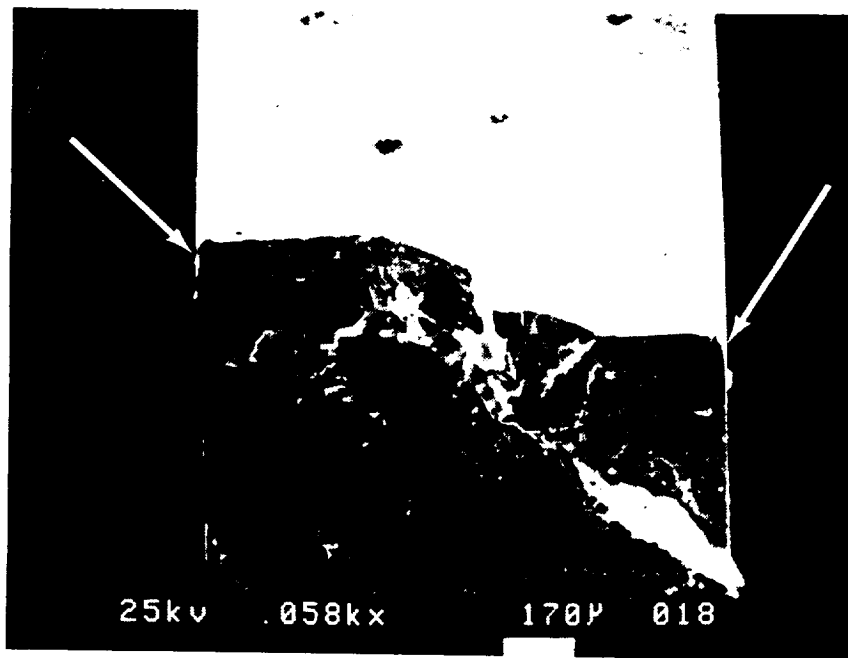
Figure 93 Fatigue Crack Origins At Casting Micropores Located Near the
Maximum Stress/Maximum Slip System Shear Stress

131

Testing of notched Hot Isostatically Pressed (HIP'd) specimens has been initiated. Substantial life improvements are observed for HIP'd material when compared to un-HIP'd material. The fatigue crack initiation sites of HIP'd specimens correspond to the maximum stress location in the notch. They are neither casting pores (as would be expected since the material is HIP'd to eliminate pores) nor slip bands at the surface. The smooth HIP'd data, although limited, indicates that a life improvement remains at 871°C (1600°F) for <001> bars (although possibly somewhat diminished from that observed at 649°C (1200°F)), but virtually no life improvement remained at 871°C (1600°F) for the HIP'd <111> specimen tested.

13.3 CONSTITUTIVE TESTS

Two room temperature tensile tests were conducted using tube specimens rather than the solid cylindrical specimens used in previous constitutive tests. Unlike the solid specimens, the tube specimens exhibited very fine, evenly distributed slip lines throughout the gage section. The stress-strain response of the tube specimen did not display an unstable strain burst at the onset of yielding. The 0.2% yield strength measured from the tube specimens compared very well to the solid bar data.

The first load cycle of each 649°C (1200°F) smooth bar fatigue test was examined to obtain a larger data base for modulus and yield strength. In addition, the complete tensile curves from the Base Program and Option 1 were compiled to provide a more complete picture of material response as the materal becomes inelastic. Typical data representation is shown in Figures 94 and 95.
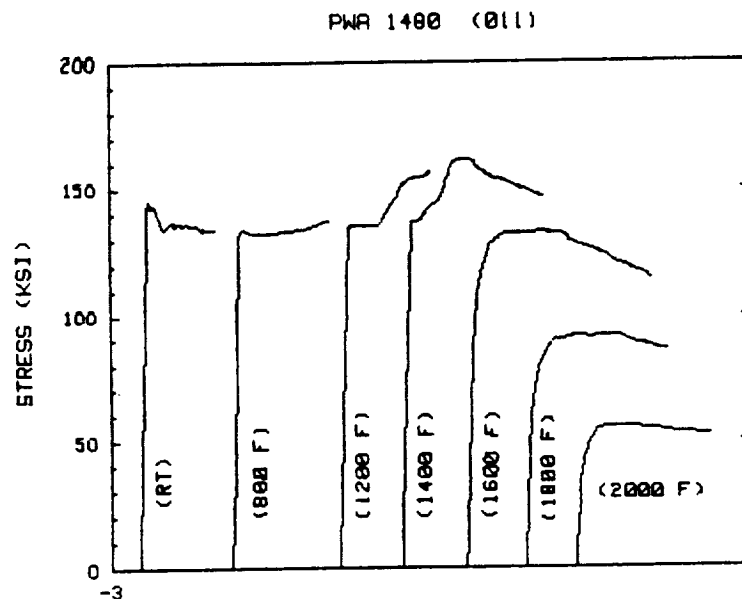
Figure 94   PWA 1480 <011> Monotonic Tensile Response From Room Temperature to 2000°F

132
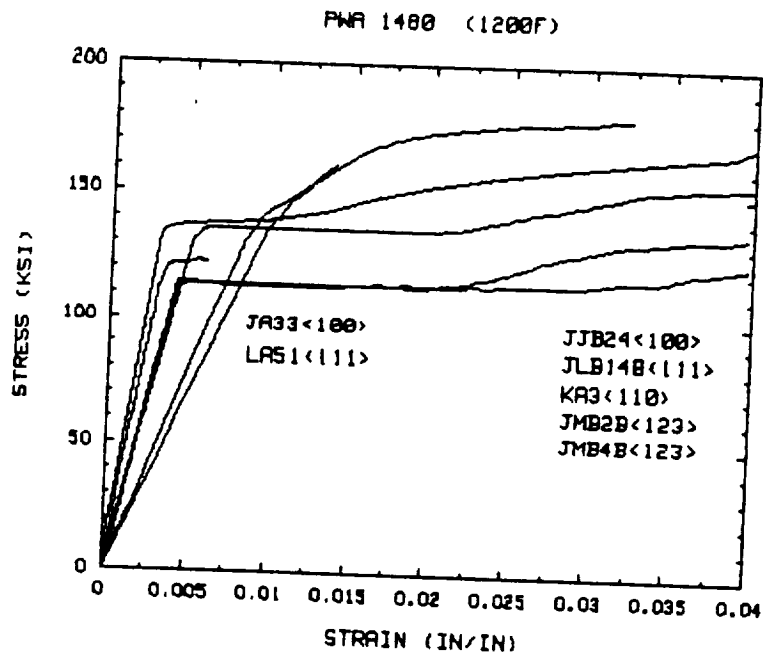
Figure 95 PWA 1480 Monotonic Tensile Response At 1200°F for Four Primary
Orientations: <001>, <111>, <011> and <213>

133

SECTION 14.0

REFERENCES

1. Swanson, G.A.; Linask, I.; Nissley, D.M.; Norris, P.P.; Meyer, T.G.; and Walker, K.P.: "Life Prediction and Constitutive Models for Engine Hot Section Anisotropic Materials Program." NASA CR-174952, February, 1986.

2. Swanson, G.A.; Linask, I.; Nissley, D.M.; Norris, P.P.; Meyer, T.G.; and Walker, K.P.: "Life Prediction and Constitutive Models for Engine Hot Section Anisotropic Materials Program." NASA CR-179594, April, 1987.

3. DeLuca, D.P. and Cowles, B.A.: "Fatigue and Fracture of Advanced Blade Materials." AFWAL-TR-84-4167, February, 1985.

4. Heine, J.E., Warren, J.R., and Cowles, B.A.: "Thermal Fatigue of Coated Blade Materials, Final Report." WRDC-TR-89-4027, December, 1988.

5. Moreno, V., Nissley, D.M., and Lin, L.S.: "Creep Fatigue Life Prediction for Engine Hot Section Materials (Isotropic), Second Annual Report." NASA CR-174844, December, 1984.

6. Nelson, R.S., Schoendorf, J.F., and Lin, L.S.: "Creep Fatigue Life Prediction for Engine Hot Section Materials (Isotropic), Interim Report." NASA CR-179550, December, 1986.

7. Moreno, V.: "Development of a Simplified Analytical Method for Representing Material Cyclic Response," NASA CR-168100, January, 1983.

8. Walker, K. P.: "Research and Development Program for Nonlinear Structural Modeling with Advanced Time-Temperature Dependent Constitutive Relationships," NASA CR-165533, November, 1981.

9. Pokhmurskii, V.I.: "Strength and Plasticity of Diffusion-Coated Steels," Protective Coatings on Metals, Vol. 6, 1972, pp. 259-266, Translated from Russian 1984.

10. Kolomytsev, P.T.: "Heat-Resistant Diffusion Coatings For Parts of Energy-Conversion Machines," Protective Coatings on Metals, Vol. 6, 1972, pp. 267-276, Translated from Russian 1984.

11. Lozitskii, A.A., et al.: "Effect of Protective Diffusion Coating on Thermal Fatigue Strength of Creep-Resistant Materials," Protective Coatings on Metals, Vol. 6, 1972, pp. 294-300, Translated from Russian 1984.

12. Leis, B.N. and Forte, T.P.: "Nonlinear Damage Analysis: Postulate and Evaluation," Final Report on Contract NAS3-22825 to NASA Lewis Research Center, February, 1983.

13. Cetel, A.D. and Duhl, D.N.: "Microstructure-Property Relationships in Advanced Nickel Base Superalloy Airfoil Castings," Presented at the 2nd Metals Conf. sponsored by the Society for the Advancement of Material and Process Engineering (SAMPE), August 2-4, 1988.

14. Shah, D.M. and Duhl, D.N.: "The Effect of Orientation, Temperature and Gamma Prime Size on the Yield Strength of a Single Crystal Nickel Base Superalloy," Superalloys 1984, Ed. by M. Gell et al., Met. Soc. AIME, pp. 105-114.

15. Takeuchi, S. and Kuramoto, E.: "Temperature and Orientation Dependence of the Yield Stress in Ni3Ga Single Crystals," Acta Met., 21(4), pp. 415-425, 1973.

16. Lall et al.: "The Orientation and Temperature Dependence of Yield Stress of Ni3 (Al, Nb) Single Crystals," Met. Trans. A, 10A(9), pp. 1323-1332, 1979.

17. MARC General Purpose Finite Element Program, MARC Corporation, Palo Alto, Ca.

18. Cassenti, B.N.: "Research and Development Program for Nonlinear Structural Modeling with Advanced Time-Temperature Dependent Constitutive Relationships, Vol. I - Theoretical Discussion." NASA CR-168191, July 1983.

19. Hill, J.T.; Weber, R.M.; and Meyer, T.G.: "Constitutive Modeling for Isotropic Materials," Addendum to Second Annual Status Report, NASA CR-174980, 1985.

20. Ostergren, W.J.: "A Damage Function and Associated Failure Equations for Predicting Hold Time and Frequency Effects in Elevated-Temperature Low-Cycle Fatigue," Jl. of Testing and Evaluation, Vol. 4, No. 5, Sept. 1976, pp. 327-339.

21. Garud, Y.S.: "A New Approach to the Evaluation of Fatigue Under Multiaxial Loadings." ASME Jl. of Eng. Mat. and Tech., Vol. 103, April 1981, pp. 118-125.

22. Newman, J.C. Jr. and Raju, I.S.: "Analysis of Surface Cracks in Finite Plates Under Tension Or Bending Loads." NASA Technical Paper 1578, 1979.

23. Tada, H., Paris, P.C., and Irwin, G.R.: "The Stress Analysis of Cracks Handbook, Second Edition." Paris Productions Inc. (and Del Research Corporation), St. Louis, Missouri, 1985.

APPENDIX A

SCHEMATICS OF TMF CYCLES

* NOTE: SEE SECTION 9 FOR AIRFOIL LE CYCLE SCHEMATIC
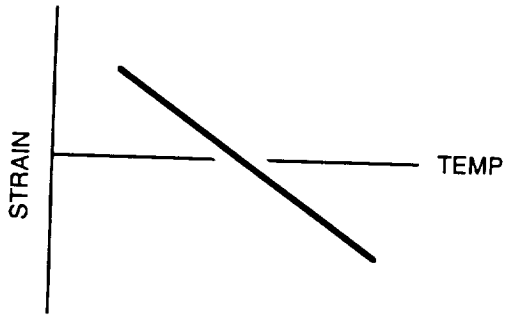
OUT-OF-PHASE
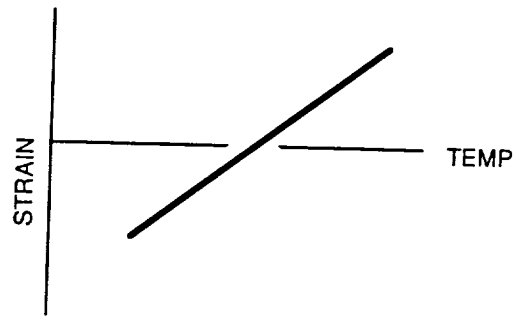
IN-PHASE
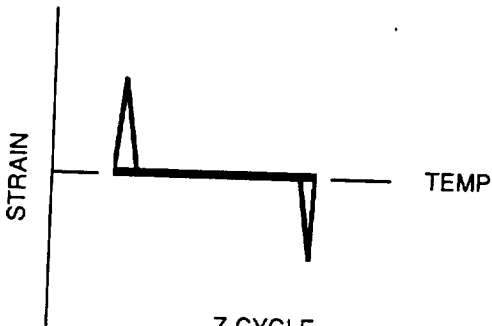
Z-CYCLE
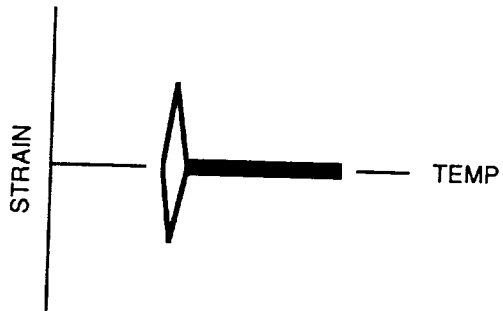
T-CYCLE
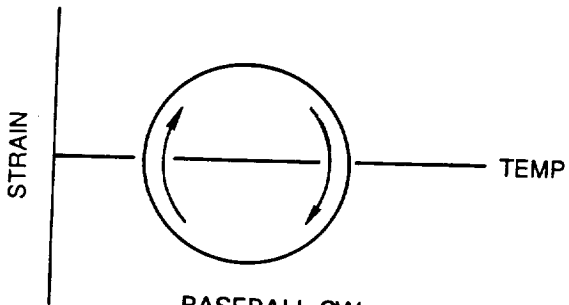
BASEBALL-CW
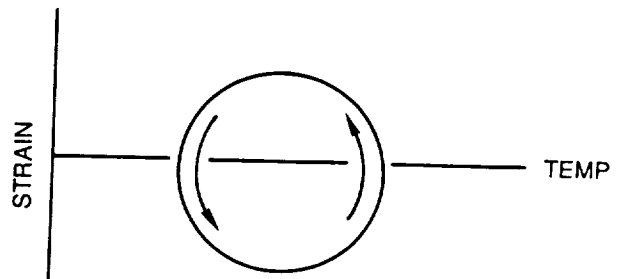
BASEBALL-CW
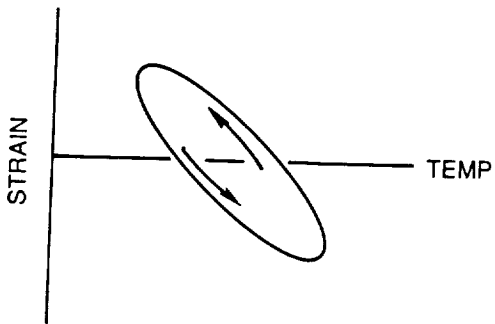
ELLIPTICAL-CCW
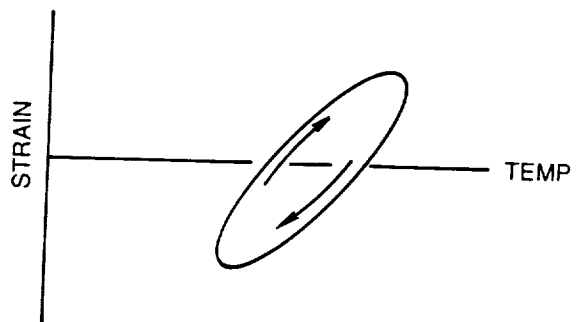
FOOTBALL-CW

LIFE DATA SUMMARY FOR PWA1480 FATIGUE TESTS

NOMENCLATURE

T = Task Number
S = Specimen Type
    r   Internally Ridged Specimen 44C (Figure 1A).
    r   Internally Ridged Specimen without Internal Ridges or Specimen 73C (Figure 1B).
    s   44C Specimen without Internal Ridges or Specimen 73C (Figure 1B).
Spec ID = Specimen Identification Number: JB = <001>; LB = <111>; KB = <011>; MB = <123>.
Tmax = Maximum Cycle Temperature (F), TMF Tmin = 800F.
Cycle Type = Test Waveform Information. All TMF Waveforms are 1 cpm Sine Waves Except as Noted.
DE = Test Mechanical Strain Range (%).
V = Test Strain Ratio. V=(Emax+Emin)/(Emax-Emin); Where Emax = Maximum Strain and Emin = Minimum Strain.
Init = Specimen Crack Initiation Location Which Led to Failure. Note: A "/" indicates that two modes were observed.
    c   Coating
    cs Coating Diffusion Zone
    sc Coating-Substrate Interfacial Region
    s   Substrate (Subsurface)
    ID Uncoated ID Surface of the Specimen
    IDc Uncoated ID Surface of the Specimen; Coating Cracks Observed Along the OD Surface
    IDs Substrate (Subsurface) Initiation Near the Uncoated ID Surface
    d   Test Discontinued with No Observed Cracks
    dc Test Discontinued with Coating Cracks Observed Along the OD Surface
    dcs Test Discontinued with Cracks Along OD Surface which Initiated at the Coating Diffusion Zone
    dsc Test Discontinued with Cracks Along OD Surface which Initiated at the Coating-Substrate Interfacial Region
Fail = Specimen Failure Location.
    gag Gage Section
    but Buttonhead Fillet
    ext Failure Caused by Cracking Underneath MTS Extensometer Quartz Rods
    IDr ID Ridge Region (44C Specimen Design)
    gagr OD Failure in Gage Section Near ID Ridge Region (44C Specimen Design)
    ogag Failure Occurred Outside Monitored Gage Section, but within the Constant Cross-Section Region
Exam = Inspection Technique Used to Define Initiation and Failure Locations and/or Crack Aspect Ratio and Crack Depth
    O   Optical Microscopy; 7X-500X
    S   Scanning Electron Microscopy; Backscatter and/or Secondary Electron Images
    T   Transmission Electron Microscopy for Observing Dislocation Activity
Tc = Coating Thickness in Mils (1 Mil = .001 In).
Nc = Cycles to Initiate a Crack Through the Coating.
AR = OD Crack Aspect Ratio (Surface Length/Depth).
    E   Estimated AR = Average of Specimen AR's at the Same Test Temperature
Ring Crack AR Associated With Cracks Which "Ring" Specimen OD
Nmin = Lower Bound on (Nc+Nsc) or Nsi.
Nmax = Upper Bound on (Nc+Nsc) or Nsi.
Ind = Denotes Method Used to Determine Nmin and Nmax. See Descriptions in Section 6.3.2.
    rep Replica Data   Method 1)
    xtr Linear Extrapolation of Replica Data   Method 2))--- Nomenclature Used in Section 6.3.2.
    grf Graphical Method   Method 3))
    ld Specimen Load Drop Tangency Point   Method 4)
Nsc = Cycles to Grow a Coating Crack .010" into the Substrate.
Nsi = Cycles to Initiate a Substrate Crack Due to Macroscopic Slip, Oxidation Effects, or Defects.
5% = Cycles to 5% Stress Range Drop from Stress Range at Nf/2.
10% = Cycles to 10% Stress Range Drop from Stress Range at Nf/2.
Nf = Cycles to Specimen Failure (50% Tensile Load Drop or Separation, Whichever Comes First).

138

<001> PWA 1480 / PWA 273 ISOTHERMAL FATIGUE SUMMARY

T	S	Spec ID	Tmax (F)	Cycle Type	DE	V	Init	Fail	Exam	Tc	Nc	AR	Nmin	Ind	Nmax	Ind	Nsc	Nsi	5%	10%	Nf
5	s	JB-103	1400	PP, 8 cpm	.6	0	dc	gag	0	2.2	7200	4.0	63050	xtr	82680	xtr	56-76k	-	No load	drop	>63050
5	s	JB-109	1400	PP, 8 cpm	.6	1	dc	gag	0	2.5	7700	5.0E	59800	-	-	-	>52k	-	No load	drop	>59797
5	s	JB-96	1400	PP, 6 cpm	.8	0	dc	gag	0	3.2	1-2k	6.0	28254	xtr	42350	xtr	26-43k	-	No load	drop	>28354
5	s	JB-23	1700	PP, 8 cpm	.6	0	c	gag	0	3.3	11500	5.6	20000	rep	20000	rep	8500	-	26000	26500	26833
5	s	JB-159	1700	CP, 8cpm+30s	.6	0	dc	gag	0	2.9	1.6-3.1k	7.0	19662	xtr	40030	xtr	16-38k	-	No load	drop	>19662
5	s	JB-28	1700	PP, 7 cpm	.68	0	c	gag	0,s	2.6	1950	4.5	6600	rep	6600	rep	4650	-	12000	12500	12830
3	r	JB-31	1700	PP, 6 cpm	.8	0	c	gag	0	3.4	550	2.0	3000	rep	3000	rep	2450	-	6000	6070	6474
5	s	JB-120	1900	PP, 8 cpm	.6	0	c	gag	0	2.5	5900	2.2	11600	rep	11600	rep	5700	-	16500	-	17981
5	s	JB-65	1900	PP, 1 cpm	.6	0	IDc	gag	0	3.1	1700	2.2E	>5485	-	-	-	>3800	-	4000	5300	5485
5	s	JB-100	1900	PC, 8cpm+60s	.6	0	c	gag	0	3.0	900	2.4	1850	rep	1850	rep	950	-	3250	-	4096
5	s	JB-170	1900	CP, 8cpm+60s	.68					Specimen failed on loading. Loose grips caused extensometer slippage.											
3	s	JB-34	1900	PP, 7 cpm	.8	0	c	gag	0,s	3.3	1050	1.9	2600	rep	2600	rep	1550	-	5800	-	6183
3	s	JB-39	1900	PP, 6 cpm	.8	0	c	gag	0	3.1	1100	1.8	2830	rep	2830	rep	1730	-	5080	5150	5325
3	r	JB-50	1900	PP, 1 cpm	.8	0	c	gag	0,s	2.9	<770	2.7	1000	rep	1000	rep	<1000	-	4550	5100	5158
3	r	JB-33	1900	PC,10cpm+60s	.8	0	IDc	1Dr	0	4.0	660	2.5	1970	rep	1970	rep	1310	-	3020	3300	3742
3	r	JB-36	1900	CP,10cpm+60s	.8	0	c	gag	0,s	3.7	220	2.2E	>745	-	-	-	>525	-	720	730	745
3	s	JB-35	1900	PP, 6 cpm	.8	0	c	gag	0,s	4.0	170	2.0	720	rep	720	rep	550	-	3000	3500	3954
3	s	JB-79	1900	PP, 4.6 cpm	1.04	0	c	gag	0,s	3.4	640	3.7	1280	grf	1600	1d	640-960	-	1580	1630	1856
5	s	JB-163	2100	PP, 10 cpm	.5	0	c	gag	0	2.6	2000	2.2	5000	rep	9300	1d	3-7.3k	-	5900	6500	9652
5	s	JB-168	2100	PP, 8 cpm	.6	0	c	gag	0	2.9	1440	2.4	4000	rep	4000	rep	2560	-	3600	4400	6146

139

<001> PWA 1480 / PWA 286 ISOTHERMAL FATIGUE SUMMARY

T	S	Spec ID	Tmax (F)	Cycle Type	DE	V	Init	Fail	Exam	Tc	Nc	AR	Nmin	Ind	Nmax	Ind	Nsc	Nsi	5%	10%	Nf
3	s	JB-102	800	PP, 8 cpm	.6	0	d	-	-	4.1	>41578	-	-	-	-	-	-	-	No load drop	No load drop	>41578
5	s	JB-97	800	PP, 6 cpm	.8	0	c	gag	O	4.1	6000	3.0	10450	rep	10450	rep	4480	-	No load drop		14475
5	s	JB-99	800	PP, 5 cpm	1.0	0	c	gag	O	4.6	2120	3.0	3640	grf	3770	grf	-	1.5-1.7k	No load drop		5047
5	s	JB-37	1400	PP, 6 cpm	.8	0	c	but	O	4.6	3600	3.3	23630	xtr	87120	xtr	-	20-84k	No load drop		>23630
5	s	JB-94	1400	PC, 6cpm+60s	.8	0	dc	gag	O	4.8	1920	4.2	7400	xtr	26830	xtr	-	5.5-25k	No load drop		>7400
5	s	JB-63	1400	PP, 5cpm sin	1.0	0	c	gag	O	5.2	1220	3.3	3460	grf	10836	grf	-	2.2-9.6k	No load drop		14936
5	s	JB-75	1400	PP, .5cpm sin	1.0	0	dc	gag	O	4.2	920	3.3	3409	xtr	50700	xtr	-	2.5-50k	No load drop		>3409
5	s	JB-158	1400	CP, 5cpm+300s	1.0	0	dc	gag	O	5.8	>1540	3.6E	2350	grf	3560	grf	-	1.2-2.4k	No load drop		>1540
5	s	JB-69	1400	PP, 4.4cpm sin	1.1	0	c	gag	O	4.6	1170	3.7	-	-	-	-	-	-	5620	5640	5650
5	s	JB-7	1400	PP, 4 cpm	1.2	0	IDc	but	O	5.7	1300	3.6E	-	-	-	-	-	-	No load drop		4090
5	s	JB-123	1700	PP, 8 cpm	.6	0	c	gag	O	5.3	8100	7.0	23200	grf	-	-	>15100	-	76000	77000	78168
5	s	JB-169	1700	PP, 6 cpm	.8	0	c	gag	O	5.8	2420	4.2	6800	grf	-	-	>4400	-	20000	-	21760
5	s	JB-129	1700	PP, 6 cpm	.8	0	c	gag	O	3.6	2820	2.8	6500	rep	6500	rep	3680	-	22100	22300	22462
3	r	JB-2	1700	PP, 1 cpm	.8	0	IDc	IDr	O	5.1	2000	2.0	>7162	-	-	-	>5160	-	6930	7010	7167
5	s	JB-155	1700	PP, 1 cpm	.8	0	ID/c	gag	O	5.1	2820	2.5	6600	rep	6600	rep	3780	-	13800	-	13900
5	s	JB-139	1700	PC, 6cpm+60s	.8	0	IDc	gag	O	4.4	780	2.6	>3128	-	-	-	>2350	-	2980	3020	3128
5	s	JB-160	1700	CP, 5cpm+60s	1.0	0	c	gag	O	5.6	960	2.5	1640	rep	1640	rep	680	-	5200	5400	5645
5	s	JB-126	1900	PP, 10 cpm	.5	0	IDc	gag	O	6.3	8200	2.0	>27338	-	-	-	>19200	-	26800	27000	27338
5	s	JB-130	1900	PP, 1.33 cpm	.6	0	IDc	gag	O	5.6	2560	2.7	>7290	-	-	-	>4730	-	6250	7150	7290
3	s	JB-25	1900	PP, 6 cpm	.8	0	IDc	gag	O	4.6	>1750	2.6	>4285	-	-	-	>2500	-	4100	4200	4285
5	s	JB-85	1900	PP, 6 cpm	.8	0	IDc	gag	O	5.1	2280	2.5	>6766	-	-	-	>4490	-	-	-	6766
3	r	JB-5	1900	PP, 1 cpm	.8	0	IDc	IDr	O,s	5.1	550	1.8	>2595	-	-	-	>2045	-	2130	-	2595
5	s	JB-24	1900	PP, 1 cpm	.8	0	IDc	gag	O	4.6	1550	3.0	>4471	-	-	-	>2920	-	2450	3700	4471
3	s	JB-20	1900	PC, 10cpm+60s	.8	0	IDc	IDr	O	4.4	1320	2.6	>2192	-	-	-	>870	-	1800	2010	2192
3	r	JB-6	1900	PC, 10cpm+60s	.8	0	IDc	gag	O,s	4.7	610	2.0	>1100	-	-	-	>480	-	-	-	1100
3	s	JB-71	1900	CP, 6cpm+120s	.8	0	IDc	gag	O,s	4.7	990	2.6E	>1514	-	-	-	>520	-	1400	1420	1514
5	s	JB-134	1900	PP, 4.6 cpm	.8	0	IDc	gag	O	4.9	810	3.8	>1335	-	-	-	>540	-	-	-	1335
3	s	JB-78	1900	PP, 4.6 cpm	1.04	0	IDc	gag	O	5.2	1210	2.6E	>1929	-	-	-	>720	-	1640	1860	1929
5	s	JB-171	2100	PP, 8 cpm	.6	.8	IDc	gag	O	5.0	3670	3.5	>5676	-	-	-	>2000	-	4250	5200	5676
5	s	JB-151	2100	PP, 1 cpm	.6	.8	?	gag	O	3.5	1400	3.5E	>5690	-	-	-	>4290	-	5000	5470	5690
5	s	JB-162	2100	PP, 7 cpm	.68	0	IDc	gag	O,s	5.8	2230	3.5	>3856	-	-	-	>1620	-	2370	2900	3856

*The following specimens were exposed 100 hr. at 2000F prior to test.

T	S	Spec ID	Tmax (F)	Cycle Type	DE	V	Init	Fail	Exam	Tc	Nc	AR	Nmin	Ind	Nmax	Ind	Nsc	Nsi	5%	10%	Nf
5	s	JB-138	1400	PP, 6 cpm	.8	0	c	but	O	5.0	2170	3.8E	>61k	-	-	-	>59300	-	60890	61400	61470
5	s	JB-150	1900	PP, 6 cpm	.8	0	IDc	gag	O	5.6	1-2k	3.8	>2097	-	-	-	-	-	2000	2040	2097

T	S	Spec ID	Tmax (F)	Cycle Type	DE	V	Init Fail	Exam	Tc	Nc	AR	Nmin	Ind	Nmax	Ind	Nsc	Nsi	5%	10%	Nf
3	r	JB-42	1900	PC,10cpm+60s	.8	0	-	gag		Cracks were from OD Copper deposit from induction coil.								1730	1760	2013

T	S	Spec ID	Tmax (F)	Cycle Type	DE	V	Init Fail	Exam	Tc	Nc	AR	Nmin	Ind	Nmax	Ind	Nsc	Nsi	5%	10%	Nf
5	s	JB-76	1700	Football,cw	.4	1	d	o	4.0	No cracks observed in the gage section.								No load drop	-	>21758
5	s	JB-98	1900	Out-of-phase	.4	0	c	gag O,S	2.9	4-6k	7-9	9000	grf	13400	grf	3.0-9.4k	-	15900	-	16169
5	s	JB-61	1900	Out-of-phase	.4	0	c	gag O	3.3	2.6-5k	Ring		-	6150	ld	<3550	-	6200	-	6216
5	s	JB-91	1900	Out-of-phase	.5	0	c	gag O	3.4	.6-1k	7.0	1840	grf	2730	grf	840-2130	-	-	-	3283
3	r	JB-22	1900	Out-of-phase	.52	0	c	gagr O,S,T	3.3	400-800	14.	1960	grf	2940	grf	1.1-2.5k	-	3710	3740	3772
3	r	JB-29	1900	In-phase	.75	0	dc	gag O	3.4	1250	4-6	10340	xtr	92160	xtr	9.1-91k	-	No load drop		>10339
3	r	JB-19	1900	Out-of-phase	.76	0	c	gagr O,S,T	2.8	<12	Ring	215	xtr	570	ld	200-560	-	572	-	580
3	r	JB-38	1900	Z-cycle .5cpm	.76	0	c	gag O,S	4.0	650	Ring	1060	rep	1200	ld	410-550	-	1480	-	1505
3	s	JB-81	1900	Out-of-phase	.8	-1	c	gag O	3.0	<21	Ring	187	xtr	460	ld	160-440	-	530	540	541
3	s	JB-72	1900	Z-cycle .5cpm	.8	0	c	gag O,S	3.0	<50	Ring	353	xtr	870	ld	300-820	-	870	-	876
5	s	JB-64	1900	In-phase	1.0	0	c	gag O	3.6	400	5.5	-	-	-	-	-	-	No load drop		615
5	s	JB-88	2100	Out-of-phase	.3	0	c	gag O	4.0	<3000	3.0	8600	grf	10000	ld	<7000	-	10100	10700	12756
5	s	JB-82	2100	Out-of-phase	.5	0	c	gag O	3.6	<<550	Ring		-	780	grf	<780	-	1300	-	1326

*The following specimens were exposed 100 hr. at 2000F prior to test.

T	S	Spec ID	Tmax (F)	Cycle Type	DE	V	Init Fail	Exam	Tc	Nc	AR	Nmin	Ind	Nmax	Ind	Nsc	Nsi	5%	10%	Nf
5	s	JB-154	1900	Out-of-phase	.4	0	c	gag O,S	2.5	<1020	4.7	1000	rep	2000	rep	1-2k	-	5580	6200	6562
5	s	JB-161	1900	Out-of-Phase	.4	0	c	gag O	2.7	<425	Ring	2150	xtr	2540	-	1.7-2.5k	-	No load drop		2543

T	S	Spec ID	Tmax (F)	Cycle Type	DE	V	Init Fail	Exam	Tc	Nc	AR	Nmin	Ind	Nmax	Ind	Nsc	Nsi	5%	10%	Nf
5	s	JB-174	1900	Out-of-phase	60	.5	c	gag 0	4.4	2050	4.6	4400	rep			2350	-	No load	drop	9900
				Note: JB-174 was a load controlled test. DE = Test stress range, V = Test stress ratio																
5	s	JB-147	1900	Out-of-phase	.45	0	c	gag 0,S	4.0	1400	4.5	2250	rep	2250	rep	850	-	7100	7900	8174
5	s	JB-121	1900	Out-of-phase +30s @Tmax	.45	-1	c	gag 0	5.4	1350	4.5	2400	rep	2400	rep	1050	-	4200	5630	6014
5	s	JB-137	1900	Out-of-phase +60s @Tmax	.45	-1	c	gag 0	4.9	1070	3.0	2050	rep	2050	rep	980	-	3830	4600	4946
7	s	JB-135	1900	Airfoil LE .25cpm +60s @Tmax	.45	-1	c	gag 0	4.3	1280	4.4	2070	rep	2070	rep	790	-	3570	4730	5059
3	r	JB-10	1900	Out-of-phase	.5	0	c	gagr 0,S	4.7	500	2.2	840	rep	3000	1d	.34-2.5k	-	3230	4050	4105
3	s	JB-104	1900	T-cycle .5cpm	.6	0	c	ext 0	4.7	3300	4.0	6000	-	6000	-	2700	-	No load	drop	6032
3	r	JB-9	1900	Out-of-phase	.76	0	c	gag 0,S,T	5.0	370	2.5	820	grf	1600	1d	.5-1.2k	-	1730	1870	1878
3	r	JB-11	1900	In-phase	.79	0	-	IDr 0,S,T	5.0	>10000	-	-		-		-	-	10050	10400	10535
3	s	JB-80	1900	Out-of-phase	.8	-1	c	gag 0,S	5.5	300	2.2	600	grf	1100	1d	300-800	-	1450	1470	1472
3	s	JB-21	1900	Z-cycle .5cpm	.8	0	c	gagr 0,S	5.6	820	3.0	1380	grf	1490	grf	560-670	-	1840	-	1847
5	s	JB-102	1900	Baseball,ccw	.8	0	IDc	gag 0	4.1	1260	2.6	3430	xtr	-		>2170	-	No load	drop	3426
				Note: JB-102 previously was run for 41578 cycles at 800F, +-.3%, 8 cpm.																
5	s	JB-111	2100	Out-of-phase	.35	0	c	ext 0	5.0	3000	4.3	4830	grf	6865	grf	1.8-3.9k	-	4980	5100	7205
5	s	JB-89	2100	Out-of-phase	.5	0	c	gag 0	5.0	770	2.0	1930	grf	2320	grf	1.1-1.6k	-	2410	2730	2912

*The following specimens were exposed 100 hr. at 2000F prior to test.

T	S	Spec ID	Tmax (F)	Cycle Type	DE	V	Init Fail	Exam	Tc	Nc	AR	Nmin	Ind	Nmax	Ind	Nsc	Nsi	5%	10%	Nf
5	s	JB-146	1900	Out-of-phase	.4	0	c	gag 0	4.5	1400	4.4	3022	xtr	3610	xtr	1.6-2.2k	-	No load	drop	3022
5	s	JB-133	1900	Out-of-phase	.45	0	c	gag 0,S	4.7	740	3.5	1650	rep	1650	rep	910	-	2200	2900	3804

T	S	Spec ID	Tmax (F)	Cycle Type	DE	V	Init Fail	Exam	Tc	Nc	AR	Nmin	Ind	Nmax	Ind	Nsc	Nsi	5%	10%	Nf
3	s	JB-51	1900	Out-of-phase	.55	0	ID	gag 0	No data available.									11400	11700	11806
3	s	JB-46	1900	Out-of-phase	.8	0	ID	gag 0,S	No data available.									2460	2550	2589
3	s	JB-47	1900	In-phase	.8	0	ID	gag 0,S	No data available.									5000	6000	6075

T	S	Spec ID	Tmax (F)	Cycle Type	DE	V	Init Fail	Exam	Tc	Nc	AR	Nmin	Ind	Nmax	Ind	Nsc	Nsi	5%	10%	Nf
5	s	LB-106	800	PP, 12 cpm	.4	0	-	but O	3.1	>27800	-	-	-	-	-	-	-	No load drop	drop	27800
5	s	LB-22	1400	PP, 10 cpm	.5	0	cs	gag O,S	3.0	1000	8.6	-	-	7600	ld	<6600	-	No load drop	drop	7623
3	s	LB-25	1400	PP, 8 cpm	.6	0	sc	gag O,S	2.9	>925	Ring	-	-	1720	ld	-	<1720	1720	-	1724
3	s	LB-19	1400	PP,8 cpm sin	.6	0	cs	gag O,S	2.7	>1370	Ring	-	-	1800	ld	<430	-	1850	1880	1953
3	s	LB-121	1400	PP, .5 cpm	.6	0	cs	gag O,S	2.9	300	Ring	-	-	400	ld	<100	-	420	480	565
3	s	LB-120	1400	PP, .5 cpm	.6	0	s	gag O	2.5	>975	Ring	-	-	1202	ld	-	<1202	1200	-	1202
3	s	LB-124	1400	PP, .5 cpm	.6	0	s	gag O,S	3.1	>1110	Ring	-	-	1320	ld	-	<1320	1320	-	1362
5	s	LB-236	1700	PP, 14 cpm	.34	0	s	gag O,S	2.0	>11.5k	2.5	18000	rep	19400	rep	-	18-20k	20700	-	21042
5	s	LB-195	1700	PP, 12.5 cpm	.4	0	s	gag O	2.4	>3620	2.0	5080	rep	5080	rep	-	5080	6600	7000	7680
5	s	LB-180	1700	PP, 10 cpm	.5	0	s	gag O	2.1	>3600	-	-	-	3600	ld	-	<3600	3750	3800	3941

T	S	Spec ID	Tmax (F)	Cycle Type	DE	V	Init Fail	Exam	Tc	Nc	AR	Nmin	Ind	Nmax	Ind	Nsc	Nsi	5%	10%	Nf
5	s	LB-30	800	PP, 10 cpm	.5	0	-	but O	5.5	>7130	-	-	-	-	-	-	-	No load drop	drop	7130
5	s	LB-209	1400	PP, 12.5 cpm	.4	0	s	but O	5.8	>38000	2.8	-	-	42600	-	-	<42600	No load drop	drop	42603
5	s	LB-241	1400	PP, 10 cpm	.5	0	s	gag O	5.5	>11850	-	-	-	11800	ld	-	<11800	11800	-	11850
5	s	LB-235	1400	PP, .5 cpm	.5	0	s	gag O	5.7	>6900	2.0	6200	rep	7320	grf	-	6.2-7.3k	9200	-	9220
5	s	LB-185	1700	PP, 16 cpm	.3	0	s	gag O	5.7	>96700	-	-	-	119000	ld	-	<119k	-	119000	120k
5	s	LB-192	1700	PP, 14 cpm	.34	0	IDs	gag O	5.9	>42.6k	-	-	-	42600	-	-	<42600	45600	46500	46583
5	s	LB-188	1700	PP, 12.5 cpm	.4	0	s	gag O	5.0	>8000	-	-	-	9200	ld	-	<9200	9210	9220	9233
5	s	LB-233	1900	PP, 14 cpm	.34	0	s	gag O	4.5	>6340	2.5	6340	rep	8870	ld	-	6.3-8.9k	8700	8900	9062
5	s	LB-232	1900	PP, .5 cpm	.34	0	IDc	gag O	5.3	10000	-	-	-	-	-	-	-	7500	10300	10761
5	s	LB-179	2100	PP, 10 cpm	.5	0	ID	gag O	5.6	>911									770	900	911

>911 Constitutive test, no replica data taken.

143

T	S	Spec ID	Tmax (F)	Cycle Type	DE	V	Init	Fail	Exam	Tc	Nc	AR	Nmin	Ind	Nmax	Ind	Nsc	Nsi	5%	10%	Nf
3	s	LB-59	1400	PP, 8 cpm	.6	0		s	gag O	-	-	2.0	1220	rep	1300	rep	-	1.2-1.3k	-	-	1445
3	s	LB-36	1400	PP, 8 cpm sin	.6	0		s	gag O,S	-	-	2.0	1550	rep	1750	rep	-	1.5-1.8k	2260	-	2331

<111> PWA 1480 / PWA 273 THERMOMECHANICAL FATIGUE SUMMARY

T	S	Spec ID	Tmax (F)	Cycle Type	DE	V	Init	Fail	Exam	Tc	Nc	AR	Nmin	Ind	Nmax	Ind	Nsc	Nsi	5%	10%	Nf
3	s	LB-23	1900	Out-of-phase	.25	0	ID	gag	O	2.4	>6900	-	-	-	-	-	-	-	8150	8200	8211
3	s	LB-20	1900	Out-of-phase	.3	0	cs	ogag	O,S	2.7	400	7.-10.	1220	rep	1408	rep	.8-1k	-	-	-	1408
3	s	LB-21	1900	Baseball,ccw	.3	0	s	gag	O,S	3.6	>4700	-	5250	rep	6500	ld	-	5.2-6.5k	6600	6650	6689
3	s	LB-156	1900	Baseball,cw	.3	0	sc/ID	gag	O,S	3.0	>860	2.2-3.4	1230	rep	1370	rep	-	370-510	-	-	1639
3	s	LB-155	1900	Baseball,cw 0.5 cpm	.6	0	-	gag	O	-	Tensile failure								No load drop		31
5	s	LB-189	2100	Out-of-phase	.25	0	c	gag	O	3.2	860	4.0	1800	rep	3700	ld	1-3k	-	3870	4000	4131
5	s	LB-240	2100	In-phase	.4	0	s	gag	O	2.0	>2233	-	1200	rep	2000	ld	-	1.2-2k	2180	-	2233

<111> PWA 1480 / PWA 286 THERMOMECHANICAL FATIGUE SUMMARY

T	S	Spec ID	Tmax (F)	Cycle Type	DE	V	Init	Fail	Exam	Tc	Nc	AR	Nmin	Ind	Nmax	Ind	Nsc	Nsi	5%	10%	Nf
5	s	LB-170	1900	Out-of-phase	.25	0	c	ext	O,S	5.5	5720	2.8	6480	rep	6480	rep	760	-	6250	-	6290
5	s	LB-181	1900	Out-of-phase	.25	0	dc	gag	O,S	5.7	5720	2.4	6720	rep	6720	rep	1000	-	7630	7670	7675
5	s	LB-27	1900	Out-of-phase	.3	0	c	ext	O	4.4	2500	2.1	3030	rep	3030	rep	530	-	No load drop		2936

Note: LB-27 encountered specimen cooling problems during testing.

T	S	Spec ID	Tmax (F)	Cycle Type	DE	V	Init	Fail	Exam	Tc	Nc	AR	Nmin	Ind	Nmax	Ind	Nsc	Nsi	5%	10%	Nf
5	s	LB-31	1900	Out-of-phase	.3	0	ID	gag	O	5.0	>3219	-	-		-		-	-	3200	-	3219
5	s	LB-32	1900	Baseball,ccw	.3	0	d	-		4.8	>11852	-	-		-		-	-	No load drop		>11852
5	s	LB-29	1900	Baseball,cw	.3	0	c	ext	O	5.3	2000	2.5-4.	2580	rep	3150	rep	.6-1.2k	-	3250	3550	3773
5	s	LB-26	1900	T-cycle .5cpm	.5	0	c	ext	O	5.2	2560	2.6E	3530	-	-		>1000	-	3500	3500	3532
5	s	LB-216	2100	Out-of-phase	.23	0	c	ext	O	5.5	3090	2.6	3820	rep	3820	rep	730	-	3900	4200	4654
5	s	LB-239	2100	Out-of-phase	.25	0	c	ext	O	5.6	2160	2.7	2800	rep	2800	rep	640	-	No load drop		3787

T	S	Spec ID	Tmax (F)	Cycle Type	DE	V	Init	Fail	Exam	Tc	Nc	AR	Nmin	Ind	Nmax	Ind	Nsc	Nsi	5%	10%	Nf
3	s	LB-56	1900	Out-of-phase	.3	0	s	gag	O,S	-	-	3.0	360	rep	360	rep	-	360	1530	1610	2067
3	s	LB-35	1900	Out-of-phase	.4	0	s	gag	O	-	-		300	-	530	-	-	300-530	535	-	537
3	s	LB-34	1900	Out-of-phase	.55	0	s	gag	O	-	Bulged	specimen	110	rep	150	-	-	110-150	150	-	151
3	s	LB-33	1900	Out-of-phase	.8	0	ID	gag	O	-	Bulged	specimen	100	rep	160	-	-	100-160	160	-	162

T	S	Spec ID	Tmax (F)	Cycle Type	DE	V	Init	Fail	Exam	Tc	Nc	AR	Nmin	Ind	Nmax	Ind	Nsc	Nsi	5%	10%	Nf
5	s	KB-47	1400	PP, 8 cpm	.6	0	c	but	O	2.0	10800	3.3E	18530	-	-	-	>7730	-	No load drop		18530
5	s	KB-64	1400	PP, 7 cpm	.68	-1	c	gag	O	2.1	4750	3.1	10500	rep	10500	rep	5750	-	19500	19800	19822
5	s	KB-67	1400	PP, 1 cpm	.68	-1	c	gag	O	3.0	3000	3.-4.	5200	rep	6000	rep	2.2-3k	-	18950	-	18987
5	s	KB-31	1700	PP, 12.5 cpm	.4	0	cs	gag	O,S	2.8	25-30k	4.6	-	-	40000	Id	<15000	-	52100	54100	54521
5	s	KB-23	1700	PP, 10 cpm	.5	0	s	gag	O,S	2.4	>6800	3.3	-	-	10200	Id	-	<10200	12700	12900	13000
5	s	KB-69	1700	PP, 1 cpm	.6	0	s	gag	O	3.4	2000	-	2800	rep	3000	rep	-	2.8-3k	2980	3050	3163
5	s	KB-28	1700	CP, 8cpm+60s	.6	0	s	gag	O	2.5	2200	2.4	3580	rep	3580	rep	-	3580	4350	4420	4556
5	s	KB-97	1900	PC,1.25cpm+60s	.3	0	IDc	gag	O	3.3	4300	3.8E	6300	rep	-	-	>2000	-	-	-	9234
5	s	KB-90	1900	CP,12.5cpm+60s	.4	0	ID	gag	O	2.7	>1870	-	-	-	-	-	-	-	1660	1700	1869
5	s	KB-86	1900	PP, 1 cpm	.4	0	ID/c	gag	O	3.8	2770	5.0	6200	rep	6700	grf	3.4-4k	-	4610	6190	6797
5	s	KB-35	1900	PP, 10 cpm	.5	0	s	gag	O,S	2.8	>2350	2.6	3320	rep	3320	rep	-	3320	-	-	3899

*The following specimens were exposed 100 hr. at 2000F prior to test.

T	S	Spec ID	Tmax (F)	Cycle Type	DE	V	Init	Fail	Exam	Tc	Nc	AR	Nmin	Ind	Nmax	Ind	Nsc	Nsi	5%	10%	Nf
5	s	KB-111	1700	PP, 10 cpm	.5	0	sc	gag	O	3.3	4100	5.0	4100	rep	4640	Id	-	4.1-4.7k	4900	5100	5338

<011> PWA 1480 / PWA 286 ISOTHERMAL FATIGUE SUMMARY

T	S	Spec ID	Tmax (F)	Cycle Type	DE	V	Init	Fail	Exam	Tc	Nc	AR	Nmin	Ind	Nmax	Ind	Nsc	Ind	Nsi	5%	10%	Nf
5	s	KB-89	1200	PP, 7 cpm	.68	0	c	but	0	4.4	>6516	-	-	-	-	-	-	-	-	6200	6400	6516
5	s	KB-85	1200	PP, 7 cpm	.68	-1	-	but	0	5.5	>8536	-	-	-	-	-	-	-	-	No load drop		>8535
5	s	KB-71	1400	PP, 10 cpm	.5	-1	dc	gag	0	4.3	25000	4.5	>63080	-	-	-	>38000	-	-	No load drop		>63080
5	s	KB-21	1400	PP, 6 cpm	.5	0	dc	gag	0	5.3	15750	10.0	61660	xtr	130500	xtr	46-115k	-	-	No load drop		>61660
5	s	KB-100	1400	PC, 7cpm+70s	.68	-1	c	gag	0	5.4	700	2.5	1300	rep	2170	ld	.6-1.5k	-	-	-	-	2283
5	s	KB-98	1400	CP, 7cpm+10s	.68	-1	dc	gag	0	4.6	8000	5.3E	44500	xtr	-	-	>36000	-	-	No load drop		>44561
5	s	KB-29	1400	PP, 6 cpm	.8	0	c	but	0	5.0	2750	4.3	3400	xtr	9200	xtr	.6-6.5k	-	-	-	-	3396
5	s	KB-68	1700	PP, 10 cpm	.5	0	s	gag	0	6.4	>7150	1.7	10100	rep	10100	rep	-	-	10100	17300	17600	17810
5	s	KB-65	1700	PP, 1 cpm	.5	0	s	gag	0	5.7	>3700	2.0	5080	rep	5080	rep	-	-	5080	6200	6300	6624
5	s	KB-70	1700	PC,10cpm+10s	.5	-1	s/c	gag	0	5.5	3600	2.5	-	-	3600	ld	-	-	<3600	3530	3600	3627
5	s	KB-96	1700	CP,10cpm+60s	.5	0	s	gag	0	4.6	>4056	-	2180	rep	3550	ld	-	-	2.2-3.6k	3880	3940	4056
5	s	KB-54	1700	PP, 8 cpm	.6	0	s	gag	0	6.1	>3500	2.7	-	-	4450	ld	-	-	<4450	-	-	4509
5	s	KB-79	1900	PP, .5 cpm	.34	0	dc	gag	0	4.3	9400	-	-	-	-	-	-	-	-	6700	9000	9420
5	s	KB-72	1900	PP, 12.5 cpm	.4	0	IDs/c	gag	0	6.0	8-11k	4.2	>15532	-	11000	rep	-	-	<11000	12300	12500	12929
5	s	KB-91	1900	PP, 12.5 cpm	.4	0	IDc	gag	0	3.8	12500	-	-	-	-	-	>4500	-	-	15100	15500	15532
5	s	KB-83	1900	PC,12.5cpm+10s	.4	0	IDc	gag	0	5.3	4100	-	-	-	-	-	-	-	-	3920	4000	4106
5	s	KB-77	1900	CP,10cpm+11s	.5	0	ID	gag	0	6.3	>2642	-	-	-	-	-	-	-	-	2060	2130	2642
5	s	KB-25	1900	PP, 8 cpm	.6	0	ID	gag	0	5.5	>1187	-	-	-	-	-	-	-	-	1140	1060	1187
5	s	KB-87	2100	PP, 2 cpm	.3	0	IDc	gag	0	5.2	3000	4.-6.	-	-	-	-	-	-	-	2150	2520	3266
5	s	KB-78	2100	PP, 2 cpm	.4	0	ID	gag	0	3.9	>1464	-	-	-	-	-	-	-	-	900	1060	1464

*The following specimens were exposed 100 hr. at 2000F prior to test.

T	S	Spec ID	Tmax (F)	Cycle Type	DE	V	Init	Fail	Exam	Tc	Nc	AR	Nmin	Ind	Nmax	Ind	Nsc	Ind	Nsi	5%	10%	Nf
5	s	KB-74	1400	PP, 10 cpm	.5	-1	c	gag	0	5.6	21000	3.5	23325	xtr	25200	rep	2.3-4.2k	-	-	26600	-	26833
5	s	KB-108	1700	PP, 10 cpm	.5	0	c	gag	0	5.5	5300	4.0	8100	rep	9050	ld	2.8-3.8k	-	-	9300	9440	9655
5	s	KB-81	1900	PP, 12.5 cpm	.4	0	c	ogag	0	4.6	10100	3.5	13100	rep	13100	rep	3000	-	-	24300	24700	24913

<011> PWA 1480 / PWA 273 THERMOMECHANICAL FATIGUE SUMMARY

T	S	Spec ID	Tmax (F)	Cycle Type	DE	V	Init Fail	Exam	Tc	Nc	AR	Nmin	Ind	Nmax	Ind	Nsc	Nsi	5%	10%	Nf
5	s	KB-33	1900	Out-of-phase	.3	0	d	- 0	2.5	>17003	-	-	-	-	-	-	-	No load drop		>17003
5	s	KB-80	2100	Out-of-phase	.25	0	c	gag 0	4.0	-	Fracture surface melted at end of test								-	6335
5	s	KB-49	2100	Out-of-phase	.25	0	c	gag 0	Note: KB-49 encountered specimen cooling problems during testing.			860	rep	1400	ld	220-760	-	1590	1700	1903
5	s	KB-27	2100	Out-of-phase	.35	0	cs	gag 0	2.6	620	3.-4.5	850	rep	1900	ld	230-1280	-	2360	2650	2900

*The following specimens were exposed 100 hr. at 2000F prior to test.

T	S	Spec ID	Tmax (F)	Cycle Type	DE	V	Init Fail	Exam	Tc	Nc	AR	Nmin	Ind	Nmax	Ind	Nsc	Nsi	5%	10%	Nf
5	s	KB-92	1900	Out-of-phase	.34	0	c	gag 0	4.2	<857	Ring Test failed before first inspection							760	790	857

<011> PWA 1480 / PWA 286 THERMOMECHANICAL FATIGUE SUMMARY

T	S	Spec ID	Tmax (F)	Cycle Type	DE	V	Init Fail	Exam	Tc	Nc	AR	Nmin	Ind	Nmax	Ind	Nsc	Nsi	5%	10%	Nf
5	s	KB-32	1900	Out-of-phase	.3	0	c	gag 0	6.0	2680	3.1	5050	rep	5050	rep	2370	-	6450	6500	6569
5	s	KB-24	1900	Out-of-phase	.3	0	c	gag 0	5.9	2900	2.2	4000	rep	4000	rep	1100	-	5550	5650	5927
5	s	KB-36	1900	Ellipt.,ccw	.3	1	d	ext 0	5.1	>9743	No cracks observed in gauge section.								9050	9400	9743
5	s	KB-34	1900	Out-of-phase	.4	0	c	gag 0	6.0	900	2.5	1610	grf	1610	grf	710	-	2240	-	2266
5	s	KB-48	2100	Out-of-phase	.25	0	c	ext 0	6.2	2460	2.0	3400	rep	3400	rep	940	-	2760	2850	3411
5	s	KB-52	2100	Out-of-phase	.25	0	dc	ext 0	5.5	4300	3.6	5150	rep	5150	rep	850	-	No load drop		5227

*The following specimens were exposed 100 hr. at 2000F prior to test.

T	S	Spec ID	Tmax (F)	Cycle Type	DE	V	Init Fail	Exam	Tc	Nc	AR	Nmin	Ind	Nmax	Ind	Nsc	Nsi	5%	10%	Nf
5	s	KB-93	1900	Out-of-phase	.3	0	c	gag 0	4.7	2420	3.3	-	-	2940	ld	<520	-	3010	-	3026

<123> PWA 1480 / PWA 273 ISOTHERMAL FATIGUE SUMMARY

T	S	Spec ID	Tmax (F)	Cycle Type	DE	V	Init Fail	Exam	Tc	Nc	AR	Nmin	Ind	Nmax	Ind	Nsc	Nsi	5%	10%	Nf
5	s	MB-21	1700	PP, 10 cpm	.5	0	cs	gag 0,s	2.0	5500	2.6	-	-	9000	ld	<3500	-	10400	10900	11648
5	s	MB-18	1700	PP, 8 cpm	.6	0	s	gag 0	2.4	>2500	2.7	3500	rep	3500	rep	-	3500	3750	-	3861
5	s	MB-4	1700	CP, 8cpm+60s	.6	0	sc	gag 0	2.4	>1100	2.4	1900	rep	1900	rep	-	1900	2000	2330	2407
5	s	MB-88	1900	PC,12.5cpm+60s	.3	0	ID/c	ogag 0	3.5	900	3.8	2940	rep	2940	rep	2040	-	2700	2800	2947

T	S	Spec ID	Tmax (F)	Cycle Type	DE	V	Init	Fail	Exam	Tc	Nc	AR	Nmin	Ind	Nmax	Ind	Nsc	Ind	Nsi	5%	10%	Nf
5	s	MB-26	1400	PP, 10 cpm	.5	-1	dc	gag	0	5.7	18600	5.0	30000				>11400			No load drop		>30000
5	s	MB-64	1700	PP, 10 cpm	.5	0	s/c	gag	0	4.2	9900	3.8	14500	rep	14500	rep	4600			19200	20000	21215
5	s	MB-40	1700	PC, 10cpm+60s	.5	0	IDc	gag	0	4.8	1650									2650	2670	2683
5	s	MB-41	1900	CP, 12.5cpm+60s	.3	0	ID	gag	0	5.9	>3680									2780	3350	3681
5	s	MB-6	1900	PP, 10 cpm	.5	0	ID	gag	0	6.0	>2540		4000	rep	6000	rep			4-6k			2540
5	s	MB-38	1900	PP, 10 cpm	.5	0	s	gag	0	5.8	>8250									8050	8220	8253
5	s	MB-33	1900	PP, 8 cpm	.6	0	IDs	gag	0	5.6	>2640									2610	2630	2640
5	s	MB-2	1900	PP, 8 cpm	.6	0	ID	gag	0	6.4	>3900									3700	3780	3919

High porosity level; Not typical for PWA1480

T	S	Spec ID	Tmax (F)	Cycle Type	DE	V	Init	Fail	Exam	Tc	Nc	AR	Nmin	Ind	Nmax	Ind	Nsc	Ind	Nsi	5%	10%	Nf
5	s	MB-25	1900	Out-of-phase	.3	0	ID	gag	0	2.6	>8000									8400	8500	8516
5	s	MB-1	1900	Out-of-phase	.4	0	c	gag	0,s	2.6	<<500	8.0			500	ld	<500			740		749
5	s	MB-16	2100	Out-of-phase	.25	0	c	gag	0	2.6	1400	6.5	2860	rep	3800	rep	1.4-2.4k			3000	3850	4961
5	s	MB-24	2100	Out-of-phase	.25	0	c	gag	0	3.0	760	4.5	1900	rep	1900	rep	1140			3450	3740	3910

T	S	Spec ID	Tmax (F)	Cycle Type	DE	V	Init	Fail	Exam	Tc	Nc	AR	Nmin	Ind	Nmax	Ind	Nsc	Ind	Nsi	5%	10%	Nf
5	s	MB-17	1900	Out-of-phase	.25	0	dc	ext	0	5.5	4600	3.1	6570	rep	6570	rep	1970			7150		7294
5	s	MB-23	1900	Out-of-phase	.25	0	c	gag	0	5.6	5050	4.3	7700	rep	7700	rep	2650			10300	10800	12172
5	s	MB-22	1900	Out-of-phase	.3	0	c	ext	0	5.3	3500	3.0	4400	xtr	5180	xtr	.9-1.7k			No load drop		4358
5	s	MB-8	1900	Out-of-phase	.3	0	c	gag	0	5.8	3930	2.5	5500	rep	5500	rep	1570			6500	6600	6745
5	s	MB-19	1900	Out-of-phase	.3	0	c	ext	0	6.2	3700	3.6	5540	xtr	7240	xtr	1.8-3.5k			4300	4530	5539
5	s	MB-62	1900	Out-of-phase	.3	1	c	gag	0	4.4	1800	3.7	3560	rep	3560	rep	1760			4000	4030	4098
5	s	MB-27	1900	Out-of-phase +300s @Tmax	.3	0	c	gag	0	4.7	1170	3.8	2100	rep	2100	rep	930			2180	2520	3002
5	s	MB-35	2100	Out-of-phase	.23	0	c	ext	0	6.1	3620	2.8	4520	rep	4520	rep	900			4570	4880	6786
5	s	MB-37	2100	Out-of-phase	.25	0	c	ext	0	6.0	2840	2.3	3780	rep	3780	rep	940			3980	4050	4130

APPENDIX B

STRESS/INELASTIC STRAIN DATA SUMMARY FOR PWA1480 FATIGUE TESTS

NOMENCLATURE

Spec ID = Specimen Identification Number: JB = <001>; LB = <111>; KB = <011>; MB = <123>

SigO Range = Initial Stress Range (ksi).
SigO Mean = Initial Mean Stress (ksi).
EinO Range = Initial Inelastic Strain Range (%).
SigNc Range = Stress Range at Nc Cycles (ksi).
SigNc Mean = Mean Stress at Nc Cycles (ksi).
EinNc Range = Inelastic Strain Range at Nc Cycles (%).
SigNs Range = Stress Range at (Nc+Nsc) or Nsi, Depending on Initiation Mode (ksi).
SigNs Mean = Mean Stress at (Nc+Nsc) or Nsi, Depending on Initiation Mode (ksi).
EinNs Range = Inelastic Strain Range at (Nc+Nsc) or Nsi, Depending on Initiation Mode (%).
Sig.5 Range = Stress Range at Nf/2 Cycles (ksi).
Sig.5 Mean = Mean Stress at Nf/2 Cycles (ksi).
Ein.5 Range = Inelastic Strain Range at Nf/2 Cycles (%).
SNmin Range = Stress Range at Nmin (ksi).
SNmin Mean = Mean Stress at Nmin (ksi).
SNmax Range = Stress Range at Nmax (ksi).
SNmax Mean = Mean Stress at Nmax (ksi).
Nc = Cycles to Initiate a Crack Through the Coating.
Nmin = Lower Bound on (Nc+Nsc) or Nsi.
Nmax = Upper Bound on (Nc+Nsc) or Nsi.
Nsc = Cycles to Grow a Coating Crack .010" into the Substrate.
Nsi = Cycles to Initiate a Substrate Crack Due to Macroscopic Slip, Oxidation Effects, or Defects.
Nf = Cycles to Specimen Failure (50% Tensile Load Drop or Separation, Whichever Comes First).
Dsig = Stress Change During Hold Times = Stress at End of Hold - Stress at Beginning of Hold (ksi).

*** Note : All stresses were calculated using substrate cross sectional area only.
      ===> Stress = Po/As = (observed specimen load)/(substrate area)
              As = Ao - Ac
              As = Substrate area.
              Ao = Specimen area based on measured specimen ID & OD.
              Ac = Coating area calculated based on constant coating thickness.
                    Coating thicknesses assumed were: PWA 273 = .003" ; PWA 286 = .005".

150

Spec ID	SigO Range (ksi)	SigO Mean (ksi)	EinO Range (%)	SigNc Range (ksi)	SigNc Mean (ksi)	EinNc Range (%)	SigNs Range (ksi)	SigNs Mean (ksi)	EinNs Range (%)	Sig.5 Range (ksi)	Sig.5 Mean (ksi)	Ein.5 Range (%)
JB-103	97.0	0.7	0.009	102.1	2.4	0.006	102.6	1.3	0.006	Test discontinued		
JB-109	94.7	-	0.010	97.2	41.3	0.010	95.9	40.3	0.008	Test discontinued		
JB-96	130.4	2.9	0.022	129.4	3.1	0.022	126.4	3.6	-	Test discontinued		
JB-23	80.8	0.5	0.029	82.8	1.4	0.032	82.4	-1.2	0.028	82.4	0.3	0.028
JB-159	83.3	0.6	0.027	78.3	-17.6	0.046	77.5	-18.9	0.048	Test discontinued		
Dsig	-2.0	-0.2		-2.7			-2.9			-		
JB-28	90.5	-0.2	0.030	89.3	0.1	0.033	89.9	2.2	0.034	89.9	2.2	0.034
JB-31	110.7	1.0	0.043	107.6	2.5	0.051	107.1	3.4	0.055	106.1	4.0	0.055
JB-120	67.0	0.3	0.042	62.3	0.3	0.072	62.6	0.0	0.074	63.1	0.5	0.070
JB-65	65.0	-0.5	0.064	57.3	0.4	0.119	-	-	-	56.2	1.2	0.143
JB-100	68.1	0.0	0.039	64.3	8.1	0.095	63.2	10.0	0.107	62.1	9.3	0.110
Dsig	+3.0			+3.4			+3.3			+3.3		
JB-170	Specimen failed during initial loading. No data is available.											
JB-34	74.3	-0.4	0.071	70.1	-0.5	0.100	70.5	0.4	0.104	71.2	-0.1	0.106
JB-39	86.3	-0.9	0.112	75.7	1.3	0.158	71.8	0.2	0.177	71.9	0.2	0.175
JB-50	84.9	0.2	0.096	81.2	0.0	0.126	78.8	-0.7	0.131	76.2	-0.1	0.141
JB-33	71.6	0.0	0.155	64.5	0.7	0.215	58.2	0.4	0.255	58.8	0.5	0.252
JB-36	80.3	1.2	0.128	80.9	9.2	0.190	-	-	-	80.0	10.2	0.203
Dsig	+6.5			+5.9			-			+5.7		
JB-35	84.5	0.0	0.117	81.0	-7.4	0.185	76.0	-10.0	0.200	69.9	-12.4	0.210
Dsig	-6.3			-5.4			-5.7			-4.6		
JB-79	99.0	1.1	0.218	89.1	0.6	0.225	90.0	0.6	0.257	91.1	0.8	0.248
JB-163	43.6	-1.0	0.101	39.5	0.0	0.118	34.0	0.1	0.154	34.0	0.1	0.154
JB-168	50.1	-0.5	0.138	42.2	0.5	0.200	34.4	0.0	0.244	37.7	0.4	0.233

Spec ID	SigO Range (ksi)	SigO Mean (ksi)	EinO Range (%)	SigNc Range (ksi)	SigNc Mean (ksi)	EinNc Range (%)	SigNs Range (ksi)	SigNs Mean (ksi)	EinNs Range (%)	Sig.5 Range (ksi)	Sig.5 Mean (ksi)	Ein.5 Range (%)
JB-102	116.9	0.8	0.0	Test discontinued before load drop. Nf/2 = 20800						115.8	0.0	0.0
JB-97	153.5	2.8	0.006	154.0	3.1	0.005	153.6	1.5	0.006	153.8	0.9	0.006
JB-99	190.0	3.3	0.010	192.2	4.7	0.011	189.8	5.1	0.007	187.7	5.3	0.010
JB-37	118.5	-1.7	0.036	119.0	2.8	0.030	117.6	3.9	0.018	117.6	3.9	0.018
JB-94	128.4	0.9	0.036	125.8	9.2	0.031	123.8	10.6	0.020	Test discontinued		
Dsig	+3.1			+1.5			+1.0			+1.3		
JB-63	157.6	1.6	0.046	155.4	3.8	-	150.0	4.3	0.027	150.0	4.3	0.027
JB-75	147.0	0.0	0.037	145.6	8.1	0.043	145.5	8.7	0.042	Test discontinued		
JB-158	154.6	1.0	0.043	149.7	-14.8	0.048	-	-	-	Test discontinued		
Dsig	-2.9			-2.7								
JB-69	169.3	0.0	0.049	170.9	9.9	0.047	169.9	11.4	0.042	167.7	12.5	0.042
JB-7	168.9	0.7	0.060	176.0	8.0	0.056	-	-	-	171.4	5.0	0.048
JB-123	76.5	0.7	0.020	79.8	2.1	-	77.9	3.0	0.023	77.9	3.0	0.021
JB-169	111.1	-1.8	0.039	109.2	1.2	0.036	108.3	2.0	0.034	106.9	2.2	0.033
JB-129	105.9	0.0	0.034	101.2	0.6	0.038	103.1	-0.2	0.037	98.7	-0.9	0.037
JB-2	103.4	0.0	0.030	99.4	-0.9	0.063	-	-	-	96.0	-1.8	0.077
JB-155	98.4	-1.1	0.025	96.5	-1.2	0.032	94.7	-2.5	0.045	94.7	-2.5	0.045
JB-139	109.3	2.4	0.035	108.5	23.4	0.092	-	-	-	108.5	24.6	0.091
Dsig	+2.9			+2.9			-			+2.5		
JB-160	121.0	-3.9	0.111	118.4	-25.4	0.132	113.6	-25.4	0.141	110.6	-25.3	0.142
Dsig	-6.4			-6.8			-6.6			-6.4		
JB-126	58.0	0.1	0.025	55.4	1.1	0.044	-	-	-	53.4	0.4	0.052
JB-130	80.9	0.0	0.055	70.8	0.5	0.104	-	-	-	67.5	1.3	0.129
JB-25	81.8	1.5	0.118	74.3	0.8	0.159	-	-	-	72.1	0.8	0.168
JB-85	84.4	-0.3	0.103	79.9	1.1	0.152	-	-	-	78.7	0.7	0.156
JB-5	77.8	-0.5	0.133	70.0	0.9	0.200	-	-	-	66.2	0.3	0.248
JB-24	76.7	0.0	0.143	63.5	0.9	0.260	-	-	-	62.1	1.2	0.260
JB-20	82.3	0.6	0.080	73.0	11.1	0.217	-	-	-	73.3	11.1	0.217
Dsig	+5.5			+5.1			-			+5.1		
JB-6	85.4	4.1	0.112	76.7	11.1	0.198	-	-	-	77.2	11.1	0.194
Dsig	+8.0			+4.9			-			+4.9		
JB-71	75.0	-0.5	0.112	67.9	-10.6	0.227	-	-	-	68.8	-10.4	0.224
Dsig	-5.7			-6.2			-			-6.6		
JB-134	85.1	-1.0	0.099	78.8	-12.9	0.196	-	-	-	78.2	-13.9	0.202
Dsig	-8.9			-6.1			-			-6.1		
JB-78	94.3	-1.4	0.194	78.5	1.1	0.308	-	-	-	78.5	1.1	0.308
JB-171	48.3	-1.3	0.120	39.1	0.4	0.195	-	-	-	39.1	0.4	0.195
JB-151	46.8	-0.7	0.145	30.0	-0.1	0.294	-	-	-	25.6	-0.3	0.344
JB-162	53.4	-1.5	0.164	43.8	0.3	0.240	-	-	-	42.2	0.1	0.261

*The following specimens were exposed 100 hr. at 2000F prior to test.

Spec ID	SigO Range (ksi)	SigO Mean (ksi)	EinO Range (%)	SigNc Range (ksi)	SigNc Mean (ksi)	EinNc Range (%)	SigNs Range (ksi)	SigNs Mean (ksi)	EinNs Range (%)	Sig.5 Range (ksi)	Sig.5 Mean (ksi)	Ein.5 Range (%)
JB-138	125.0	0.4	0.024	121.9	-0.3	0.021	-	-	-	114.0	-0.8	0.013
JB-150	84.1	-0.9	0.164	78.7	0.9	0.158	-	-	-	78.7	0.9	0.158

<001> PWA 1480 / UNCOATED ISOTHERMAL FATIGUE SUMMARY

Spec ID	SigO Range (ksi)	SigO Mean (ksi)	EinO Range (%)	SigNc Range (ksi)	SigNc Mean (ksi)	EinNc Range (%)	SigNs Range (ksi)	SigNs Mean (ksi)	EinNs Range (%)	Sig.5 Range (ksi)	Sig.5 Mean (ksi)	Ein.5 Range (%)
JB-42 Dsig	79.4 +5.0	4.3	0.148	-	-	-	-	-	-	73.7 +5.2	11.0	0.199

<001> PWA 1480 / PWA 273 THERMOMECHANICAL FATIGUE SUMMARY

Spec ID	SigO Range (ksi)	SigO Mean (ksi)	SigNc Range (ksi)	SigNc Mean (ksi)	SNmin Range (ksi)	SNmin Mean (ksi)	SNmax Range (ksi)	SNmax Mean (ksi)	Sig.5 Range (ksi)	Sig.5 Mean (ksi)
JB-76	60.5	22.0	Test discontinued before load drop. Nf/2 = 10800						60.3	-1.2
JB-125 Dsig	48.6 +2.4	7.0	52.8 +0.8	16.9	52.3 +1.0	17.8	52.8 +0.5	25.0	55.8 +0.7	21.0
JB-98	60.9	5.7	62.5	18.4	64.3	20.3	66.3	24.6	65.7	24.6
JB-61	60.6	6.6	-	-	-	-	63.7	17.1	59.8	16.2
JB-66 Dsig	65.9 +4.7	10.2	66.4 +0.9	26.4	70.4 +0.6	28.1	69.1 +0.3	31.5	69.2 +0.6	30.2
JB-62 Dsig	65.6 +1.5	9.5	73.7 +0.8	33.3	74.8 +0.8	37.8	77.0 +0.4	38.6	73.3 +0.8	34.5
JB-91	79.3	10.0	81.3	22.6	81.7	25.1	83.2	25.5	81.4	24.6
JB-22	78.2	10.0	83.4	15.8	79.9	21.0	80.1	21.6	79.9	21.0
JB-59	111.1	-20.1	112.5	-35.9	101.0	-37.3	-	-	Test discontinued	
JB-59 plus	57.7	9.9	-	-	58.8	22.3	58.4	23.8	58.5	21.8
JB-29	117.0	-17.3	117.7	-38.9	117.0	-44.4	-	-	Test discontinued	
JB-19	110.5	16.0	112.9	23.8	115.3	30.9	113.5	33.3	115.3	32.1
JB-38	121.7	21.0	122.2	34.9	124.4	38.5	124.4	38.5	122.6	38.0
JB-81	143.5	-8.4	123.9	25.3	123.0	36.9	121.4	39.6	122.5	38.5
JB-72	122.1	17.8	125.6	32.2	126.0	36.5	123.2	36.1	127.4	38.0
JB-64	159.4	-33.1	154.9	-48.6	-	-	-	-	154.9	-49.3
JB-88	48.1	6.1	48.0	22.0	46.2	21.7	45.4	20.9	47.0	22.7
JB-82	86.4	16.8	86.9	39.0	-	-	86.9	40.9	85.7	40.9

*The following specimens were exposed 100 hr. at 2000F prior to test.

Spec ID	SigO Range (ksi)	SigO Mean (ksi)	SigNc Range (ksi)	SigNc Mean (ksi)	SNmin Range (ksi)	SNmin Mean (ksi)	SNmax Range (ksi)	SNmax Mean (ksi)	Sig.5 Range (ksi)	Sig.5 Mean (ksi)
JB-154	64.9	10.9	65.4	15.5	65.4	15.5	66.8	19.6	66.4	22.0
JB-161	64.6	12.0	63.1	15.0	63.9	18.5	63.1	18.1	63.6	18.8

<001> PWA 1480 / PWA 286 THERMOMECHANICAL FATIGUE SUMMARY

Spec ID	/	Sig0 Range (ksi)	Sig0 Mean (ksi)	/	SigNc Range (ksi)	SigNc Mean (ksi)	/	SNmin Range (ksi)	SNmin Mean (ksi)	/	SNmax Range (ksi)	SNmax Mean (ksi)	/	Sig.5 Range (ksi)	Sig.5 Mean (ksi)	/
JB-174		58.3	14.5		58.2	14.6		58.3	14.6		58.3	14.6		58.4	14.5	
JB-147		71.4	10.6		76.3	23.4		74.3	26.7		74.3	26.7		70.0	26.3	
JB-121		66.6	-5.5		72.8	22.0		66.8	26.7		66.8	26.7		65.4	24.5	
Dsig		+3.6			+0.5			+0.6			+0.6			+0.6		
JB-137		65.9	-7.9		72.9	25.4		70.9	27.6		70.9	27.6		68.7	32.9	
Dsig		+6.0			+1.5			+1.4			+1.4			+1.2		
JB-135		61.5	-8.1		69.1	24.1		72.6	32.8		72.6	32.8		72.6	32.9	
Dsig		+1.9			+1.3			+0.4			+0.4			+0.3		
JB-10		-	-		88.1	20.9		91.3	22.2		89.7	27.0		91.0	26.7	
JB-104		108.6	-1.5		112.2	1.5		107.1	5.1		107.1	5.1		111.2	3.0	
JB-9		115.5	17.7		122.9	36.2		123.4	36.8		121.4	37.2		124.0	36.7	
JB-11		125.3	-18.2		125.1	-44.3		-	-		-	-		127.8	-44.2	
JB-80		148.4	-2.6		133.6	47.8		132.6	55.8		134.7	57.9		132.6	56.3	
JB-21		132.2	21.9		135.5	36.4		131.8	39.6		131.8	40.5		132.2	37.3	
JB-102		135.3	-7.0		135.1	-11.9		133.5	-8.0		-	-		135.3	-10.2	
JB-111		54.9	15.6		55.0	25.3		52.3	25.0		31.0	15.0		53.4	23.8	
JB-89		84.7	18.3		80.4	38.3		76.8	35.6		76.8	38.1		80.9	37.6	

*The following specimens were exposed 100 hr. at 2000F prior to test.

Spec ID	/	Sig0 Range (ksi)	Sig0 Mean (ksi)	/	SigNc Range (ksi)	SigNc Mean (ksi)	/	SNmin Range (ksi)	SNmin Mean (ksi)	/	SNmax Range (ksi)	SNmax Mean (ksi)	/	Sig.5 Range (ksi)	Sig.5 Mean (ksi)	/
JB-146		65.1	15.1		69.0	23.6		67.1	31.5		67.1	31.5		67.8	26.5	
JB-133		77.4	14.5		79.0	23.6		77.6	25.2		77.6	25.2		76.0	24.8	

<001> PWA 1480 / UNCOATED THERMOMECHANICAL FATIGUE SUMMARY

Spec ID	/	Sig0 Range (ksi)	Sig0 Mean (ksi)	/	SigNc Range (ksi)	SigNc Mean (ksi)	/	SNmin Range (ksi)	SNmin Mean (ksi)	/	SNmax Range (ksi)	SNmax Mean (ksi)	/	Sig.5 Range (ksi)	Sig.5 Mean (ksi)	/
JB-51		81.2	16.5		-	-		-	-		-	-		88.8	29.1	
JB-46		112.8	23.8		-	-		-	-		-	-		113.2	35.7	
JB-47		127.9	-14.0		-	-		-	-		-	-		123.5	-37.5	

154

Spec ID	SigO Range (ksi)	SigO Mean (ksi)	EinO Range (%)	SigNc Range (ksi)	SigNc Mean (ksi)	EinNc Range (%)	SigNs Range (ksi)	SigNs Mean (ksi)	EinNs Range (%)	Sig.5 Range (ksi)	Sig.5 Mean (ksi)	Ein.5 Range (%)
LB-106	156.1	0.1	0.002	-	-	-	-	-	-	172.1	11.1	0.003
LB-22	190.6	0.0	0.010	188.7	0.7	0.009	192.0	0.1	0.010	188.7	0.7	0.009
LB-25	234.5	0.0	0.011	-	-	-	231.5	0.0	0.015	230.5	3.0	0.013
LB-19	222.6	1.0	0.020	-	-	-	222.6	3.1	-	225.7	3.1	0.018
LB-121	238.7	-4.7	0.006	237.2	3.7	0.025	234.3	2.9	0.026	237.2	3.7	0.025
LB-120	229.8	-4.1	0.014	-	-	-	220.6	5.0	0.030	223.0	3.1	0.021
LB-124	232.5	-0.9	0.014	-	-	-	223.5	6.8	-	226.4	1.0	0.026
LB-236	114.3	-0.9	0.015	-	-	-	116.2	1.1	-	113.1	-0.1	0.017
LB-195	132.0	0.0	0.024	-	-	-	132.2	2.7	0.028	132.0	3.5	0.029
LB-180	152.6	-1.0	0.097	-	-	-	152.9	1.3	-	152.5	-1.3	0.106

Spec ID	SigO Range (ksi)	SigO Mean (ksi)	EinO Range (%)	SigNc Range (ksi)	SigNc Mean (ksi)	EinNc Range (%)	SigNs Range (ksi)	SigNs Mean (ksi)	EinNs Range (%)	Sig.5 Range (ksi)	Sig.5 Mean (ksi)	Ein.5 Range (%)
LB-30	219.0	-3.5	0.006	-	-	-	-	-	-	212.4	-2.1	0.004
LB-209	155.1	-1.3	0.007	-	-	-	170.5	14.7	0.005	157.0	8.3	0.006
LB-241	192.5	-3.1	0.011	-	-	-	191.5	1.0	-	194.6	2.1	0.011
LB-235	182.8	-3.3	0.013	-	-	-	182.8	2.4	0.017	182.3	1.0	0.017
LB-185	103.7	-0.4	0.016	-	-	-	99.3	0.0	0.017	103.7	0.5	0.013
LB-192	115.6	1.4	0.012	-	-	-	117.9	2.2	-	117.0	3.9	0.016
LB-188	130.6	-1.3	0.031	-	-	-	133.7	0.0	-	132.3	2.5	0.036
LB-233	101.2	-1.3	0.046	-	-	-	90.5	1.7	-	90.2	1.2	0.075
LB-232	75.7	2.2	0.113	52.0	1.0	-	-	-	-	63.1	2.3	0.131
LB-179	56.6	0.4	0.292	-	-	-	-	-	-	51.1	0.1	-

Spec ID	SigO Range (ksi)	SigO Mean (ksi)	EinO Range (%)	SigNc Range (ksi)	SigNc Mean (ksi)	EinNc Range (%)	SigNs Range (ksi)	SigNs Mean (ksi)	EinNs Range (%)	Sig.5 Range (ksi)	Sig.5 Mean (ksi)	Ein.5 Range (%)
LB-59	231.7	-0.5	0.019	-	-	-	234.0	10.1	0.005	233.5	8.5	0.007
LB-36	219.6	0.0	0.006	-	-	-	219.5	0.0	-	225.1	3.1	0.007

Spec ID	SigO Range (ksi)	SigO Mean (ksi)	SigNc Range (ksi)	SigNc Mean (ksi)	SNmin Range (ksi)	SNmin Mean (ksi)	SNmax Range (ksi)	SNmax Mean (ksi)	Sig.5 Range (ksi)	Sig.5 Mean (ksi)
LB-23	102.3	18.3	-	-	-	-	-	-	95.1	29.9
LB-20	118.7	27.0	116.8	39.8	123.9	44.0	118.2	47.3	111.6	45.4
LB-21	124.4	-9.5	-	-	128.4	-16.7	129.6	-14.3	125.2	-14.3
LB-156	125.6	14.8	-	-	127.9	22.5	129.4	22.5	124.3	19.4
LB-155	220.7	33.1	-	-	-	-	-	-	209.4	35.4
LB-189	115.0	27.7	104.6	46.1	109.6	50.0	109.6	50.0	109.2	49.6
LB-240	178.6	-32.8	-	-	160.4	-48.6	154.7	-49.3	159.8	-47.4

<111> PWA 1480 / PWA 286 THERMOMECHANICAL FATIGUE SUMMARY

Spec ID	/ SigO Range (ksi)	SigO Mean (ksi)	/ SigNc Range (ksi)	SigNc Mean (ksi)	/ SNmin Range (ksi)	SNmin Mean (ksi)	/ SNmax Range (ksi)	SNmax Mean (ksi)	/ Sig.5 Range (ksi)	Sig.5 Mean (ksi)	/
LB-170	97.5	17.1	101.3	57.6	86.6	49.1	86.6	49.1	99.1	54.5	
LB-181	100.1	17.5	105.7	56.7	100.2	60.6	100.2	60.6	99.8	49.9	
LB-27	121.7	18.7	124.6	43.8	132.5	45.3	132.5	45.3	121.2	39.9	
LB-31	124.6	17.2	-	-	-	-	-	-	117.7	52.7	
LB-32	122.2	-13.4	Test discontinued before load drop. Nf/2 = 6000						117.3	-5.4	
LB-29	126.5	7.1	113.3	9.7	112.2	7.1	112.2	7.1	113.3	8.2	
LB-26	212.4	-8.5	209.7	0.0	217.4	1.9	-	-	203.9	1.0	
LB-216	95.4	25.5	94.5	40.5	92.0	37.6	92.0	37.6	90.5	40.1	
LB-239	119.6	23.8	94.1	45.7	103.1	45.3	103.1	45.3	94.2	45.7	

<111> PWA 1480 / UNCOATED THERMOMECHANICAL FATIGUE SUMMARY

Spec ID	/ SigO Range (ksi)	SigO Mean (ksi)	/ SigNc Range (ksi)	SigNc Mean (ksi)	/ SNmin Range (ksi)	SNmin Mean (ksi)	/ SNmax Range (ksi)	SNmax Mean (ksi)	/ Sig.5 Range (ksi)	Sig.5 Mean (ksi)	/
LB-56	114.1	31.3	-	-	118.9	46.3	118.9	46.3	120.3	52.9	
LB-35	143.2	48.0	-	-	161.2	46.7	156.1	43.9	160.3	46.7	
LB-34	180.8	38.4	-	-	189.0	45.1	183.7	41.2	192.8	45.6	
LB-33	215.2	31.6	-	-	236.9	42.4	226.3	37.8	236.0	42.5	

<011> PWA 1480 / PWA 273 ISOTHERMAL FATIGUE SUMMARY

Spec ID	SigO Range (ksi)	SigO Mean (ksi)	EinO Range (%)	/	SigNc Range (ksi)	SigNc Mean (ksi)	EinNc Range (%)	/	SigNs Range (ksi)	SigNs Mean (ksi)	EinNs Range (%)	/	Sig.5 Range (ksi)	Sig.5 Mean (ksi)	Ein.5 Range (%)	/
KB-47	185.0	-2.1	0.026		178.6	-2.6	0.014		181.9	-3.1	0.016		186.4	-4.5	0.011	
KB-64	190.7	-59.1	0.017		186.4	-35.6	0.012		179.3	-35.6	-		179.3	-35.6	-	
KB-67	164.8	-80.5	0.029		174.1	-32.8	0.020		173.4	-25.9	0.021		172.0	-21.8	0.023	
KB-31	101.5	-1.8	0.018		101.9	-0.2	0.014		100.3	0.4	0.014		101.9	-0.2	0.014	
KB-23	118.9	-0.1	0.023		-	-	-		120.1	2.4	0.024		120.3	1.6	0.026	
KB-69	125.8	-3.3	0.062		124.0	-0.7	0.067		122.9	-0.4	0.075		123.6	0.0	0.067	
KB-28	138.5	-1.5	0.043		133.0	-22.5	-		130.0	-23.0	-		133.8	-22.6	0.090	
Dsig	-3.8				-9.1				-9.0				-9.1			
KB-97	63.7	2.7	0.023		48.7	1.6	0.064		47.6	2.3	-		48.7	1.6	0.064	
Dsig	+1.6				+3.2				+3.0				+3.2			
KB-90	82.6	-0.7	0.036		-	-	-		-	-	-		72.2	-7.3	0.101	
Dsig	-7.7				-				-				-7.2			
KB-86	74.4	-1.3	0.056		59.9	0.0	0.106		52.7	-1.5	0.130		58.8	-1.7	0.116	
KB-35	98.2	-2.9	0.070		-	-	-		-	-	-		94.0	-1.3	0.078	

*The following specimens were exposed 100 hr. at 2000F prior to test.

| KB-111 | 108.6 | -2.1 | 0.065 | | 105.0 | 0.3 | 0.057 | | 105.0 | 0.3 | 0.057 | | 106.5 | 0.3 | 0.059 | |

Spec ID	SigO Range (ksi)	SigO Mean (ksi)	EinO Range (%)	SigNc Range (ksi)	SigNc Mean (ksi)	EinNc Range (%)	SigNs Range (ksi)	SigNs Mean (ksi)	EinNs Range (%)	Sig.5 Range (ksi)	Sig.5 Mean (ksi)	Ein.5 Range (%)
KB-89	199.2	-5.6	0.011	-	-	-	-	-	-	195.9	-0.6	0.012
KB-85	208.6	-60.0	0.024	-	-	-	-	-	-	205.0	-26.9	0.014
KB-71	141.0	-60.8	0.011	140.4	-49.0	0.009	144.2	-5.5	0.010	Test discontinued		
KB-21	138.5	-1.6	0.010	140.7	-3.2	0.010	176.8	28.4	0.045	Test discontinued		
KB-100	192.7	-67.7	0.025	178.9	21.7	0.037	+7.5			176.7	24.2	0.043
Dsig	+26.0			+7.6						+7.2		
KB-98	190.5	-69.3	0.104	183.7	-46.1	0.029	180.9	-39.7	0.023	Test discontinued		
Dsig	-4.6			-4.3			-3.5			-		
KB-29	220.0	-2.9	0.020	221.5	-3.4	0.024	221.0	-1.3	0.025	221.5	-3.4	0.024
KB-68	129.0	0.1	0.030	-	-	-	122.2	0.9	0.031	122.8	1.1	0.031
KB-65	104.3	-1.4	0.030	-	-	-	105.7	1.5	-	106.7	-0.5	0.129
KB-70	113.0	-30.3	0.061	120.3	15.3	-	120.3	15.5	-	116.9	14.3	0.052
Dsig	+4.8			+4.8			+4.8			+4.8		
KB-96	115.1	-3.9	0.031	-	-	-	111.3	20.5	0.060	113.2	23.6	0.057
Dsig	-6.8			-			-6.0			-5.7		
KB-54	145.6	-0.9	0.049	-	-	-	144.6	-0.9	0.049	141.7	1.0	0.049
KB-79	68.6	0.0	0.024	47.5	0.0	0.108	-	-	-	Test discontinued		
KB-72	87.7	0.7	0.017	80.8	2.0	-	80.6	2.0	-	83.5	1.7	0.035
KB-91	84.8	0.5	0.037	77.3	0.7	0.056	-	-	-	78.0	0.2	0.053
KB-83	82.3	-0.3	0.042	75.5	4.9	0.075	-	-	-	75.5	4.9	0.075
Dsig	+6.3			+4.7						+5.1		
KB-77	89.2	-1.5	0.088	-	-	-	-	-	-	83.8	-5.1	0.121
Dsig	-6.7			-						-7.7		
KB-25	110.8	0.3	0.118	-	-	-	-	-	-	106.8	-0.3	0.133
KB-87	46.0	-0.4	0.053	-	-	-	-	-	-	34.5	0.0	0.113
KB-78	54.8	-0.6	0.134	-	-	-	-	-	-	47.4	0.0	0.169

*The following specimens were exposed 100 hr. at 2000F prior to test.

Spec ID	SigO Range (ksi)	SigO Mean (ksi)	EinO Range (%)	SigNc Range (ksi)	SigNc Mean (ksi)	EinNc Range (%)	SigNs Range (ksi)	SigNs Mean (ksi)	EinNs Range (%)	Sig.5 Range (ksi)	Sig.5 Mean (ksi)	Ein.5 Range (%)
KB-74	134.3	0.0	0.009	134.7	2.4	0.009	134.3	5.1	0.009	134.0	2.2	0.009
KB-108	107.3	-4.5	0.062	105.5	-1.4	0.053	104.4	-2.3	-	105.5	-1.4	0.053
KB-81	75.0	-1.1	0.081	70.3	-0.2	0.087	69.6	-0.2	0.089	69.8	-0.1	0.089

<011> PWA 1480 / PWA 273 THERMOMECHANICAL FATIGUE SUMMARY

Spec ID	/	SigO Range (ksi)	SigO Mean (ksi)	/	SigNc Range (ksi)	SigNc Mean (ksi)	/	SNmin Range (ksi)	SNmin Mean (ksi)	/	SNmax Range (ksi)	SNmax Mean (ksi)	/	Sig.5 Range (ksi)	Sig.5 Mean (ksi)	/
KB-33		85.9	10.7		Test discontinued before load drop. Nf/2 = 8500									87.5	39.2	
														49.9	-2.8	
KB-80		71.7	28.8		-	-		-	-		-	-		89.3	38.7	
KB-49		69.6	20.1		96.2	41.2		90.0	39.9		90.7	40.1		99.5	44.2	
KB-27		101.7	22.7		96.0	42.2		98.0	41.5		97.3	42.6				

*The following specimens were exposed 100 hr. at 2000F prior to test.

Spec ID	SigO Range	SigO Mean	SigNc Range	SigNc Mean	SNmin Range	SNmin Mean	SNmax Range	SNmax Mean	Sig.5 Range	Sig.5 Mean
KB-92	94.3	16.9	-	-	-	-	-	-	98.9	27.7

<011> PWA 1480 / PWA 286 THERMOMECHANICAL FATIGUE SUMMARY

Spec ID	/	SigO Range (ksi)	SigO Mean (ksi)	/	SigNc Range (ksi)	SigNc Mean (ksi)	/	SNmin Range (ksi)	SNmin Mean (ksi)	/	SNmax Range (ksi)	SNmax Mean (ksi)	/	Sig.5 Range (ksi)	Sig.5 Mean (ksi)	/
KB-32		81.1	10.5		83.3	15.4		88.6	25.0		88.6	25.0		81.4	25.7	
KB-24		87.7	14.1		91.8	41.0		84.1	48.1		89.1	48.1		91.4	41.0	
KB-36		85.6	42.7		-	-		-	-		-	-		89.0	42.3	
KB-34		120.8	18.4		127.0	35.2		128.0	51.1		128.0	51.1		128.2	43.1	
KB-48		74.1	10.0		78.8	38.1		53.3	26.6		53.3	26.6		75.3	36.9	
KB-52		75.3	8.0		69.2	27.2		76.5	33.2		76.5	33.2		Test discontinued		

*The following specimens were exposed 100 hr. at 2000F prior to test.

Spec ID	SigO Range	SigO Mean	SigNc Range	SigNc Mean	SNmin Range	SNmin Mean	SNmax Range	SNmax Mean	Sig.5 Range	Sig.5 Mean
KB-93	92.9	18.3	101.2	38.1	-	-	103.6	38.9	103.6	38.9

Spec ID	SigO Range (ksi)	SigO Mean (ksi)	EinO Range (%)	/	SigNc Range (ksi)	SigNc Mean (ksi)	EinNc Range (%)	/	SigNs Range (ksi)	SigNs Mean (ksi)	EinNs Range (%)	/	Sig.5 Range (ksi)	Sig.5 Mean (ksi)	Ein.5 Range (%)	/
MB-21	119.3	-3.3	0.026		119.1	2.2	0.032		119.3	2.4	0.029		119.1	2.2	0.032	
MB-18	143.9	-2.0	0.055		-	-	-		144.7	3.1	-		144.9	3.6	0.052	
MB-4	155.8	-2.3	0.065		-	-	-		142.4	-18.7	0.144		145.2	-18.4	0.137	
Dsig	-				-				-14.5				-15.1			
MB-88	60.2	1.3	0.016		57.2	4.4	0.040		41.6	1.5	0.073		55.0	6.6	0.046	
Dsig	+2.8				+3.6				+3.6				+4.3			

Spec ID	SigO Range (ksi)	SigO Mean (ksi)	EinO Range (%)	/	SigNc Range (ksi)	SigNc Mean (ksi)	EinNc Range (%)	/	SigNs Range (ksi)	SigNs Mean (ksi)	EinNs Range (%)	/	Sig.5 Range (ksi)	Sig.5 Mean (ksi)	Ein.5 Range (%)	/
MB-26	140.7	-63.6	0.016		138.6	-29.5	0.017		135.6	-27.6	0.014		Test discontinued			
MB-64	119.0	2.0	0.018		117.6	-2.0	0.027		116.2	5.0	0.024		117.6	-2.0	0.027	
MB-40	118.3	-0.8	0.031		110.8	20.7	0.075		-	-	-		112.5	18.1	0.073	
Dsig	+13.2				+7.3				-				+7.7			
MB-41	68.3	-1.6	0.031		-	-	-		-	-	-		61.2	-4.8	0.071	
Dsig	-4.5				-				-				-6.0			
MB-6	105.2	-0.7	0.082		-	-	-		-	-	-		99.3	0.9	0.102	
MB-38	90.2	-2.6	0.108		-	-	-		-	-	-		81.4	0.7	0.122	
MB-33	103.3	-1.4	0.164		-	-	-		81.7	0.7	0.123		99.3	0.9	0.167	
MB-2	105.4	0.6	0.141		-	-	-		-	-	-		98.0	0.3	0.161	

16. Abstract

This report presents the results from a 35 month period of a program designed to develop generic constitutive and life prediction approaches and models for nickel-based single crystal gas turbine airfoils. The program is composed of a base program and an optional program. The base program addresses the high temperature coated single crystal regime above the airfoil root platform. The optional program investigates the low temperature uncoated single crystal regime below the airfoil root platform including the notched conditions of the airfoil attachment.

Both base and option programs involve experimental and analytical efforts. Results from uniaxial constitutive and fatigue life experiments of coated an uncoated PWA 1480 single crystal material form the basis for the analytical modeling effort. Four single crystal primary orientations were used in the experiments: <001>, <011>, <111>, and <213>. Specific secondary orientations were also selected for the notched experiments in the optional program. Constitutive models for an overlay coating and PWA 1480 single crystal material were developed based on isothermal hysteresis loop data and verified using thermomechanical (TMF) hysteresis loop data. A fatigue life approach and life models were selected for TMF crack initiation of coated PWA 1480. An initial life model used to correlate smooth and notched fatigue data obtained in the option program shows promise. Computer software incorporating the overlay coating and PWA 1480 constitutive models was developed.